Oxidative Medicine and Cellular Longevity

ROS and Oxidative Stress in Stem Cells

Lead Guest Editor: Artur Cieślar-Pobuda
Guest Editors: Jianbo Yue, Hsin-chen Lee, Magdalena Skonieczna, and Yau-Huei Wei

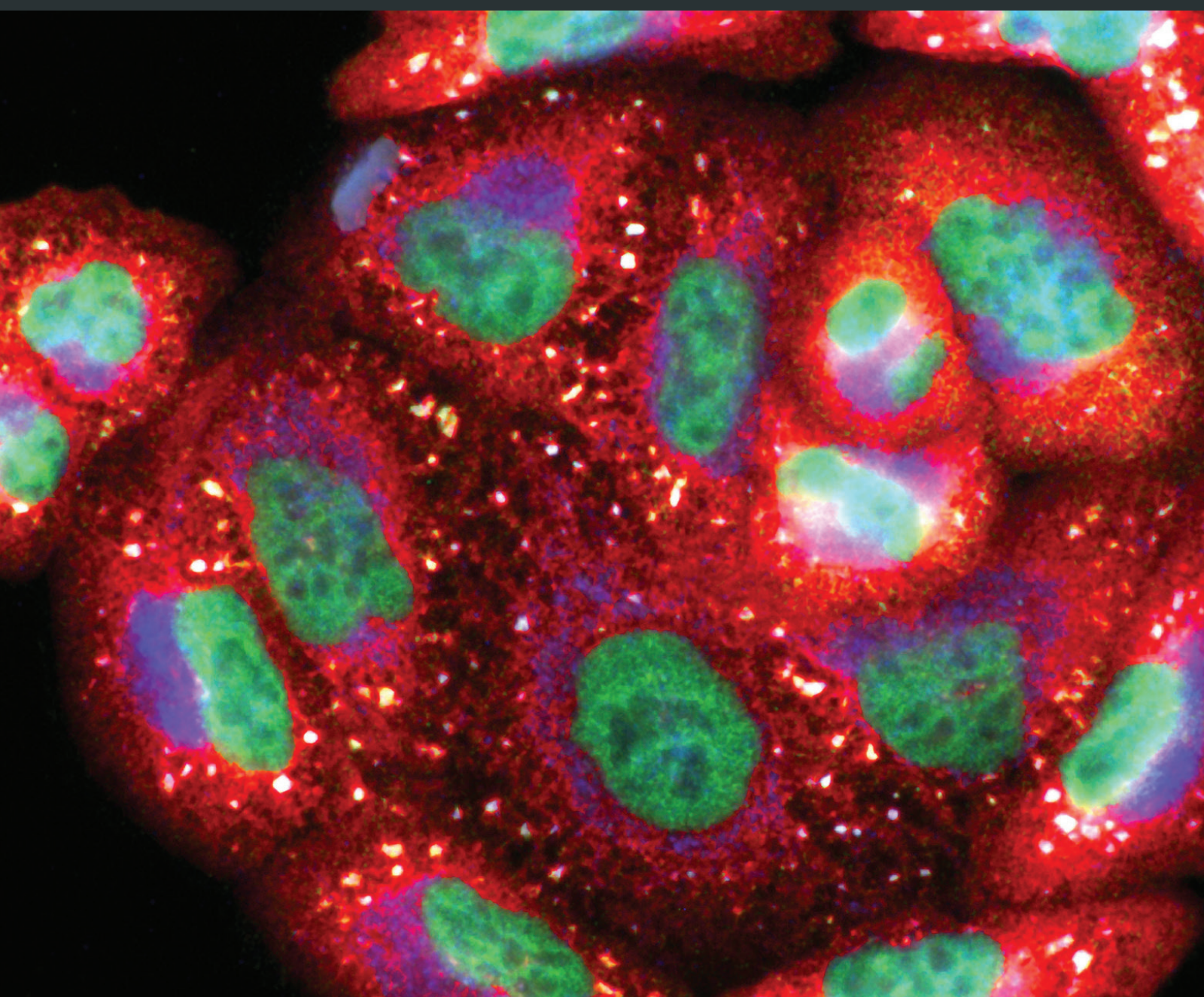

ROS and Oxidative Stress in Stem Cells

Oxidative Medicine and Cellular Longevity

ROS and Oxidative Stress in Stem Cells

Lead Guest Editor: Artur Cieslar-Pobuda
Guest Editors: Jianbo Yue, Hsin-chen Lee, Magdalena Skonieczna, and Yau-Huei Wei

Editorial Board

Contents

Hindawi
Oxidative Medicine and Cellular Longevity
Volume 2017, Article ID 5047168, 2 pages
https://doi.org/10.1155/2017/5047168

Editorial

ROS and Oxidative Stress in Stem Cells

Artur Cieślar-Pobuda,[1] Jianbo Yue,[2] Hsin-Chen Lee,[3] Magdalena Skonieczna,[4] and Yau-Huei Wei[3,5]

[1]*Stem Cell Group, Nordic EMBL Partnership, Centre for Molecular Medicine Norway (NCMM), University of Oslo, Oslo, Norway*
[2]*City University of Hong Kong, Kowloon, Hong Kong*
[3]*Center for Mitochondrial Medicine and Free Radical Research, Changhua Christian Hospital, Changhua City, Taiwan*
[4]*Biotechnology Centre, Silesian University of Technology, Gliwice, Poland*
[5]*Mackay Medical College, New Taipei City, Taiwan*

Correspondence should be addressed to Artur Cieślar-Pobuda; artur.cieslar-pobuda@ncmm.uio.no

Received 19 June 2017; Accepted 20 June 2017; Published 6 September 2017

Reactive oxygen species (ROS) are well known to be implicated in various important cellular processes including signaling, regulation of homeostasis, or induction of death. Oxidative stress resulting from increased ROS production and impaired free radical scavenging systems can cause severe damage to biological macromolecules, affecting cell proliferation and causing genomic instability and cellular senescence. Although ROS are involved in a wide range of cellular processes, a limited number of studies have examined the generation and function of ROS in stem cells. It is known that ROS may enhance differentiation of stem cells and facilitate reprogramming into induced pluripotent stem cells (iPSCs), but on the other hand, they are also associated with malignant transformation or premature aging. Stem cells have also been shown to possess defective DNA repair machinery, which may have serious consequences for cells exposed to extensive oxidative stress. Since stem cells are considered as a promising tool in regenerative medicine, it is crucial to know and better understand all the processes related to ROS to prevent potential generation of mutations causing genomic instability and to avoid unwanted ROS-driven differentiation. Thus, the mechanisms by which genomic integrity of stem cells is maintained under oxidative stress and the role of ROS should be elucidated before stem cells finally find their place in clinical applications.

The paper by C.-J. Li et al. demonstrates that treatment with antioxidants not only increases proliferation and mitochondrial integrity of human mesenchymal stem cells (hMSCs) but also enhances the therapeutic potential of hMSCs by promoting the formation of tunneling nanotubes (TNTs) between hMSCs and oxidatively injured cells in a coculture system. The authors demonstrate that TNTs enable hMSCs to "export" their healthy mitochondria to the injured cells and hence decrease their oxidative stress and stabilize the mitochondrial membrane potential of the injured cells. Concurrently, the rescued cells also show enhanced mitophagy, implicating that their damaged mitochondria are eliminated in order to maintain normal cell physiology. The findings highlight that antioxidants enhance mitochondrial transfer from hMSCs to the injured cells and provide them with a repair mechanism.

A similar topic is presented by Y.-C. Chuang et al. who show that Wharton's jelly mesenchymal stem cells (WJMSCs) are able to transfer healthy mitochondria to cybrid cells from a patient with myoclonus epilepsy associated with ragged-red fibers (MERRF) through intercellular connections. This mitochondrial transfer is found to be

associated with reduction of oxidative stress and improvement of mitochondrial bioenergetics in MERRF cybrid cells. The ability of WJMSCs to "help" cells with defective mitochondrial function (e.g., MERRF cells) through donating healthy mitochondria is an intriguing phenomenon that may provide new cues for the development of more effective treatment of diseases caused by or associated with mitochondrial dysfunction.

V. A. Sergeeva et al. contributed an interesting study, in which the adaptive response of MSCs to low doses of ionizing radiation (IR) is described. The authors show that such a response may be mediated by oxidized cell-free DNA (cfDNA) fragments. It is demonstrated that treatment of MSCs with low doses of IR leads to cell death of part of the cell population and release of oxidized cfDNA, which has the ability to penetrate into the cytoplasm of other cells. Oxidized cfDNA, like low doses of IR, induces ROS production, ROS-induced oxidative DNA damage, cell cycle arrest, activation of DNA repair mechanisms, and inhibition of apoptosis. The MSCs pretreated with a low dose of irradiation or oxidized cfDNA are equally effective in induction of an adaptive response to the challenge of further doses of radiation. This study suggests that oxidized cfDNA is a stress-triggered signaling molecule that mediates radiation-induced bystander effects and that it is an important component of radioadaptive responses of cells to low doses of IR.

D. Sainz de la Maza et al. explore the role of ROS and autophagy on reprogramming of primordial germ cells (PGCs) into pluripotent cells. The authors demonstrate that a metabolic shift from oxidative phosphorylation toward glycolysis, autophagy, and mitochondrial inactivation and an early rise in ROS levels are necessary for PGC reprogramming. It is shown that all these processes are regulated by a correct (right) HIF1/HIF2 balance and Oct4. The cells obtained are unable to self-renew, and it is postulated that *Blimp1* may be responsible for this.

J. Kučera et al. focus in their work on the effect of hypoxia on intracellular signaling pathways responsible for mouse embryonic stem (ES) cell maintenance. By employing wild-type and hypoxia inducible factor 1- (HIF-1-) deficient ES cells and measuring phosphorylation of proteins of the ERK, Akt, and STAT3 pathways, the authors investigate the response of ES cells to hypoxia. The study shows that ERK signaling is downregulated in hypoxia in a ROS-dependent manner, but without the involvement of hypoxia-inducible factor HIF-1. The authors also observe a decreased ROS level in hypoxia and a similar phosphorylation pattern for ERK when the cells are supplemented with glutathione.

Finally, the review article by M. Skonieczna et al. gives an extensive overview about NADPH oxidases (NOX) and their role in various cellular systems. The article describes the functions and mechanisms of action of NOX and NOX-derived ROS in stem cells, cancer cells, and cancer stem cells. It also points out the importance of understanding NOX-dependent cellular processes, as a future perspective for regenerative medicine and development of new therapies toward cancers.

In conclusion, the aim of this special issue is to provide updated information for readers to better understand the role of oxidative stress and ROS in stem cell physiology. All the articles selected for this special issue present important findings that will undoubtedly provide useful cues for future research.

Artur Cieślar-Pobuda
Jianbo Yue
Hsin-Chen Lee
Magdalena Skonieczna
Yau-Huei Wei

Hindawi
Oxidative Medicine and Cellular Longevity
Volume 2017, Article ID 9515809, 22 pages
https://doi.org/10.1155/2017/9515809

Research Article

Low-Dose Ionizing Radiation Affects Mesenchymal Stem Cells via Extracellular Oxidized Cell-Free DNA: A Possible Mediator of Bystander Effect and Adaptive Response

V. A. Sergeeva,[1] E. S. Ershova,[1,2] N. N. Veiko,[1,2] E. M. Malinovskaya,[1] A. A. Kalyanov,[1] L. V. Kameneva,[1] S. V. Stukalov,[1] O. A. Dolgikh,[1] M. S. Konkova,[1] A. V. Ermakov,[1] V. P. Veiko,[3] V. L. Izhevskaya,[1] S. I. Kutsev,[1,4] and S. V. Kostyuk[1]

[1]*Research Centre for Medical Genetics (RCMG), Moscow 115478, Russia*
[2]*V. A. Negovsky Research Institute of General Reanimatology, Moscow 107031, Russia*
[3]*Bach Institute of Biochemistry and Russian Academy of Sciences, 33 Leninskii Ave., Moscow 119071, Russia*
[4]*N. I. Pirogov Russian National Research Medical University, Moscow 117997, Russia*

Correspondence should be addressed to V. A. Sergeeva; tracytheplane@gmail.com

Received 20 January 2017; Revised 17 April 2017; Accepted 18 May 2017; Published 22 August 2017

Academic Editor: Magdalena Skonieczna

We have hypothesized that the adaptive response to low doses of ionizing radiation (IR) is mediated by oxidized cell-free DNA (cfDNA) fragments. Here, we summarize our experimental evidence for this model. Studies involving measurements of ROS, expression of the NOX (superoxide radical production), induction of apoptosis and DNA double-strand breaks, antiapoptotic gene expression and cell cycle inhibition confirm this hypothesis. We have demonstrated that treatment of mesenchymal stem cells (MSCs) with low doses of IR (10 cGy) leads to cell death of part of cell population and release of oxidized cfDNA. cfDNA has the ability to penetrate into the cytoplasm of other cells. Oxidized cfDNA, like low doses of IR, induces oxidative stress, ROS production, ROS-induced oxidative modifications of nuclear DNA, DNA breaks, arrest of the cell cycle, activation of DNA reparation and antioxidant response, and inhibition of apoptosis. The MSCs pretreated with low dose of irradiation or oxidized cfDNA were equally effective in induction of adaptive response to challenge further dose of radiation. Our studies suggest that oxidized cfDNA is a signaling molecule in the stress signaling that mediates radiation-induced bystander effects and that it is an important component of the development of radioadaptive responses to low doses of IR.

1. Introduction

Human beings are constantly exposed to background sources of IR both of natural (terrestrial and cosmic) and artificial origin (nuclear energy, nuclear accidents, radiation for medical purposes) [1]. The use of IR in research, industry, homeland security, and contemporary medicine is continuously growing and increasing the potential for human exposures [2]. However, the biological effects of low-dose ionizing radiation (LDIR) exposure are still not adequately understood. It is possible that even if there is a potential beneficial hormetic effect, there might still be risks of negative effects that have not been detected [3]. Although there are many published reports available, the understanding of fundamental biological processes and signaling pathways involved in the response to LDIR in human cells is still inconsistent and not fully conclusive [2]. A number of epidemiological studies are available for LDIR exposures below 0.1 Gy on stochastic effects such as cancer incidence and effects on heredity [4, 5], and it was reported that 0.06 Gy of LDIR exposure might increase the risk of brain cancer threefold [6]. It is well accepted that one of the major problems in radiation research is how to extrapolate the data obtained for high-dose IR exposures to the LDIR

range (0.1 Gy and less). There is a "linear, no-threshold" hypothesis [7] according to which even the smallest doses of IR could potentially increase the cancer risk. However, the evidence for nonlinearity in biological effects of LDIR is growing [8, 9]. The nontargeted effects of IR, such as radioadaptive responses (RAR), radiation-induced bystander effects (RIBE), and LDIR hypersensitivity, add to the uncertainties of assessing the biological effects of LDIR.

The effects of information transfer from irradiated (target) cells to adjacent, nontargeted cells (RIBE) have been observed for a number of damaging agents of both physical and chemical nature in many types of eukaryotic cells and cover a variety of physiological effects including genomic instability, cell death, and/or RAR [10]. RIBE and RAR are closely interconnected biologically and have many similarities and characteristic features [10–12]. There are three possible pathways of signal transfer from the irradiated cell to the bystander cell: through direct cellular contact with the formation of common membranous structures, through interaction involving gap junctions, or via signals released to the culture medium of the irradiated cells [13], a pathway typical for the RIBE induced by radiation with low linear energy transfer [14]. Many candidate molecules, mainly soluble proteins, have been proposed as mediators of bystander signaling [15, 16].

Research on the role of cell-free DNA (cfDNA) circulating in the blood of healthy persons and patients has led to the hypothesis that oxidized cfDNA (cfDNAox) released from dying cells could mediate RIBE and RAR, and further information on our own research on this subject can be found here [17–20]. We researched the bystander effect in various cell types including G0 lymphocytes of peripheral blood [17] and HUVECs [20]. As we have showed previously, one of the known markers for irradiation-induced chromatin rearrangement, the position of pericentromeric loci of chromosome 1 (1q12) [21], undergoes the same change after 10 cGy of IR and when treated with cfDNAox from the medium from irradiated cells (cfDNAoxR) [18].

Stem cells are undifferentiated cells that have a potential for unlimited division and differentiation into many types of cells. As they have a longer life span, they are more likely to accumulate mutations and lead to cancer [22]. IR can affect the fate of stem cells by inducing DNA damage, arresting the cell cycle or apoptosis, both at genetic and epigenetic levels. Researching the signaling pathways that allow stem cells to survive IR is of importance, and the aim of our work was to assess the development of the RAR to low-dose IR in mesenchymal stem cells (MSCs) and to describe the role of cfDNAox as a stress signaling molecule that mediates RIBE.

2. Methods

2.1. Cell Culture. MSCs were derived from adipose tissue of patients subjected to surgical operation. To obtain stromal cells, minced adipose tissue was digested with collagenase as described previously [23]. Tissue samples were mechanically disrupted in Dulbecco's Modified Eagle medium (DMEM) (Paneko, Moscow) containing 250 μg/ml gentamycin, 60 U/ml penicillin, and 60 U/ml streptomycin (Paneko). Cells were dissociated by incubation with 0.04% collagenase (Sigma) in DMEM with 10% fetal bovine serum (FBS) (PAA, Austria) at 37°C for 16 h. Cells were centrifuged at 200g for 10 min, transferred into slide flasks and cultivated at 37°C in AmnioMax Basal Medium with AmnioMax Supplement C100 (Gibco). Cultures were split no more than four times before experiments.

MSCs were characterized by standard markers using fluorescence-activated cell sorting (FACS): MHC molecules (HLA-ABC+) and adhesion molecules (CD44+, CD54 (low), CD90+, CD106+, CD29+, CD49b (low), and CD105); however, they were negative for hematopoietic markers (CD34−, CD45−, and HLA-DR−) and the marker CD117 (Dominici et al. 2006). Moreover, cells differentiated into adipocytes in the presence of inducers in a kit for adipogenic differentiation (STEMCELL Technologies). Ethical approval for the use of MSCs was obtained from the Regional Committees for Medical and Health Research Ethics (approval number 5).

2.2. Irradiation of Cells. MSCs were irradiated in a growth medium at 20°C using a pulsed Röntgen radiation unit (ARINA-3, Spectroflash, Russia). The voltage on the X-tube was ~160 kV (~60 keV), peak energy in the spectrum was 60 keV, and dose rate was 10 cGy/min. Nonirradiated cells were used as controls.

2.3. Flow Cytometry (FACS). MSCs were washed in Versene solution (PanEco, Moscow, Russia) and then treated with 0.25% trypsin, washed with medium, and suspended in PBS. Cells were fixed with paraformaldehyde (PFA, Sigma, 2%, 37°C, 10 min), washed three times with 0.5% BSA-PBS, and permeabilized with 0.1% Triton X-100 in PBS (15 min, 20°C) or with 90% methanol (3 h, 4°C). The cells were washed 3× with 0.5% BSA-PBS and labeled with primary antibodies (1 μg/ml) for 2 h (4°C) and then washed 3× with 0.5% BSA-PBS. The following antibodies were used: γH2AX-Dylight488 (pSer139) (NB100-78356G, Novus Biologicals); NOX4 (Sc-30141, Santa Cruz Biotechnology); 8OHDG (Sc-66036, Santa Cruz Biotechnology); BRCA2 (NBP1-88361, Novus Biologicals); PCNA (ab2426, Abcam); Ki-67FITC (sc-23900 FITC, Santa Cruz Biotechnology); and BCL2 (Sc-783, Santa Cruz Biotechnology). Cells were then incubated for 2 h (20°C) with FITC-conjugated goat anti-rabbit IgG (Sc-2012, Santa Cruz Biotechnology) or goat anti-mouse IgG (Sc-2010, Santa Cruz Biotechnology). To quantify the background fluorescence, we stained portions of the cells with secondary FITC-conjugated antibodies only. To quantify DNA, cells were treated with propidium iodide (PI) and RNase A. The cells were analyzed using a CyFlowSpace flow cytometer (Partec, Germany).

2.4. Annexin V Binding Assays. Cells were detached, washed with PBS, and treated with annexin V-FITC and PI in buffer (10 mM HEPES, pH 7.4, 140 mM NaCl, 2.5 mM $CaCl_2$) at 20°C for 15 min and immediately analyzed using an automated cell counter (Countess II FL, Thermo Fisher) or FACS (CyFlow Space).

2.5. ROS Assays

2.5.1. FACS ROS Assay. After irradiation or treatment with cfDNA, cells were washed with PBS and incubated with 10 μM H2DCFH-DA (Invitrogen) at 37°C in the dark for 20 min. Cells were detached, washed with PBS, and immediately analyzed by FACS.

2.5.2. Fluorescence Microscopy. Cells were grown in slide flasks and washed in PBS. Then, 10 μM H2DCFH-DA (Molecular Probes/Invitrogen, CA, USA) was added for 20 min, and cells were washed 3× with PBS and immediately photographed.

2.5.3. Plate ROS Assay. Cells were grown to 80–90% confluency in 96-well plates (Nunclon, Germany). After irradiation or treatment with DNA, cells were incubated with 10 μM H2DCFH-DA (Invitrogen) at 37°C in the dark. Fluorescence was measured with λex = 503 nm and λem = 524 nm (EnSpire, PerkinElmer, Finland).

2.6. Fluorescence Microscopy. Cells were grown in slide flasks, fixed in 2% PFA (4°C, 20 min), washed with PBS, and then permeabilized with 0.1% Triton X-100 in PBS (15 min, 20°C), followed by blocking with 0.5% BSA in PBS (1 h, 4°C), and incubated overnight with rabbit polyclonal antibody against LC3 (Epitomics, Cambridge, MA), γH2AX (pSer139), or NF-κB (p65) (Abcam). After washing with 0.01% Triton X-100 in PBS, cells were incubated for 2 h (20°C) with FITC goat anti-rabbit IgG, washed with PBS, and then stained with DAPI or PI. Nuclear fragmentation was examined in cells washed and stained with Hoechst 33342 (Sigma, 10 μg/ml) for 10 min at 37°C. Images were obtained using an AxioScope A1 microscope (Carl Zeiss).

2.7. Quantification of mRNA Levels. Total mRNA was isolated using RNeasy Mini kits (Qiagen, Germany), treated with DNAse I, and reverse transcribed by a Reverse Transcriptase kit (Sileks, Russia). The expression profiles were obtained using qRT-PCR with SYBR Green PCR Master Mix (Applied Biosystems). The mRNA levels were analyzed using the StepOnePlus (Applied Biosystems); the technical error was approximately 2%. The following primers were used (Sintol, Russia):

NOX4 (TTGGGGCTAGGATTGTGTCTA; GAGTGTT CGGCACATGGGTA);
BCL2 (TTTGGAAATCCGACCACTAA; AAAGAAAT GCAAGTGAATGA);
BCL2A1 (TACAGGCTGGCTCAGGACTAT; CGCAA CATTTTGTAGCACTCTG);
BCL2L1 (CGACGAGTTTGAACTGCGGTA; GGGAT GTCAGGTCACTGAATG);
CCND1 (TTCGTGGCCTCTAAGATGAAGG; GAGCA GCTCCATTTGCAGC);
CDKN2A (ATGGAGCCTTCGGCTGACT; GTAACTA TTCGGTGCGTTGGG);
BRCA1 (GGCTATCCTCTCAGAGTGACATTTTA; GC TTTATCAGGTTATGTTGCATGGT);
BIRC2 (GAATCTGGTTTCAGCTAGTCTGG; GGTGG GAGATAATGAATGTGCAA);
BIRC3 (AAGCTACCTCTCAGCCTACTTT; CCACTG TTTTCTGTACCCGGA);
BAX (F: CCCGAGAGGTCTTTTTCCGAG, R: CCAG CCCATGATGGTTCTGAT);
BRCA2 (F: CCTCTGCCCTTATCATCACTTT, R: CCA GATGATGTCTTCTCCATCC);
TBP (reference gene) (F: GCCCGAAACGCCGAATAT, R: CCGTGGTTCGTGGCTCTCT).

The standard curve method was used for the quantification of RNA levels.

2.8. Quantitation of 8-OxodG. DNAs were dissolved in 20 μl HPLC-purified water and digested for 1 h at 37°C using 0.5 μl of DNase I (2000 U/μl), 2.3 μl 100 mM $MgCl_2$, and 0.5 μl 1 M Tris-HCl (pH 7.4). After adjusting the pH to 5.2 with 0.5 μl of 3 M sodium acetate (pH 5.2), the DNA was further digested with 1 μl of NP1 (1 unit/μl) for 1 h followed by neutralization with 2.3 μl of 1 M Tris-HCl (pH 8.0); 0.5 μl of alkaline phosphatase (1 unit/μl) was added and further incubated for 1 h. Quantitative analysis of 8-oxodG was performed using electrospray ionization mass spectrometry (ESI-MS/MS) on an AB SCIEX 3200 Qtrap machine. The sensitivity of this assay was one molecule of 8-oxodG per 10^7 molecules of dG.

2.9. DNA Oxidation In Vitro. Genomic DNA was isolated from MSCs by phenol-chloroform extraction. Hydrolysis by DNAse I (Invitrogen, USA) was performed until the maximal length of the DNA fragments was below 15 kb. The resulting DNA solution (100 μg/ml) was combined with 300 mM H_2O_2 under UV light (312 nm), 30 min, 25°C (gDNAox). The modified DNA was precipitated with 2 volumes of ethanol in the presence of 2 M ammonium acetate, washed twice with 75% ethanol, and then dried and dissolved in water. DNA concentrations were assessed by UV spectrophotometry.

2.10. Plasmid Construction. Plasmid pEGFP-C1 that contains the *EGFP* gene (http://www.bdbiosciences.com, GenBank accession number U55763) was used as vector. The DNA fragment to be inserted was synthesized and consisted of 59 base pairs flanked with BamHI restriction sites (italics) and containing the poly-G (underlines) sequence.

∨BamH1
GGGCCCG*GGATCCA*CCGGATCTAGATAATCGCCGT

∨BamH1
CCCGCCCGCCGCCTTGGGGGGGGGGG*GATCCA*AAAAA

In order to obtain the DNA fragment, PCR with primers GF_601 gggcccgggatccaccggatctagataatcgccgtcccgc ccgccgcctt and C10 tttttggatccccccccccccaaggcggcgggcggga cggcga was used.

The fragment was purified by agarose gel electrophoresis and treated with BamHI. The vector pEGFP-C1 was treated with BamHI and added to the DNA fragments with subsequent ligation with T4 DNA ligase. Competent *E. coli* (strain JM110) were then transformed and grown on LB with agarose and kanamycin (50 μg/ml). The clones were analyzed by PCR with oligonucleotides

Table 1: Sources and characteristics of MSC lines. Cell lines were obtained from the Research Centre for Medical Genetics, Moscow.

Cell	Source	Surface markers			
MSC	Adipose tissue from mammary gland	CD34−	CD45−	HLA-ABC+	HLA-DR−
		CD44+	CD29+	CD49b low	CD54 low
		CD90+	CD106−	CD105 low	CD117−

R_SEQ_N and SEQ_C in order to confirm the insertion of the DNA fragment (SEQ_C = catggtcctgctggagttcgtg, R_SEQ_N = caataaacaagttaacaacaacaattgc). Selected clones were grown in liquid medium and plasmids were isolated. After confirmation of the designed DNA sequence by sequencing, the plasmids were extracted using an Invisorb Plasmid Maxi Kit (http://www.invitek.de).

2.11. Comet Assays. A cell suspension in low-melting-point agarose was dropped onto slides precoated with 1% normal-melting-point agarose. The slides were placed in a solution (10 mM Tris-HCl, pH 10, 2.5 M NaCl, 100 mM EDTA, 1% Triton X-100, 10% DMSO, 4°C, 1 h) and then in electrophoresis buffer (300 mM NaOH, 1 mM EDTA, pH > 13). Electrophoresis was performed for 20 min at 1 V/cm, 300 mA. The slides were fixed in 70% ethanol and stained with SYBR Green I (Invitrogen, USA).

2.12. Statistics. All the reported results were reproduced at least three times as independent biological replicates. In FACS, the median of signal intensities was analyzed. The figures show the mean and standard deviation (SD) values. The significance of the observed differences was analyzed with nonparametric Mann–Whitney U tests. p values < 0.05 were considered statistically significant and are marked in the figures with $*$. Data were analyzed with StatPlus 2007 professional software (http://www.analystsoft.com/).

3. Results

3.1. Experimental Design. This study was performed using human MSC lines obtained from different donors and characterized by their CD marker expression (Table 1). We first demonstrated that treatment of MSCs with LDIR (10 cGy) increases the level of 8-oxodG in cfDNA obtained from the culture medium 2–2.5-fold. We also constructed a plasmid containing a DNA fragment that contains a (G)n repeat that is easy to oxidize, which penetrates into the cytoplasm of MSCs when they are irradiated as shown by fluorescence microscopy. In the second series of experiments, we compared the effects of various types of oxidized cfDNA with those of LDIR on the levels of ROS production, DNA breaks, and expression levels of several adaptive response genes. Unless otherwise stated, the IR dose was 10 cGy and the concentration of oxidized cfDNA fragments (cfDNAox and cfDNAoxR) added to cultures was 50 ng/ml with an exposure time of 5 min up to 24 h.

3.2. Low-Dose Radiation Causes Oxidation of cfDNA In Vitro. The concentrations of cfDNA in the growth medium used here are 12 ± 2 ng/ml [24]. Previously published studies have reported that genomic DNA (gDNA) from cultured cells contains ~0.1 to 0.5 8-oxodG per 10^6 nucleotides [25, 26]. cfDNA in the medium used here contains ~1 to 5 8-oxodG per 10^6 nucleotides.

LDIR can lead to death of a part of the cell population during the first min of exposure. The amount of apoptotic cells after irradiation was assessed using the marker of apoptosis annexin V. 10–20 min after irradiation, cells exhibited signs of apoptosis, and the fraction of apoptotic cells increases 2–2.5-fold (Figure 1(b)). Cell death leads to an increase in the cfDNA concentration in the medium; the concentration 20 min after irradiation with 10 cGy averaged 40 ± 5 ng/ml. IR causes oxidative stress [27] and 10 cGy of LDIR increased the level of 8-oxodG in cfDNA up to 100–200 8-oxodG per 10^6 nucleotides 20 min after irradiation. The latter will be referred to here as cfDNAoxR.

CG-rich cfDNA fragments are prone to oxidation. We further investigated if the CG-rich oxidized cfDNA penetrates into cells after treating them with 10 cGy of IR.

3.3. Oxidized cfDNA Penetrates into Cells Treated with 10 cGy of I ∗ R. A plasmid containing a marker GFP gene and (G)n repeats that are easy to oxidize was constructed, and its penetration into cells was investigated by fluorescence microscopy and flow cytometry. The cells were treated with plasmids in two ways: (1) the plasmid was added to the medium at a concentration of 100 ng/ml and the cells were then incubated for 24 h and (2) cells were irradiated directly after adding the plasmid to the medium. After cultivation, cells were imaged with the same exposure and magnification. Cells treated by method (1) exhibited weak fluorescence in the cytoplasm, while cells treated by method (2) had a higher level of fluorescence which indicates penetration of the plasmids into the cytoplasm (Figure 1(a)).

As CG-rich oxidized cfDNA penetrates into cells, it might mediate early responses to LDIR (10 cGy).

3.4. Oxidized cfDNA Mediates Early Responses to LDIR (10 cGy). As we showed previously, GC-rich cfDNA can play a role of a signaling molecule in RIBE when lymphocytes from peripheral blood are exposed to LDIR [17]. We hypothesized that oxidized GC-rich cfDNA fragments can be mediators of rapidly repaired DNA breaks in cells exposed to LDIR.

cfDNA from medium of cells 15 min after irradiation was added to MSCs. As the cfDNA in these conditions contains a high level of oxidized bases, model fragments of oxidized DNA were prepared (Table 2) which allowed us to exclude the effect of other factors such as level of methylation and differences in sequence.

cfDNAox fragments were prepared by treatment of gDNA with H_2O_2 and Fe^{2+}/EDTA and the level of 8-oxodG was

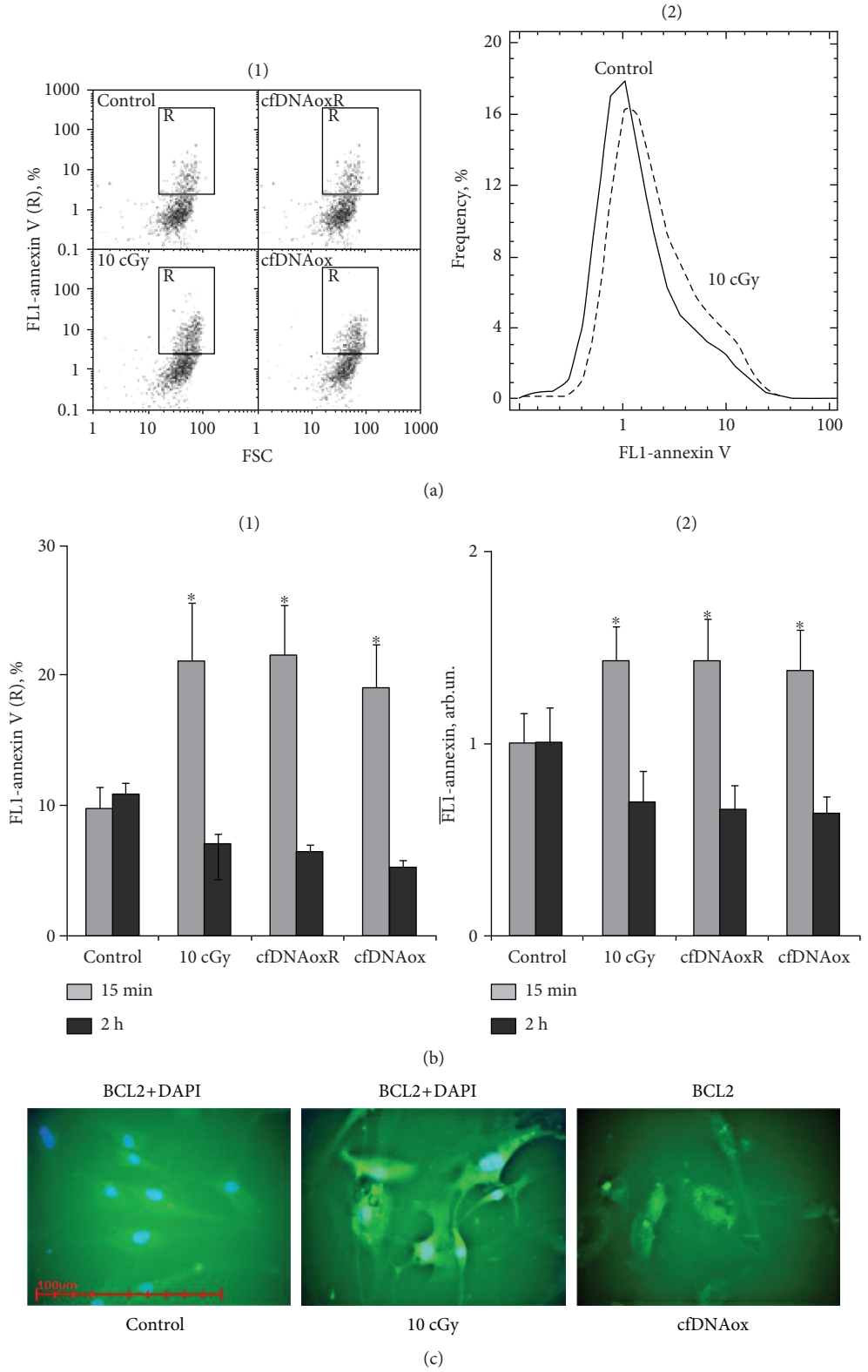

Figure 1: Low-dose radiation causes a strong antiapoptotic response. (a) (1) Flow cytometric enumeration of cells with signs of early apoptosis by FL1 versus FSC. R: gated area, annexin V-positive cells in total population; (2) distribution of fluorescence intensities of cells stained with annexin V-FITC. (b) Signal intensity of FL1-R (1) and average signal intensity of FL1-annexin V-FITC (2) in irradiated (10 cGy, 15 min and 2 h after exposure) and exposed to cfDNAox and cfDNAoxR (50 ng/ml, 15 min and 2 h) cells (flow cytometry). (c) Fluorescence microscopy of irradiated and exposed to cfDNAox MSCs stained with BCL2 (anti-BCL2-antibody and secondary FITC-conjugated antibodies) and DAPI (40×), $^{*}p < 0.05$.

Table 2: Content of 8-oxodG per 10^6 nucleotides in different types of DNA.

	Content of 8-oxodG per 10^6 nucleotides
gDNA	<0.01
cfDNAox	400
cfDNAoxR	200

assessed (Table 2). Intact genomic DNA contains less 8-oxodG than the threshold of sensitivity of the analysis (0.1 per 10^6 nucleotides), cfDNAox contains ~400 per 10^6 nucleotides, and cfDNA from irradiated medium (cfDNAoxR) contains ~200 per 10^6 nucleotides.

The effect of cfDNAox, cfDNAoxR, or LDIR on the levels of ROS and DNA breaks was investigated. In order to confirm the role of DNA oxidation in these processes, cells were also treated with unoxidized genomic DNA and unoxidized cfDNA from the medium of control cells.

3.4.1. cfDNAox Fragments, like LDIR, Induce a Short-Term Increase in ROS Production. LDIR induces oxidative stress in cells, increasing ROS production. Intracellular ROS level was assessed using H2DCFH-DA (2,7-dichlorofluorescin diacetate) [28, 29] which rapidly penetrates into the cytoplasm where intracellular esterases deacetylate it to form nonfluorescent DCFH [28] which reacts with ROS forming fluorescent DCF [30]. DCF is then detected with a plate reader to provide quantitation of total ROS in the cells. Both IR and oxidized cfDNAox and cfDNAoxR lead to a 2-fold increase of ROS 5–15 min after exposure (Figures 2(b) and 2(d)). However, 30 min after exposure the ROS level decreases and in another 60 min has returned to the control level (Figures 2(b) and 2(d)). These results were confirmed by FACS analysis of the amount of ROS in individual cells (Figures 2(b), 2(c), and 2(d)) and by fluorescence microscopy (Figure 2(e)). Unoxidized gDNA and cfDNA fragments at 50 ng/ml caused an insignificant elevation of ROS synthesis 2 h after addition, most likely due to gradual oxidation of the added fragments. Thus, both intact and oxidized DNA stimulate a short increase in the level of ROS.

Increase in ROS production by cfDNAox fragments can be connected with increased expression of *NOX4*.

3.4.2. cfDNAox Fragments, like LDIR, Induce an Increase in NOX4 Expression. The main producer of ROS is the NADPH oxidase family (NOX) that includes *NOX* 1–5, DUOX 1, and DUOX2 [31]. *NOX 1–5* are membrane-bound enzyme complexes whose activity is determined by NADPH binding and transfer of an electron to molecular oxygen with formation of a short-living $O_2^-\bullet$ that is further transformed into oxygen peroxide (H_2O_2) and a hydroxyl radical (•OH) [32]. The *NOX4* expression level is regulated by many factors and changes in response to IR [33]. Since LDIR and cfDNAox had the same effect on ROS production, we expected that they will have a very similar effect on *NOX4* expression.

And indeed, LDIR and cfDNAox and cfDNAoxR fragments induce a 2–2.5-fold increase in *NOX4* gene expression after 10–20 min exposure, which after 1 h, it returns to the control level (Figure 3(a)). *NOX4* enzyme expression increases by 30% right after irradiation, and by 60% after adding cfDNAox and cfDNAoxR fragments to the medium, and 1 h after irradiation, the level of *NOX4* expression is 2–2.2-fold increased compared to control, and 3 h after irradiation, it returns to control levels (Figures 3(b) and 3(c)).

The increased level of ROS can induce damage to the cells and cause oxidation of genomic DNA.

3.4.3. cfDNAox and Oxidized cfDNA Fragments Cause Oxidation in Nuclear DNA. LDIR, as well as cfDNAox and cfDNAoxR, causes an increase in ROS production that leads to oxidation of nuclear DNA. An FITC-labeled antibody was used to detect 8-oxodG. Control cells did not contain FITC-labeled antibody; there were single cells in the population that had labeled cytoplasm, possibly due to oxidized mitochondrial DNA. Three main types of cells are present after irradiation: (1) with labeled nuclei, (2) with labeled cytoplasm, and (3) both nucleus and the cytoplasm are labeled. Fifteen–20 min after irradiation with 10 cGy, the fluorescent intensity of the cytoplasm and the amount of stained nuclei increased (Figures 4(a) and 4(b)). Two h after irradiation, the staining returns to the control level. CfDNAox and cfDNAoxR fragments have a similar effect; 20 min after treatment, the intensity increases compared to control (Figures 4(a) and 4(b)).

Two subpopulations of cells were detected by flow cytometry; 3–5% of the total population showed high levels of 8-oxodG (Figure 4(c), subpopulation R) and others with low levels of 8-oxodG (Figure 4(c)), cells outside of R). In control cells, the R fraction comprises $3 \pm 2\%$ of the total population. The R fraction and its level of intensity increase 8–10-fold 20–30 min after irradiation or treatment with cfDNAox and cfDNAoxR fragments (Figure 4(d) (1)) and after 2 h the intensity returns to control (Figure 4(d) (1)).

The total amount of 8-oxodG fluorescence 20–30 min after irradiation or treatment with cfDNAox and cfDNAoxR fragments increases 7-8-fold (Figure 4(d) (2)) and after 2 h decreases but remains 1.5–2-fold higher than the control (Figure 4(d) (2)). Unoxidized gDNA and cfDNA fragments at 50 ng/ml did not induce oxidative modification of nuclear DNA during 2 h of incubation. Thus, LDIR stimulates ROS production by activation of NOX4 and leads to oxidative modification of nuclear DNA.

Oxidative modification of nuclear DNA can lead to DNA breaks in cell nuclei.

3.4.4. Oxidized cfDNA Fragments, like LDIR, Cause DNA Damage and Breaks in Nuclear DNA. Since oxidation of DNA can cause single- and double-strand breaks [31], we assessed DNA damage by comet assays and flow cytometry for γH2AX labeling. The comet assay allows detection of both single- and double-strand breaks and is widely used to determine the extent of DNA damage [34].

Comet assays were performed 5 min and 3 h after exposure to LDIR (10 cGy) or to cfDNAox and cfDNAoxR fragments. Four types of cells were present in control populations: (1) cells without DNA breaks, (2) cells with few DNA breaks, (3) cells with fragmented DNA, and (4)

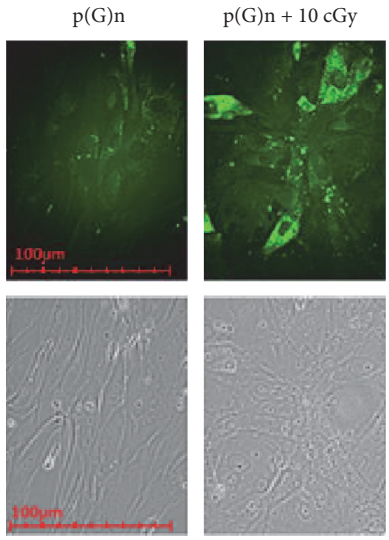

(a)

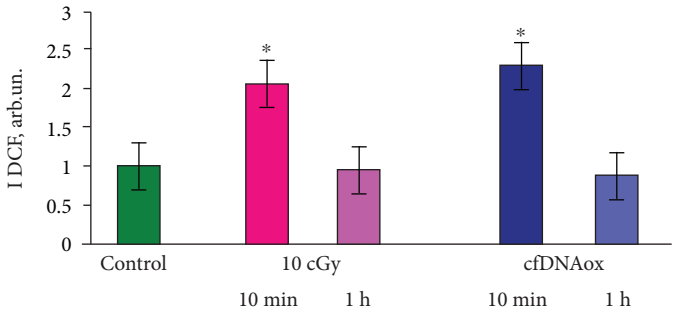

(b)

(1)

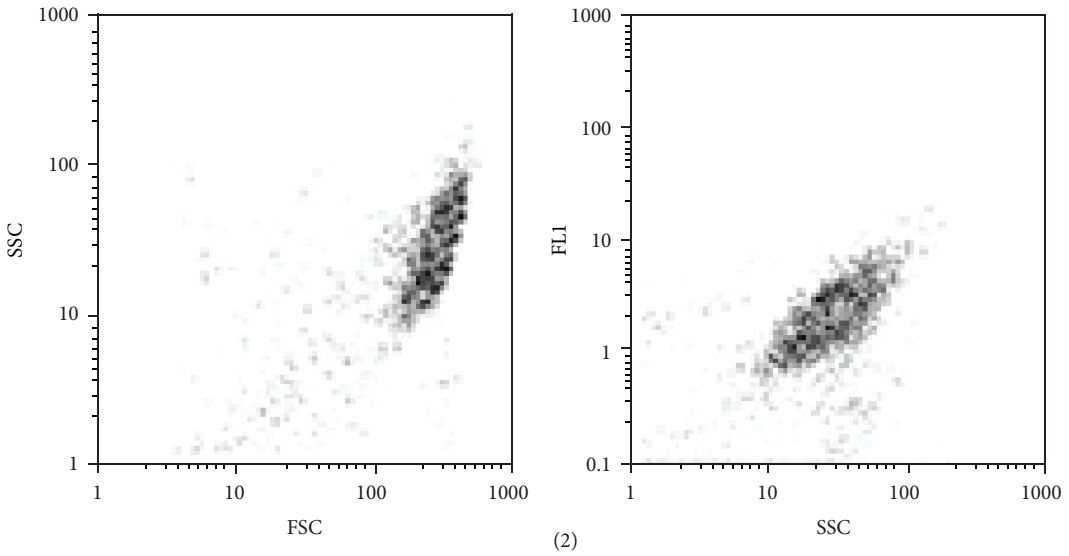

(2)

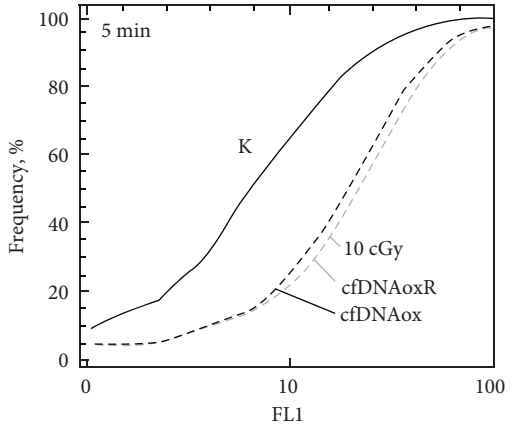

(c)

Figure 2: Continued.

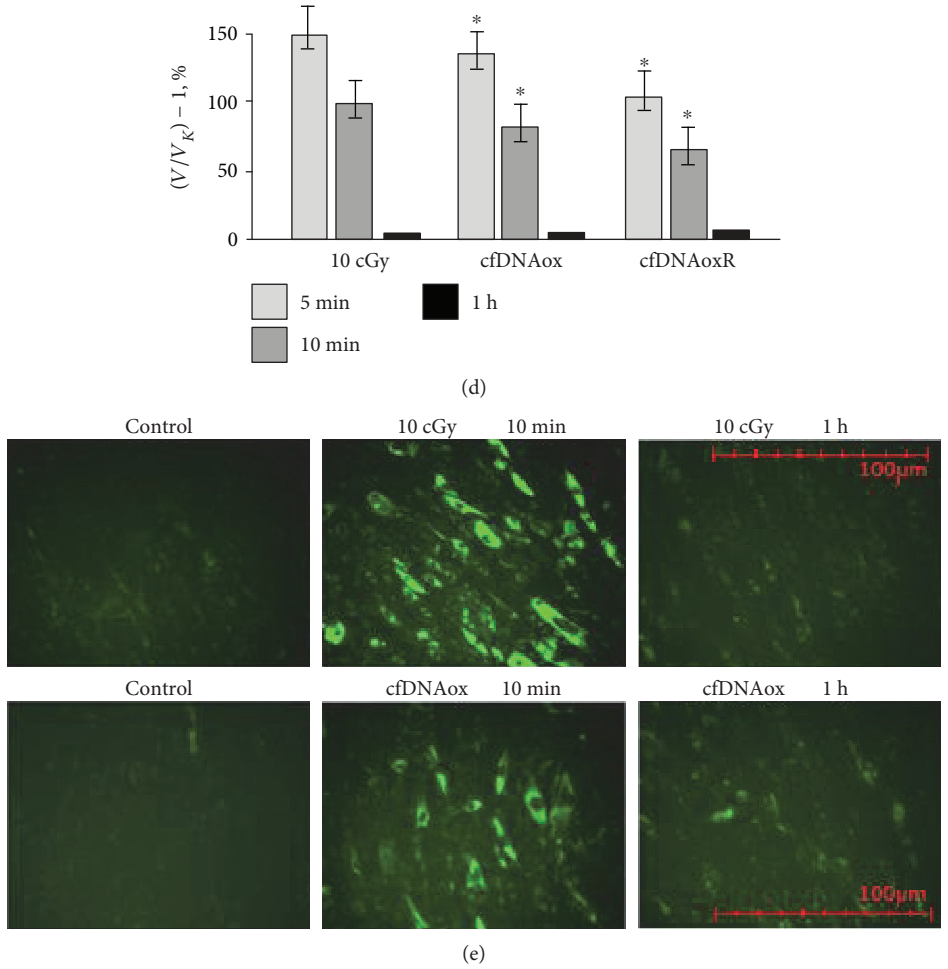

Figure 2: (a) A plasmid containing a marker GFP-gene and containing (G)n repeats that are easy to oxidate penetrates into cells treated with 10 cGy of IR (fluorescent microscopy, 40x). (b–e) Both low-dose radiation (10 cGy) and cfDNAox fragments induce a short-term increase in ROS production. (a, b) Change of DCF fluorescence in the presence of 10 μM of H2DCFH-DA. (c) (1) SSC versus FSC and FL1-DCF versus SSC plots; (2) cumulative histogram of DCF intensity distribution measured by FACS; $^*p < 0.001$, nonparametric U test. (d) Ratio of I(DCF) change rate in treated samples (v) to the control samples (vk) (flow cytometry). The light-grey, dark-grey, and black bars correspond to 5, 10, and 60 min time points, respectively. Data points were averaged and represented as mean ± SD for three biological replicates. $^*p < 0.01$, nonparametric Mann–Whitney U test. (e) Increase in ROS level measured by fluorescence microscopy 10 min after 10 cGy irradiation or addition of cfDNAox fragments (50 ng/ml); 60 min after exposure ROS returns to control level.

apoptotic cells with very damaged DNA (Figure 5(a)). Exposure to 10 cGy of radiation, as well as to cfDNAox and cfDNAoxR, stimulated DNA breaks; after 5–20 min of exposure, most cells were of 3 types (Figures 5(b), 5(c), and 5(d)). After 3 h, the amount of cells with damaged DNA was significantly reduced in both cases (Figures 5(b), 5(c), and 5(d)).

DSBs were revealed by immunostaining with antibodies against the histone γH2AX phosphorylated on Ser-139 that rapidly accumulates at DNA loci flanking DSB sites [35]. Cells were fixed and stained with FITC-labeled antibodies for γH2AX and FACS was used for quantitative assessment of the phospho-γH2AX level (Figure 6(a)). Two subpopulations of cells were present, one with a high level of fluorescence (R) and the main fraction with low fluorescence (Figure 6(a)). Control cells from the R subpopulation comprise 3 ± 2% of the total cell count. The amount of cells in R and their intensity of fluorescence increases 7-8-fold 15–30 min after LDIR or treatment with cfDNAox and cfDNAoxR fragments (Figure 6(b)). Two h after 10 cGy of radiation, the level of gamma-H2AX fluorescence of R decreased 2-fold, and after treatment with cfDNAox and cfDNAoxR fragments, it decreased to control levels (Figure 6(b) (1)). The total amount of γH2AX after LDIR or treatment with cfDNAox and cfDNAoxR fragments increases 3.4–3.8-fold, and after 2 h, it returns to control (Figure 6(b) (2)).

FACS allows assessing the average amount of H2AX histone in cells, but these numbers do not always reflect the real degree of DNA damage [36]. To find the reason for the quantitative changes in the level of γH2AX in cells after LDIR or after treating them with cfDNAox and cfDNAoxR, we analyzed fixed cells stained with antibodies for γH2AX by fluorescence microscopy (Figures 6(c) and 6(d)). Exposure to

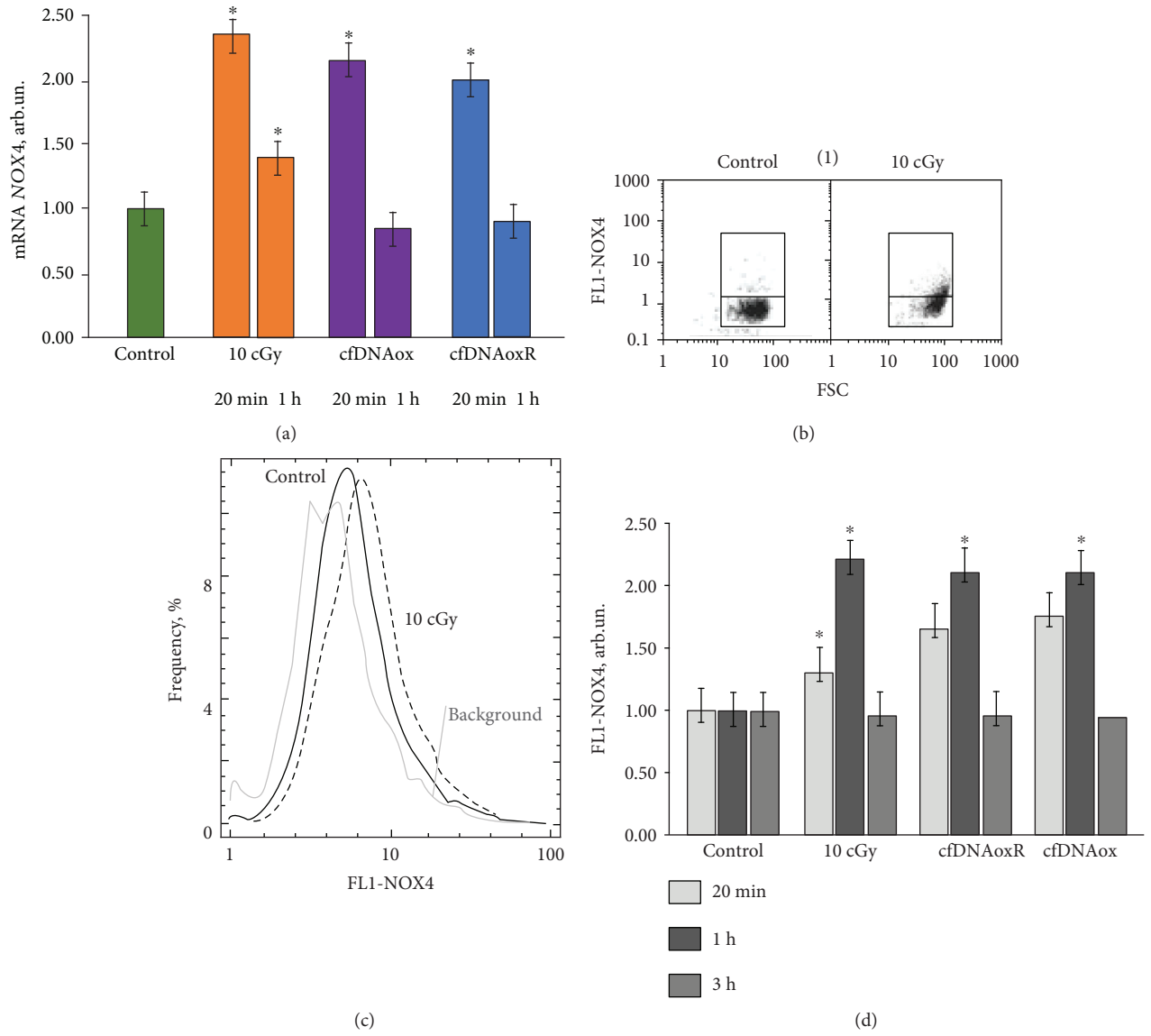

Figure 3: Both low-dose radiation (10 cGy) and cfDNAox and cfDNAoxR (50 ng/ml) fragments induce an increase in *NOX4* expression. (a) Changes in the levels of mRNAs encoding NOX4. NOX4 mRNA in treated cells compared to control (three biological replicates). Reference gene was *TBP*. $^*p < 0.001$, nonparametric *U* test (qRT-PCR). (b) FL1-NOX4 versus SSC plots. Gate R encircles the fraction of MSCs with elevated values of FL1-NOX4 (flow cytometry). (c) Distribution of cells treated with 10 cGy radiation according to the FL1-NOX4 signal strength (flow cytometry). (d) NOX4 level after irradiation with 10 cGy and treatment with 50 ng/ml of cfDNAox and cfDNAoxR and the dynamic change of average fluorescence intensity of NOX4. $^*p < 0.001$, nonparametric *U* test (flow cytometry).

LDIR or addition of cfDNAox and cfDNAoxR fragments to the medium elevates the level of cells with multiple DNA breaks 3–5-fold within 20 min (Figures 6(c) and 6(d)), but after 2 h, this level decreases and only cells containing very few breaks are present (Figure 6(d)). Unoxidized gDNA and cfDNA fragments do not induce DNA breaks during the first 2 h of incubation.

Thus, the damage to the cell nuclei that is induced by LDIR can be mediated by oxidized DNA fragments. cfDNAox penetrates into cells increasing ROS production and leading to oxidative stress and multiple DNA breaks the amount of which decreases 2 h after irradiation or start of incubation with oxidized cfDNA. We researched if the DNA breaks are repaired or that cells with multiple DNA breaks undergo cell death within these 2 h.

3.4.5. Oxidized cfDNA Fragments, like LDIR, Activate Repair of Nuclear DNA. DNA damage induced by IR activates signaling cascades that control DNA repair [37]. Double-strand breaks (DSB) are one of the most dangerous forms of DNA damage. BRCA1 is a nuclear protein that takes part in the regulation of the cell cycle and DSB repair by homologous recombination [38].

LDIR or treatment with cfDNAox and cfDNAoxR fragments leads to a 3.5–4.5-fold increment in the level of mRNA transcripts from the *BRCA1* and *BRCA2* genes after 30 min

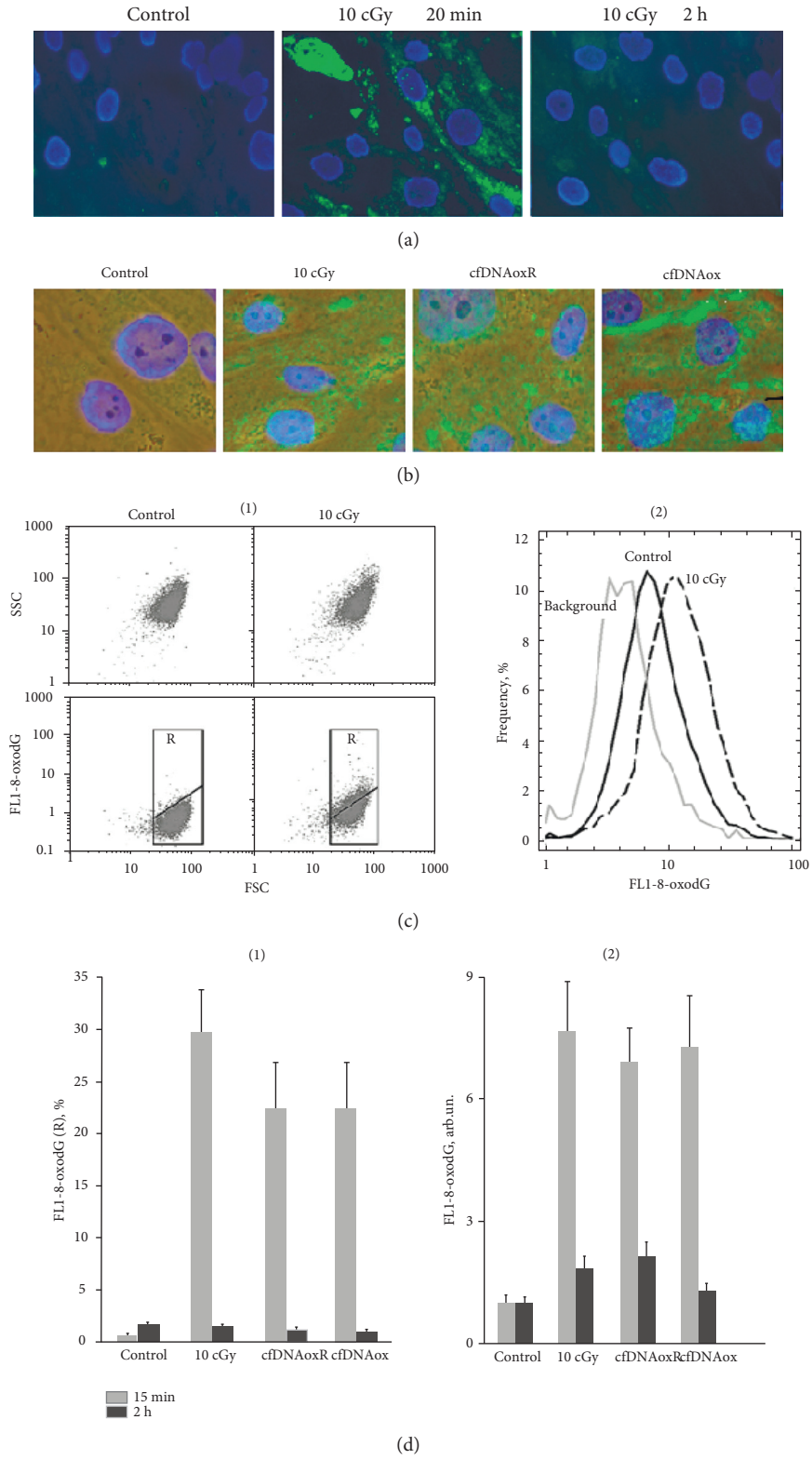

Figure 4: Low-dose radiation and cfDNAox and cfDNAoxR fragments cause oxidation in nuclear DNA. (a, b) Cells stained with antibodies to 8-oxodG (secondary FITC-conjugated antibodies) and DAPI (fluorescence microscopy, 40x (a), 100x (b)). (c, d) Flow cytometry detection of 8-oxodG: (c) (1) analysis of irradiated MSCs stained with antibodies to 8-oxodG FL1-8-oxodG versus SSC plots. Gate R encircles the fraction of MSCs with elevated values of 8-oxodG (secondary FITC-conjugated antibodies); (c) (2) distribution of the cells with varying 8-oxodG contents. (d) (1) Signal intensity of FL1-R; (d) (2) median signal intensity of FL1 (mean value for three independent experiments). $^{*}p < 0.01$ against control group of cells, nonparametric U test.

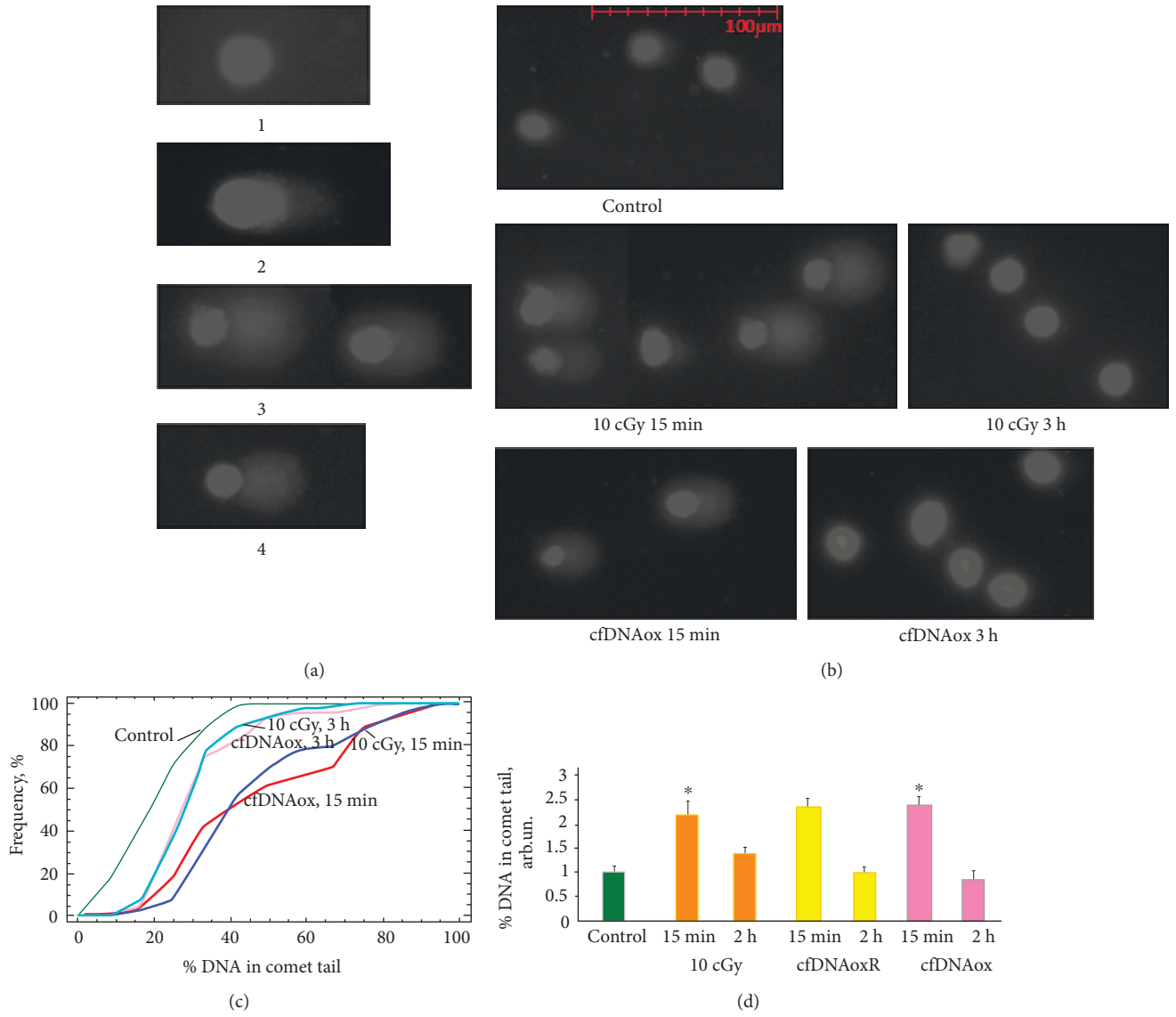

Figure 5: Low-dose radiation and cfDNAox and cfDNAoxR fragments (50 ng/ml) cause DNA breaks in nuclear DNA of exposed MSCs. (a) Different types of nuclei with varying degree of DNA damage (100×). (b) Nuclei of irradiated (10 cGy) and exposed to cfDNAox (50 ng/ml) MSCs, 5 min and 3 h after exposure; (c) cumulative histograms for tail moment of irradiated (10 cGy, 5 min and 3 h) and exposed to cfDNAox (50 ng/ml, 5 min and 3 h) MSCs; (d) percentage of DNA within tails. The significance of differences with the control in the obtained distributions was analyzed by means of the Kolmogorov-Smirnov statistics. ∗ means that $p < 0.05$.

(Figures 7(d) and 7(e)), and after 2 h, this level remains 2–2.5-fold higher than the control level (Figures 7(d) and 7(e)). These results were confirmed at the protein level. Figure 7(b) is a histogram of BRCA2 protein expression where R is an area of cells with high fluorescence (Figures 7(a) and 7(b)). Thirty min after irradiation or addition of cfDNAox and cfDNAoxR fragments to the medium, the level of BRCA2 in R is increased 4-5-fold (Figure 7(b)). The total BRCA2 level increased 30 min after irradiation with 10 cGy and 2.5–3.5-fold after the addition of cfDNAox and cfDNAoxR fragments (Figure 7(b)) and remained increased 2–2.5-fold 2 h after. Thus, there is a correlation between DSB formation and the level of BRCA2 that reflects the efficacy of DNA repair after irradiation (Figure 7(c)). LDIR or oxidized DNA fragments increase the amount of DSBs but, at the same time, activate DNA repair which leads to the minimization of the amount of breaks in the cell DNA. Unoxidized gDNA and cfDNA fragments at 50 ng/ml did not affect the level of BRCA2 2 h after the start of incubation.

Thus, DNA breaks activate DNA reparation system in the treated cells. As DNA reparation requires time, we were expecting to see a short-term arrest of the cell cycle after treating cells with LDIR or cfDNAox or cfDNAoxR fragments.

3.4.6. cfDNAox and cfDNAoxR Fragments, like LDIR, Cause a Short-Term Arrest of the Cell Cycle and Decrease Proliferation. Oxidative stress and DNA damage lead to the arrest of the cell cycle at all stages and block proliferation [39]. We analyzed the effect of low-dose radiation and cfDNAox and

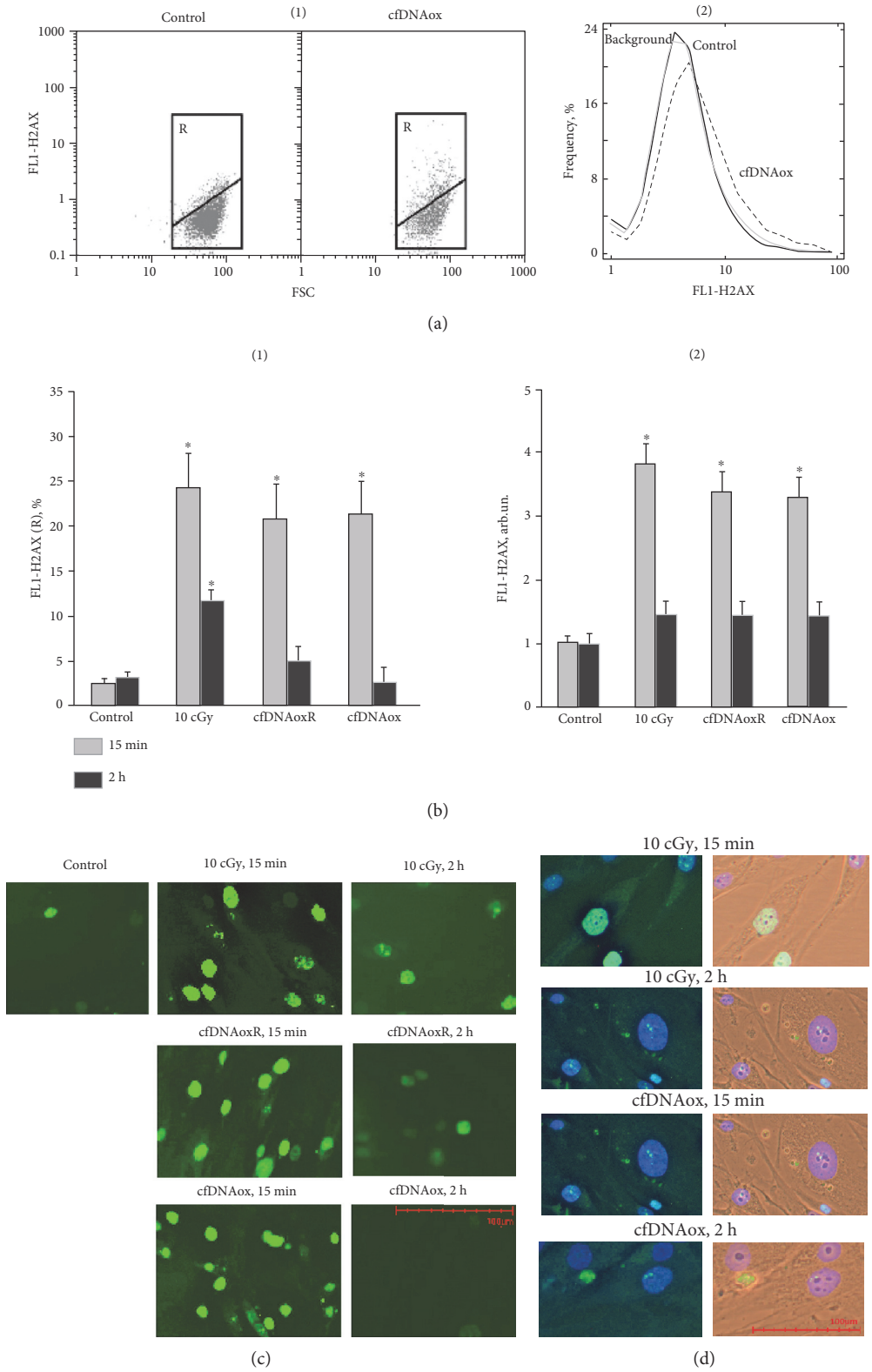

FIGURE 6: Low-dose radiation and cfDNAox and cfDNAoxR fragments cause DNA breaks and γH2AX foci in nuclear DNA. (a) (1) Flow cytometry detection of DSB in cells exposed to cfDNAox and cfDNAoxR fragments. Cells were processed for immunofluorescence staining with anti γH2AX antibody-DyLight488 (FL1). Gate R encircles the fraction of cells with elevated values of FL1-γH2AX. (2) Distribution of γH2AX fluorescence intensities with varying DSB levels. (b) Median signal intensity of FL1 (mean value for three independent experiments). (c, d) DSB in irradiated cells (10 cGy, 15 min and 2 h after exposure) and cells exposed to cfDNAox and cfDNAoxR (50 ng/ml, 15 min and 2 h, fluorescence microscopy). Cells stained with anti γH2AX antibodies (c) and DAPI (d), $^{*}p < 0.05$.

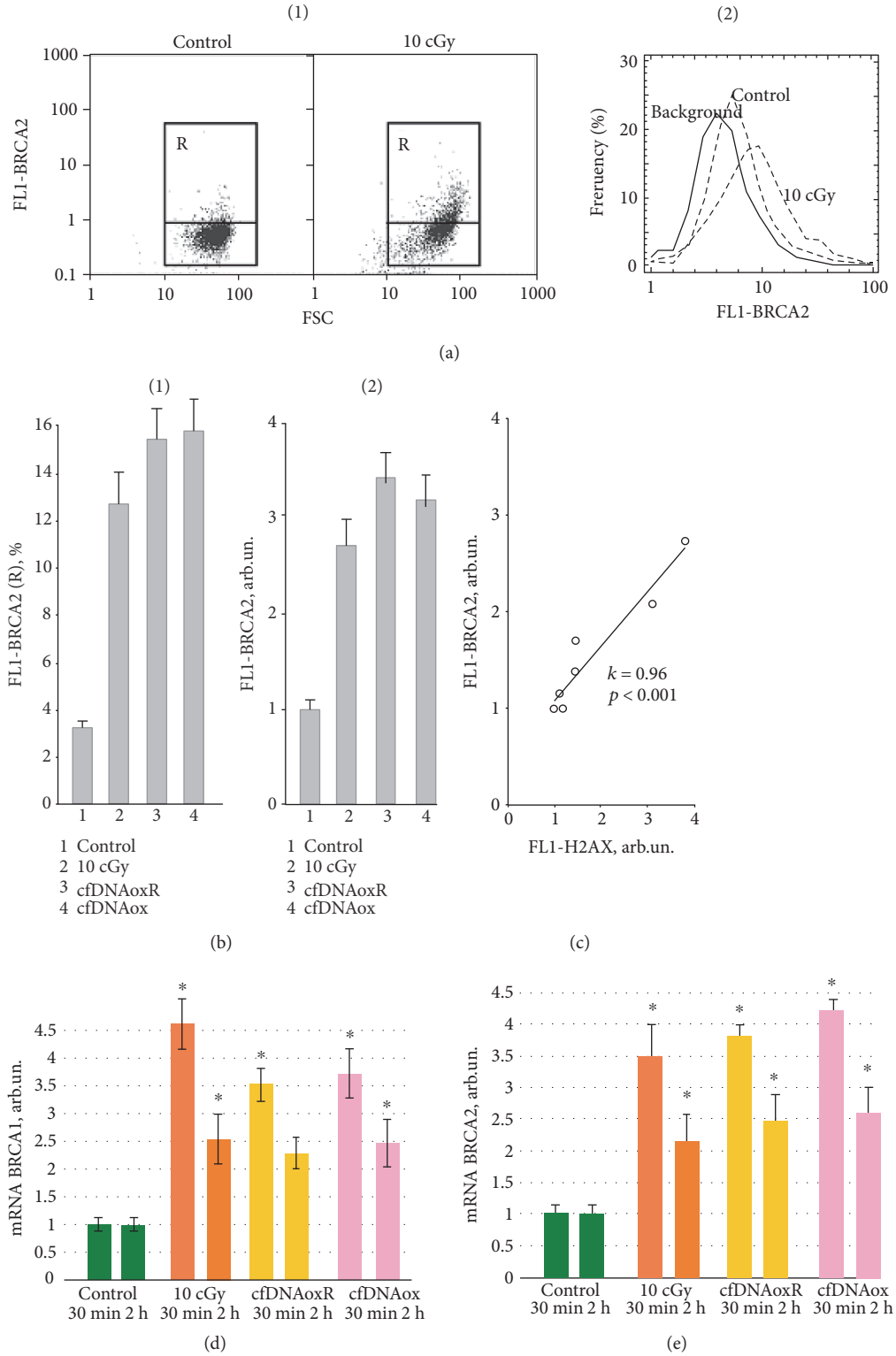

FIGURE 7: DNA damage induced by low-dose radiation and cfDNAox and cfDNAoxR fragments activates reparation of nuclear DNA. (a) (1) Flow cytometry detection of BRCA2 in irradiated (10 cGy) and control cells stained with anti-BRCA2 antibodies and secondary FITC-conjugated antibodies. Gate R encircles the fraction of MSCs with elevated values of FL1- BRCA2; (2) distribution of cells with varying BRCA2 contents. (b) The signal intensity of FL1-R (1) and average signal intensity of FL1-BRCA2 (2) in irradiated cells (10 cGy, 15 min and 2 h after exposure) and cells exposed to cfDNAox and cfDNAoxR (50 ng/ml, 15 min and 2 h) (flow cytometry). (c) Linear correlation between the levels of γH2AX and BRCA2 ($k = 0.96$; $p < 0.0001$). (d, e) Dependence of the changes in the levels of mRNA BRCA1 (d) and BRCA2 (e) in irradiated cells and cells exposed to cfDNAox and cfDNAoxR (RT-PCR); mRNA level—average expression of genes in treated cells compared to control (for three biological replicates). Reference gene, *TBP*. $^{*}p < 0.001$, nonparametric *U* test (qRT-PCR).

cfDNAoxR fragments on the level of proliferation using antibodies to the proliferation markers Ki-67 and PCNA [40] and flow cytometry. All types of cells express Ki-67 and PCNA during all stages of the cell cycle [40]. Cells were stained with propidium iodide in order to assess the total amount of DNA. LDIR or cfDNAox fragments decrease the level of Ki-67 protein; 30 min after treatment, Ki-67 is 40–50% lower than that in the control, and 2 h after, it starts increasing and almost reaches control level (Figure 8(b)).

PCNA is a transcription factor for polymerase Δ that is a part of the DNA repair system. We observed a 40–60% increase of the level of PCNA 30 min after irradiation or treatment of cells with oxidized cfDNA (Figure 8(c)), indicating that repair processes are active and proliferation is decreased. As a decrease of proliferation usually occurs when the cell cycle is arrested [40], we assessed the stage at which the cycle stops after irradiation and treatment with oxidized DNA.

Ten cGy of radiation or addition of cfDNAox and cfDNAoxR fragments to the medium increases the number of cells in G1 and G0/G1 30 min after exposure, and thus, these factors arrest the cell cycle in G1 (Figure 8(a) (2)). Three h after irradiation or start of incubation with oxidized DNA, the cell cycle returns to normal.

Exposure to LDIR or addition of cfDNAox and cfDNAoxR fragments causes a 1.5–2-fold decrease in the level of expression of CCND1 and a 1.5–2-fold increase in expression of *CDKN2* and *CDKN1A* 30 min after the exposure, indicating that the cell-cycle undergoes a short-term arrest. However, 3 h after the exposure, the level of expression of *CCND1* increases 20–25% compared to control and *CDKN2* and *CDKN1A* decrease to control level. Thus, the cell cycle is shortly arrested at the G1-phase and the cells have time for repair of the damage and then they can progress further through the cycle.

Thus, DNA damage leads to a short-term arrest of the cell cycle and activation of DNA reparation. As a result, the level of proliferation, as well as the amount of cells in the population, increases in 2-3 h after treatment. The increased amounts of cells in the population can be a result of low level of apoptosis.

3.4.7. LDIR Causes a Strong Antiapoptotic Response. The amount of apoptotic cells after irradiation or treatment with cfDNAox and cfDNAoxR fragments was assessed using a marker of apoptosis, annexin V, and FACS (Figure 1). After 15 min, cells exhibit signs of apoptosis, and the fraction of apoptotic cells increases ≈2-fold and the apoptosis level 30–40% (Figure 1(b)). Despite that, 2 h after irradiation, the level of apoptosis decreases compared to control (Figure 1(b)). These results were confirmed using an automated cell counter after propidium iodide and annexin V FITC staining; the amount of apoptotic cells increases 3-fold 10 min after irradiation, but decreases 3-fold compared to control 3 h after irradiation.

Bcl2 is a family of proteins that are crucial for cell survival and apoptosis regulation. It includes three groups of interacting and functionally different proteins [41]. Bcl-2 and its 4 relative proteins (BCL-XL, Bcl-W, A1, and Mcl-1) are antiapoptotic, whereas Bax, Bak, Box and Bik, Bad, Bim, Puma, Bid, Noxa, Hrk, Bmf are proapoptotic. Other important factors that decide the cell fate are apoptotic protein inhibitors like BIRC2 and BIRC3 that inhibit the activity of caspase-3, caspase-7, and caspase-9 [42].

Antiapoptotic processes are activated 20 min after irradiation or the addition of cfDNAox and cfDNAoxR fragments to the medium, and the levels of antiapoptotic genes *BCL2*, *BCL2A1 (Bfl-1/A1)*, *BCL2L1 (BCL-X)*, *BIRC2 (c-IAP1)*, and *BIRC3 (c-IAP2)* increase 1.5–2.5-fold (Table 3). The level of proapoptotic *BAX* is increased 20 min after irradiation or treatment with cfDNAox and cfDNAoxR fragments, in agreement with the increased apoptosis level 15 min after exposure. *Bcl2* family genes have increased expression 2–72 h after irradiation or treatment with cfDNAox and cfDNAoxR fragments. Unoxidized gDNA and cfDNA fragments at 50 ng/ml increased the expression level of the antiapoptotic genes *BCL2*, *BCL2A1 (Bfl-1/A1)*, *BCL2L1 (BCL-X)*, *BIRC2 (c-IAP1)*, and *BIRC3 (c-IAP2)* only 20–30% 3 h after the start of incubation. As these fragments caused an extended ROS production and the activation of antiapoptotic genes after only 3 h, the effect is most likely connected to these fragments being gradually oxidized. Flow cytometry and fluorescence microscopy show that Bcl2 protein expression is increased 30 min after irradiation or addition of cfDNAox and cfDNAoxR fragments, and it remains increased 2–72 h after exposure (Figure 1(b)). Thus, the antiapoptotic response to LDIR or addition of oxidized DNA fragments is strong.

3.4.8. cfDNAox Fragments, like LDIR, Activate the Antioxidant Response. Oxidative stress caused by an increase of ROS production can activate an antioxidant response in which one of the main regulators is transcription factor NRF2 [43]. One h after LDIR, the level of *NRF2* gene expression increases 5.5-fold. CfDNAox and cfDNAoxR fragments increase the expression of the *NRF2* gene 3-4-fold 1 h after the addition to the medium (Figure 9(a)). Two h after irradiation or cfDNAox and cfDNAoxR fragments, *NRF2* expression is 7-8-fold increased compared to control, and after 3 h, it goes down but still remains 3–5-fold higher than in control cells (Figure 9(a)). The level of protein NRF2 is increased 2-fold after irradiation or addition of cfDNAox and cfDNAoxR fragments (Figure 9(b)), but 24 h after the initial exposure, it returns to control levels (Figure 9(b)).

The key event of antioxidant response development is the translocation of NRF2 to the nucleus. To analyze the effect of oxidized DNA fragments on the location of NRF2, antibodies against NRF2 and fluorescence microscopy were used (Figure 9(c)). When cells are irradiated or treated with cfDNAox and cfDNAoxR fragments, NRF2 expression increases both in the cytoplasm and in the nucleus 1 h after the exposure (Figure 9(c)). Three h after irradiation, NRF2 expression decreases yet the factor remains in the nucleus and can activate antioxidant genes (Figure 9(c)). Unoxidized gDNA and cfDNA fragments (50 ng/ml) did not affect NRF2 expression within 2 h after the start of incubation. Thus, both LDIR and cfDNAox induce a strong antioxidant response.

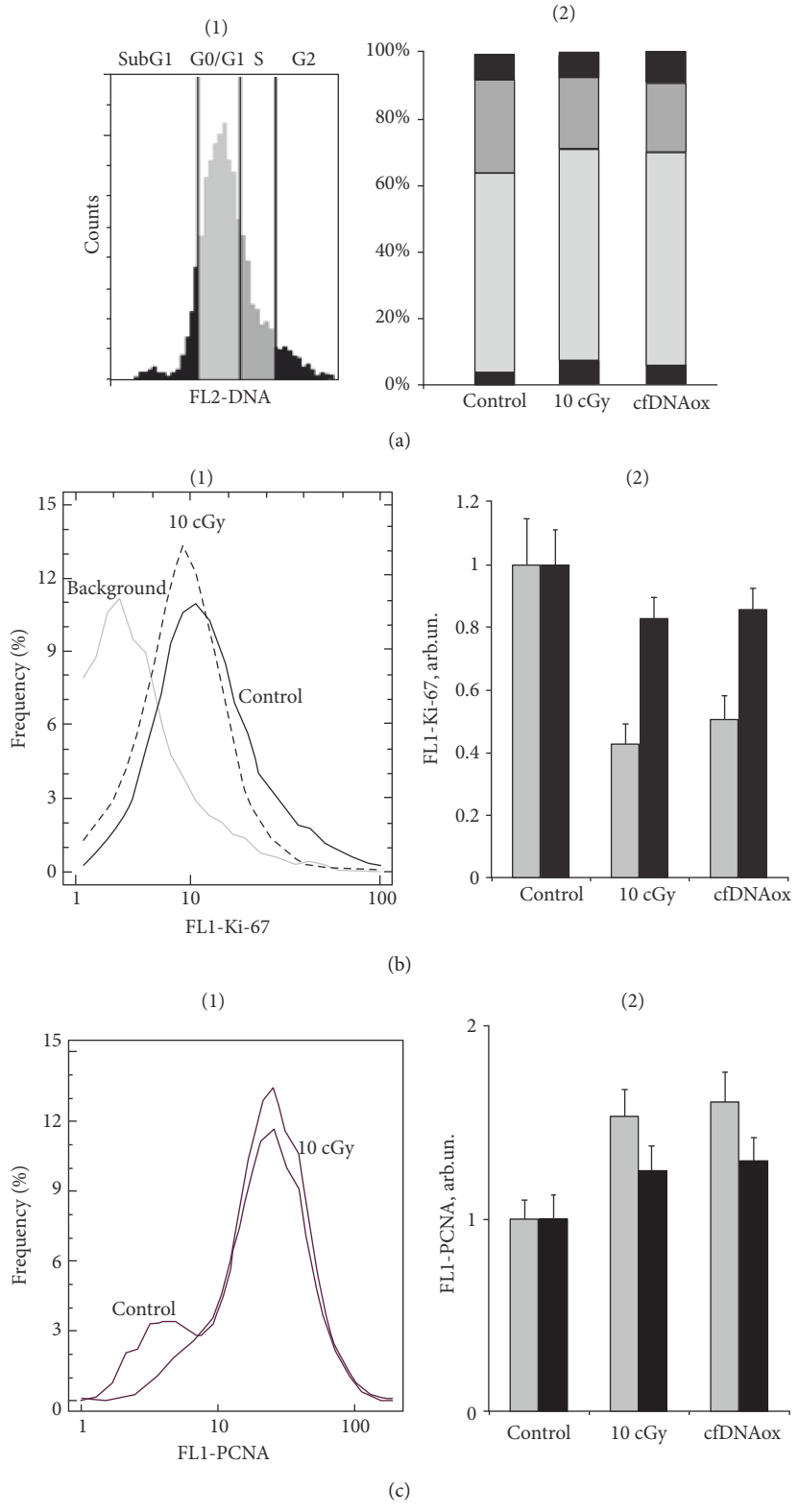

Figure 8: Low-dose radiation and cfDNAox fragments cause a short-term arrest of cell cycle and decreases proliferation. (a) (1) Proportions of cells that contain the amount of DNA characteristic for G1, S, and G2/M phases of the cell-cycle (flow cytometry). (a) (2) Proportions for control cells,10 cGy irradiated cells, and cells treated with oxidized DNA. (b) Dynamics of the change of fraction of proliferating cells (Ki-67+ fraction) in the population (flow cytometry): (1) distribution of cells with varying Ki-67 content; (2) average signal intensity of FL1-Ki-67+ in irradiated cells (10 cGy, 15 min and 2 h after exposure) and cells exposed to cfDNAox (50 ng/ml, 30 min and 2 h). *Significantly differs from control ($p < 0.05$). (c) Change of PCNA level in control and exposed cells (flow cytometry): (1) distribution of cells with varying Ki-67 contents; (2) average PCNA fluorescence. *Significantly different from control ($p < 0.05$).

Table 3: Dependence of the changes in the levels of antiapoptotic genes *BCL2*, *BCL2A1 (Bfl-1/A1)*, *BCL2L1 (BCL-X)*, *BIRC2 (c-IAP1)*, and *BIRC3 (c-IAP2)* and proapoptotic *BAX* expression in irradiated and exposed to cfDNAox, cfDNAoxR, and gDNA in MSCs on the time after exposure (RT-PCR). mRNA level—average expression of genes in treated MSCs compared to control (for three biological replicates). Reference gene—*TBP*. $^*p < 0.001$, nonparametric *U* test (qRT-PCR).

Gene		Changes in the expression levels, arb.un.			
Treatment	Time	10 cGy	cfDNAox	cfDNAoxR	gDNA
BCL2	30 min	2.6 ± 0.3*	2.3 ± 0.2*	2.4 ± 0.2*	1.1 ± 0.2
	2 h	4.1 ± 0.4*	3.1 ± 0.2*	3.3 ± 0.3*	1.0 ± 0.2
	24 h	3.9 ± 0.3*	2.9 ± 0.2*	2.9 ± 0.3*	1.3 ± 0.3
	48 h	2.8 ± 0.3*	3.1 ± 0.3*	2.6 ± 0.2*	1.8 ± 0.3*
BCL2A1 (Bfl-1/A1)	30 min	1.6 ± 0.2*	2.4 ± 0.2*	2.5 ± 0.3*	1.0 ± 0.2
	2 h	2.1 ± 0.2*	2.2 ± 0.1*	2.4 ± 0.2*	1.1 ± 0.2
	24 h	2.1 ± 0.3*	2.8 ± 0.3*	2.3 ± 0.2*	1.3 ± 0.2
	48 h	1.8 ± 0.3*	1.6 ± 0.2*	2.2 ± 0.2*	1.7 ± 0.3*
BCL2L1 (BCL-X)	30 min	1.4 ± 0.2	1.6 ± 0.1*	1.6 ± 0.1*	1.1 ± 0.2
	2 h	1.9 ± 0.3*	1.5 ± 0.2*	1.7 ± 0.2*	1.2 ± 0.3
	24 h	2.3 ± 0.2*	2.7 ± 0.3*	2.4 ± 0.2*	1.1 ± 0.3
	48 h	2.8 ± 0.3*	2.4 ± 0.3*	1.9 ± 0.2*	1.6 ± 0.2
BIRC2 (c-IAP1)	30 min	2.4 ± 0.2*	1.4 ± 0.2	1.8 ± 0.2*	1.0 ± 0.3
	2 h	2.6 ± 0.2*	2.1 ± 0.2*	2.3 ± 0.3*	1.0 ± 0.2
	24 h	2.6 ± 0.3*	2.7 ± 0.3*	2.6 ± 0.2*	1.6 ± 0.3*
	48 h	2.4 ± 0.2*	2.4 ± 0.3*	2.5 ± 0.2*	2.5 ± 0.3*
BIRC3 (c-IAP2)	30 min	2.2 ± 0.1*	1.2 ± 0.2	1.2 ± 0.2	1.0 ± 0.2
	2 h	2.5 ± 0.2	1.9 ± 0.2*	1.8 ± 0.2*	1.2 ± 0.3
	24 h	2.5 ± 0.2	2.6 ± 0.3*	2.5 ± 0.3*	1.6 ± 0.3
	48 h	2.0 ± 0.3	2.5 ± 0.4*	2.5 ± 0.4*	2.0 ± 0.4*
BAX	30 min	1.6 ± 0.2*	1.5 ± 0.2*	1.4 ± 0.2	1.0 ± 0.2
	2 h	0.8 ± 0.2	0.8 ± 0.2	0.9 ± 0.2	1.1 ± 0.3
	24 h	0.8 ± 0.2	0.9 ± 0.2	1.1 ± 0.2	0.9 ± 0.2

3.5. Oxidized cfDNA Fragments, as well as LDIR, Cause an Adaptive Response. We assessed the effect of oxidized cfDNA and LDIR on the survival of human adipose-derived mesenchymal stem cells (haMSCs) that were subsequently exposed to irradiation at 2 Gy. haMSCs were grown for 3 h in presence of cfDNAox and cfDNAoxR and then irradiated with 2 Gy. In a different experiment, we first irradiated cells with 10 cGy, cultivated them for 3 h, and then irradiated again with a dose of 2 Gy and grew them in fresh media for 48 h more. MTT tests demonstrated a statistically significant decrease in the cell death induced by 2 Gy of irradiation in cells that were pretreated with oxidized cfDNA or preirradiated with 10 cGy ($p < 0.01$; Mann–Whitney test, Figure 10(a)). Moreover, both preconditioning with cfDNAox at 50 ng/ml and preirradiation with 10 cGy 3 h before irradiation with a dose of 2 Gy decrease the proportion of cells containing gamma-H2AX foci (Figure 10(b)).

4. Discussion

The predominant hypothesis concerning the origin of cfDNA is that its main source is dead cells [44], but another hypothesis suggests that cfDNA could be actively excreted by living cells [45]. The main reasons for enrichment of the cfDNA pool with oxidized DNA fragments are the death of cells with a high level of DNA oxidation and the GC enrichment of cfDNA compared to total nuclear DNA [13]. The proportion of mitochondrial DNA in cfDNA increases under conditions of oxidative stress [46–48], and this process is relevant as mitochondrial DNA, on average, contains larger amounts of 8-oxodG compared to genomic DNA and thus contributes to the pool of oxidized cfDNA [49].

Increased levels of 8-oxodG in cfDNA can be a sign of oxidative stress, in our case, as a consequence of LDIR. It should be noted that GC-rich fragments within genomic DNA tend to accumulate oxidative damage as well. We have previously demonstrated that chronic exposure to gamma-neutron or tritium β-radiation evokes an increase in the content of GC-rich sequences (69% GC) in the transcribed region of human ribosomal repeat (rDNA) in cfDNA from 166 individuals [50]. The reason for this phenomenon is the increased stability of GC repeats to hydrolysis [51]. The transcribed area of rDNA is one of the examples of preferentially oxidized DNA [52]. Thus, in addition to enrichment of cfDNA pools with oxidized DNA of dying cells, the content of 8-oxodG in cfDNA may depend on the somewhat slowed-down degradation in human serum of GC-rich fragments as compared to AT-rich fragments [53].

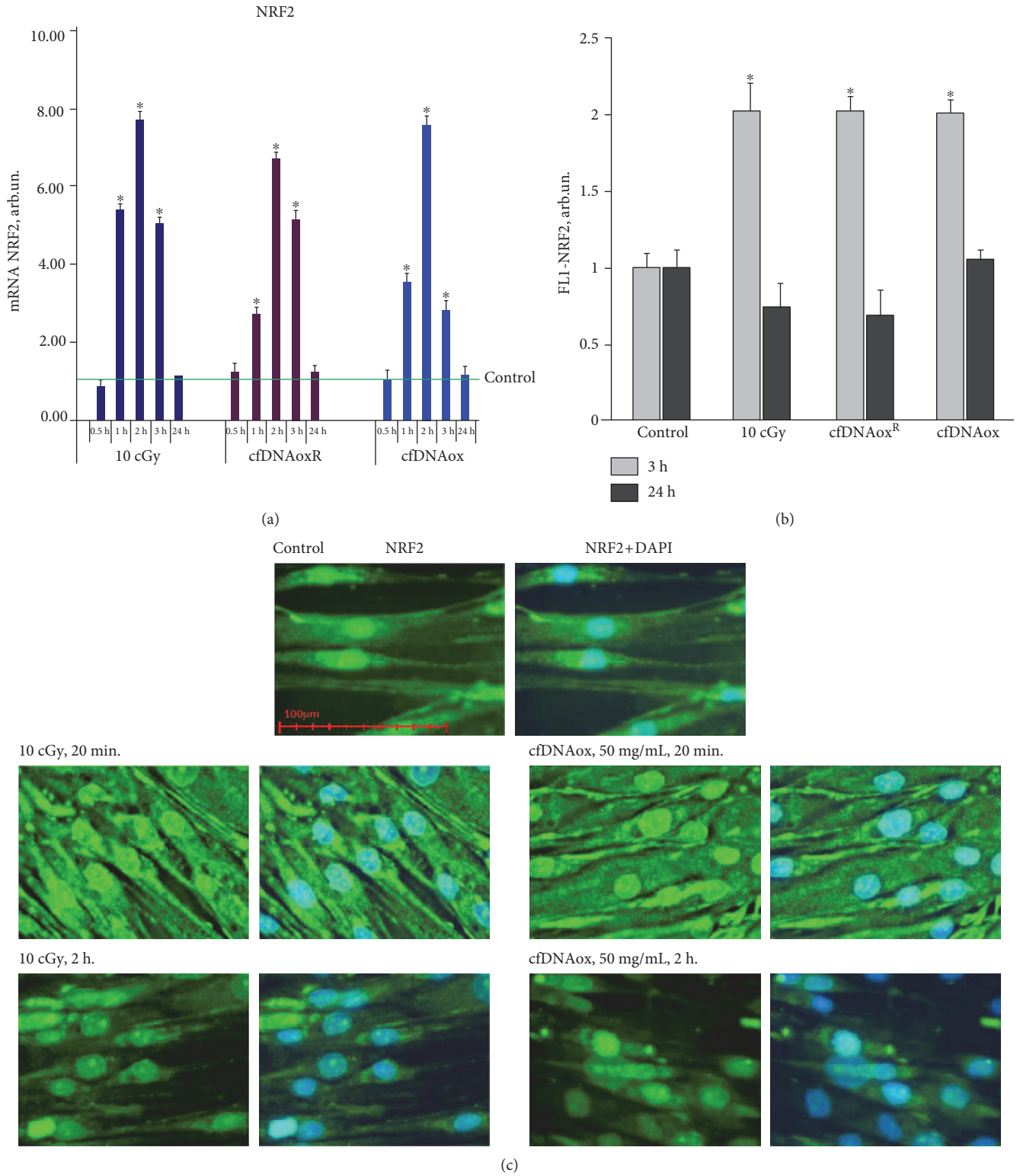

Figure 9: Low-dose radiation and cfDNAox and cfDNAoxR fragments activate antioxidant response. (a) Dependence of changes in the levels of NRF2 mRNA in irradiated cells and cells exposed to cfDNAox and cfDNAoxR on the time after exposure (RT-PCR); mRNA levels—average expression of genes in treated cells compared to controls (three biological replicates). Reference gene, *TBP*. $^{*}p < 0.001$, nonparametric *U* test (qRT-PCR). (b) Average median signal intensities in cells stained with anti-NRF2-FITC antibodies after various exposures (3 h and 24 h after exposure, flow cytometry). (c) Fluorescence microscopy of irradiated cells and cells exposed to cfDNAox stained with anti-NRF2-FITC antibodies and DAPI.

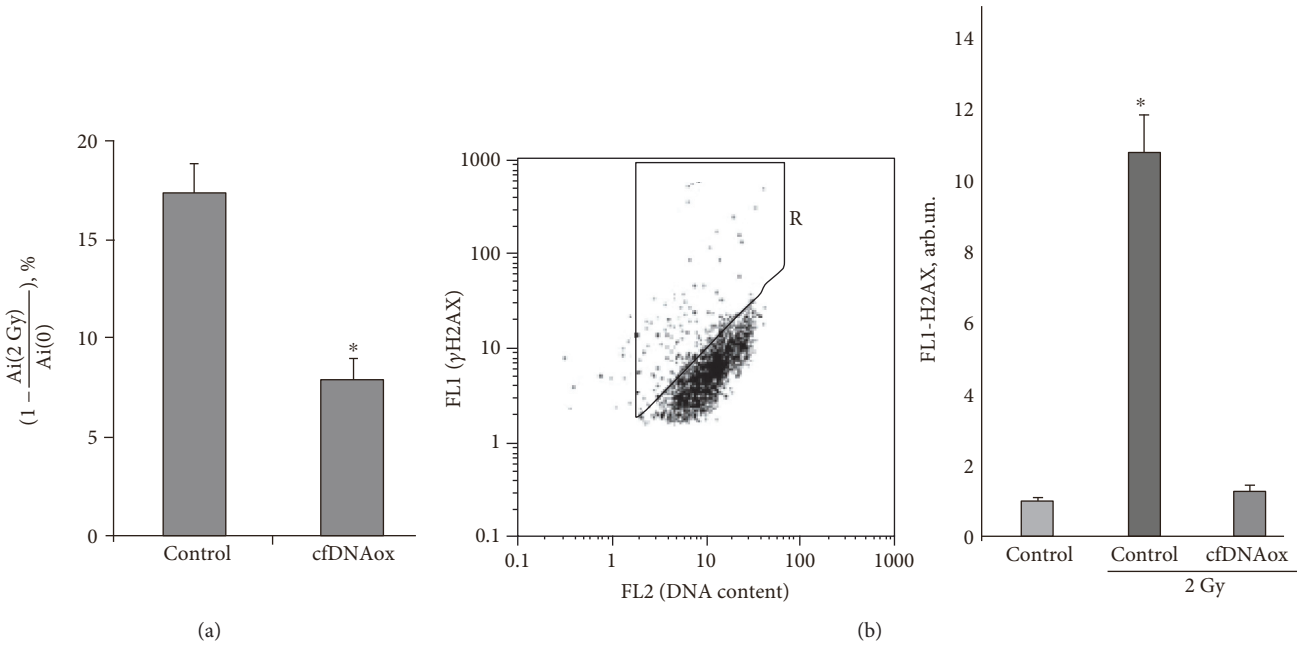

Figure 10: The effect of cfDNAox on the survival of cells and formation of γH2AX foci after exposure to radiation (2 Gy). haMSCs were grown for 3 h in presence of cfDNAox and then irradiated with 2 Gy and grown in fresh media for 48 h more before GG assay. Ai (0), Ai (2 Gy)—absorbance of MTT derivative as normalized to the number of assayed cells in control and irradiated cell populations after preconditioning. *The differences are significant at $p < 0.01$. (b) (1) Fluorescence-activated cell sorting (FACS) analysis was used to assess the accumulation of gH2AX foci in haMSCs. The plot of FL1 (gH2AX) versus FL2 (DNA content, PI) is shown as drawn for the control cells. The Gate R denotes the fraction of haMSCs, with type 2 nuclei and large number of gH2AX foci. (b) (2) Mean relative fluorescence of the main population of haMSCs (b) after subtraction of the background. Means for the three experiments and SD are shown. *The difference from the control is statistically significant ($p < 0.05$).

The cellular response to irradiation depends on a wide variety of factors, but the most important of these is a substantial increase in the level of ROS within a time frame of several seconds to 2–5 min [13]. ROS induces damage to cellular DNA, including the rupture of deoxyribose rings, the appearance of apurinic and apyrimidinic sites, single- and double-strand breaks, DNA protein crosslinks, and formation of oxidized bases [13].

Ionizing low-LET irradiation increases the rate of apoptosis in various cell types within min after irradiation. Dying cells release fragments of chromatin, contributing to the pool of cfDNA and increasing its concentration in the medium. cfDNA from irradiated cells contains significantly larger amounts of the oxidation marker 8-oxodG than cfDNA of control (nonirradiated) cells or cellular DNA of irradiated cells [54]. Here, cfDNA collected from the medium of LDIR (10 cGy)-irradiated cells and DNA oxidized in vitro affects control nonirradiated cells in the same way, indicating that cfDNA released from dying irradiated cells can serve as a stress signal and be a factor in stress signaling of radiation-induced bystander effects and of radioadaptive responses. It is of importance that the cfDNA of nonirradiated cells and unoxidized genomic DNA are not stress signals, as neither of them induces ROS synthesis in control cells.

A variety of studies concern RIBE and RAR based on various parameters of target and bystander cells [10, 54], and we have previously studied the bystander effect in diverse cell types [12, 20, 54]. One marker for irradiation-induced chromatin rearrangement is the position of pericentromeric loci of chromosome 1 (1q12) [20]. Exposure to cfDNA extracted from the culture media of irradiated MSCs leads to similar structural rearrangements of chromatin [55]. All these effects were primarily dependent on an increase in the production of ROS in cells because when a scavenger of ROS, α-tocopherol, was added to the medium, they were blocked [56]. We have shown that the addition of cfDNA from the medium of irradiated cells to the medium of endotheliocytes leads to a decrease in the number of cells with DNA breaks [57], an effect similar to that observed when cells were irradiated in low doses. The incubation medium of irradiated cells induces the initial stages of the apoptotic cascade in bystander cells that is accompanied by an increase in the content of ROS within a 6 h time frame [58]. These examples indicate that the patterns of the effects caused by LDIR can be transmitted via the culture medium (or via the extracellular space in the organism) and cfDNA is the most likely molecule to be the stress signal in RIBE. Further evidence for this hypothesis is the fact that cfDNA from the medium of control nonirradiated cells does not produce any of the effects described above, and no adaptive response is observed. Moreover, if the cfDNA from irradiated cells is treated with DNAse I, it loses its ability to cause an adaptive response [27, 28].

The goal of this work was to compare the action of model oxidized DNA fragments (cfDNAox) and cfDNA from the

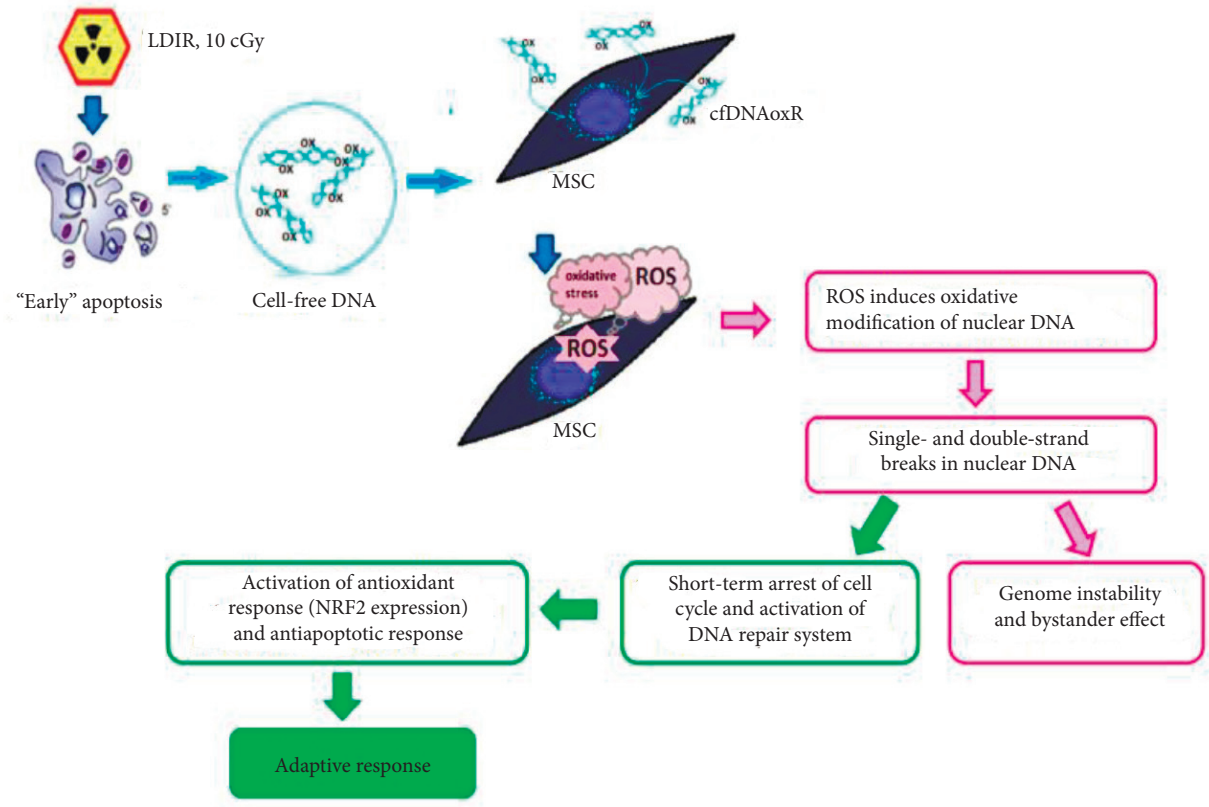

Figure 11: Proposed mechanisms for the development of radioadaptive responses and bystander effect. Irradiation induces primary oxidative stress and oxidation of genomic DNA → apoptosis of some irradiated cells → release of oxidized cfDNAoxR → reactive oxygen species (ROS) production → ROS induces oxidative modifications of nuclear DNA, rapidly repaired DNA breaks, short-term arrest of the cell cycle → activation of DNA reparation systems and antioxidant response → inhibition of apoptosis. Thus, we conclude that cfDNAox that appears after irradiation is a signaling molecule in the stress signaling that mediates radiation-induced bystander effects.

medium of irradiated cells (cfDNAoxR) with those of LDIR (10 cGy) on human adipose-derived MSCs, and we obtained hard evidence that their reaction to LDIR can be mediated by oxidized GC-rich cfDNA fragments. Firstly, the responses of cells to these fragments are identical to those to 10 cGy of radiation. Thus, cfDNA fragments are stress signaling molecules that regulate RAR to LDIR. We demonstrated that the radiation leads to the increase of oxidized cfDNA in the culture medium. We used a genetic construction containing an easy-to-oxidize (G)n repeat to show that the oxidized cfDNA can rapidly penetrate into the cytoplasm and induce a short-term increase in ROS production, a process implemented by the NOX4 oxidase. This, on the one hand, leads to a short-term oxidative modification of nuclear DNA, but, on the other hand, activates antioxidant systems. An increased level of ROS leads to DNA damage and DSBs, but, at the same time, activates DNA repair and minimizes damage. Moreover, 10 cGy of radiation evoke a strong antiapoptotic response.

Taken together, these data indicate that the cascade of events in cfDNAox signaling may be the following: irradiation → primary oxidative stress → oxidation of genomic DNA → apoptosis of some irradiated cells → release of oxidized cfDNAoxR → ROS production → ROS induces oxidative modifications of nuclear DNA, rapidly repaired DNA breaks, and short-term arrest of the cell cycle → activation of DNA repair systems and antioxidant response → inhibition of apoptosis → radioadaptive responses (RAR) (Figure 11). We believe that oxidized DNA is one of the components of damage-associated molecular pattern molecules. The supposed mechanism of penetration of our plasmids into cells includes the oxidation of dG (in dG repeats) on the cell surfaces. Oxidized DNA fragments penetrate into cells, as shown previously [59]. When the oxidation is moderate, the unchanged promotor allows the inserted GFP gene to be transcribed. In order to optimize the amount of plasmids in the cytoplasm, we conducted an experiment in conditions with a slightly elevated level of ROS on cell surfaces and in the medium by addition of H_2O_2. In these conditions, the fluorescence intensity of the cytoplasm was elevated more than without H_2O_2. Thus, the level of GFP fluorescence increases when the cells are under a moderate oxidative stress caused by either radiation or H_2O_2. This indicates that cfDNA needs to be oxidized in order to penetrate into the cells.

The secondary oxidative stress that is evoked in bystander cells occurs after interaction of cfDNAox with its receptors on the cell surface or inside, possibly transmembrane proteins of the toll-like receptor family, namely TLR9 [60], whose ligation may lead to the elevation of ROS

[60, 61]. Binding of CpG-DNA to TLR9 increases the ROS level in human monocytes, [62] and in neutrophils, it leads to the production of peroxynitrite [61]. In addition, oxidized DNA seems to be a stronger TLR9-stimulating ligand than nonoxidized DNA [18]. As we showed previously, GC-rich cfDNA fragments can activate TLR9 [63]. In this cascade, the formation of the "DNA-TLR9" complex initiates the cellular signaling pathway that leads to an activation of NF-κB [63], which in many different ways augments the biosynthesis of ROS. However, when the TLR9 pathway was blocked in irradiated lymphocytes, there were no substantial changes in the localization of 1q12 loci or in the level of ROS [64], indicating that in addition to oxidized DNA-stimulated TLR9 receptors, cells possess other sensors whose activation leads to the changes in ROS and that RIBE may be regulated through more than one molecular pathway. Evidence pointing at the existence of toll-like receptor-independent stress signal transfer pathways was demonstrated by other authors, including cytoplasmic DNA-dependent STING, AIM2, RIG-1, and DAI sensor pathways [65]. Apart from that, cells may possess a variety of molecules that sense the damage in cfDNA and may respond differentially to oxidized DNA bases. The reception of cfDNAox produced by irradiated cells warrants further investigations.

ROS level increases drastically during the first minutes after the addition of cfDNAox or cfDNAoxR to the medium, but decreases 30 min after the addition. We propose that activation of ROS production is connected to a changed expression of ROS-coding enzyme/enzymes such as the *NOX* family enzymes of NADPH oxidases [24]. One-2 h after treatment, cells have a moderately elevated level of ROS if the DNA is not oxidized. The reaction of MSCs to oxidized DNA is more rapid compared that of differentiated cells [55]. Oxidative stress is the key stage that initiates the cfDNAox signaling pathway which, on the one hand, triggers DNA oxidation and damage in the cells but on the other hand allows the development of the adaptive response (activation of DNA repair, activation of antioxidant transcription factor NRF2, and apoptosis inhibition) (Figure 11). Our evidence suggests that cfDNAoxR that appears after irradiation is responsible for the stress signaling that mediates radiation-induced bystander effects (RIBE) and moreover is an important component of the development of radioadaptive responses (RAR) to low doses of IR. Since they are a pool of reserve cells for critical situations and a tool for tissue regeneration with a relatively high proliferative potential [66], changes in cfDNA properties can be crucial for MSCs because DNA breaks can lead to chromosomal aberrations and insertions of DNA into the breakpoints.

Conflicts of Interest

The authors do not have any competing interests.

Acknowledgments

This work was supported by the Russian Foundation for Basic Research (Grant nos. 16-04-01099 A and 16-04-00576 A).

References

[1] M. Hauptmann, S. Haghdoost, M. Gomolka et al., "Differential response and priming dose effect on the proteome of human fibroblast and stem cells induced by exposure to low doses of ionizing radiation," *Radiation Research*, vol. 185, no. 3, pp. 299–312, 2016.

[2] M. Sokolov and R. Neumann, "Global gene expression alterations as a crucial constituent of human cell response to low doses of ionizing radiation exposure," *International Journal of Molecular Sciences*, vol. 17, no. 1, 2015.

[3] M. Tubiana, L. E. Feinendegen, C. Yang, and J. M. Kaminski, "The linear no-threshold relationship is inconsistent with radiation biologic and experimental data," *Radiology*, vol. 251, pp. 13–22, 2009.

[4] Z. Tao, Y. Zha, S. Akiba et al., "Cancer mortality in the high background radiation areas of Yangjiang, China during the period between 1979 and 1995," *Journal of Radiation Research*, vol. 41, pp. 31–41, 2000.

[5] G. Jaikrishan, K. R. Sudheer, V. J. Andrews et al., "Study of stillbirth and major congenital anomaly among newborns in the high-level natural radiation areas of Kerala, India," *Journal of Community Genetics*, vol. 4, pp. 21–31, 2013.

[6] M. S. Pearce, J. A. Salotti, M. P. Little et al., "Radiation exposure from CT scans in childhood and subsequent risk of leukaemia and brain tumours: a retrospective cohort study," *Lancet*, vol. 380, pp. 499–505, 2012.

[7] J. E. Cleaver, "Biology and genetics in the biological effects of ionizing radiation (BEIR VII) report," *Health Physics*, vol. 89, pp. S32–S32, 2005.

[8] M. Tubiana, A. Aurengo, D. Averbeck, and R. Masse, "Recent reports on the effect of low doses of ionizing radiation and its dose-effect relationship," *Radiation and Environmental Biophysics*, vol. 44, pp. 245–251, 2006.

[9] P. Kundrát and W. Friedland, "Non-linear response of cells to signals leads to revised characteristics of bystander effects inferred from their modelling," *International Journal of Radiation Biology*, vol. 88, no. 10, pp. 743–750, 2012.

[10] H. Matsumoto, A. Takahashi, and T. Ohnishi, "Radiation-induced adaptive responses and bystander effects," *Uchu Seibutsu Kagaku*, vol. 18, no. 4, pp. 247–254, 2004.

[11] C. Mothersill and C. Seymour, "Radiation-induced bystander effects and adaptive responses—the yin and yang of low dose radiobiology?," *Mutation Research*, vol. 568, no. 1, pp. 121–128, 2004.

[12] F. Ballarini, M. Biaggi, A. Ottolenghi, and O. Sapora, "Cellular communication and bystander effects: a critical review for modelling low-dose radiation action," *Mutation Research*, vol. 501, no. 1-2, pp. 1–12, 2002.

[13] A. V. Ermakov, M. S. Konkova, S. V. Kostyuk, V. L. Izevskaya, A. Baranova, and N. N. Veiko, "Oxidized extracellular DNA as a stress signal in human cells," *Oxidative Medicine and Cellular Longevity*, vol. 2013, Article ID 649747, 12 pages, 2013.

[14] C. Mothersill and C. B. Seymour, "Cell-cell contact during gamma irradiation is not required to induce a bystander effect in normal human keratinocytes: evidence for release during irradiation of a signal controlling survival into the medium," *Radiation Research*, vol. 149, no. 3, pp. 256–262, 1998.

[15] J. Rzeszowska-Wolny, W. M. Przybyszewski, and M. Widel, "Ionizing radiation-induced bystander effects, potential targets for modulation of radiotherapy," *European Journal of Pharmacology*, vol. 625, no. 1–3, pp. 156–164, 2009.

[16] K. M. Prise and J. M. OSullivan, "Radiation-induced bystander signaling in cancer therapy," *Nature Reviews Cancer*, vol. 9, no. 5, pp. 351–360, 2009.

[17] M. S. Kon'kova, A. V. Ermakov, L. V. Efremova, S. V. Kostyuk, and N. N. Veiko, "Influence of X-ray and/or CpG-DNA induced oxidative stress on adaptive response in human lymphocytes," *International Journal of Low Radiation*, vol. 7, no. 6, pp. 446–452, 2010.

[18] A. V. Ermakov, M. S. Kon'kova, S. V. Kostyuk et al., "Development of the adaptive response and bystander effect induced by low-dose ionizing radiation in human mesenchymal stem cells," *Proceedings of the 6th International Conference on Circulating Nucleic Acids in Plasma and Serum (CNAPS '11)*, pp. 225–231, Springer Netherlands, 2011.

[19] K. V. Glebova, I. L. Konorova, A. V. Marakhonov, I. V. Barskov, L. G. Khaspekov, and N. N. Veiko, "Oxidative modification of ecDNA alter its biological action on rat neurons," *Journal of Nucleic Acids Investigation*, vol. 2, no. 1, p. 28, 2011.

[20] S. V. Kostyuk, A. V. Ermakov, A. Y. Alekseeva et al., "Role of extracellular DNA oxidative modification in radiation induced bystander effects in human endotheliocytes," *Mutation Research*, vol. 729, no. 1-2, pp. 52–60, 2012.

[21] D. M. Spitkovskiĭ, N. N. Veĭko, A. V. Ermakov et al., "Structural and functional changing induced by exposure to adaptive doses of X-rays in the human lymphocytes both normal and defective by reparation of DNA double strands breaks," *Radiation Biology, Radioecology*, vol. 43, no. 2, pp. 136–143, 2003.

[22] T. Reya, S. J. Morrison, M. F. Clarke, and I. L. Weissman, "Stem cells, cancer, and cancer stem cells," *Nature*, vol. 414, no. 6859, pp. 105–111, 2011.

[23] S. Kostyuk, T. Smirnova, L. Kameneva et al., "GC-rich extracellular DNA induces oxidative stress, double-strand DNA breaks, and DNA damage response in human adipose-derived mesenchymal stem cells," *Oxidative Medicine and Cellular Longevity*, vol. 2015, Article ID 782123, 15 pages, 2015.

[24] P. Loseva, S. Kostyuk, E. Malinovskaya et al., "Extracellular DNA oxidation stimulates activation of NRF2 and reduces the production of ROS in human mesenchymal stem cells," *Expert Opinion on Biological Therapy*, vol. 12, Supplement 1, pp. 85–97, 2012.

[25] D. Mangal, D. Vudathala, J. Park, H. L. Seon, T. M. Penning, and I. A. Blair, "Analysis of 7,8-dihydro-8-oxo-2′-deoxyguanosine in cellular DNA during oxidative stress," *Chemical Research in Toxicology*, vol. 22, no. 5, pp. 788–797, 2009.

[26] J. Ravanat, T. Douki, P. Duez et al., "Cellular background level of 8-oxo-7,8-dihydro-2′-deoxyguanosine: an isotope based method to evaluate artefactual oxidation of DNA during its extraction and subsequent work-up," *Carcinogenesis*, vol. 23, no. 11, pp. 1911–1918, 2002.

[27] J. K. Leach, G. van Tuyle, P. S. Lin, R. Schmidt-Ullrich, and R. B. Mikkelsen, "Ionizing radiation-induced, mitochondria-dependent generation of reactive oxygen/nitrogen," *Cancer Research*, vol. 61, no. 10, pp. 3894–3901, 2001.

[28] L. B. CP, H. Ischiropoulos, and S. C. Bondy, "Bondy evaluation of the probe 2′,7′-dichlorofluorescin as an indicator of reactive oxygen species formation and oxidative stress," *Chemical Research in Toxicology*, vol. 5, pp. 227–231, 1992.

[29] A. Cossarizza, R. Ferraresi, L. Troiano et al., "Simultaneous analysis of reactive oxygen species and reduced glutathione content in living cells by polychromatic flow cytometry," *Nature Protocols*, vol. 4, no. 12, pp. 1790–1797, 2009.

[30] H. Zhu, G. L. Bannenberg, P. Moldeus, and H. G. Shertzer, "Oxidation pathways for the intracellular probe 2_,7_-dichlorofluorescein," *Archives of Toxicology*, vol. 68, pp. 582–587, 1994.

[31] U. Weyemi and C. Dupuy, "The emerging role of ROS-generating NADPH oxidase NOX4 in DNA-damage responses," *Mutation Research*, vol. 751, no. 2, pp. 77–81, 2012.

[32] F. Chen, S. Haigh, S. Barman, and D. J. Fulton, "From form to function: the role of Nox4 in the cardiovascular system," *Frontiers in Physiology*, vol. 1, no. 3, p. 412, 2012.

[33] A. N. Lyle, N. N. Deshpande, Y. Taniyama et al., "Poldip 2, a novel regulator of Nox4 and cytoskeletal integrity in vascular smooth muscle cells," *Circulation Research*, vol. 105, pp. 249–259, 2009.

[34] A. R. Collins, "Measuring oxidative damage to DNA and its repair with the comet assay," *Biochimica et Biophysica Acta*, vol. 13, pp. 150–155, 2013.

[35] M. Löbrich, A. Shibata, A. Beucher et al., "GammaH2AX foci analysis for monitoring DNA double strand break repair: strengths, limitations and optimization," *Cell Cycle*, vol. 9, no. 4, pp. 662–669, 2010.

[36] K. J. McManus and M. J. Hendzel, "ATM-dependent DNA damage-independent mitotic phosphorylation of H2AX in normally growing mammalian cells," *Molecular Biology of the Cell*, vol. 16, no. 10, pp. 5013–5025, 2005.

[37] A. A. Goodarzi and P. A. Jeggo, "The repair and signaling responses to DNA double-strand breaks," *Advances in Genetics*, vol. 82, pp. 1–45, 2013.

[38] I. Mermershtain and J. N. Glover, "Structural mechanisms underlying signaling in the cellular response to DNA double strand breaks," *Mutation Research*, vol. 750, no. 1-2, pp. 15–22, 2013.

[39] R. E. Shackelford, W. K. Kaufmann, and R. S. Paules, "Oxidative stress and cell cycle checkpoint function," *Free Radical Biology & Medicine*, vol. 28, no. 9, pp. 1387–1404, 2000.

[40] R. Bologna-Molina, A. Mosqueda-Taylor, N. Molina-Frechero, A. D. Mori-Estevez, and G. Sánchez-Acuña, "Comparison of the value of PCNA and Ki-67 as markers of cell proliferation in ameloblastic tumors," *Medicina Oral, Patología Oral y Cirugía Bucal*, vol. 18, no. 2, pp. 174–179, 2013.

[41] A. Wells, L. Griffith, J. Z. Wells, and D. P. Taylor, "The dormancy dilemma: quiescence versus balanced proliferation," *Cancer Research*, vol. 73, no. 13, pp. 3811–3816, 2013.

[42] S. Cory, D. C. Huang, and J. M. Adams, "The Bcl-2 family: roles in cell survival and oncogenesis," *Oncogene*, vol. 22, no. 53, pp. 590–607, 2003.

[43] T. W. Kensler and N. Wakabayashi, "Nrf2: friend or foe for chemoprevention?," *Carcinogenesis*, vol. 31, no. 1, pp. 90–99, 2010.

[44] S. Jahr, H. Hentze, S. Englisch et al., "DNA fragments in the blood plasma of cancer patients: quantitations and evidence for their origin from apoptotic and necrotic cells," *Cancer Research*, vol. 61, no. 4, pp. 1659–1665, 2001.

[45] M. van der Vaart and P. J. Pretorius, "Circulating DNA: its origin and fluctuation," *Annals of the New York Academy of Sciences*, vol. 1137, pp. 18–26, 2008.

[46] J. Hajizadeh, J. DeGroot, M. TeKoppele, A. Tarkowski, and L. V. Collins, "Extracellular mitochondrial DNA and oxidatively damaged DNA in synovial fluid of patients with

rheumatoid arthritis," *Arthritis Research & Therapy*, vol. 5, no. 5, pp. R234–R240, 2001.

[47] B. Zhang, A. Angelidou, K. D. Alysandratos et al., "Mitochondrial DNA and anti-mitochondrial antibodies in serum of autistic children," *Journal of Neuroinflammation*, vol. 7, pp. 80–85, 2010.

[48] A. Cossarizza, M. Pinti, M. Nasi et al., "Increased plasma levels of extracellular mitochondrial DNA during HIV infection: a new role for mitochondrial damage-associated molecular patterns during inflammation," *Mitochondrion*, vol. 11, no. 5, pp. 750–755, 2011.

[49] M. Suter and C. Richter, "Fragmented mitochondrial DNA is the predominant carder of oxidized DNA bases," *Biochemistry*, vol. 38, no. 1, pp. 459–464, 1999.

[50] I. B. Korzeneva, S. V. Kostuyk, E. S. Ershova et al., "Human circulating ribosomal DNA content significantly increases while circulating satellite III (1q12) content decreases under chronic occupational exposure to low-dose gamma- neutron and tritium beta-radiation," *Mutation Research*, vol. 791-792, pp. 49–60, 2016.

[51] A. V. Ermakov, S. V. Kostyuk, M. S. Konkova, N. A. Egolina, E. M. Malinovskaya, and N. N. Veiko, "Extracellular DNA fragments," *Annals of the New York Academy of Sciences*, vol. 1137, pp. 41–46, 2008.

[52] E. M. Malinovskaya, T. D. Smirnova, and N. A. Egolina, "Changes in human ribosomal genes ensemble with ageing," *Medical Genetics*, vol. 7, no. 2, pp. 10–16, 2008.

[53] N. N. Veĭko, N. V. Bulycheva, O. A. Roginko et al., "Ribosomal repeat in cell free DNA as a marker for cell death," *Biochemistry (Moscow) Supplement Series B: Biomedical Chemistry*, vol. 2, no. 2, pp. 198–207, 2008.

[54] A. V. Ermakov, M. S. Kon'kova, S. V. Kostyuk et al., "An extracellular DNA mediated bystander effect produced from low dose irradiated endothelial cells," *Mutation Research*, vol. 712, no. 1-2, pp. 1–10, 2011.

[55] A. V. Ermakov, M. S. Kon'kova, S. V. Kostiuk et al., "Bystander effect development in human mesenchymal stem cells after exposure to adaptive dose of X-radiation," *Radiatsionnaia Biologiia, Radioecologiia*, vol. 50, no. 1, pp. 42–51, 2010.

[56] S. V. Kostyuk, T. D. Smirnova, L. V. Efremova et al., "Enhanced expression of iNOS in human endothelial cells during long-term culturing with extracellular DNA fragments," *Bulletin of Experimental Biology and Medicine*, vol. 149, no. 2, pp. 191–195, 2010.

[57] L. V. Efremova, A. Y. Alekseeva, M. S. Kon'kova et al., "Extracellular DNA affects NO content in human endothelial cells," *Bulletin of Experimental Biology and Medicine*, vol. 149, no. 2, pp. 196–200, 2010.

[58] F. M. Lyng, C. B. Seymour, and C. Mothersill, "Early events in the apoptotic cascade initiated in cells treated with medium from the progeny of irradiated cells," *Radiation Protection Dosimetry*, vol. 99, no. 1–4, pp. 169–172, 2002.

[59] S. V. Kostyuk, M. S. Konkova, E. S. Ershova et al., "An exposure to the oxidized DNA enhances both instability of genome and survival in cancer cells," *PLoS One*, vol. 8, no. 10, article e77469, 2013.

[60] P. Henneke, O. Takeuchi, R. Malley et al., "Cellular activation, phagocytosis, and bactericidal activity against group B streptococcus involve parallel myeloid differentiation factor 88-dependent and independent signaling pathways," *The Journal of Immunology*, vol. 169, no. 7, pp. 3970–3977, 2002.

[61] L. József, T. Khreiss, D. El Kebir, and J. G. Filep, "Activation of TLR-9 induces IL-8 secretion through peroxynitrite signaling in human neutrophils," *The Journal of Immunology*, vol. 176, no. 2, pp. 1195–1202, 2006.

[62] Y. Adachi, A. L. Kindzelskii, A. R. Petty et al., "IFN-γ primes RAW264 macrophages and human monocytes for enhanced oxidant production in response to CpG DNA via metabolic signaling: roles of TLR9 and myeloperoxidase trafficking," *The Journal of Immunology*, vol. 176, no. 8, pp. 5033–5040, 2006.

[63] S. V. Kostiuk, E. M. Malinovskaia, A. V. Ermakov et al., "Cell-free DNA fragments increase transcription in human mesenchymal stem cells, activate TLR-dependent signal pathway and suppress apoptosis," *Biomeditsinskaya Khimiya*, vol. 58, no. 6, pp. 673–683, 2012.

[64] A. V. Ermakov, M. S. Kon'kova, S. V. Kostyuk, N. A. Egolina, L. V. Efremova, and N. N. Veiko, "Oxidative stress as a significant factor for development of an adaptive response in irradiated and nonirradiated human lymphocytes after inducing the bystander effect by low-dose X-radiation," *Mutation Research*, vol. 669, no. 1-2, pp. 155–161, 2009.

[65] V. Hornung and E. Latz, "Intracellular DNA recognition," *Nature Reviews Immunology*, vol. 10, no. 2, pp. 123–130, 2010.

[66] P. Nagaria, C. Robert, and F. V. Rassool, "DNA double-strand break response in stem cells: mechanisms to maintain genomic integrity," *Biochimica et Biophysica Acta*, vol. 1830, no. 2, pp. 2345–2353, 2013.

Hindawi
Oxidative Medicine and Cellular Longevity
Volume 2017, Article ID 4386947, 16 pages
https://doi.org/10.1155/2017/4386947

Research Article

Hypoxia Downregulates MAPK/ERK but Not STAT3 Signaling in ROS-Dependent and HIF-1-Independent Manners in Mouse Embryonic Stem Cells

Jan Kučera,[1] Julie Netušilová,[1] Stanislava Sladeček,[1] Martina Lánová,[1] Ondřej Vašíček,[2,3] Kateřina Štefková,[1] Jarmila Navrátilová,[1] Lukáš Kubala,[2,3] and Jiří Pacherník[1,3]

[1]*Institute of Experimental Biology, Faculty of Science, Masaryk University, Kotlářská 267/2, 61137 Brno, Czech Republic*
[2]*Institute of Biophysics, Academy of Sciences of the Czech Republic, Královopolská 2590/135, 61200 Brno, Czech Republic*
[3]*International Clinical Research Center, Centre of Biomolecular and Cellular Engineering, St. Anne's University Hospital, Pekařská 53, 65691 Brno, Czech Republic*

Correspondence should be addressed to Jiří Pacherník; jipa@sci.muni.cz

Received 18 January 2017; Revised 27 April 2017; Accepted 15 May 2017; Published 27 July 2017

Academic Editor: Magdalena Skonieczna

Hypoxia is involved in the regulation of stem cell fate, and hypoxia-inducible factor 1 (HIF-1) is the master regulator of hypoxic response. Here, we focus on the effect of hypoxia on intracellular signaling pathways responsible for mouse embryonic stem (ES) cell maintenance. We employed wild-type and HIF-1α-deficient ES cells to investigate hypoxic response in the ERK, Akt, and STAT3 pathways. Cultivation in 1% O_2 for 24 h resulted in the strong dephosphorylation of ERK and its upstream kinases and to a lesser extent of Akt in an HIF-1-independent manner, while STAT3 phosphorylation remained unaffected. Downregulation of ERK could not be mimicked either by pharmacologically induced hypoxia or by the overexpression. Dual-specificity phosphatases (DUSP) 1, 5, and 6 are hypoxia-sensitive MAPK-specific phosphatases involved in ERK downregulation, and protein phosphatase 2A (PP2A) regulates both ERK and Akt. However, combining multiple approaches, we revealed the limited significance of DUSPs and PP2A in the hypoxia-mediated attenuation of ERK signaling. Interestingly, we observed a decreased reactive oxygen species (ROS) level in hypoxia and a similar phosphorylation pattern for ERK when the cells were supplemented with glutathione. Therefore, we suggest a potential role for the ROS-dependent attenuation of ERK signaling in hypoxia, without the involvement of HIF-1.

1. Introduction

Embryonic development in its early stages takes place in a hypoxic microenvironment, and oxygen (O_2) has a significant impact on cellular differentiation or cell fate decisions [1]. ES are derived from preimplantation blastocyst, and hypoxia is thus suggested to modify cellular differentiation and regulate pluripotency. However, the outcome of stem cell cultivation in reduced O_2 tension remains highly controversial [2–5].

Cellular response to hypoxia is primarily orchestrated by hypoxia-inducible factor (HIF). HIF is a heterodimeric protein belonging to a family of environmental sensors known as a bHLH-PAS (basic-helix-loop-helix-Per-Arnt-Sim) transcription factors. HIF consists of a constitutively expressed HIF-β subunit and O_2-regulated HIF-α subunit [6]. Three α isoforms termed HIF-1α, HIF-2α, and HIF-3α are currently described [7]. When O_2 is not a limiting factor, the HIF-α subunit is rapidly hydroxylated by the family of proline hydroxylases (PHD) and targeted for subsequent proteasomal degradation [8–10]. Hypoxia inactivates PHD leading to the accumulation of the α subunit. After dimerization with the β subunit in the nucleus, HIF binds to a conserved DNA sequence known as the hypoxia-responsive element (HRE) to transactivate a myriad of hypoxia-responsive genes. HIF-1 heterodimer consisting of HIF-1α and HIF-β is the most important for cell adaptation to hypoxia [11]. Notably, O_2-dependent hydroxylation is implicated also

in the modification of other (non-HIF) targets, and O_2 is also a substrate for other various enzymes such as NADPH oxidases and monooxygenases [12]. Further, sensing and cellular response to low O_2 levels are also associated with the modulation of reactive oxygen species formation (ROS) and alterations in the metabolism of mitochondria, including ATP production [13]. A particular cellular response to reduced O_2 levels is thus complex and might be mediated in both HIF-dependent and -independent fashion.

The self-renewal and differentiation of murine ES cells is regulated by several signaling pathways. Among others, the signal transducer and activator of transcription 3 (STAT3) and phosphatidylinositol-4,5-bisphosphate-3-kinase/Akt (PI3K/Akt) signaling maintain ES cells in an undifferentiated pluripotent state [14, 15]. Conversely, mitogen-activated protein kinase/extracellular signal-regulated kinase (MAPK/ERK) signaling promotes the differentiation of ES cells [16]. Here, we focus on changes elicited in the activity of the mentioned signaling pathways in wild-type and HIF-1α deficient ES cells upon 24 h cultivation in 1% O_2. The activity of these signaling pathways is regulated through phosphorylation and by an opposing process of dephosphorylation mediated by phosphatases. DUSPs are the MAPK-specific phosphatases that impede the activity of ERK and also stress-activated kinases. DUSP1, DUSP5, and DUSP6 are suggested as hypoxia-sensitive and responsible for ERK downregulation [17, 18]. Further, serine/threonine PP2A regulates both the MAPK/ERK and Akt pathways, and its modulation by hypoxia is proposed in various models [19, 20].

Our study demonstrates the sensitivity of ES cells to chronic hypoxia in the context of the dephosphorylation of ERK and Akt with the possible involvement of ROS-dependent mechanisms. In agreement with other studies [21–23], we suggest that cultivation in 1% O_2 is in our system also associated with the decline of markers associated with the undifferentiated status of ES cells, despite the impairment of prodifferentiation ERK signaling.

2. Materials and Methods

2.1. Cell Culture and Treatment. Feeder-free R1-adapted mouse ES cells (wild-type HIF-1α +/+) and HIF-1α −/− (a generous gift from Professor Carmeliet, Katholieke Universiteit Leuven, Belgium) [24] were propagated as described previously [25] in an undifferentiated state by cell culturing on tissue culture plastic coated with gelatin (0.1% porcine gelatin solution in water) in Dulbecco's modified Eagle's medium (DMEM) containing 15% fetal bovine serum (FBS), 100 IU/ml penicillin, 0.1 mg/ml streptomycin, and 1× nonessential amino acid (all from Gibco-Invitrogen, UK) and 0.05 mM β-mercaptoethanol (β-ME; Sigma-Aldrich, USA), supplemented with 1000 U/ml of leukemia inhibitory factor (LIF, Chemicon, USA), referred to here as the complete medium. Cells were seeded and after 24 h were cultivated in normoxia or hypoxia for 24 h, unless specified otherwise. Normoxia was defined as 95% ambient air and 5% CO_2, hypoxia as 1% O_2, 94% N_2, and 5% CO_2.

Cobalt (II) chloride ($CoCl_2$), desferoxamine (DFO), dimethyloxalylglycine (DMOG), okadaic acid (OA), and glutathione (GSH) were provided by Sigma-Aldrich, USA. JNJ-42041935 (JNJ) was generously provided by Terry Barrett, Ph.D. (Johnson & Johnson Pharmaceutical Research & Development).

2.2. Cell Transfection and Luciferase Reporter Assay. Cell transfection and luciferase reporter assay were performed as described elsewhere [22]. Briefly, for the luciferase reporter assay, cells were transfected using polyethyleneimine (PEI) in a stoichiometric ratio of 4 μl per 1 μg of DNA 24 h after seeding.

0.5 μg of pT81/HRE-*luc* construct containing three tandem copies of the erythropoietin HRE in front of the herpes simplex thymidine kinase promoter and the luciferase gene, expression vectors for murine HIF-1α and HIF-2α under cytomegalovirus promoter, and GFP [26] (all generously provided by Professor L. Poellinger, Karolinska Institutet, Sweden), APRE-luciferase gene reporter plasmid (STAT3-responsive acute-phase response element, luciferase reporter; APRE-*luc* [27]; kindly provided by Professor A. Miyajima, Institute of Molecular and Cellular Biosciences, University of Tokyo, Japan) and *Renilla* luciferase construct (Promega, USA) were used per one well in a 24-well plate. The cell culture medium was changed 6 h after transfection. For experiments involving APRE-*luc*, the medium was exchanged for fresh complete medium or medium without LIF. Dual-Luciferase Assay Kit (Promega, USA) was used for the evaluation of luciferase activity according to the manufacturer's instructions. Relative luciferase units were measured using a ChameleonTM V plate luminometer (Hidex, Finland) and normalized to the *Renilla* luciferase expression.

2.3. Small Interfering RNA (siRNA) Transfection. Cells were transfected by commercially available siRNA against DUSP1 (sc-35938), DUSP5 (sc-60555), DUSP6 (sc-39001) transcripts (each consisting of a pool of 3 target-specific 19-25 nt siRNAs designed to knock down gene expression), or related nonsilencing control (all Santa Cruz Biotechnology, USA) using Lipofectamine RNAiMAX Reagents (Thermo Fisher Scientific Inc., USA) according to the manufacturer's instructions. Cells were harvested at the indicated time, and the expression of particular DUSP transcripts was assessed by qRT-PCR, or the expressions of selected proteins and posttranslational modification were analyzed by western blot.

2.4. Quantitative Real-Time RT-PCR (qRT-PCR) Analysis. Total RNA was extracted using the UltraClean Tissue & Cells RNA Isolation Kit (MO BIO Laboratories, USA). Complementary DNA was synthesized according to the manufacturer's instructions for M-MLV reverse transcriptase (Sigma-Aldrich); 0.5 μg of total RNA was used for cDNA synthesis. qRT-PCR was performed in a Roche Light-Cycler 480 instrument using LightCycler SYBRE Green Master Mix (Roche, Germany) according to the manufacturer's instructions. The primers, appropriate annealing temperatures, and PCR product lengths for the determined transcripts are listed in Table 1. The gene expression of each

Table 1: Primers, appropriate annealing temperatures, and PCR product lengths.

Transcript	Forward 5′→3′	Reverse 5′→3′	Annealing (°C)	Product (bp)
DUSP1	tctcagccaattgtgctaac	tgatggagtctatgaagtcaa	56	126
DUSP5	cgcctacagaccagcctatg	ccttcttccctgacacagtcaat	61	264
DUSP6	acctggaaggtggcttcagt	tccgttgcactattggggtc	62	187
FGF5	accggtgaaaccaaaggtg	gcgaaacttcagtctgtacttcact	57	76
GDF15	ccgagaggactcgaactcag	ggttgacgcggagtagcag	60	104
NANOG	aagcagaagatgcggactgt	gtgctgagcccttctgaatc	59	232
OCT4	cgttctctttggaaaggtgttc	gaaccatactcgaaccacatcc	59	319
PGK1	ggtgttgccaaaatgtcgcttt	cagccttgatcctttggttgtt	58	139
PP2A	gtggatgggcagatcttctgt	gcagcttggttaccacaacg	60	347
TBP	gcacaggagccaagagtgaag	acacgtggatagggaaggca	60	397
TNAP	aggcaggattgaccacgg	tgtagttctgctcatgga	59	440
VEGF	agaaggagagcagaagtccc	gatccgcatgatctgcatgg	62	235
ZFP42	gcacacagaagaaagcagga	cactgatccgcaaacacct	57	94
β-actin	gatcaagatcattgctcctcct	taaaacgcagctcagtaacag	59	177

sample was expressed in terms of the threshold cycle normalized to the mean of β-actin and TATA-box binding protein (TBP) expression.

2.5. Western Blot Analysis. Western blot analysis and cell sample harvesting and preparation were performed by a standard procedure as presented previously [28]. We used primary antibodies against HIF-1α (GeneTex, USA), HIF-2α, Nanog (Novus Biologicals, USA), β-actin, Oct4 (Santa Cruz), p-Akt (S473), Akt, p-STAT3 (Y705), STAT3, p-ERK (T202/Y204), ERK, p-glycogen synthase kinase 3 (S9) (p-GSK3β), RAF1, p-RAF1 (S259), p-RAF1 (S338), early growth response protein 1 (EGR1), DUSP6, p-MAP/ERK (S217/221) (p-MEK), and MEK (all Cell Signaling Technology, USA). Following immunodetection, each membrane was stained by Amido black to confirm the transfer of the protein samples. The total level of β-actin was detected as loading control. Typical representative western blots from at least three independent experiments are shown. Densitometry analysis was performed using ImageJ software (NIH, USA) and relative protein expression was calculated after normalization to the total protein of interest or β-actin. Data are presented as the mean + SEM.

2.6. High-Performance Liquid Chromatography (HPLC) Analysis of ROS Production. The HPLC detection of O_2^- was based on the detection of a specific product, 2-hydroxyethidium 2-OH-E(+), which is formed in the reaction of O_2^- with HE as described previously [25, 29, 30]. Besides specific 2-OH-E(+), also a nonspecific product of hydride acceptors in reaction with HE, ethidium (E(+)), was detected. Briefly, the cells were seeded onto 60 mm tissue culture dishes 24 h before treatment. The cells were exposed to hypoxia for 24 h or treated with 10 mM GSH for 60 minutes. Thirty minutes before the end of the experiment, HE (Sigma-Aldrich, USA) in a final concentration of 10 μM was added to the cells. The cells were washed two times with ice-cold PBS. To extract the HE products, ice-cold methanol was added to the cells for 15 minutes at 4°C in the dark and shaken. The supernatant was transferred to an Eppendorf tube and centrifuged. A 75 μl sample was injected into the HPLC system (Agilent series 1100) equipped with fluorescence and UV detectors (Agilent series 1260) to separate the 2-OH-E(+) and E(+) products. Fluorescence was detected at 510 nm (excitation) and 595 nm (emission); the mobile phase consisted of H_2O/CH_3CN. A Kromasil C18 (4.6 mm × 250 mm) column was used as the stationary phase.

2.7. Alkaline Phosphatase (ALP) Activity Determination. ALP activity determination was performed by a standard procedure as presented previously [31, 32]. Briefly, the cells were seeded 24 h before treatment and exposed to hypoxia or normoxia for 24 h. After the incubation, the cells were washed twice with PBS and lysed in ALP assay lysis buffer (50 mM Tris pH 7.4, 150 mM NaCl, 1 mM EDTA, and 0.5% NP40; all components Sigma-Aldrich, USA). Protein concentration was determined using DC protein assay (Bio-Rad, USA) kit according to manufacturer's instructions. 5 μg of protein was incubated in a 96-well plate (four parallel wells in each group) at 37°C with ALP substrate (4-p-nitrophenylphosphate; Sigma-Aldrich, USA) for 30 minutes. The reaction was stopped by adding 3 M NaOH and the optical densities were measured at 405 nm (620 nm reference) using a microplate reader (Hidex, Finland).

2.8. Statistical Analysis. Data are expressed as mean + standard error of the mean (SEM). Statistical analysis was assessed by T test or by one-way analysis of variance ANOVA and Bonferroni's Multiple Comparison posttest. Values of $P < 0.05$ were considered statistically significant ($^*P < 0.05$)

3. Results

3.1. Hypoxic Response in Wild-Type and HIF-1α-Deficient ES Cells. To determine the stabilization of HIF-1α and its role in hypoxic response in our system, we cultivated wild-type and

HIF1α-deficient ES cells in normoxia and in the presence of 1% O_2 for 24 h. In parallel, ES cells were also treated by hypoxia mimetics for 24 h ($CoCl_2$–0.3 mM, DFO–0.05 mM, DMOG–3 mM, and JNJ–0.2 mM); concentrations were selected according to a comprehensive literature search and previous study [22]. As anticipated, exposure to hypoxia led to the stabilization of HIF-1α in wild-type but not in HIF-1α −/− ES cells. The level of HIF-2α in hypoxia-treated cells was equal in wild-type and HIF-1α −/− ES cells (Figure 1(a)). In a similar manner, treatment with hypoxia mimetics also resulted in HIF-1α stabilization with a certain variability in the efficacy of the employed compounds and with $CoCl_2$ having the most pronounced effect (Figure 1(b)). The expressions of HIF-dependent (phosphoglycerate kinase 1 (PGK1), vascular endothelial growth factor (VEGF)), and HIF-independent (growth differentiation factor 15, GDF15) transcripts were determined by qRT-PCR. The increased expression of HIF downstream target genes (VEGF, PGK1) occurred in wild-type ES cells after 24 h hypoxic cultivation. The loss of HIF-1α reduced hypoxia-induced expression in both VEGF and PGK1 (Figures 1(c) and 1(d), resp.). The transcription of GDF15 was upregulated in both wild-type and HIF1α −/− cells cultivated in hypoxia (Figure 1(e)).

3.2. Hypoxia but Not HIF Stabilization Decreases ERK Signaling. The cultivation of ES cells in complete medium (supplemented with serum and LIF) results in the activation of several pathways that are responsible for ES cell maintenance. In normoxia, STAT3, Akt, and MAPK/ERK pathways are phosphorylated and, hence, active. Here, we aimed to assess how incubation in 1% O_2 affects the phosphorylation of these signaling components. The phosphorylation of STAT3 remained unchanged by hypoxia. In contrast, the phosphorylation of Akt and its downstream target GSK3β at inhibitory serine 9 was decreased in hypoxia-exposed ES cells (Figure 2(a)). Notably, we observed a strong decrease in the phosphorylation of ERK and its upstream kinase MEK. The dephosphorylation of RAF1 was also apparent at both inhibitory S259 and activating S338 residues (Figure 2(b)). The attenuation of ERK signaling correlated with the downregulation of its downstream target EGR1 (Figure 2(b)). Dephosphorylation was not dependent on HIF-1α in any of the examined proteins.

To further analyze STAT3 signaling, we employed APRE-*luc*, a luciferase reporter system that responds to the transcriptional activity of STAT3. Wild-type and HIF-1α −/− ES cells were transfected with APRE-*luc* and, after media change, were further cultivated in the presence of LIF-free medium or complete medium for 24 h in either normoxia or hypoxia. APRE-*luc* activity was significantly upregulated in an HIF-independent manner in the presence of LIF, which is a known inductor of STAT3 signaling. This effect was preserved also in hypoxia (Figure 2(c)).

Next, we assessed the effect of HIF stabilization mediated via exogenous HIF-1 or HIF-2 expression. ES cells were transiently transfected by the vectors constitutively expressing mHIF-1α or mHIF-2α. Cells treated with PEI and transfected with GFP expression vector served as a control. We observed stabilization and increased levels of HIF-1α and HIF-2α, as well as the upregulation of HIF-mediated transcription activity; however, the phosphorylation of ERK kinase remained unaffected in both cases (Figures 2(d) and 2(e)).

The administration of the hypoxia mimetics $CoCl_2$, DFO, DMOG, and JNJ for 24 h did not mimic the effect of hypoxia in the sense of ERK and Akt dephosphorylation. The phosphorylation of ERK kinase was upregulated following $CoCl_2$ and DFO treatment and remained unaffected after the addition of DMOG and JNJ. Phosphorylation of Akt was upregulated by DFO and remained unchanged following treatment with other mimetics (Figure 2(f)).

3.3. Hypoxia Upregulates DUSP1 but DUSP6 Has the Most Prominent Effect on ERK Dephosphorylation. Further, we investigated the role of DUSP phosphatases in hypoxia-driven ERK dephosphorylation. Firstly, the effect of hypoxia on DUSP1, 5, and 6 expressions was evaluated by qRT-PCR. The exposure of ES cells to hypoxia for 24 h increased DUSP1 expression (Figure 3(a)). Similar results were obtained using wild-type or HIF-1α deficient cells. In contrast to DUSP1, the level of transcripts of DUSP5 and 6 remained unaffected in hypoxia, again independently of the presence of HIF-1α (Figures 3(b) and 3(c), resp.). Next, we addressed the question of which DUSP has the most prominent effect on ERK dephosphorylation. We employed the RNA silencing of selected members of the DUSP family and screened for ERK phosphorylation. The transfection of ES cells by siRNA against DUSP1, 5, or 6 resulted in their decreased expression (Figures 3(d), 3(e), and 3(f), resp.). In the next step, we analyzed the effect of DUSP silencing on ERK phosphorylation status. Only the silencing of DUSP6 had a prominent effect on augmenting ERK phosphorylation. It was also correlated with the downregulation of DUSP6 protein (Figures 3(g), 3(h), and 3(i)).

3.4. Hypoxia Downregulates ERK Phosphorylation Regardless of DUSP6 Silencing. The RNA silencing of DUSP6 elevated the phosphorylation of ERK both in normoxia and hypoxia; however, increase in ERK phosphorylation following the DUSP6 silencing in hypoxia was not statistically significant (Figures 4(a) and 4(b)). Neither hypoxia-induced ERK dephosphorylation nor the reduction in EGR1 level were abolished following the DUSP6 silencing, as determined by western blot (Figure 4(a)). DUSP6 protein and ERK level were also determined in hypoxic conditions. Cells were cultured in 1% O_2 for 3, 6, 12, and 24 h. Western blot analysis revealed the hypoxia-mediated downregulation of DUSP6 protein in ES cells at all examined time points. Similarly, ERK phosphorylation was also progressively downregulated in hypoxia (Figure 4(c)).

3.5. Okadaic Acid Partially Rescues Hypoxia-Mediated Dephosphorylation. In an effort to clarify the involvement of PP2A phosphatase in the hypoxia-mediated regulation of ERK and Akt activation, we firstly examined its mRNA level. The gene expression of PP2A was not significantly modified by hypoxia either in parental wild-type or in HIF-1 −/− cells

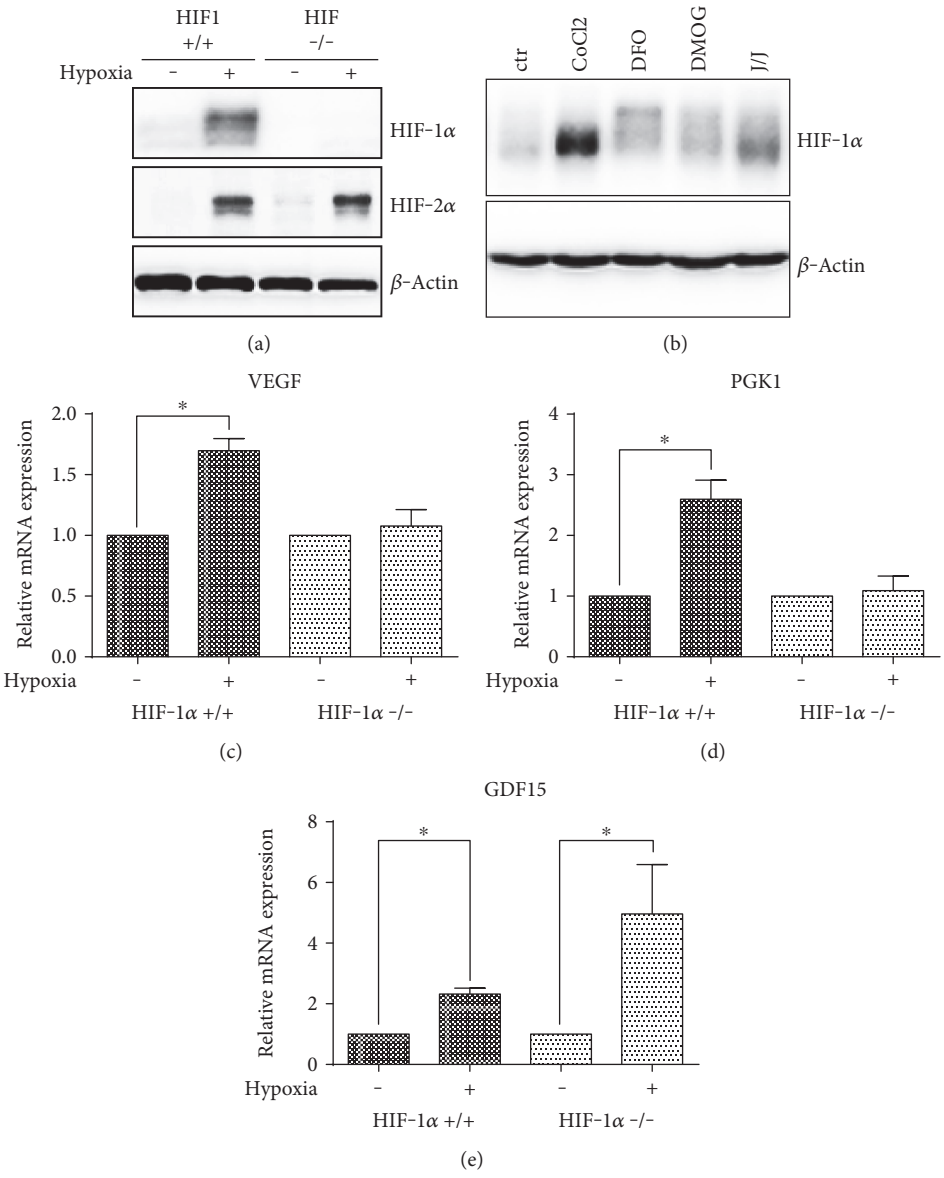

Figure 1: Stabilized HIF-1α and HIF-2α in hypoxia (24 h, 1% O_2) in parental wild-type (HIF-1α +/+) and HIF-1α −/− ES cells (a) and pharmacologically stabilized HIF-1α in wild-type ES cells (b) determined by western blot. Total level of β-actin was used as a loading control. Relative expressions of HIF-dependent ((VEGF (c), PGK1 (d)) and -independent (GDF15 (e)) genes in normoxia and hypoxia in wild-type and HIF-1α −/− ES cells. Data are presented as mean + SEM from at least three independent experiments. Statistical significance was determined by T test ($^*P < 0.05$).

(Figure 5(a)). Second, we employed OA, a potent inhibitor of PP2A. Before exposure to hypoxia or standard cultivation, OA was added to media in a 10 nM concentration. The inhibition of PP2A increased the phosphorylation of ERK independently of normoxic or hypoxic conditions and abolished its downregulation in hypoxia (Figures 5(b), 5(c), 5(d), and 5(e)). The phosphorylation of RAF1 at S259 remained intact upon treatment with OA (Figure 5(b)). The effect of OA on Akt phosphorylation was even more pronounced in hypoxia. Treatment with OA also increased the basal level of MEK phosphorylation, which was, however, reduced in hypoxia-cultivated samples. Similarly, OA induced the upregulation of RAF1 at S338 but did not prevent the reduction observed in hypoxic samples (Figures 5(b), 5(c), and 5(d)).

3.6. Hypoxia Reduces the ROS Level in ES Cells Affecting ERK and Akt Phosphorylation. To determine the involvement of hypoxia-induced changes in the cellular redox environment, we employed the ROS sensitive probe HE. Following the hypoxic cultivation, we observed a significant decline in both O_2-specific (Figure 6(a)) and -nonspecific HE oxidation products (Figure 6(b)) as assessed by HPLC analysis. The supplementation of cells with intracellular antioxidant GSH significantly reduced the amount of HE oxidation products in a manner similar to hypoxia. Further, we sought to elucidate the effect of GSH or β-ME supplementation (10 mM, 60 minutes) on the phosphorylation of selected signaling components of the ERK and Akt pathways. Following the treatment with GSH or β-ME, we revealed robust

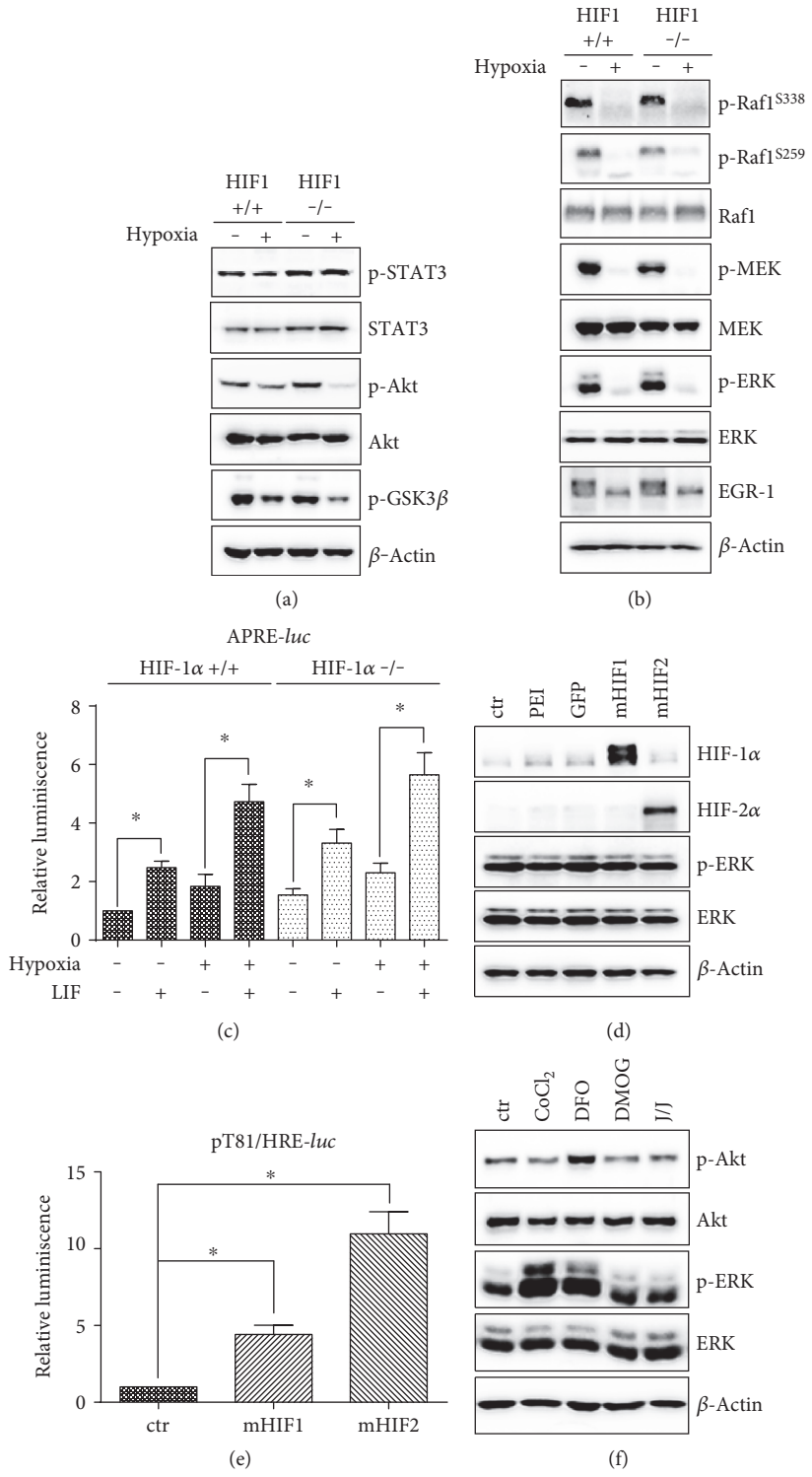

Figure 2: Effect of hypoxia on STAT3 and Akt (a) and ERK signaling (b) in wild-type and HIF-1α −/− ES cells. Analysis of STAT3 transcription activity (APRE-*luc*) in wild-type or HIF-1α −/− ES cultivated in complete medium (LIF) or LIF-free medium in normoxia or hypoxia (c). Effect of overexpression of mHIF1 and mHIF2 on ERK phosphorylation in wild-type ES cells (d). Analysis of HIF transcription activity (*pt81*/*HRE-luc*) induced by overexpression of mHIF-1 and mHIF-2 determined by luciferase reporter assay in wild-type ES cells (e). Effect of pharmacologically induced hypoxia on ERK phosphorylation in wild-type ES cells (f). The total level of β-actin was used as a loading control for western blot analyses. Data from luciferase assays are presented as mean + SEM from at least three independent experiments. Statistical significance was determined by one-way analysis of variance ANOVA and post hoc Bonferroni's multiple comparison test ($^*P < 0.05$).

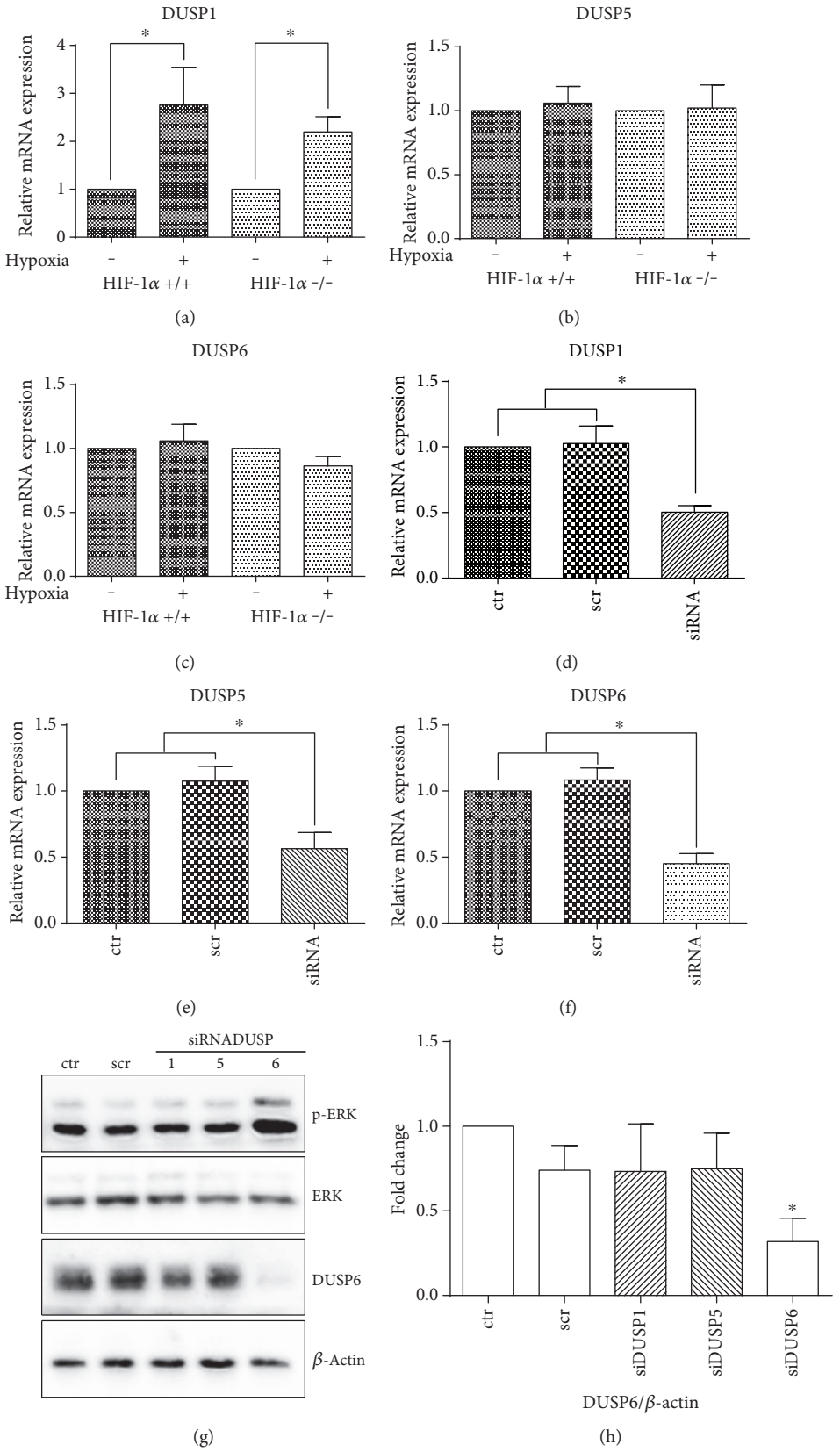

Figure 3: Continued.

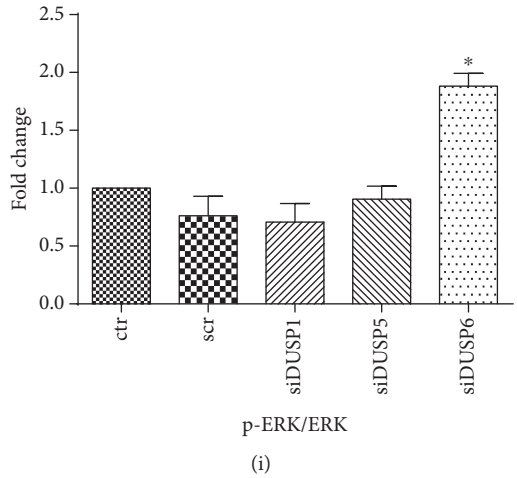

Figure 3: Relative expressions of DUSP1 (a), DUSP5 (b), and DUSP6 (c) in hypoxia in wild-type and HIF-1α −/− ES cells. Statistical significance was determined by T test ($^*P < 0.05$). Effect of siRNA-mediated silencing on DUSP1 (d), DUSP5 (e), and DUSP6 (f) expression in wild-type ES cells determined by qRT-PCR. Data are presented as mean + SEM from at least three independent experiments. Statistical significance was determined by one-way analysis of variance ANOVA and post hoc Bonferroni's multiple comparison test ($^*P < 0.05$). Effect of DUSP1, 5, and 6 siRNAs on ERK phosphorylation and DUSP6 levels in wild-type ES cells (g). The total level of β-actin was used as a loading control. Densitometry analysis of western blots expressed as fold change in DUSP6 protein expression (h) or ERK phosphorylation (i). Data are presented as mean + SEM from at least three independent experiments. Statistical significance was determined by one-way analysis of variance ANOVA and post hoc Bonferroni's multiple comparison test ($^*P < 0.05$).

dephosphorylation of the ERK pathway and its upstream kinases, as well as Akt kinase. The level of STAT3 phosphorylation remained unaffected by this intervention (Figures 6(c) and 6(d)).

3.7. Hypoxia Attenuates Markers Associated with Undifferentiated State of ES Cells. Given the suggested importance of hypoxia in stem cell cultivation, we aimed to investigate whether the attenuation of prodifferentiation ERK signaling in hypoxia affects the selected markers of stem cell maintenance. The gene expressions of critical regulators of the undifferentiated state and stem cell markers octamer-binding transcription factor 4 (OCT4), Nanog, zinc finger protein 42 homolog (ZFP42), and tissue nonspecific alkaline phosphatase (TNAP) were significantly decreased in hypoxia (Figures 7(a), 7(b), 7(c), and 7(d)), contrary to the early differentiation marker fibroblast growth factor 5 (FGF5), which was upregulated (Figure 7(e)), as determined by qRT-PCR. Protein levels of Oct4 and Nanog were reduced in hypoxia-cultivated cells as determined by western blot (Figure 7(f)), as well as alkaline phosphatase activity (Figure 7(g)).

4. Discussion

Properties of stem cells are maintained by numerous factors including O_2 level. Mouse ES cells are routinely cultivated in media supplemented with serum and LIF, which support their undifferentiated state. LIF acts mainly through activating STAT3 signaling, while serum activates other pathways including MAPK/ERK and Akt [14, 16, 33]. Here, we show that chronic hypoxia (1% O_2 for 24 h) decreases the phosphorylation of ERK and Akt but not STAT3 and attenuates markers associated with undifferentiated state. As the most striking effect of hypoxia was observed on ERK signaling, we further focused on this pathway in particular, with a minor interest also in Akt. Interestingly, chronic hypoxia downregulated not only ERK but also its upstream kinases, MEK and RAF.

As mentioned before, cellular response to hypoxia is a complex process. A decrease in O_2 level inhibits PHD, which in turn leads to HIF stabilization and transactivation of its target genes, for example, PGK1 or VEGF [34]. GDF15 is known to be upregulated by various stressors including O_2 deprivation, without evidence of direct HIF involvement [35, 36]. This process is universal virtually for every cell type, including ES cells.

To understand the mechanisms of the observed ERK signaling inhibition by hypoxia, we first aimed to assess whether HIF activity alone causes the dephosphorylation of ERK signaling pathways. We employed HIF-1α deficient ES cells, the exogenous expression of HIF-1α and HIF-2α, and treatment with the most commonly used inhibitors of PHD, (hypoxia mimetics) DMOG, JNJ, $CoCl_2$, and DFO [22, 37, 38]. Neither HIF-1α depletion nor HIF upregulation by overexpression or hypoxia mimetics manifested an effect on the studied ERK dephosphorylation. Therefore, we suggest that hypoxia and not HIF itself is responsible for the observed attenuation of ERK signaling. Moreover, DFO and $CoCl_2$ even induced ERK phosphorylation. This is in agreement with other authors reporting that iron chelation strongly activates MAPK [39–42]. Interestingly, the mechanism of ERK induction proposed by Huang and colleagues suggests that DFO inhibits DUSP1 and therefore supports ERK phosphorylation [43]. However, in our experiments, we observed the induction of DUSP1

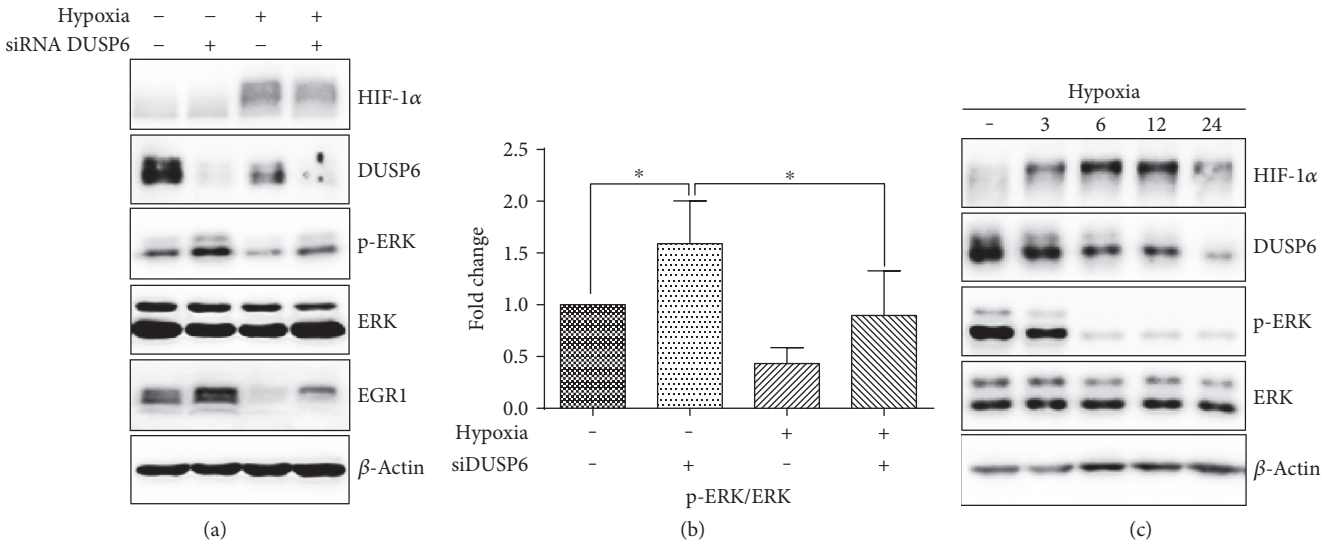

Figure 4: Effect of DUSP6 siRNA silencing on ERK signaling in normoxia and hypoxia in wild-type ES cells (a). Densitometry analysis of western blot expressed as fold change in ERK phosphorylation (b). Data are presented as mean + SEM from at least three independent experiments. Statistical significance was determined by one-way analysis of variance ANOVA and post hoc Bonferroni's multiple comparison test (* $P < 0.05$). Effect of 3 h, 6 h, 12 h, and 24 h 1% O_2 cultivation on DUSP6 protein expression and ERK phosphorylation in wild-type ES cells (c). Total level of β-actin was used as a loading control.

following DFO and $CoCl_2$ treatment (data not shown, manuscript in preparation). ROS-dependent activation of ERK signaling has been described multiple times [44, 45], and we earlier reported that in our system, ERK is also activated in a ROS-sensitive manner [25]. Therefore, we hypothesized that the activation of ERK might be mediated by drug-induced ROS elevation [46, 47].

Further, we aimed to establish whether the downregulation of ERK signaling is associated with the activity of phosphatases. In agreement with literature, the roles of selected MAPK-specific DUSPs and PP 2A were here analyzed. The elevated expression of DUSP1 following hypoxic treatment was reported earlier [48] as well as the upregulation of ERK-specific DUSP6 in the presence of 1% O_2, which was mediated in an HIF-1-dependent manner [18]. We also tested DUSP5 as a representative of nuclear inducible DUSP with specificity only towards ERK; the higher efficiency of DUSP1 in the dephosphorylation of p38 and c-Jun N-terminal kinase was described by other authors [49, 50].

In our experiments, hypoxia increased the expression of DUSP1 in an HIF1-independent manner, while the mRNA expressions of DUSP5 and DUSP6 remained unchanged upon 24 h hypoxic incubation. Others suppose that DUSP1 is induced by hypoxia in a program of gene expression controlled by HIF-1 [51, 52]. Although we do not rule out this possibility, on the basis of our results, we propose that HIF-1 is dispensable for DUSP1 gene expression in chronic hypoxia. Interestingly, in contrast to our results, Bermudez and colleagues reported the upregulation of both DUSP5 and DUSP6 mRNA levels following 24 h cultivation in 1% O_2 [18]. This divergence might be attributed to differences between the melanoma and adenocarcinoma cell lines employed in mentioned study and the ES cells used in our experiments.

Next, we employed siRNA silencing to investigate the involvement of DUSPs in the regulation of ERK phosphorylation. The downregulation of DUSP1 and DUSP5 by specific siRNAs did not have a profound effect on ERK phosphorylation. In contrary to this, the siRNA silencing of DUSP6 resulted in upregulation of the phosphorylated form of ERK, suggesting its involvement in ERK regulation in mouse ES cells. Hypoxia, however, downregulated ERK phosphorylation regardless of DUSP6 silencing. Moreover, hypoxia did not increase DUSP6 expression on either the mRNA or protein levels. It was reported that DUSP6 is subject to extensive posttranscriptional and posttranslational modifications and that mRNA level might not correspond to the protein level due to several feedback loop mechanisms that are likely to promote the proteasomal degradation of DUSP6 via ERK phosphorylation [18, 53]. Thus, it is possible that the expression of DUSP6 takes place as a part of early hypoxic response and, after 24 h, returns to its basal level. However, we observed the downregulation of DUSP6 on the protein level even after 3 h cultivation in 1% O_2. Taken together, we conclude that selected DUSP1, 5, and 6 do not play a major role in the downregulation of ERK phosphorylation during chronic hypoxia in our system. Consistent with this is the fact that not only ERK but also its upstream kinases MEK and RAF, which are not recognized as a substrate for DUSPs [54], showed a decline in phosphorylation status in hypoxia.

Further, we decided to elucidate the role of PP2A in chronic hypoxia. PP2A is one of the most abundantly expressed serine/threonine protein phosphatases that regulates the MAPK/ERK pathway in both a positive and negative fashion [55] and is also involved in the dephosphorylation of Akt [56]. Although PP2A can be induced by various stressors including hypoxia in both in vivo and in vitro models [19, 20], in our experiments, its mRNA level was not altered

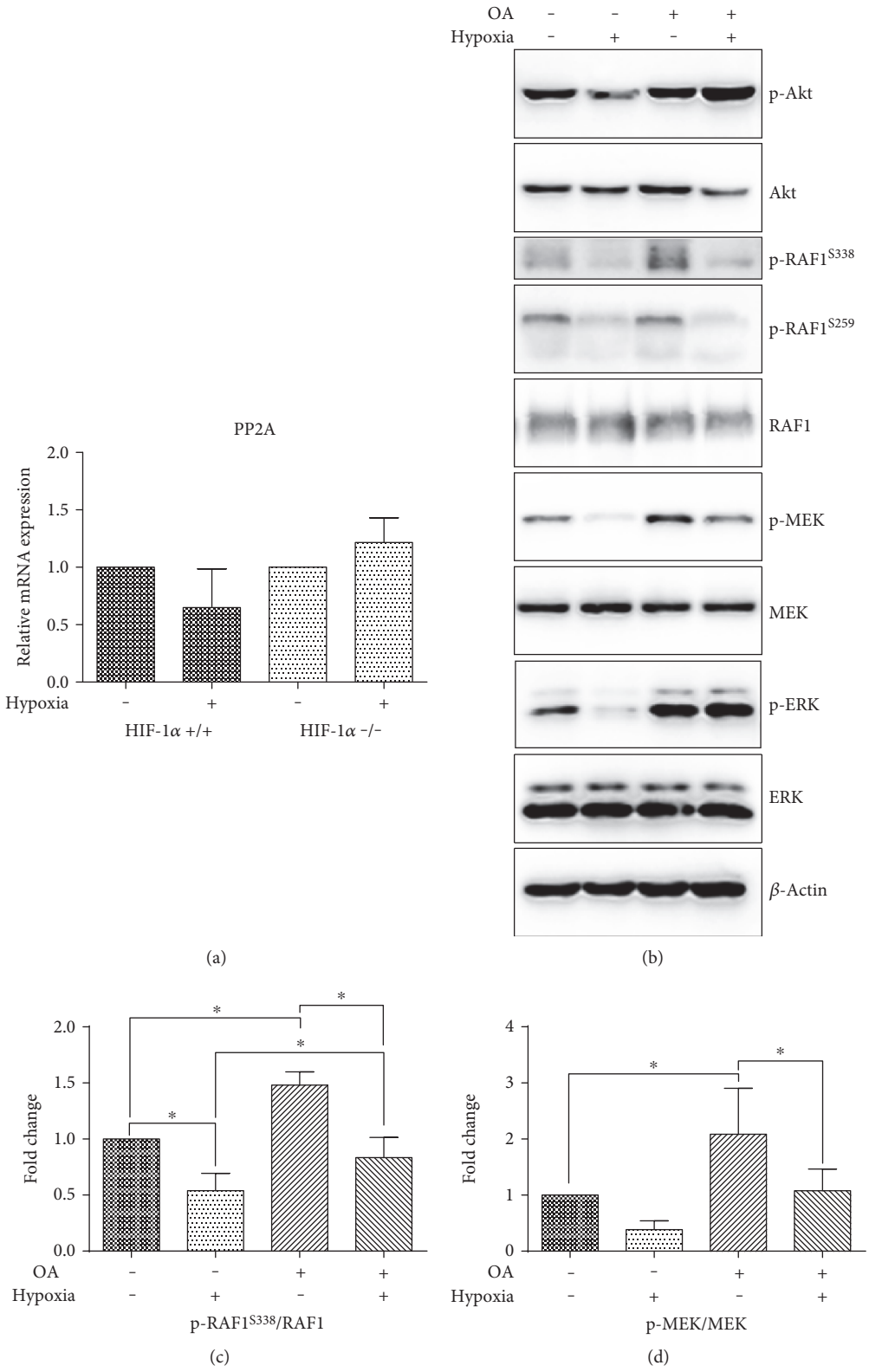

Figure 5: Continued.

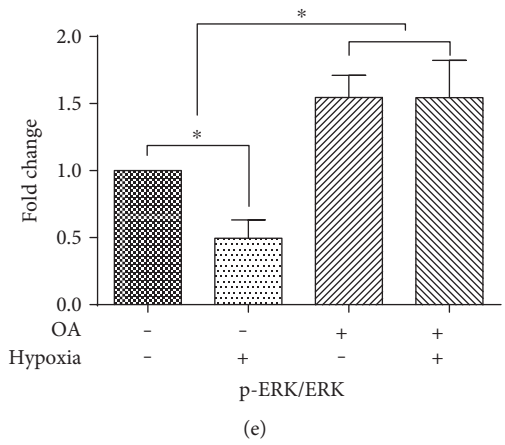

Figure 5: Relative expression of PP2A (a) in hypoxia in wild-type and HIF-1α −/− ES cells determined by qRT-PCR. Data are presented as mean + SEM from at least three independent experiments. Statistical significance was determined by T test. Effect of OA on signaling in hypoxia and normoxia in wild-type and HIF-1α −/− ES cells (b). Total level of β-actin was used as a loading control. Densitometry analysis of MAPK/ERK western blot expressed as fold change in RAF (S338) (c) MEK (d), and ERK phosphorylation (e). Data are presented as mean + SEM from at least three independent experiments. Statistical significance was determined by one-way analysis of variance ANOVA and post hoc Bonferroni's multiple comparison test ($^*P < 0.05$).

after hypoxic cultivation. We employed the PP2A inhibitor OA to further investigate the involvement of PP2A in the dephosphorylation of the ERK and Akt pathways observed in hypoxia. The hypoxia-induced impairment of ERK and Akt phosphorylation was reversed in the presence of OA. The dephosphorylation of MEK was partially rescued, but it was still downregulated by hypoxia, despite the general increase in phosphorylation, similarly to the situation with the S338 RAF1 residue. These findings suggest several modes of action of PP2A in our experiments. PP2A might dominate as a negative regulator of ERK signaling through the direct dephosphorylation of ERK and MEK, as proposed by previous studies [57, 58]. However, the increased phosphorylation of S338 at RAF1 in OA-treated ES cells suggests intervention on the level of RAF1 or, even more likely, upstream, as S338 is not reported as a PP2A target. This is in accordance with the study by Sawa and colleagues [59]. Moreover, OA also promotes the phosphorylation of epidermal growth factor receptor (EGFR) and thus activates EGF signaling, which is also connected with ERK and Akt upregulation [60]. However, we were not able to detect changes in EGFR phosphorylation in our experiments (data not shown). As the inhibitory phosphorylation of RAF1 at the S259 site which is the PP2A target [61] remained unaffected by OA treatment, we also propose that this type of RAF1 regulation has negligible importance in our system. Interestingly, S259 phosphorylation is mediated by Akt [62]; however, the phosphorylation of Akt was upregulated following OA treatment in hypoxia without the effect of RAF1 phosphorylation. This suggests the limited significance of crosstalk between PI3K/Akt and MAPK/ERK at the level of Akt and RAF1 in ES cells. Taken together, our results indicate that the impairment of ERK signaling takes place on the level of RAF1 or above via a hypoxia-driven independent mechanism that might, to a certain extent, include the involvement of PP2A.

A plausible explanation for our observations might be in the decline of intracellular ROS in cells cultivated in hypoxia. ROS are currently recognized as an important modulator of various intracellular signaling pathways [63]. Many growth factors and cytokine receptors possess cysteine-rich motifs susceptible to oxidation that may result in changes in the structure and function of the protein and lead to the activation or inhibition of several signaling pathways [64]. A proportionate level of ROS is also required for the formation of disulfide bonds in order to achieve the suitable intermolecular conformation of signaling proteins and is also vital in the process of intramolecular dimerization and protein-protein interactions (e. g., with scaffold proteins), which are necessary for proper signal transduction [65].

Previously, we and other authors demonstrated that antioxidants and inhibitors of ROS-producing enzymatic sites abolish MAPK and Akt activation. Conversely, interventions that lead to increased ROS production or the direct exposure of cells to oxidants such as H_2O_2 also activated MAPK as well as Akt in a number of different studies including ours [25, 63, 64].

To compare the effects of hypoxia-mediated decreases in ROS, we treated cells with GSH. GSH is an essential component of the ROS buffering intracellular system and a first line of defence antioxidant [66]. Cells supplemented with exogenous GSH manifested phosphopatterns of ERK and Akt signaling identical to those of cells cultivated in hypoxia. These results were further confirmed with treatment of cells with reducing agent and thiol antioxidant β-ME. Therefore, we suggest that hypoxia-mediated ROS depletion is significantly involved in the downregulation of ERK and Akt signaling in conditions of chronic hypoxia.

Signaling through ERK kinase is typically regulated by mitogens and as such is associated with cell proliferation. The inhibition of mitogen-induced ERK signaling thus also attenuates cell division [67]. The described mechanisms

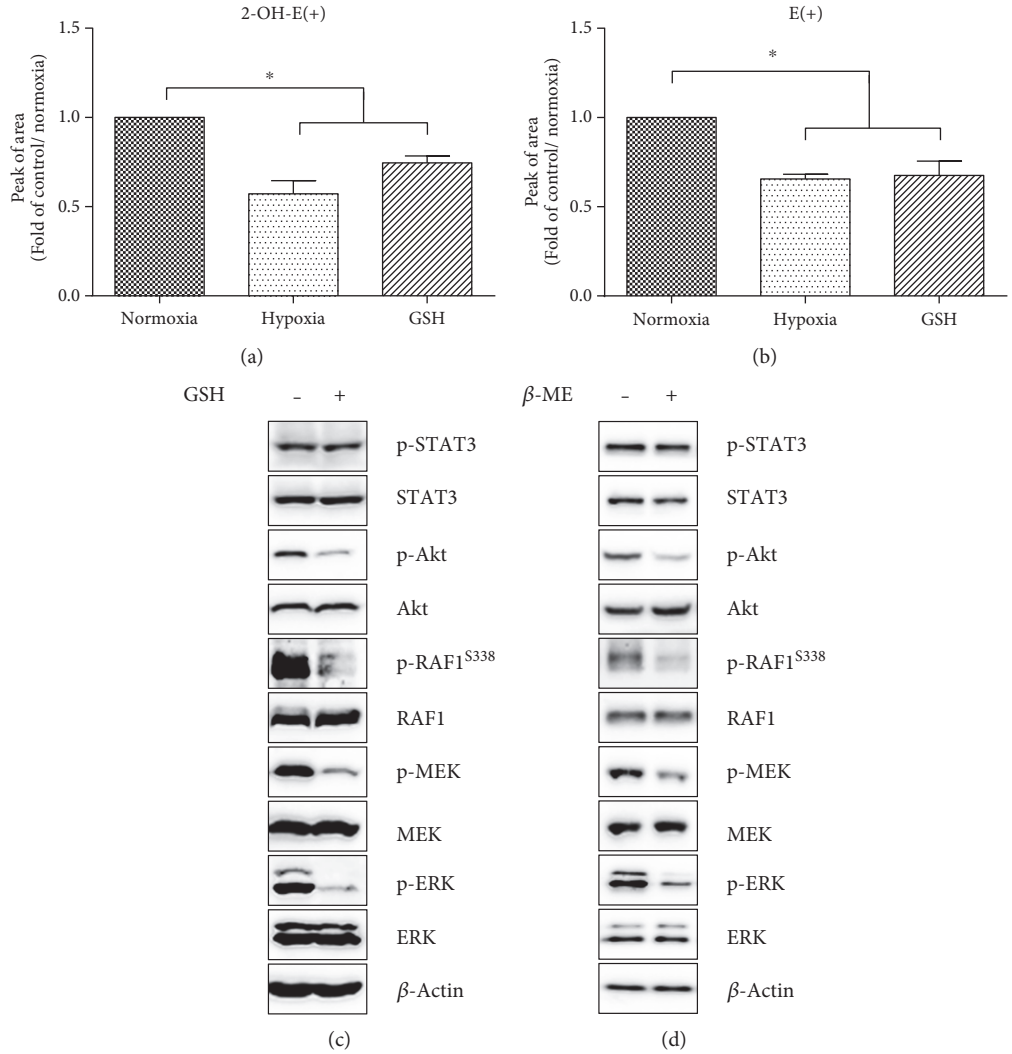

Figure 6: HPLC determination of specific 2-OH-E(+) (a) and nonspecific product E(+) (b) of HE oxidation in cells cultivated in normoxia or hypoxia or supplemented with GSH. Data are presented as mean + SEM from at least three independent experiments. Statistical significance was determined by one-way analysis of variance ANOVA and post hoc Bonferroni's multiple comparison test ($^*P < 0.05$). Effect of GSH and β-ME supplementation on phosphorylation of MAPK/ERK, Akt, and STAT3 (c, d). Total level of β-actin was used as a loading control.

may therefore serve as part of the processes that keep the low proliferation rate of stem cell in their niche, even in the presence of relatively high concentrations of growth factors. Multiple lines of evidence show that cultivation in the range between 1 and 5% of O_2 supports the maintenance of ES cells in a pluripotent state, prevents their differentiation, and even reprograms the partially differentiated cells to a stem cell-like state [2, 5, 68]. In contrast to studies proposing hypoxia to have a beneficial effect on stem cell maintenance, others reported that cultivation in reduced O_2 tension supports rather ES cell differentiation [3, 4, 69]. Although ERK signaling contributes preferably to differentiation in the context of ES cells, the hypoxia-mediated ERK attenuation observed in our experiments did not support the undifferentiated state, as shown in the reduced transcripts of markers associated with stem cell signature. This is in agreement with our earlier study in which neither PHD inhibition nor 1% or 5% hypoxia prevented the downregulation of markers associated with pluripotency induced by the depletion of LIF [22]. Here, we report similar results, even in the presence of complete medium, as shown by reduced mRNA levels of OCT4, NANOG, ZFP42, and TNAP, diminished Oct4 and Nanog protein and reduction in alkaline phosphatase activity. Thus, in our system, hypoxia is not a supportive factor with respect to the maintenance of markers of undifferentiated ES cells after 24 h cultivation in 1% O_2. PI3K/Akt was shown to be critical for supporting the self-renewal of ES; therefore, the observed reduction in transcripts associated with undifferentiated status might be attributed to hypoxia-mediated impairment of Akt and its downstream targets such as Nanog [15, 33]. However, it should be emphasized that downregulations of markers associated with undifferentiated state are highly dependent on hypoxia level, length of hypoxic incubation, cell type, and specific culture conditions, and might have only be transient [21]. It is of particular interest that we did not observe the downregulation of STAT3 signaling in hypoxia, which is central to maintenance of the undifferentiated state and pluripotency [14, 70]. This is in contrast

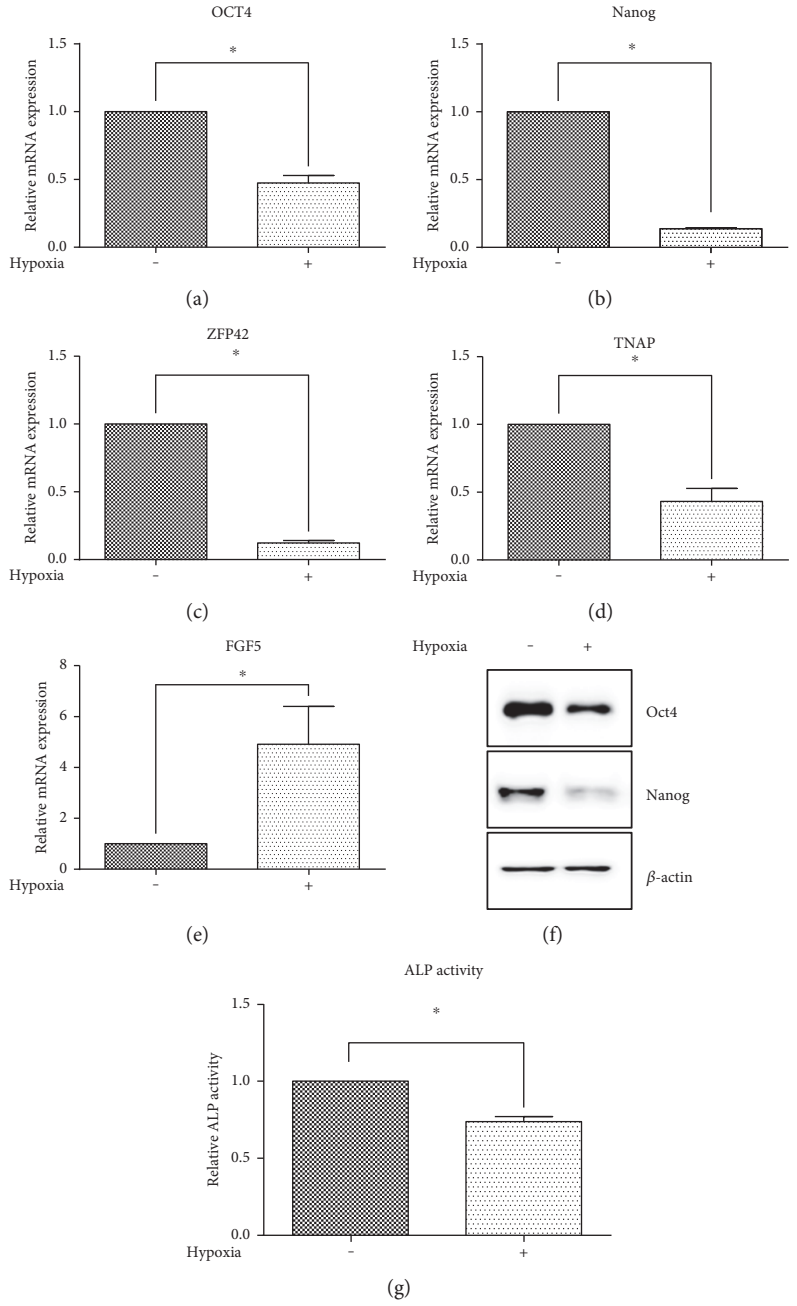

Figure 7: Relative expression of OCT4 (a), NANOG (b), ZFP42 (c), TNAP (d), and FGF5 (e) in wild-type ES cells determined by qRT-PCR. Data are presented as mean + SEM from at least three independent experiments. Statistical significance was determined by T test ($^*P < 0.05$). Protein level of Oct4 and Nanog in wild-type ES cells cultivated in normoxia or hypoxia as determined by western blot (f). Total level of β-actin was used as a loading control. Determination of alkaline phosphatase activity in wild-type ES cells cultivated in normoxia or hypoxia (g). Data are presented as mean + SEM from at least three independent experiments. Statistical significance was determined by T test ($^*P < 0.05$).

with a study by Jeong and collaborators, who also reported the hypoxia-induced differentiation of ES cells. However, in this study, the differentiation of ES was connected to the HIF-1-mediated suppression of LIF receptor transcription, which in turn attenuated STAT3 activation [3]. As we showed on the phosphorylation level and by luciferase reporter assay, STAT3 signaling is not compromised by hypoxia in our system, regardless of the presence of HIF-1. Notably, in our previous study, we also reported the resistance of LIF-induced STAT3 phosphorylation to changes in intracellular redox status [25]. This notion is of particular interest as persistent STAT3 phosphorylation is a hallmark of several cancers and leads to the gene expression responsible for malignant cell proliferation and resistance to apoptosis, as well as increased invasion and migration [71]. Further, it should be emphasized that STAT3 signaling is crucial for the regulation of cancer stem

cells in a similar way as for the regulation of ES cells [72]. The relative indifference of STAT3 phosphorylation to changes in redox environment thus might serve as one of the driving forces of cancer progression associated with poor prognosis.

Here, we report conclusively that chronic hypoxia attenuates the phosphorylation of ERK and Akt in ES cells independently of the presence of HIF-1α. On the basis of our results, we suggest that ROS plays a considerable role in the phosphorylation of ERK and Akt in ES cells, as is demonstrated by the similar effect of hypoxia-induced ROS depletion and GSH supplementation on ERK and Akt signaling cascades. However, our data do not exclude the involvement of other different mechanisms.

Conflicts of Interest

The authors declare no conflicts of interest regarding the publication of this paper. The authors alone are responsible for the content and writing of the paper.

Acknowledgments

The authors are grateful to Professor L. Poellinger and Professor A. Miyajima for providing the plasmids. The work was funded by the Faculty of Medicine of Masaryk University (Grant MUNI/A/1558/2014) and the Ministry of Education, Youth and Sport of the Czech Republic (Project no. LQ1605 NPU II; Project MSM0021622430). This research was also supported by collaboration between Masaryk University and the Karolinska Institutet under the Project KI-MU CZ.1.07/2.3.00/20.0180.

References

[1] Q. Lin, Y. Kim, R. M. Alarcon, and Z. Yun, "Oxygen and cell fate decisions," *Gene Regulation and Systems Biology*, vol. 2, pp. 43–51, 2008.

[2] T. Ezashi, P. Das, and R. M. Roberts, "Low O_2 tensions and the prevention of differentiation of hES cells," *Proceedings of the National Academy of Sciences*, vol. 102, no. 13, pp. 4783–4788, 2005.

[3] C.-H. Jeong, H.-J. Lee, J.-H. Cha, J. H. J.-H. Kim, K.-W. K. R. Kim, and D.-K. Yoon, "Hypoxia-inducible factor-1 alpha inhibits self-renewal of mouse embryonic stem cells in vitro via negative regulation of the leukemia inhibitory factor-STAT3 pathway," *The Journal of Biological Chemistry*, vol. 282, no. 18, pp. 13672–13679, 2007.

[4] S. Prado-Lopez, A. Conesa, A. Armiñán et al., "Hypoxia promotes efficient differentiation of human embryonic stem cells to functional endothelium," *Stem Cells*, vol. 28, no. 3, pp. 407–418, 2010.

[5] J. Mathieu, Z. Zhang, A. Nelson et al., "Hypoxia induces re-entry of committed cells into pluripotency," *Stem Cells*, vol. 31, no. 9, pp. 1737–1748, 2013.

[6] G. L. Wang, B. H. Jiang, E. A. Rue, and G. L. Semenza, "Hypoxia-inducible factor 1 is a basic-helix-loop-helix-PAS heterodimer regulated by cellular O2 tension," *Proceedings of the National Academy of Sciences of the United States of America*, vol. 92, no. 12, pp. 5510–5514, 1995.

[7] Y. Z. Gu, S. M. Moran, J. B. Hogenesch, L. Wartman, and C. A. Bradfield, "Molecular characterization and chromosomal localization of a third alpha-class hypoxia inducible factor subunit, HIF3alpha," *Gene Expression*, vol. 7, no. 3, pp. 205–213, 1998.

[8] L. E. Huang, J. Gu, M. Schau, and H. F. Bunn, "Regulation of hypoxia-inducible factor 1alpha is mediated by an O2-dependent degradation domain via the ubiquitin-proteasome pathway," *Proceedings of the National Academy of Sciences of the United States of America*, vol. 95, no. 14, pp. 7987–7992, 1998.

[9] P. H. Maxwell, M. S. Wiesener, G. W. Chang et al., "The tumour suppressor protein VHL targets hypoxia-inducible factors for oxygen-dependent proteolysis," *Nature*, vol. 399, no. 6733, pp. 271–275, 1999.

[10] P. Jaakkola, D. R. Mole, Y. M. Tian et al., "Targeting of HIF-alpha to the von Hippel-Lindau ubiquitylation complex by O_2-regulated prolyl hydroxylation," *Science*, vol. 292, no. 5516, pp. 468–472, 2001.

[11] R. H. Wenger, "Mammalian oxygen sensing, signalling and gene regulation," *The Journal of Experimental Biology*, vol. 203, Part 8, pp. 1253–1263, 2000.

[12] K. Bedard and K. Krause, "The NOX family of ROS-generating NADPH oxidases: physiology and pathophysiology," *Physiological Reviews*, vol. 87, no. 1, pp. 245–313, 2007.

[13] N. S. Chandel and G. R. S. Budinger, "The cellular basis for diverse responses to oxygen," *Free Radical Biology & Medicine*, vol. 42, no. 2, pp. 165–174, 2007.

[14] H. Niwa, T. Burdon, I. Chambers, and A. Smith, "Self-renewal of pluripotent embryonic stem cells is mediated via activation of STAT3," *Genes & Development*, vol. 12, no. 13, pp. 2048–2060, 1998.

[15] M. P. Storm, H. K. Bone, C. G. Beck et al., "Regulation of Nanog expression by phosphoinositide 3-kinase-dependent signaling in murine embryonic stem cells," *The Journal of Biological Chemistry*, vol. 282, no. 9, pp. 6265–6273, 2007.

[16] T. Burdon, C. Stracey, I. Chambers, J. Nichols, and A. Smith, "Suppression of SHP-2 and ERK signalling promotes self-renewal of mouse embryonic stem cells," *Developmental Biology*, vol. 210, no. 1, pp. 30–43, 1999.

[17] C. Liu, Y. Shi, Y. Du et al., "Dual-specificity phosphatase DUSP1 protects overactivation of hypoxia-inducible factor 1 through inactivating ERK MAPK," *Experimental Cell Research*, vol. 309, no. 2, pp. 410–418, 2005.

[18] O. Bermudez, P. Jouandin, J. Rottier, C. Bourcier, G. Pagès, and C. Gimond, "Post-transcriptional regulation of the DUSP6/MKP-3 phosphatase by MEK/ERK signaling and hypoxia," *Journal of Cellular Physiology*, vol. 226, no. 1, pp. 276–284, 2011.

[19] P. T. Heikkinen, M. Nummela, S.-K. Leivonen et al., "Hypoxia-activated Smad3-specific dephosphorylation by PP2A," *The Journal of Biological Chemistry*, vol. 285, no. 6, pp. 3740–3749, 2010.

[20] C. P. Hofstetter, J.-K. Burkhardt, B. J. Shin et al., "Protein phosphatase 2A mediates dormancy of glioblastoma multiforme-derived tumor stem-like cells during hypoxia," *PloS One*, vol. 7, no. 1, article e30059, 2012.

[21] H. S. C. Barbosa, T. G. Fernandes, T. P. Dias, M. M. Diogo, and J. M. S. Cabral, "New insights into the mechanisms of embryonic stem cell self-renewal under hypoxia: a multifactorial analysis approach," *PloS One*, vol. 7, no. 6, article e38963, 2012.

[22] L. Binó, J. Kučera, K. Štefková et al., "The stabilization of hypoxia inducible factor modulates differentiation status and inhibits the proliferation of mouse embryonic stem cells," *Chemico-Biological Interactions*, vol. 244, pp. 204–214, 2016.

[23] D. E. Powers, J. R. Millman, R. B. Huang, and C. K. Colton, "Effects of oxygen on mouse embryonic stem cell growth, phenotype retention, and cellular energetics," *Biotechnology and Bioengineering*, vol. 101, no. 2, pp. 241–254, 2008.

[24] P. Carmeliet, Y. Dor, J. M. Herbert et al., "Role of HIF-1alpha in hypoxia-mediated apoptosis, cell proliferation and tumour angiogenesis," *Nature*, vol. 394, no. 6692, pp. 485–490, 1998.

[25] J. Kučera, L. Binó, K. Štefková et al., "Apocynin and Diphenyleneiodonium induce oxidative stress and modulate PI3K/Akt and MAPK/Erk activity in mouse embryonic stem cells," *Oxidative Medicine and Cellular Longevity*, vol. 2016, Article ID 7409196, 14 pages, 2016.

[26] P. Carrero, K. Okamoto, P. Coumailleau, S. O'Brien, H. Tanaka, and L. Poellinger, "Redox-regulated recruitment of the transcriptional coactivators CREB-binding protein and SRC-1 to hypoxia-inducible factor 1alpha," *Molecular and Cellular Biology*, vol. 20, no. 1, pp. 402–415, 2000.

[27] T. Matsui, T. Kinoshita, T. Hirano, T. Yokota, and A. Miyajima, "STAT3 down-regulates the expression of cyclin D during liver development," *The Journal of Biological Chemistry*, vol. 277, no. 39, pp. 36167–36173, 2002.

[28] H. Kotasová, I. Veselá, J. Kučera et al., "Phosphoinositide 3-kinase inhibition enables retinoic acid-induced neurogenesis in monolayer culture of embryonic stem cells," *Journal of Cellular Biochemistry*, vol. 113, no. 2, pp. 563–570, 2012.

[29] H. Zhao, J. Joseph, H. M. Fales et al., "Detection and characterization of the product of hydroethidine and intracellular superoxide by HPLC and limitations of fluorescence," *Proceedings of the National Academy of Sciences of the United States of America*, vol. 102, no. 16, pp. 5727–5732, 2005.

[30] J. Zielonka, J. Vasquez-Vivar, and B. Kalyanaraman, "Detection of 2-hydroxyethidium in cellular systems: a unique marker product of superoxide and hydroethidine," *Nature Protocols*, vol. 3, no. 1, pp. 8–21, 2008.

[31] M. Kovarikova, J. Pachernik, J. Hofmanova, Z. Zadak, and A. Kozubik, "TNF-alpha modulates the differentiation induced by butyrate in the HT-29 human colon adenocarcinoma cell line," *European Journal of Cancer*, vol. 36, no. 14, pp. 1844–1852, 2000.

[32] K. Stefkova, J. Prochazkova, and J. Pachernik, "Alkaline phosphatase in stem cells," *Stem Cells International*, vol. 2015, Article ID 628368, 11 pages, 2015.

[33] N. R. D. Paling, H. Wheadon, H. K. Bone, and M. J. Welham, "Regulation of embryonic stem cell self-renewal by phosphoinositide 3-kinase-dependent signaling," *The Journal of Biological Chemistry*, vol. 279, no. 46, pp. 48063–48070, 2004.

[34] J. Mazumdar, V. Dondeti, and M. C. Simon, "Hypoxia-inducible factors in stem cells and cancer," *Journal of Cellular and Molecular Medicine*, vol. 13, no. 11-12, pp. 4319–4328, 2009.

[35] M. Albertoni, P. H. Shaw, M. Nozaki et al., "Anoxia induces macrophage inhibitory cytokine-1 (MIC-1) in glioblastoma cells independently of p53 and HIF-1," *Oncogene*, vol. 21, no. 27, pp. 4212–4219, 2002.

[36] P. Vaňhara, A. Hampl, A. Kozubík, and K. Souček, "Growth/differentiation factor-15: prostate cancer suppressor or promoter?," *Prostate Cancer and Prostatic Diseases*, vol. 15, no. 4, pp. 320–328, 2012.

[37] K. J. Woo, T.-J. Lee, J.-W. Park, and T. K. Kwon, "Desferrioxamine, an iron chelator, enhances HIF-1alpha accumulation via cyclooxygenase-2 signaling pathway," *Biochemical and Biophysical Research Communications*, vol. 343, no. 1, pp. 8–14, 2006.

[38] T. D. Barrett, H. L. Palomino, T. I. Brondstetter et al., "Pharmacological characterization of 1-(5-chloro-6-(trifluoromethoxy)-1H-benzoimidazol-2-yl)-1H-pyrazole-4-carboxylic acid (JNJ-42041935), a potent and selective hypoxia-inducible factor prolyl hydroxylase inhibitor," *Molecular Pharmacology*, vol. 79, no. 6, pp. 910–920, 2011.

[39] H. J. Kim, S.-J. Yang, Y. S. Kim, and T. U. Kim, "Cobalt chloride-induced apoptosis and extracellular signal-regulated protein kinase activation in human cervical cancer HeLa cells," *Journal of Biochemistry and Molecular Biology*, vol. 36, no. 5, pp. 468–474, 2003.

[40] S.-J. Yang, J. Pyen, I. Lee, H. Lee, Y. Kim, and T. Kim, "Cobalt chloride-induced apoptosis and extracellular signal-regulated protein kinase 1/2 activation in rat C6 glioma cells," *Journal of Biochemistry and Molecular Biology*, vol. 37, no. 4, pp. 480–486, 2004.

[41] S.-K. Lee, H.-J. Jang, H.-J. Lee et al., "p38 and ERK MAP kinase mediates iron chelator-induced apoptosis and -suppressed differentiation of immortalized and malignant human oral keratinocytes," *Life Sciences*, vol. 79, no. 15, pp. 1419–1427, 2006.

[42] A. Triantafyllou, P. Liakos, A. Tsakalof, E. Georgatsou, G. Simos, and S. Bonanou, "Cobalt induces hypoxia-inducible factor-1alpha (HIF-1alpha) in HeLa cells by an iron-independent, but ROS-, PI-3K- and MAPK-dependent mechanism," *Free Radical Research*, vol. 40, no. 8, pp. 847–856, 2006.

[43] X. Huang, J. Dai, C. Huang, Q. Zhang, O. Bhanot, and E. Pelle, "Deferoxamine synergistically enhances iron-mediated AP-1 activation: a showcase of the interplay between extracellular-signal-regulated kinase and tyrosine phosphatase," *Free Radical Research*, vol. 41, no. 10, pp. 1135–1142, 2007.

[44] M. Torres and H. J. Forman, "Redox signaling and the MAP kinase pathways," *BioFactors*, vol. 17, no. 1–4, pp. 287–296, 2003.

[45] D. Trachootham, W. Lu, M. A. Ogasawara, R.-D. V. Nilsa, and P. Huang, "Redox regulation of cell survival," *Antioxidants & Redox Signaling*, vol. 10, no. 8, pp. 1343–1374, 2008.

[46] N. S. Chandel, D. S. McClintock, C. E. Feliciano et al., "Reactive oxygen species generated at mitochondrial complex III stabilize hypoxia-inducible factor-1alpha during hypoxia: a mechanism of O_2 sensing," *The Journal of Biological Chemistry*, vol. 275, no. 33, pp. 25130–25138, 2000.

[47] Y. Liu, Y. Cui, M. Shi, Q. Zhang, Q. Wang, and X. Chen, "Deferoxamine promotes MDA-MB-231 cell migration and invasion through increased ROS-dependent HIF-1α accumulation," *Cellular Physiology and Biochemistry*, vol. 33, no. 4, pp. 1036–1046, 2014.

[48] C. Liu, Y. Shi, Z. Han et al., "Suppression of the dual-specificity phosphatase MKP-1 enhances HIF-1 trans-activation and increases expression of EPO," *Biochemical and Biophysical Research Communications*, vol. 312, no. 3, pp. 780–786, 2003.

[49] D. N. Slack, O. M. Seternes, M. Gabrielsen, and S. M. Keyse, "Distinct binding determinants for ERK2/p38alpha and JNK map kinases mediate catalytic activation and substrate selectivity of map kinase phosphatase-1," *The Journal of Biological Chemistry*, vol. 276, no. 19, pp. 16491–16500, 2001.

[50] A. Kucharska, L. K. Rushworth, C. Staples, N. A. Morrice, and S. M. Keyse, "Regulation of the inducible nuclear dual-specificity phosphatase DUSP5 by ERK MAPK," *Cellular Signalling*, vol. 21, no. 12, pp. 1794–1805, 2009.

[51] K. R. Laderoute, H. L. Mendonca, J. M. Calaoagan, A. M. Knapp, A. J. Giaccia, and P. J. Stork, "Mitogen-activated protein kinase phosphatase-1 (MKP-1) expression is induced by low oxygen conditions found in solid tumor microenvironments. A candidate MKP for the inactivation of hypoxia-inducible stress-activated protein kinase/c-Jun N-terminal protein kinase activity," *The Journal of Biological Chemistry*, vol. 274, no. 18, pp. 12890–12897, 1999.

[52] K. A. Seta, R. Kim, H. W. Kim, D. E. Millhorn, and D. Beitner-Johnson, "Hypoxia-induced regulation of MAPK phosphatase-1 as identified by subtractive suppression hybridization and cDNA microarray analysis," *The Journal of Biological Chemistry*, vol. 276, no. 48, pp. 44405–44412, 2001.

[53] S. Marchetti, C. Gimond, J.-C. Chambard et al., "Extracellular signal-regulated kinases phosphorylate mitogen-activated protein kinase phosphatase 3/DUSP6 at serines 159 and 197, two sites critical for its proteasomal degradation," *Molecular and Cellular Biology*, vol. 25, no. 2, pp. 854–864, 2005.

[54] O. Bermudez, G. Pages, and C. Gimond, "The dual-specificity MAP kinase phosphatases: critical roles in development and cancer," *American Journal of Physiology Cell Physiology*, vol. 299, no. 2, pp. C189–C202, 2010.

[55] D. A. Wassarman, N. M. Solomon, H. C. Chang, F. D. Karim, M. Therrien, and G. M. Rubin, "Protein phosphatase 2A positively and negatively regulates Ras1-mediated photoreceptor development in Drosophila," *Genes & Development*, vol. 10, no. 3, pp. 272–278, 1996.

[56] Y.-C. Kuo, K.-Y. Huang, C.-H. Yang, Y.-S. Yang, W.-Y. Lee, and C.-W. Chiang, "Regulation of phosphorylation of Thr-308 of Akt, cell proliferation, and survival by the B55alpha regulatory subunit targeting of the protein phosphatase 2A holoenzyme to Akt," *The Journal of Biological Chemistry*, vol. 283, no. 4, pp. 1882–1892, 2008.

[57] E. Sontag, S. Fedorov, C. Kamibayashi, D. Robbins, M. Cobb, and M. Mumby, "The interaction of SV40 small tumor antigen with protein phosphatase 2A stimulates the map kinase pathway and induces cell proliferation," *Cell*, vol. 75, no. 5, pp. 887–897, 1993.

[58] D. R. Alessi, N. Gomez, G. Moorhead, T. Lewis, S. M. Keyse, and P. Cohen, "Inactivation of p42 MAP kinase by protein phosphatase 2A and a protein tyrosine phosphatase, but not CL100, in various cell lines," *Current Biology*, vol. 5, no. 3, pp. 283–295, 1995.

[59] T. Sawa, T. Sasaoka, H. Hirai et al., "Intracellular signalling pathways of okadaic acid leading to mitogenesis in rat1 fibroblast overexpressing insulin receptors: okadaic acid regulates Shc phosphorylation by mechanisms independent of insulin," *Cellular Signalling*, vol. 11, no. 11, pp. 797–803, 1999.

[60] S. M. Hernández-Sotomayor, M. Mumby, and G. Carpenter, "Okadaic acid-induced hyperphosphorylation of the epidermal growth factor receptor. Comparison with receptor phosphorylation and functions affected by another tumor promoter, 12-O-tetradecanoylphorbol-13-acetate," *The Journal of Biological Chemistry*, vol. 266, no. 31, pp. 21281–21286, 1991.

[61] S. Ory, M. Zhou, T. P. Conrads, T. D. Veenstra, and D. K. Morrison, "Protein phosphatase 2A positively regulates Ras signaling by dephosphorylating KSR1 and Raf-1 on critical 14-3-3 binding sites," *Current Biology*, vol. 13, no. 16, pp. 1356–1364, 2003.

[62] S. Zimmermann, "Phosphorylation and regulation of Raf by Akt (protein kinase B)," *Science*, vol. 286, no. 5445, pp. 1741–1744, 1999.

[63] J. Zhang, X. Wang, V. Vikash et al., "ROS and ROS-mediated cellular signaling," *Oxidative Medicine and Cellular Longevity*, vol. 2016, Article ID 4350965, 18 pages, 2016.

[64] Y. Son, Y. Cheong, N. Kim, H. Chung, D. G. Kang, and H. Pae, "Mitogen-activated protein kinases and reactive oxygen species: how can ROS activate MAPK pathways?," *Journal of Signal Transduction*, vol. 2011, Article ID 792639, 6 pages, 2011.

[65] S. Di Meo, T. T. Reed, P. Venditti, and V. M. Victor, "Role of ROS and RNS sources in physiological and pathological conditions," *Oxidative Medicine and Cellular Longevity*, vol. 2016, Article ID 1245049, 44 pages, 2016.

[66] B. Marengo, M. Nitti, A. L. Furfaro et al., "Redox homeostasis and cellular antioxidant systems: crucial players in cancer growth and therapy," *Oxidative Medicine and Cellular Longevity*, vol. 2016, Article ID 6235641, 16 pages, 2016.

[67] R. Roskoski, "ERK1/2 MAP kinases: structure, function, and regulation," *Pharmacological Research*, vol. 66, no. 2, pp. 105–143, 2012.

[68] M. Á. Ramírez, E. Pericuesta, M. Yáñez-Mó, A. Palasz, and A. Gutiérrez-Adán, "Effect of long-term culture of mouse embryonic stem cells under low oxygen concentration as well as on glycosaminoglycan hyaluronan on cell proliferation and differentiation," *Cell Proliferation*, vol. 44, no. 1, pp. 75–85, 2011.

[69] H. F. Chen, H. C. Kuo, W. Chen, F. C. Wu, Y. S. Yang, and H. N. Ho, "A reduced oxygen tension (5%) is not beneficial for maintaining human embryonic stem cells in the undifferentiated state with short splitting intervals," *Human Reproduction*, vol. 24, no. 1, pp. 71–80, 2009.

[70] T. Matsuda, T. Nakamura, K. Nakao et al., "STAT3 activation is sufficient to maintain an undifferentiated state of mouse embryonic stem cells," *The EMBO Journal*, vol. 18, no. 15, pp. 4261–4269, 1999.

[71] P. Wu, D. Wu, L. Zhao, L. Huang, G. Shen, and J. Huang, "Prognostic role of STAT3 in solid tumors: a systematic review and meta-analysis," *Oncotarget*, vol. 7, no. 15, pp. 19863–19883, 2016.

[72] J. Yuan, F. Zhang, and R. Niu, "Multiple regulation pathways and pivotal biological functions of STAT3 in cancer," *Scientific Reports*, vol. 5, article 17663, 2015.

Hindawi
Oxidative Medicine and Cellular Longevity
Volume 2017, Article ID 4745252, 17 pages
https://doi.org/10.1155/2017/4745252

Research Article

Metabolic Reprogramming, Autophagy, and Reactive Oxygen Species Are Necessary for Primordial Germ Cell Reprogramming into Pluripotency

D. Sainz de la Maza, A. Moratilla, V. Aparicio, C. Lorca, Y. Alcaina, D. Martín, and M. P. De Miguel

Cell Engineering Laboratory, La Paz University Hospital Research Institute IDiPAZ, Madrid, Spain

Correspondence should be addressed to M. P. De Miguel; mariapdemiguel@gmail.com

Received 19 January 2017; Revised 7 April 2017; Accepted 25 May 2017; Published 5 July 2017

Academic Editor: Artur Cieślar-Pobuda

Cellular reprogramming is accompanied by a metabolic shift from oxidative phosphorylation (OXPHOS) toward glycolysis. Previous results from our laboratory showed that hypoxia alone is able to reprogram primordial germ cells (PGCs) into pluripotency and that this action is mediated by hypoxia-inducible factor 1 (HIF1). As HIF1 exerts a myriad of actions by upregulating several hundred genes, to ascertain whether the metabolic switch toward glycolysis is solely responsible for reprogramming, PGCs were cultured in the presence of a pyruvate kinase M2 isoform (PKM2) activator, or glycolysis was promoted by manipulating PPARγ. Conversely, OXPHOS was stimulated by inhibiting PDK1 activity in normoxic or in hypoxic conditions. Inhibition or promotion of autophagy and reactive oxygen species (ROS) production was performed to ascertain their role in cell reprogramming. Our results show that a metabolic shift toward glycolysis, autophagy, and mitochondrial inactivation and an early rise in ROS levels are necessary for PGC reprogramming. All of these processes are governed by HIF1/HIF2 balance and strict intermediate Oct4 levels. Histone acetylation plays a role in reprogramming and is observed under all reprogramming conditions. The pluripotent cells thus generated were unable to self-renew, probably due to insufficient *Blimp1* downregulation and a lack of Klf4 and cMyc expression.

1. Introduction

Primordial germ cells (PGCs) are the embryonic precursors of the gametes. Despite being unipotent stem cells, they share some common features with pluripotent stem cells (PSCs), such as constitutive expression of pluripotency factors *Oct4*, *Sox2*, *Lin28*, and *Nanog* [1–6], and stem cell markers stage-specific embryonic antigen 1 (SSEA1) and tissue-nonspecific alkaline phosphatase (TNAP). Functionally, PGCs are closely related to pluripotency, given that disruptions during their development can give rise to pluripotent, malignant embryonal carcinoma cells (ECCs) [3]. Furthermore, unipotent germ cells differentiate only into gametes but acquire totipotency through fertilization. Thus, germ cells are the only cells that undergo reprogramming under physiological conditions. Probably because of this, PGCs are easily reprogrammed toward pluripotent embryonic germ cells (EGCs) when cultured with basic fibroblast growth factor (bFGF) or trichostatin A (TSA) [7–9]. Previous work from our laboratory has shown that PGCs cultured under hypoxia can give rise to pluripotent cells, termed hypoxia-induced embryonic germ-like cells (hiEGLs), with hypoxia-inducible factor 1 (*HIF1*) α as a key factor in the metabolic switch toward glycolysis and subsequent *Oct4* deregulation [10].

In classical induced pluripotent stem cell (iPSC) generation with *Oct4*, *Sox2*, *cMyc*, and *Klf4* [11], reprogrammed cells also undergo metabolic reprogramming, shifting from oxidative metabolism toward a glycolytic phenotype [12, 13]. Moreover, several studies show that metabolic resetting is an active process that takes place during reprogramming [12–14] and that an increase in the expression of glycolytic genes precedes a similar increase in the expression of genes

that control self-renewal, suggesting that metabolic resetting has an active and early role in reprogramming. It has also been reported that inhibition of oxidative pathways is important to maintain pluripotency [15], and we demonstrated that hypoxia directly promotes cell reprogramming of in vivo committed cells [10]. This mechanism has also been observed in cancer cells and involves mitochondrial inactivation, which in turn renders low levels of reactive oxygen species (ROS), thus preventing oxidative damage [16, 17]. In fact, glycolysis stimulation or the addition of antioxidants such as ascorbic acid can enhance iPSC derivation [18, 19]. This metabolic shift, mitochondrial inactivation, and ROS clearance have also been observed in our hiEGL cultures when compared with nonreprogrammed PGCs [10]. These data propose a way to induce pluripotency by modifying cell metabolism. Our previous results clearly support this hypothesis and allow further characterization of the importance of cell energy metabolism in the reprogramming process.

2. Materials and Methods

Oct4-green fluorescent protein (GFP) mice from the C57BL\6 strain were used in this study. PGCs from 8.5 days post coitum (dpc) embryos were isolated and seeded onto a confluent monolayer of mitomycin C-treated Sandoz thioguanine- and ouabain-resistant (STO) cells. STO cells are immortalized mouse embryonic fibroblasts that display stem cell factor on their membrane, allowing for PGC attachment and survival.

The isolation and culture of PGCs were carried out as described in [3], and the medium was changed daily. Briefly, PGCs were cultured over nutritious mitomycin-treated STO cells in DMEM with 15% ES-qualified FBS and supplemented with LIF (Millipore) and SCF (R&D Systems), which are essential for PGC survival and proliferation but do not induce reprogramming, in normoxic or hypoxic (3% O_2) conditions, and exposed to soluble factors daily. Soluble factors were added in decreasing logarithmic concentrations according to the published literature to establish nontoxic ranges. Factors and final concentrations used were DASA at 0.1 μM, ciglitazone at 0.1 μM, dichloroacetate at 50 μM and 500 μM, 2-methoxyestradiol at 0.1 μM, resveratrol at 0.5 μM, chloroquine at 5 μM, spermidine at 1 μM, ascorbic acid at 50 μg/mL, and valproic acid at 5 mg/mL.

TNAP staining was performed as described in [3]. Colonies of 8 or more cells were regarded as reprogrammed PGCs. A *t*-test was then performed between experimental conditions with 3 technical replicates and at least 3 biological replicates.

Immunofluorescence was performed after fixation using 4% paraformaldehyde at pH 7.4. PGCs were identified by labeling for SSEA-1 (R&D Systems). Double staining together with molecules of interest was performed: phospho-pyruvate dehydrogenase (p-PDH) (Abcam), HIF1α (Abcam), HIF2α (Abcam), Nanog (Abcam), Klf4 (R&D Systems), cMyc (Santa Cruz Biotechnology), p62 (Abcam), p300 (R&D Systems), H2BacK20 (Abcam), H3acK9 (Abcam), and H4acK5K8,K12,K16 (Abcam). As controls, the mouse embryonic stem cell line E14Tg2a, monkey Cos7, human Hela, and mouse NIH3T3 cell lines were used. Images were obtained by confocal microscopy.

To show mitochondrial activity, flow cytometry was performed after addition of a mitochondrial JC-1 fluorescent probe or Cell ROX Green probe (Life Technologies) and subsequent fixation as previously described [10] or with live cells to simultaneously detect Oct4-GFP levels.

Cell sorting was also performed based on this design to isolate PGCs and to extract RNA for specific gene expression analysis, using the RNeasy Mini Kit (Qiagen). RNA was converted to cDNA using the High Capacity cDNA Reverse Transcription Kit (Applied Biosystems), which was then preamplified using TaqMan PreAmp Master Mix (Applied Biosystems) to reach enough of a sample before performing qPCR, using *β-actin* as the reference gene. Primers *PPAR* Forward 5′-3′: tggggatgtctcacaatgc, Reverse 3′-5′: tgggttcagctggtc gata, *Blimp* Forward 5′-3′: gtctgtgccaagacgttcg, Reverse 3′-5′: gaaaggccgttctccactg, *Bnip3* Forward 5′-3′: aaaacagcactctgtct gagga, Reverse 3′-5′: gcttcgggtgtttaaaaagga, *β-actin* Forward 5′-3′: ctgtattcccctccatcgtg, Reverse 3′-5′: aggagtccttctgacccattc. qPCR conditions were 10 min at 95°C and then 10 cycles of 15 s at 95°C and 4 min at 60°C in a Biometra TPersonal.

To demonstrate pluripotency, embryoid bodies (EBs) and three germ layer differentiation were obtained and demonstrated from reprogrammed PGCs as in [10]. The antibodies chosen were antialbumin (Dako) for endoderm, antivimentin (Dako) for mesoderm, and anticytokeratins AE1/AE3 (Dako) for ectoderm demonstration by immunofluorescence.

Electron microscopy was used for observing autophagic processes. PGCs and STO cells were cultured in Permanox-covered culture wells (Cultex) and embedded in epoxy resin. Standard ultrathin sections stained with uranyl and Pb were observed on an electron microscope. In addition, autophagic vacuoles were immunolabeled by anti-p62 antibody (Abcam), and confocal imaging and image analysis (ImageJ) were used to count the number of autophagic vacuoles in confocal stacks. At least 30 cells were counted per condition. Data are shown as number of autophagic vacuoles per whole cell.

Statistical significance in cultures was assessed by Student's *t*-test with Fisher modification in at least 3 separate experiments, each performed in triplicate. EBs and spontaneous differentiation were performed at least 3 times. Flow cytometry results were assessed by parametric F-Snedecor test analysis. All significances were considered at $p \leq .05$.

3. Results

3.1. Glycolysis Is Necessary but Not Sufficient for PGC Reprogramming. In a previous study, we demonstrated that hypoxia reprograms PGCs into pluripotency and that this action is mediated by *HIF1* [10]. Because HIF1 exerts a myriad of actions by upregulating several hundred genes, to ascertain if the metabolic switch toward glycolysis is solely responsible for reprogramming, we cultured PGCs in the presence of DASA, a pyruvate kinase M2 isoform (PKM2) activator. We thus hypothesized that an increase in the glycolytic flux would promote reprogramming. DASA was not able to mimic hypoxia in inducing PGC reprogramming (Figure 1(a)), suggesting that additional effects of HIF1 are required. However,

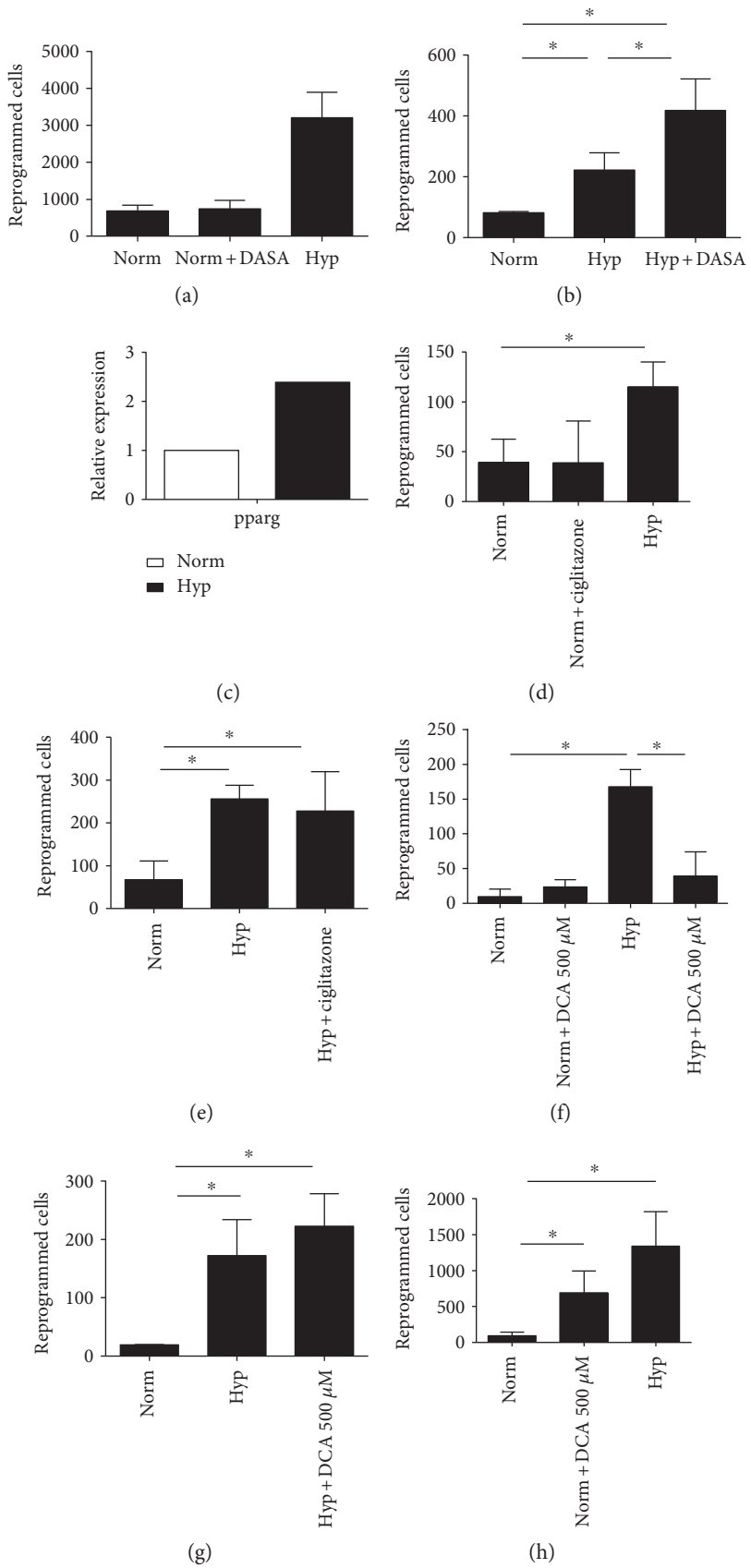

Figure 1: Continued.

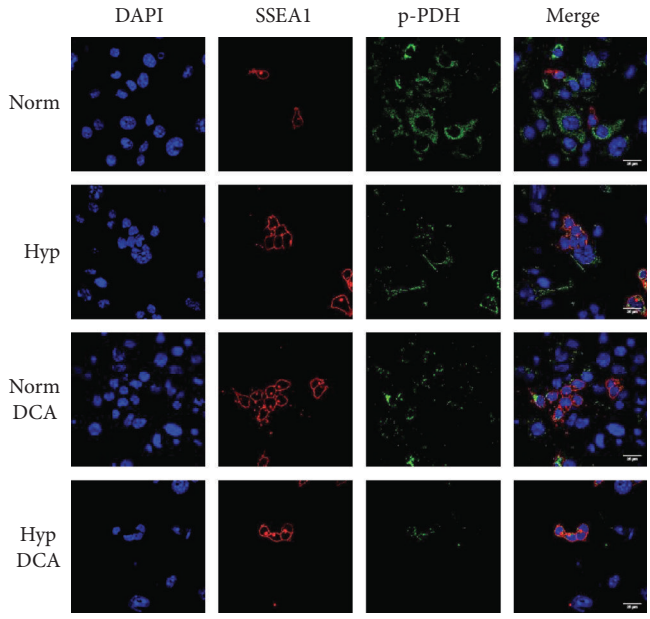

(i)

Figure 1: (a) Number of reprogrammed cells in PGC cultures supplemented with DASA (0.1 μM) for 7 days in normoxia. No differences are observed with respect to normoxia. (b) Number of reprogrammed cells in PGC cultures supplemented with DASA (0.1 μM) for 7 days in hypoxia. DASA causes a synergistic effect with hypoxia. (c) Relative expression of PPARγ in PGCs cultured under normoxia or hypoxia. Results are shown normalized with respect to normoxia. (d and e) Number of reprogrammed cells in PGC cultures supplemented with PPARγ agonist ciglitazone (0.1 μM) for 7 days in (d) normoxia or (e) hypoxia. No differences are observed by ciglitazone addition with respect to controls. (f) Number of reprogrammed cells in PGC cultures supplemented with DCA at a high dose (500 μM) for 7 days in normoxia and in hypoxia. DCA prevents hypoxia-induced reprogramming and it has no effect in normoxia. (g and h) Number of reprogrammed cells in PGC cultures supplemented with DCA at a low dose (50 μM) for 7 days. (h) DCA in normoxia is capable of reprogramming, (g) whereas it has no further effect in hypoxia. Asterisks show significance at $p < .05$. (i) Immunofluorescence against phosphorylated PDH (p-PDH) in normoxia (norm) and hypoxia (hyp) with and without 50 μM DCA for 4 days. From left to right: in blue, nuclei stained with DAPI; in red, PGCs detected as SSEA1$^+$ cells; in green, p-PDH. Scale bars represent 25 microns.

DASA exerted a synergistic effect together with hypoxic culturing (Figure 1(b)), suggesting that even in a glycolytic-prone metabolism promoted by hypoxia, an increase in the glycolytic flux further improves reprogramming efficiency.

Similarly, we then promoted glycolysis by manipulating *PPARγ*, a master regulator of metabolism. PPARγ can increase glucose uptake inducing GLUT4 expression, contributes to glycolysis initiation by inducing glucokinase expression, and inhibits the tricarboxylic acid cycle by enhancing pyruvate dehydrogenase kinase (*PDK*) 4 expression. Accordingly, we found an increase in PPARγ expression under hypoxia (Figure 1(c)), which indicates that a metabolic reprogramming is taking place during PGC reprogramming. The use of ciglitazone, a PPARγ agonist, in normoxia did not lead to PGC reprogramming (Figure 1(d)), indicating that PPARγ alone is unable to provoke a metabolic shift that, in turn, induces PGC reprogramming. Also, ciglitazone did not synergize with hypoxia (Figure 1(e)), consistent with the observed upregulation of *PPARγ* by hypoxia alone.

Conversely, we stimulated oxidative phosphorylation (OXPHOS) by inhibiting PDK1 activity in hypoxia by dichloroacetate, a PDK inhibitor. We hypothesized that inhibition of PDK would inhibit PGC reprogramming. As expected, dichloroacetate (DCA) impaired hypoxia-induced PGC reprogramming (Figure 1(f)), suggesting that a glycolytic metabolism is required for reprogramming, whereas it had no effect in normoxia (Figure 1(f)). Nonetheless, when a 10-time lower dose of DCA was used, no impairment of reprogramming in hypoxia was observed (Figure 1(g)), and most importantly, a significant increase in the number of reprogrammed cells was shown in normoxia (Figure 1(h)).

A possible explanation is that in low-DCA dose conditions, a glycolytic signature is observed in PGCs, as confirmed by the fact that in such cultures PDH is phosphorylated and thus inactive; thus, the low dose of 50 μM DCA does not inhibit PDK1, and p-PDH can still be found in cultures under normoxia or hypoxia in combination with DCA (Figure 1(i)).

We next investigated how a low dose of DCA induces reprogramming. First, we confirmed the pluripotent capacity of these cells by embryoid body generation and three germ layer spontaneous differentiations. Positive staining for the three germ layers proved that, as with hiEGLs, DCA-reprogrammed cells display pluripotency at least in vitro (Figure 2(a)).

We next explored the possible stabilization of HIF1 in DCA cultures. In fact, HIF1 was stabilized in PGCs by a low dose of DCA, similarly to hypoxic cultures (Figure 2(b)), revealing a possible and similar mechanism of PGC reprogramming by hypoxia and DCA.

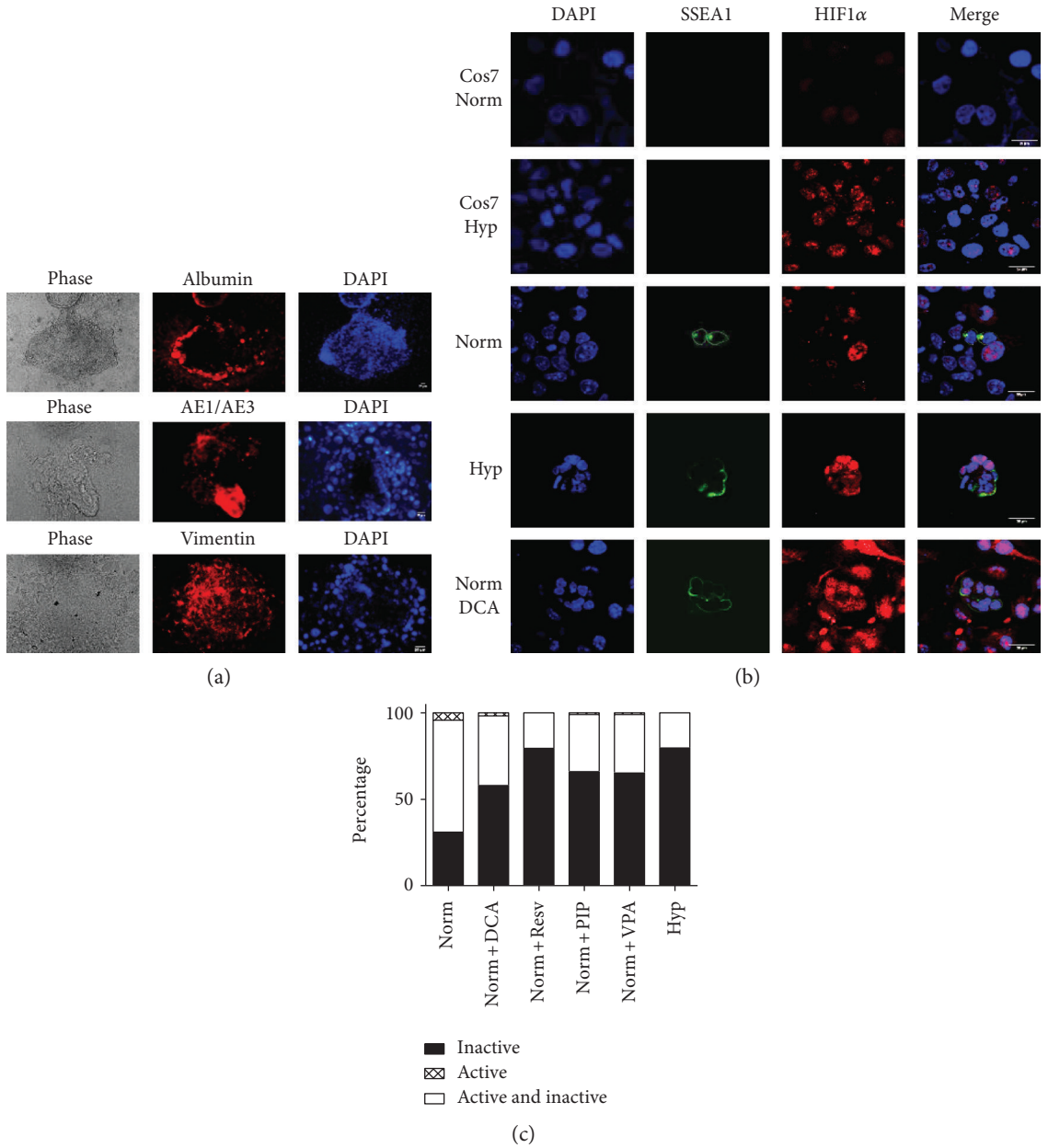

Figure 2: (a) EB formation and spontaneous differentiation of reprogrammed PGCs with a low dose of DCA (50 μM) in normoxia. The markers of endoderm, ectoderm, and mesoderm are, respectively, albumin, AE1/AE3 cytokeratins, and vimentin. Scale bars correspond to 25 μm. (b) Confocal microscopy images for immunofluorescence against SSEA1 and HIF1α in PGC cultures. Samples include Cos7 cells cultured in normoxic conditions as a negative control and in hypoxia as a positive control. Images also show PGCs cultured in normoxia (norm), hypoxia (Hyp), and dichloroacetate (50 μM) in normoxia (norm + DCA) for 48 h. Scale bars correspond to 25 μm. (c) Flow cytometry data of PGC cultures showing the percentage of SSEA1$^+$ cells displaying green signal from the JC-1 probe (inactive mitochondria), red signal (active mitochondria), or bivalent (both types). An increase in inactive mitochondria in detriment of bivalent mitochondria is observed in normoxia together with either low DCA dose (50 μM), resveratrol (0.5 μM), or VPA (5 mg/mL) and in hypoxia after 5 days with respect to normoxic cultures.

We hypothesized that HIF1 inhibition would impair PGC reprogramming under hypoxia. For that purpose, we used a HIF1 inhibitor, 2-methoxyestradiol (2-ME), expecting to see an impairment in reprogramming. The 2-ME showed no effect at low doses and shown to be toxic to PGCs at high doses (not shown), suggesting that HIF1 is essential not only for reprogramming but also for PGC survival in hypoxia.

We then explored the possible effects of a low dose of DCA in mitochondrial activity. In normoxia, most PGCs show both inactive and active mitochondria, followed by a large percentage of PGCs with inactive mitochondria and a minimal amount with active ones. Cells with DCA showed an increase in the percentage of inactive mitochondria with respect to normoxia, as demonstrated by JC-1 labeling and flow cytometry (Figure 2(c)). This decrease in mitochondrial

activity is related to the glycolytic signature of PGC metabolism under low DCA and points to the possible involvement of autophagic mechanisms in PGC reprogramming.

3.2. Autophagy Is Necessary but Not Sufficient for PGC Reprogramming. We next explored the possibility that autophagy, and specifically mitophagy, has a direct role in PGC reprogramming exerted by both hypoxia or normoxia and a low dose of DCA. In fact, *Bnip3*, a key regulator of mitophagy and a HIF1 target, demonstrated a 14-fold increased expression in hypoxia in comparison to normoxia by qRT-PCR (Figure 3(a)). As expected, we confirmed the presence of mitophagic vacuoles in normoxia and also in hypoxia and DCA conditions by electron microscopy (Figure 3(b)). DCA (and the rest of reprogramming conditions, see below) caused a slight increase in the number of p62-positive autophagic vacuoles at day 3 (Figures 3(c) and 3(d)), although it was not significant due to high SD between cells.

To demonstrate the role of autophagy in PGC reprogramming, we next prevented autophagy in PGC cultures subjected to hypoxia with the autophagy inhibitor chloroquine. In fact, hypoxia-induced reprogramming was prevented (Figure 3(e)), demonstrating that autophagy is required for reprogramming. When we induced autophagy with spermidine, no reprogramming was achieved (Figure 3(f)), suggesting that autophagy alone is not sufficient for PGC reprogramming.

However, when we induced mitophagy with resveratrol, reprogramming was achieved in normoxia (Figure 4(a)). Mitophagy was also observed by electron microscopy (Figure 4(b)), and the number of p62-positive autophagic vacuoles was slightly increased respect to normoxia at day 3 (Figures 3(d) and 4(c)). There was also an increase in the percentage of cells with inactive mitochondria, higher than that observed with DCA, and similar to that achieved under hypoxic conditions (Figure 2(c)). Pluripotency induction by resveratrol was also confirmed by EB formation and spontaneous differentiation into cells of the three germ layers (Figure 4(d)).

3.3. A Precise Level of ROS Is Required for PGC Reprogramming. In addition to inducing autophagy similarly to spermidine, resveratrol is also a potent antioxidant capable of reducing ROS levels. In fact, after 20 h of culture, we detected lower ROS levels in PGCs exposed to resveratrol with respect to normoxia, and also, we detected ROS in DCA-exposed cultures (Figure 4(d)). To explore the possibility of inducing pluripotency in PGCs by reducing ROS levels, we cultured PGCs in normoxia in the presence of the potent antioxidant ascorbic acid (vitamin C). The ascorbic acid did not have a reprogramming effect (Figure 4(e)), suggesting that the sole reduction of ROS is not capable of inducing reprogramming. However, when we tested whether ROS clearance could disrupt reprogramming, we observed that ascorbic acid is capable of preventing hypoxia-induced reprogramming (Figure 4(e)), suggesting that a specific level of ROS is necessary for PGC reprogramming. Also, in DCA-induced PGC reprogramming, ROS removal impaired the event of cell reprogramming as well (Figure 4(f)), further supporting our hypothesis that a rise in ROS is necessary for reprogramming.

In addition to its mitophagy induction and antioxidant and ROS clearance actions, resveratrol also induces sirtuins, which in turn might stabilize HIF1, and thus the rest of HIF1 actions. In fact, HIF1 immunofluorescence in resveratrol-cultured PGCs demonstrated HIF1 stabilization (Figure 4(g)). Thus, resveratrol induces pluripotency in PGCs by simultaneously acting on mitophagy, ROS levels, and glycolysis induction via HIF1a stabilization.

3.4. PGC Reprogramming Pathways Converge in HIF1 Stabilization and Oct4 Deregulation. In PGC hypoxic cultures, HIF1 stabilization promotes deregulation of Oct4 levels, which in PGCs are already high, lowering them to promote reprogramming [10]. To ascertain whether reprogramming in normoxia by low DCA and resveratrol uses the same mechanism, we performed flow cytometry for Oct4-GFP in such cultures (Figure 5(a)). In fact, both DCA and resveratrol showed a similar pattern of Oct4 expression to hypoxia and statistically different from normoxia, suggesting that the same Oct4 deregulating mechanism is being used.

Because HIF2 has been described to be the HIF responsible for Oct4 regulation, we studied the expression of HIF2 in our PGC cultures in order to ascertain whether the HIF1/HIF2 equilibrium could be responsible for PGC reprogramming. HIF2 expression was found in all the conditions studied, even in normoxia (Figure 5(b)), suggesting that HIF1 is responsible for PGC reprogramming. Interestingly, both HIF1 and HIF2 expression disappeared after 6 days in every condition studied (not shown).

We also studied the possible effects of the reprogramming factors in *Nanog* expression, given that *Nanog* has been demonstrated to be a master regulator of pluripotency that is also expressed in PGCs. Nanog was expressed in every condition studied, as expected (Figure 5(c)), adding to the evidence that reprogramming toward pluripotency has been achieved. These results also agree with the reduction of Blimp1 expression, a gene related to germ cell identity that downregulates in hypoxia-induced reprogramming (not shown).

Similarly to hypoxia, DCA and resveratrol did not induce self-renewal in induced PGCs, leading to the generation of a stable cell line. For that reason, we investigated the expression of Klf4 and cMyc in cultures under DCA and resveratrol. Neither factor was able to upregulate either gene (Figures 6(a) and 6(b)), providing an explanation for the lack of self-renewal of the reprogrammed cells similar to hypoxia.

3.5. Epigenetic Control of PGC Reprogramming. To characterize the implication of epigenetics in the reprogramming with DCA and resveratrol in normoxic conditions, *p300* (*CREB-binding protein-CBP-coactivator*) acetyltransferase expression was investigated. p300 was expressed in the PGCs' nuclei in all reprogramming conditions (Figure 7). Actual histone acetylation was evaluated by immunocytochemistry against H2BacK20, H3acK9, and H4acK5K8,K12,K16. Our results show that whereas histones H2B, H3, and H4 are nonacetylated in normoxic PGCs, they become acetylated both in

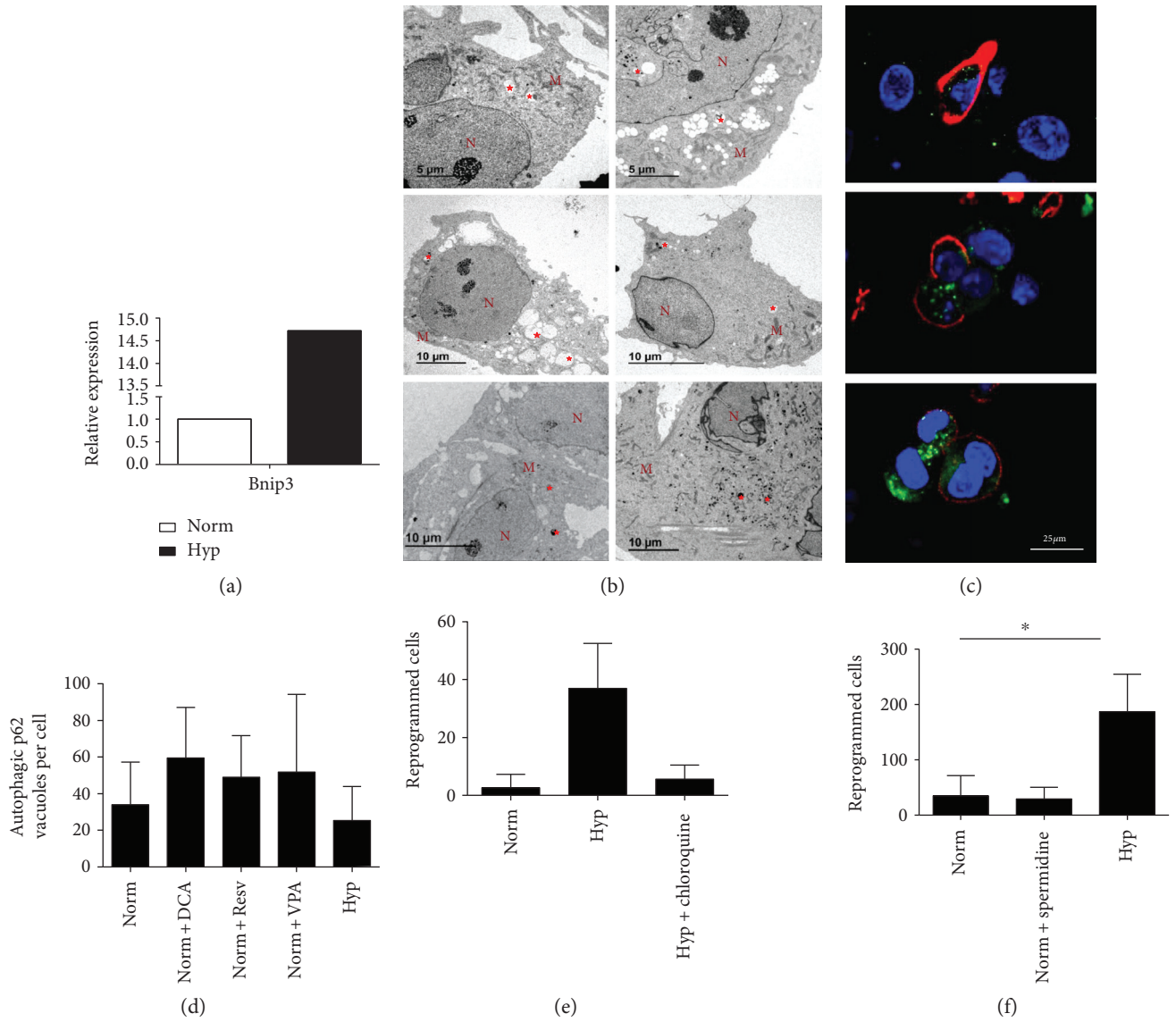

FIGURE 3: (a) Relative expression of *Bnip3* gene carried out by quantitative PCR from PGCs cultured under normoxia or hypoxia. Results are shown normalized with respect to normoxia. (b) Electron microscopy photographs of PGCs in normoxia (top row), hypoxia (second row), and normoxia with 50 μM DCA (bottom). Left column day 3 and right column day 6 cultures. Autophagic vacuoles are labeled with red stars. M: mitochondria. N: nucleus. (c) Confocal microscopy merge images for immunofluorescence against SSEA1 in red (PGCs) and p62 autophagic vacuoles in green in cytoplasms of PGC cultures subjected to normoxia (top row), hypoxia (second row), and normoxia with 50 μM DCA (bottom) for 3 d. Nuclei are seen in blue with DAPI. Scale bars correspond to 25 μm. (d) Quantification of p62-positive autophagic vacuoles in confocal stacks shows a nonstatistically significant increase with respect to normoxia. (e) Inhibition of autophagy with chloroquine (5 μM) for 7 days prevents hypoxia-induced reprogramming. (f) Induction of autophagy with spermidine (1 μM) in normoxia for 7 days does not induce reprogramming. Asterisks show significance at $p < .05$.

normoxic DCA and resveratrol-supplemented cultures as early as 48 h of treatment (Figure 7).

As histone acetylation was positive in all the reprogramming conditions in normoxia, and also in hypoxia alone, we explored the possibility that manipulation of histone acetylation was in fact capable of reprogramming directly. We made use of valproic acid (VPA), a wide histone deacetylases inhibitor. We demonstrate that VPA is capable of PGC reprogramming in normoxia (Figure 8(a)), whereas no further effect was seen in hypoxic conditions (Figure 8(a)). Reprogramming toward pluripotency was characterized by EB formation (Figure 8(b)). Similarly to DCA and resveratrol, Oct4 expression levels were also altered by VPA (Figure 5(a)). Mitochondrial activity was diminished as well with respect to normoxia (Figure 2(c)). HIF1 and HIF2 expression were confirmed as well (Figure 8(c)). VPA-treated cultures were positive for Nanog and negative for Klf4 expression as assessed by immunofluorescence (Figure 8(c)). Interestingly, VPA-treated cultures were positive for cMyc (Figure 8(c)). Autophagy was also slightly increased at day 3 as shown by electron microscopy (Figure 8(d)) and p62 immunolabeling (Figure 8(e)) and quantification of autophagic vacuoles (Figure 3(d)).

4. Discussion

Our results show that a mere soluble factor is able to induce acquisition of pluripotency in PGCs, as we had previously shown using only hypoxia [10]. Previous work from our laboratory showed that PGCs and EGCs display a differential expression profile, which differs in energetic metabolism genes [10]. Our results indicated an essential role of *HIF1* in PGC reprogramming, due to direct metabolic reprogramming that drives pluripotency acquisition. It is known that HIF1 induces the glucose transporter (GLUT), *pyruvate dehydrogenase kinase 1*, *lactate dehydrogenase A*, and *hexokinase* expression [20–26]. HIF stabilization through prolyl hydroxylase inhibition was sufficient to induce PGC reprogramming [10]. Our results show that PKM2 activation using soluble factor DASA and the consequent boost in glycolytic flux promote a higher number of reprogrammed cells in hypoxia, but not in normoxia. *PKM2* expression can be enhanced by HIF1 or PPARγ [27, 28], thus it is probable that a PKM2 activation in hypoxia (in which it is likely that PKM2 is operating and where there certainly is a glycolytic profile) contributes to more reprogramming. On the other hand, HIF1 absence in normoxia is not able to induce *PKM2* expression or glycolytic profile establishment, which makes PKM2 activation useless.

Regarding *PPARγ*, we also found no effect of the agonist ciglitazone on PGC reprogramming. *PPARγ* is a direct target of HIF1 and vice versa; therefore, *PPARγ* and *HIF1* might establish a positive loop that could cause an enhancement of glycolysis. However, in normoxic conditions in which no HIF1α is detected, PPARγ would be incapable of creating a glycolytic profile. Our data showing that a PPARγ agonist does not improve PGC reprogramming in hypoxia could indicate that the metabolic circuit had already been established through HIF1 activity and PDH inhibition. Thus, enhancement of PPARγ activity would have no effect on PGC reprogramming.

Taking into account that *PDK1* is a HIF1 target, it appears likely that hypoxia-induced HIF1α expression provokes metabolic reprogramming in low-oxygen conditions [10, 22, 23]. This same observation has been found in DCA- and resveratrol-induced reprogramming in this study. However, it is rather surprising that DCA, a *PDK1* inhibitor, induces PGC reprogramming. In particular, this effect is unexpected because *PDH* inhibition through *PDK1* action is one of the characteristics of PGC reprogramming [10]. In fact, *OSKM* induction results in an increase of *PDK1* expression in other cell types [29]. There are many examples in which DCA causes a metabolic shift toward glycolysis, leading to stem cell differentiation, a decrease in iPSC derivation efficiency, or cancer cell apoptosis [12, 30–32]. Our results also show that a high DCA dose provokes an inhibition of PGC reprogramming. However, a low DCA dose maintains a glycolytic profile, as supported by immunofluorescence and flow cytometry analysis, and induces PGC reprogramming, demonstrated by three germ layer differentiation. A plausible explanation is that at the low concentration, DCA is not inhibiting *PDK1* but is exerting another crucial event in PGC reprogramming. In fact, different cell types do not react identically to DCA addition. For instance, glioma cancer stem cells are DCA sensitive, showing an oxidative metabolic profile that causes their differentiation and death, whereas neural stem cells do not show this behavior [32, 33]. DCA can even induce an increase in proliferation, as observed in neuroblastoma cells in a mouse xenograft model [34]. Interestingly, DCA induces a greater *Oct4*/*PKM2* interaction [32], indicating that DCA might directly contribute to lower Oct4 levels, which might in turn promote reprogramming.

Autophagy is required for iPSC derivation, although there are discrepancies concerning the molecular pathway involved. It has been reported that a transitory *Sox2* overexpression takes place during the first days of reprogramming, leading to canonical autophagy induction, with Atg5 and LC3-II as major regulators. It has also been reported that pluripotency induction in cells lacking *Atg5* shows a reprogramming impairment [35]. However, another study established that this impairment could be reversed, augmenting *OSKM* expression, and that the essential pathway was Atg5-independent, relied on *Rab9* and *sintaxin 7*, and included AMP-kinase (AMPK) activation, endoplasmic reticulum autophagy, and mitophagy [36, 37].

PGC reprogramming shares aspects of both hypotheses. PGCs and hiEGLs are Sox2 positive, which is necessary for autophagy. In addition, HIF1 induces *Bnip3* expression, which in turn inhibits mTORC1 binding Rheb, an mTOR activator. Thus, Bnip3 triggers autophagy [38]. Our results show an important increase in *Bnip3* expression in hypoxia, which likely inhibits *mTOR* and induces autophagy. However, resveratrol's mechanism of action occurs through Sirt1 activation, an NAD^+-dependent deacetylase [39, 40]. Because spermidine addition did not show an effect in PGC reprogramming and the resveratrol and spermidine pathways share *Atg5*, *Atg7*, and *LC3* deacetylation [41, 42], it appears likely that the autophagy observed in PGC reprogramming does not take place through the canonical pathway.

Inhibition of autophagy using chloroquine diminished the number of reprogrammed cells, indicating the importance of autophagy in PGC reprogramming. It appears logical that the energetic stress and metabolic reprogramming that takes place during PGC culture in hypoxia drives a rearrangement of cellular structures in order to adapt to a new environment; in fact, we have observed mitophagy by electron microscopy not only in hypoxia but also with DCA and resveratrol. Mitophagy logically provokes lower ROS production and, consequently, prevents cell death [43, 44]. It has been reported that autophagy inhibition in cells overexpressing Bnip3 causes cell death, given that these cells are incapable of generating, in turn, their protective response [44]. Because Sirt1 can deacetylate *forkhead box O3* (*FOXO3*), which in turn induces *Bnip3* expression [45], it is probable that resveratrol-induced autophagy occurs through this pathway. In fact, this mechanism has already been observed in rat kidney cells [46].

PPARγ is also important in autophagy induction. Apart from its role in energetic metabolism triggering *PKM2* expression, *PPARγ* can induce autophagy [47]. PPARγ levels are also oxygen dependent, given that it is a HIF1 direct

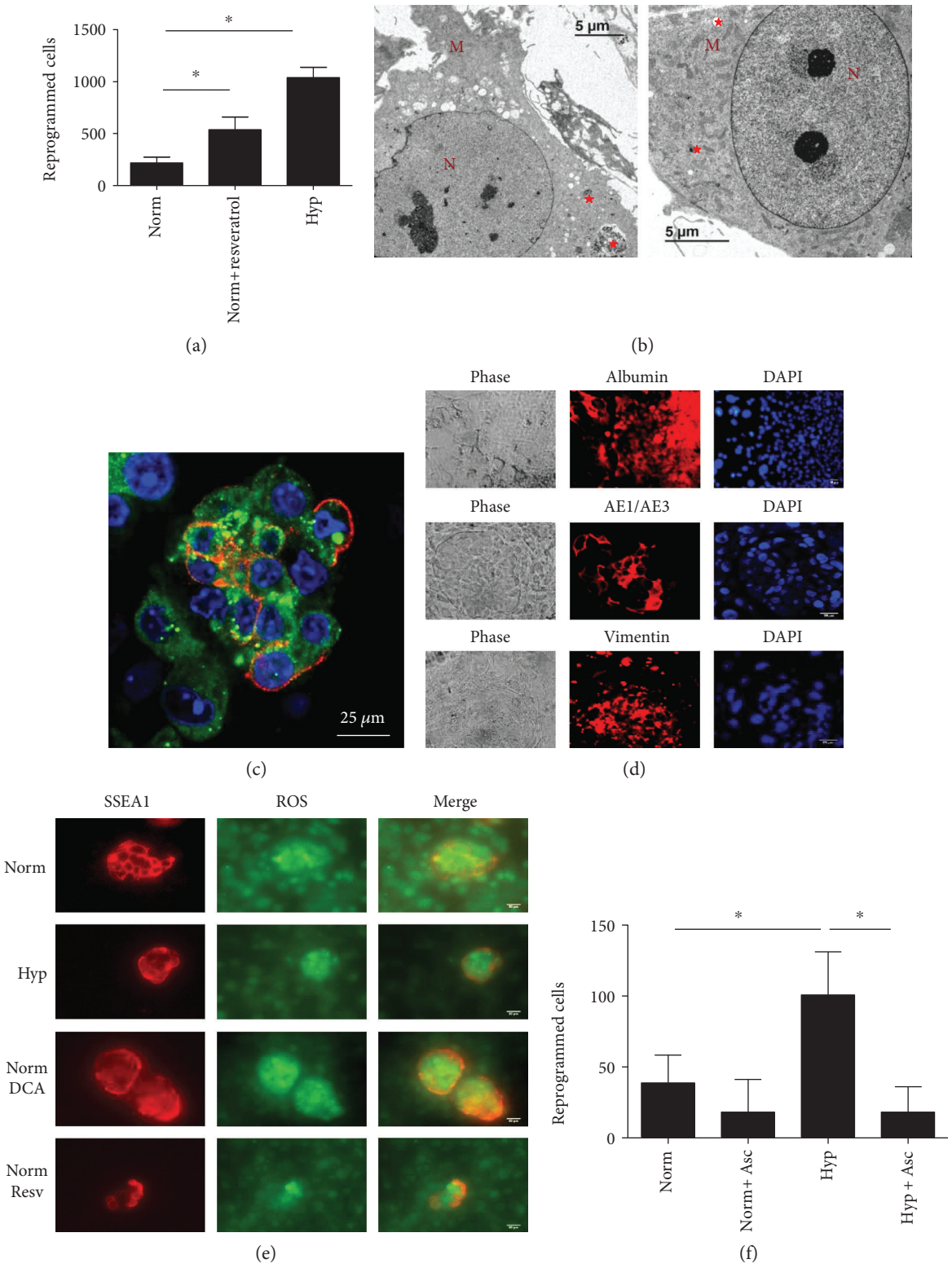

Figure 4: Continued.

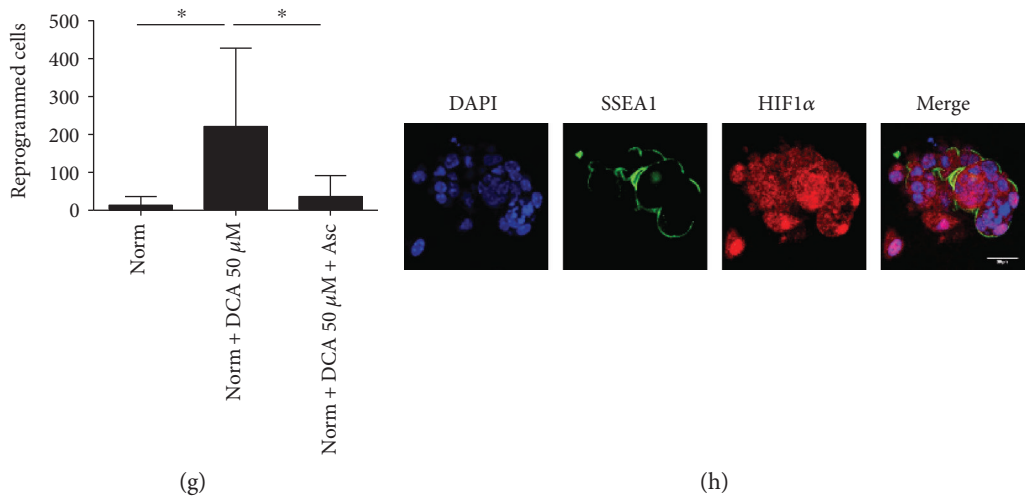

Figure 4: (a) Number of reprogrammed PGCs in conditions of normoxia, normoxia and resveratrol (0.5 μM), and hypoxia for 7 days. Resveratrol induces PGC reprogramming. Asterisks show significance at $p < .05$. (b) Electron microscopy photographs showing 0.5 μM resveratrol-induced mitophagy at day 3 (left) and day 6 (right). Autophagic vacuoles are labeled with red stars. M: mitochondria. N: nucleus. (c) Confocal microscopy merge image for immunofluorescence against SSEA1 in red (PGCs) and p62 autophagic vacuoles in green in PGC cytoplasms of cultures subjected to normoxia with 0.5 μM resveratrol for 3 d. Nuclei are seen in blue with DAPI. Scale bars correspond to 25 μm. (d) Embryoid body formation and spontaneous differentiation of reprogrammed cells into cells of the three germ layers by resveratrol (0.5 μM). (e) Immunofluorescence images of ROS levels in PGC (SSEA1+) cultures exposed to normoxia, hypoxia, normoxia and low DCA dose (50 μM), and normoxia and resveratrol (0.5 μM) for 20 h. Scale bars correspond to 20 μm. (f) Number of reprogrammed PGCs in conditions of normoxia, normoxia and ascorbic acid (50 μg/mL), hypoxia, and hypoxia and ascorbic acid (50 μg/mL), for 7 days. Ascorbic acid does not induce reprogramming in normoxia and prevents hypoxia-induced reprogramming. (g) Number of reprogrammed PGCs in conditions of normoxia, normoxia and DCA (50 μM), normoxia and DCA (50 μM), and ascorbic acid (50 μg/mL) for 7 days. Ascorbic acid prevents reprogramming induced by DCA. Asterisks show significance at $p < .05$. (h) Confocal microscopy images for immunofluorescence against SSEA1 and HIF1α in PGC cultures subjected to resveratrol for 48 h. Controls are the same as in Figure 2(b). Scale bars correspond to 25 μm.

target [48]. Among PPARγ targets are *HIF1α*, *PDK*, and *Bnip3* [28, 47, 48]. Thus, the observed increase in *PPARγ* in PGCs cultured in hypoxia, added to an increase in *Bnip3* expression, an increase in PDK activity and HIF1 stabilization, could establish an axis responsible for fixing a metabolic profile in which autophagy and mitophagy are essential to the adaptation to hypoxia. These observations agree with other studies in which hypoxia-induced and PPARγ-induced autophagy required HIF1α [47, 49].

In terms of ROS, metabolic reprogramming in response to low oxygen levels prevents ROS generation from mitochondria as a result of OXPHOS [17]. Pluripotent stem cells show reduced ROS levels, preventing oxidative stress [16]. Ascorbic acid addition to the culture medium enhances iPSC induction using *OSK* and *OSKM*, whereas resveratrol did not show any effect [19]. Our results fit with these facts, because PGCs cultured in hypoxia show lower levels of ROS compared with those in normoxia after 3 days in culture [10]. However, ROS removal is not sufficient to induce PGC reprogramming, as shown in ascorbic acid experiments, but probably contributes to PGC survival in hypoxia. However, ROS might play another role in PGCs. Specifically, our study suggests that a transient and small increase in ROS in DCA cultures might stabilize HIF1α, consequently inducing PGC reprogramming. Once HIF1α is stabilized, it would induce a metabolic reprogramming, which is shown by PDH inactivation and inactive mitochondria. This peak in ROS production has also been observed in iPSC generation from human fibroblasts, immediately before HIF1 stabilization. In this case, ROS increase induces an elevation in the expression of *nuclear factor-* (*erythroid-derived 2-*) *like 2 (NRF2)*, a master regulator of response against ROS production that promotes a metabolic shift toward glycolysis via *HIF1* [50].

With respect to the epigenetic control of reprogramming, our present results show that *CREB-binding protein* (*CBP*) coactivator, p300, is not expressed in the PGCs' nuclei in normoxic cultures whereas it becomes expressed in all the reprogramming conditions after 48 h of culture. Similarly, acetylation of histones appears evident in all reprogramming conditions + normoxia and in hypoxia alone as early as after 48 h of treatment. In fact, histone acetylation has a close implication in PGC reprogramming. Similar to our results with VPA that reprograms PGCs even in normoxia in the absence of bFGF, another histone deacetylase (HDAC) inhibitor, trichostatin A (TSA) can reprogram PGCs into pluripotent EGCs also in the absence of bFGF [9]. HDAC inhibitors have been widely used in the field of cell reprogramming, since their addition to culture increases the efficiency. Specifically, VPA has been shown to display this mentioned improvement in the arising of iPSCs, even making *Klf4* and *cMyc* dispensable from the reprogramming cocktail [51], by reducing senescence of reprogrammed cells [52]. However, *CBP*-specific knockout in PGCs did not alter their histone acetylation levels [53], suggesting that histone

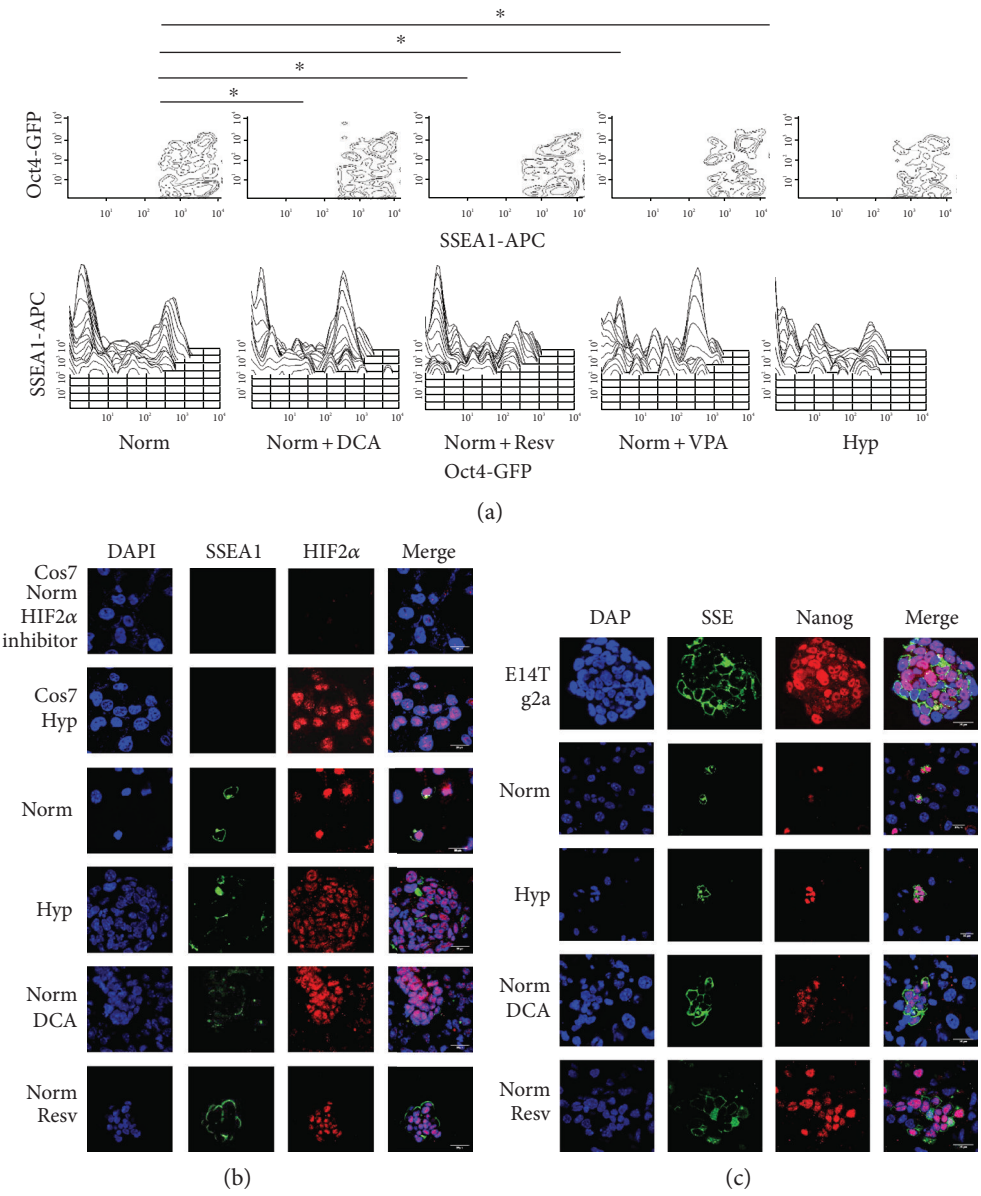

Figure 5: (a) Oct4-GFP flow cytometry in PGC cultures under normoxia, normoxia and 50 μM DCA, normoxia and 0.5 μM resveratrol, normoxia and 5 mg/mL VPA, and hypoxia for 4 days. Normoxic cultures show two separate populations with high and low Oct4-GFP levels, whereas reprogramming cultures under normoxia with DCA, resveratrol and VPA, and hypoxia show a statistically significant appearance of a population with intermediate Oct4 levels. Asterisks show significance at $p < .05$. (b) HIF2 immunofluorescence in normoxic, hypoxic, normoxia + DCA (50 μM), and normoxia + resveratrol (0.5 μM) cultures showing positive reaction in SSEA1+ cell (PGC) nuclei under every condition. (c) Nanog immunofluorescence in normoxic, hypoxic, normoxia + DCA (50 μM), and normoxia + resveratrol (0.5 μM) cultures showing positive reaction in SSEA1+ cell (PGC) nuclei under every condition.

acetylation in PGCs is dependent on other histone acetylases different than *CBP*. In addition to their histone acetylation properties, *CBP*/*p300* exerted an antiapoptotic effect in PGCs in vivo [53]. In our cultures, p300 expression could aid in the survival of reprogramming cells.

It is remarkable that distinct pathways that lead to reprogramming share *HIF1α* expression as a common feature. All reprogrammed cells show HIF1α protein stabilization after 48 h of culture, turning into HIF1α negative at approximately the sixth day of culture. Because PGCs in normoxia are always negative for HIF1α, this molecule appears to be essential for PGC reprogramming. In fact, iPSC derivation through *OSKM* induction is impaired if HIF1α is absent [29]. Also, ectopic expression of *HIF1α* during the reprogramming process promotes appearance of iPSC colonies [54]. In our experimental model, HIF1 is essential for both reprogramming and survival of PGCs in hypoxia. This observation might indicate that adaptation of PGCs to hypoxia involves metabolic reprogramming and cellular rearrangement through autophagy. Our results in all reprogrammed

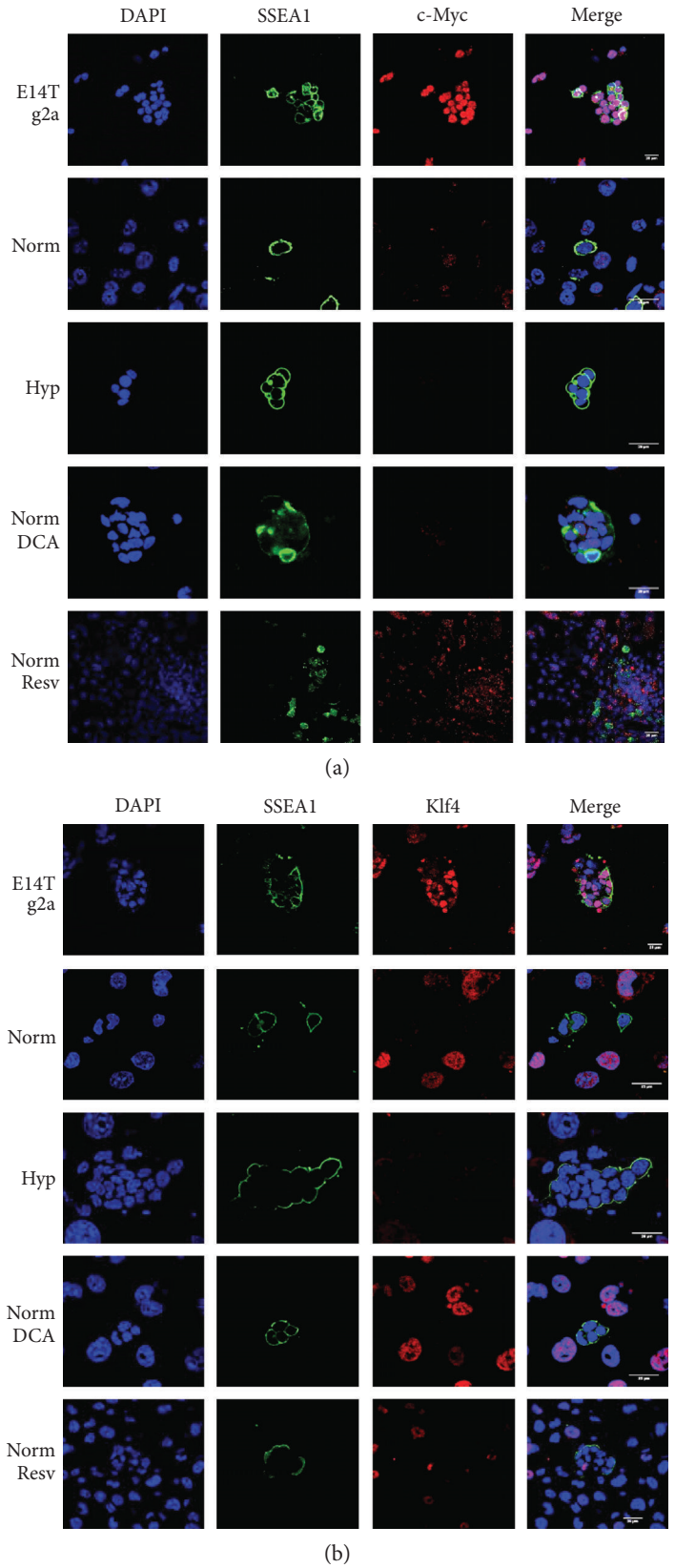

Figure 6: (a) cMyc immunofluorescence in normoxic, hypoxic, normoxia + DCA (50 μM), and normoxia + resveratrol (0.5 μM) cultures showing lack of reaction in SSEA1+ cell (PGC) nuclei under every condition. (b) Klf4 immunofluorescence in normoxic, hypoxic, normoxia + DCA (50 μM), and normoxia + resveratrol (0.5 μM) cultures showing negative reaction in SSEA1+ cell (PGC) nuclei under every condition. Positive controls are the ES cell line E14Tg2. Scale bars correspond to 25 μm.

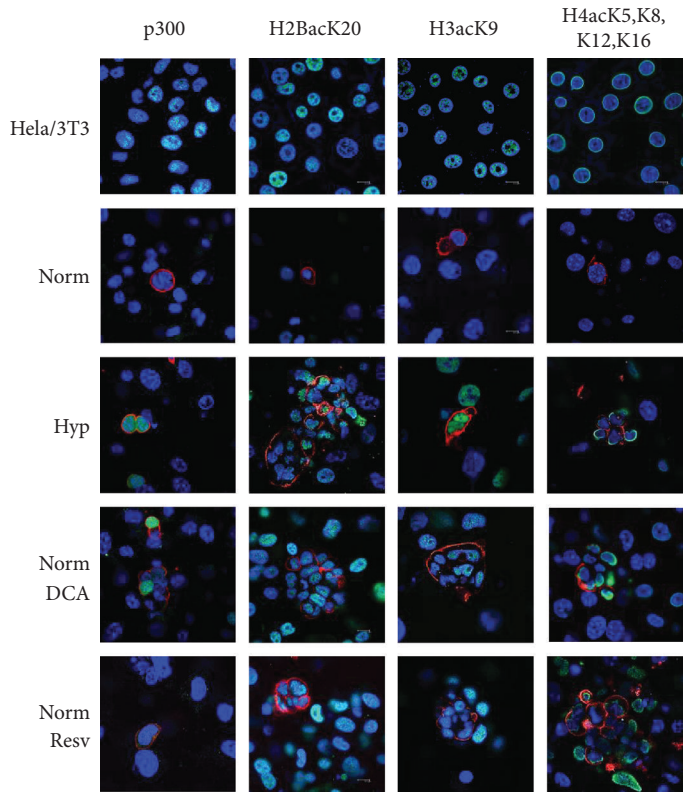

Figure 7: Confocal merge images of p300, H2BacK20, H3acK9, and H4acK5K8,K12,K16 immunofluorescence (in green in the nuclei) in normoxic, hypoxic, normoxia + DCA, and normoxia + resveratrol cultures, showing positive reaction in SSEA1+ cells (PGCs, membranes in red). Blue shows nuclei with DAPI stain. Colocalization is seen as light blue. p300 and histone acetylations were negative in the nuclei of normoxic SSEA1+ cells (PGCs) and positive under reprogramming conditions (DCA at 50 μM and resveratrol at 0.5 μM, all conditions maintained for 48 h). Positive controls are the human untreated Hela cell line for p300 and the NIH3T3 mouse cell line subjected to the histone deacetylase inhibitor Na^+ butyrate at 0.25 μM for 16 hours for histone acetylations. Scale bars correspond to 100 μm in every photograph.

cells show a predominance of inactive mitochondria and observation of autophagic events. Our data also show that HIF1α is lost at approximately the sixth day of culture, indicating that metabolic reprogramming has been fulfilled by that time and HIF1α is then downregulated. Similarly, transient expression of HIF1α has also been reported in human embryonic stem cells (ESCs) cultured in hypoxia, where it only lasts for 48 h [55].

Regarding *HIF2α*, its expression was shown to be constitutive in PGCs, given that it is detectable from the beginning of the culture, even in PGCs cultured in normoxia. This observation is not surprising, considering that PGCs are the only cell type that retains Oct4 expression in 8.5 dpc embryos and that the transcription factor responsible for that expression is *HIF2* [56]. *HIF2α* is also involved in *Sox2* and *Nanog* expression, both of which are present in PGCs [55]. HIF2α is absent from the sixth day of culture in all reprogrammed cells. In agreement, it has been reported that *HIF2α* overexpression favors iPSC derivation if this overexpression takes place during the early phase of reprogramming and it exerts an inhibitory effect if it occurs in later phases [54]. On the other hand, human ESCs maintain the nuclear location of HIF2α for a longer time and cells deficient for *HIF2α* are unable to proliferate and cannot be maintained in culture [55]. This loss of HIF2α might explain the lack of self-renewal in our reprogrammed cells. We propose that *HIF1α* induction alters *HIF1*/*HIF2* balance and, once metabolic reprogramming has been accomplished, HIF2α does not reach its previous levels and reprogrammed cells fail to establish self-renewal. This HIF2 impairment might be the cause behind the heterogeneous Oct4 pattern and the rise of Oct4 low populations that enter the reprogramming process. It has recently been reported that it is a reduced Oct4 expression that directs a robust pluripotent state in ESCs [57] and that a higher range of Oct4 levels in ESCs causes heterogeneity in Nanog expression. This idea is also supported by redefinition of the low *Oct4* levels required for pluripotency entry as well as the higher *Oct4* levels required for differentiation [58]. Our data show that hypoxia, low DCA, resveratrol, and VPA induce a wider range of Oct4 levels in PGCs, accounting both for pluripotency induction and differentiation-prone colony formation. This HIF balance could also be involved in the cMyc negativity in our reprogrammed cells, given that *HIF1α* and *cMyc* compete for *Sp1* cofactor binding, whereas *HIF2α* allows *cMyc*/*Sp1* binding [59]. As shown in the results, we hypothesize that the lack of Klf4 and cMyc observed in the reprogrammed cells (except VPA where cMyc is positive) is responsible for this inability to self-renew. In turn, this lack of expression might be also

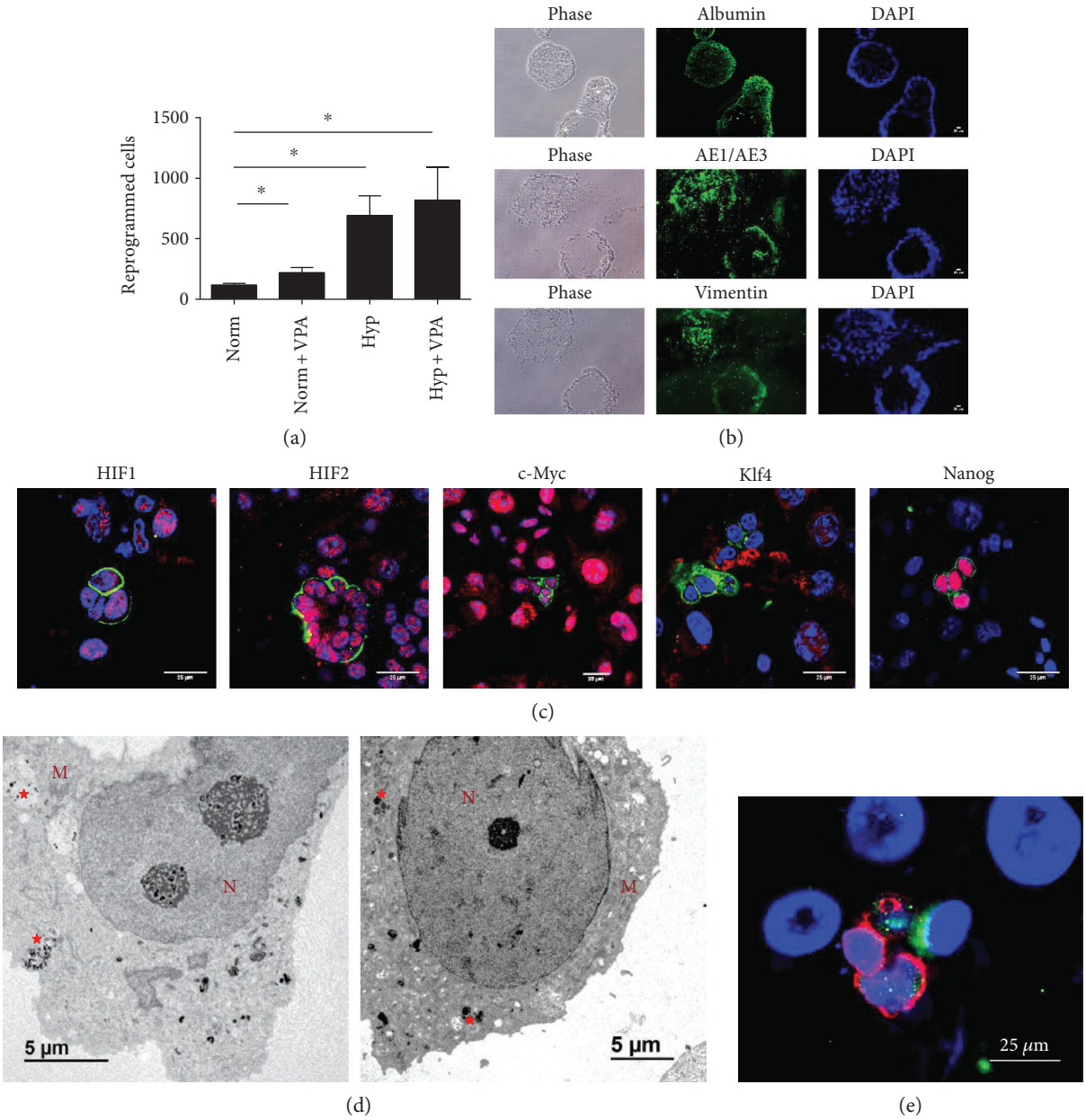

Figure 8: (a) Number of reprogrammed PGCs in conditions of normoxia, normoxia and valproic acid (VPA), hypoxia, and hypoxia and VPA (5 mg/mL) for 7 days. VPA induces PGC reprogramming in normoxia but does not synergize with hypoxia. Asterisks show significance at $p < .05$. (b) EB formation and spontaneous differentiation of reprogrammed cells into cells of the three germ layers by VPA in normoxia (5 mg/mL). Markers of endoderm, ectoderm, and mesoderm are, respectively, albumin, AE1/AE3 cytokeratins, and vimentin. Scale bars correspond to 25 μm. (c) Confocal microscopy merge images for immunofluorescence against SSEA1 in green (PGCs), and HIF1α, HIF2α, cMyc, Klf4, and Nanog in red in nuclei of PGC cultures subjected to 5 mg/mL VPA for 48 h. Colocalization is seen as bright pink. Controls are the same as in Figure 2(b). Scale bars correspond to 25 μm. (d) Electron microscopy photographs showing VPA-induced mitophagy at day 3 (left) and day 6 (right). Autophagic vacuoles are labeled with red stars. M: mitochondria. N: nucleus. (e) Confocal microscopy merge image for immunofluorescence against SSEA1 in red (PGCs) and p62 autophagic vacuoles in green in cytoplasms of PGC cultures subjected to normoxia with 5 mg/mL VPA for 3 d. Nuclei are seen in blue with DAPI. Scale bars correspond to 25 μm.

due to insufficient downregulation of *Blimp1*. Reprogramming PGCs toward EGCs with classical bFGF shows a critical downregulation of *Blimp1* as a major step, which drives *Klf4* and *cMyc*. Although we observed a downregulation of *Blimp1* by qRT-PCR in reprogrammed PGCs, this event might occur in a lower intensity as it occurs in classical EGC derivation.

Our data collectively suggest that pluripotency and immortality are two distinctly regulated processes, the first exerted by HIF1 control of the processes of glycolysis, autophagy, and an early peak in ROS, with an intermediate downregulation of Oct4; and the second exerted by *Blimp1* downregulation, *HIF1*/*HIF2* balance, and expression of cMyc and Klf4. Further studies on which genes are separately

responsible for these two characteristics will be of significant interest, not only for EGCs and iPSCs but for their implications in oncogenic transformation.

Disclosure

The authors declare that the research was conducted without any commercial or financial relationships that could be considered a potential conflict of interest.

Conflicts of Interest

The author's declare that they have no conflicts of interest.

Acknowledgments

Authors thank financing from the Roche Farma SA and Foundation Domingo Martínez. Aparicio V. and Moratilla A. are financed by the Consejería de Educación, Juventud y Deporte of Comunidad de Madrid and by the Fondo Social Europeo (Programa Operativo de Empleo Juvenil and Iniciativa de Empleo Juvenil (YEI), (PEJ15/BIO/AI/0045 and PEJ15/BIO/AI/0093, resp.). Martín D. is financed by Grant PIE15/00065 of ISCIII and cofinanced by FEDER, Programa Operativo Crecimiento Inteligente 2014-2020. Authors thank Juliette Siegfried and her team at http://servingmed.com for the English editing, the Statistics Facility of La Paz Hospital for statistical advice, and Victor Toledano for flow cytometry.

References

[1] H. R. Scholer, S. Ruppert, N. Suzuki, K. Chowdhury, and P. Gruss, "New type of POU domain in germ line-specific protein Oct-4," *Nature*, vol. 344, pp. 435–439, 1990.

[2] M. Boiani, S. Eckardt, H. R. Scholer, and K. J. McLaughlin, "Oct 4 distribution and level in mouse clones: consequences for pluripotency," *Genes & Development*, vol. 16, pp. 1209–1219, 2002.

[3] M. P. De Miguel and P. J. Donovan, "Isolation and culture of embryonic germ cells," *Methods in Enzymology*, vol. 365, pp. 351–363, 2003.

[4] S. Yamaguchi, H. Kimura, M. Tada, N. Nakatsuji, and T. Tada, "Nanog expression in mouse germ cell development," *Gene Expression Patterns*, vol. 5, pp. 639–646, 2005.

[5] Y. Yabuta, K. Kurimoto, Y. Ohinata, Y. Seki, and M. Saitou, "Gene expression dynamics during germline specification in mice identified by quantitative single-cell gene expression profiling," *Biology of Reproduction*, vol. 75, pp. 705–716, 2006.

[6] J. A. West, S. R. Viswanathan, A. Yabuuchi et al., "A role for Lin 28 in primordial germ-cell development and germ-cell malignancy," *Nature*, vol. 460, pp. 909–913, 2009.

[7] Y. Matsui, K. Zsebo, and B. L. Hogan, "Derivation of pluripotential embryonic stem cells from murine primordial germ cells in culture," *Cell*, vol. 70, pp. 841–847, 1992.

[8] J. L. Resnick, L. S. Bixler, L. Cheng, and P. J. Donovan, "Long-term proliferation of mouse primordial germ cells in culture," *Nature*, vol. 359, pp. 550-551, 1992.

[9] G. Durcova-Hills, F. Tang, G. Doody, R. Tooze, and M. A. Surani, "Reprogramming primordial germ cells into pluripotent stem cells," *PloS One*, vol. 3, article e3531, 2008.

[10] P. Lopez-Iglesias, Y. Alcaina, N. Tapia et al., "Hypoxia induces pluripotency in primordial germ cells by HIF1alpha stabilization and Oct 4 deregulation," *Antioxidants & Redox Signaling*, vol. 22, pp. 205–223, 2015.

[11] K. Takahashi and S. Yamanaka, "Induction of pluripotent stem cells from mouse embryonic and adult fibroblast cultures by defined factors," *Cell*, vol. 126, pp. 663–676, 2006.

[12] C. D. L. Folmes, T. J. Nelson, A. Martinez-Fernandez et al., "Somatic oxidative bioenergetics transitions into pluripotency-dependent glycolysis to facilitate nuclear reprogramming," *Cell Metabolism*, vol. 14, pp. 264–271, 2011.

[13] A. D. Panopoulos, O. Yanes, S. Ruiz et al., "The metabolome of induced pluripotent stem cells reveals metabolic changes occurring in somatic cell reprogramming," *Cell Research*, vol. 22, pp. 168–177, 2012.

[14] S. Zhu, W. Li, H. Zhou et al., "Reprogramming of human primary somatic cells by OCT4 and chemical compounds," *Cell Stem Cell*, vol. 7, pp. 651–655, 2010.

[15] O. Yanes, J. Clark, D. M. Wong et al., "Metabolic oxidation regulates embryonic stem cell differentiation," *Nature Chemical Biology*, vol. 6, pp. 411–417, 2010.

[16] L. Armstrong, K. Tilgner, G. Saretzki et al., "Human induced pluripotent stem cell lines show stress defense mechanisms and mitochondrial regulation similar to those of human embryonic stem cells," *Stem Cells*, vol. 28, pp. 661–673, 2010.

[17] R. A. Cairns, I. S. Harris, and T. W. Mak, "Regulation of cancer cell metabolism," *Nature Reviews. Cancer*, vol. 11, pp. 85–95, 2011.

[18] Y. Yoshida, K. Takahashi, K. Okita, T. Ichisaka, and S. Yamanaka, "Hypoxia enhances the generation of induced pluripotent stem cells," *Cell Stem Cell*, vol. 5, pp. 237–241, 2009.

[19] M. A. Esteban, T. Wang, B. Qin et al., "Vitamin C enhances the generation of mouse and human induced pluripotent stem cells," *Cell Stem Cell*, vol. 6, pp. 71–79, 2010.

[20] G. L. Semenza, "HIF-1 and tumor progression: pathophysiology and therapeutics," *Trends in Molecular Medicine*, vol. 8, pp. S62–S67, 2002.

[21] M. Hayashi, M. Sakata, T. Takeda et al., "Induction of glucose transporter 1 expression through hypoxia-inducible factor 1alpha under hypoxic conditions in trophoblast-derived cells," *The Journal of Endocrinology*, vol. 183, pp. 145–154, 2004.

[22] J. W. Kim, I. Tchernyshyov, G. L. Semenza, and C. V. Dang, "HIF-1-mediated expression of pyruvate dehydrogenase kinase: a metabolic switch required for cellular adaptation to hypoxia," *Cell Metabolism*, vol. 3, pp. 177–185, 2006.

[23] I. Papandreou, R. A. Cairns, L. Fontana, A. L. Lim, and N. C. Denko, "HIF-1 mediates adaptation to hypoxia by actively downregulating mitochondrial oxygen consumption," *Cell Metabolism*, vol. 3, pp. 187–197, 2006.

[24] Y. Liu, Y. M. Li, R. F. Tian et al., "The expression and significance of HIF-1alpha and GLUT-3 in glioma," *Brain Research*, vol. 1304, pp. 149–154, 2009.

[25] N. Wong, J. De Melo, and D. Tang, "PKM2, a central point of regulation in cancer metabolism," *International Journal of Cell Biology*, vol. 2013, Article ID 242513, 11 pages, 2013.

[26] H. Sakagami, Y. Makino, K. Mizumoto et al., "Loss of HIF-1alpha impairs GLUT4 translocation and glucose uptake by the skeletal muscle cells," *American Journal of Physiology. Endocrinology and Metabolism*, vol. 306, pp. E1065–E1076, 2014.

[27] W. Luo, H. Hu, R. Chang et al., "Pyruvate kinase M2 is a PHD3-stimulated coactivator for hypoxia-inducible factor 1," *Cell*, vol. 145, pp. 732–744, 2011.

[28] G. Panasyuk, C. Espeillac, C. Chauvin et al., "PPARgamma contributes to PKM2 and HK2 expression in fatty liver," *Nature Communications*, vol. 3, p. 672, 2012.

[29] A. Prigione, N. Rohwer, S. Hoffmann et al., "HIF1alpha modulates cell fate reprogramming through early glycolytic shift and upregulation of PDK1-3 and PKM2," *Stem Cells*, vol. 32, pp. 364–376, 2014.

[30] S. Bonnet, S. L. Archer, J. Allalunis-Turner et al., "A mitochondria-K^+ channel axis is suppressed in cancer and its normalization promotes apoptosis and inhibits cancer growth," *Cancer Cell*, vol. 11, pp. 37–51, 2007.

[31] M. G. Vander Heiden, L. C. Cantley, and C. B. Thompson, "Understanding the Warburg effect: the metabolic requirements of cell proliferation," *Science*, vol. 324, pp. 1029–1033, 2009.

[32] M. Morfouace, L. Lalier, L. Oliver et al., "Control of glioma cell death and differentiation by PKM2-Oct 4 interaction," *Cell Death & Disease*, vol. 5, article e1036, 2014.

[33] M. Morfouace, L. Lalier, M. Bahut et al., "Comparison of spheroids formed by rat glioma stem cells and neural stem cells reveals differences in glucose metabolism and promising therapeutic applications," *The Journal of Biological Chemistry*, vol. 287, pp. 33664–33674, 2012.

[34] B. Feuerecker, C. Seidl, S. Pirsig, G. Bruchelt, and R. Senekowitsch-Schmidtke, "DCA promotes progression of neuroblastoma tumors in nude mice," *American Journal of Cancer Research*, vol. 5, pp. 812–820, 2015.

[35] S. Wang, P. Xia, B. Ye, G. Huang, J. Liu, and Z. Fan, "Transient activation of autophagy via Sox2-mediated suppression of mTOR is an important early step in reprogramming to pluripotency," *Cell Stem Cell*, vol. 13, pp. 617–625, 2013.

[36] Y. Nishida, S. Arakawa, K. Fujitani et al., "Discovery of Atg5/Atg7-independent alternative macroautophagy," *Nature*, vol. 461, pp. 654–658, 2009.

[37] T. Ma, J. Li, Y. Xu et al., "Atg5-independent autophagy regulates mitochondrial clearance and is essential for iPSC reprogramming," *Nature Cell Biology*, vol. 17, pp. 1379–1387, 2015.

[38] Y. Li, Y. Wang, E. Kim et al., "Bnip3 mediates the hypoxia-induced inhibition on mammalian target of rapamycin by interacting with Rheb," *The Journal of Biological Chemistry*, vol. 282, pp. 35803–35813, 2007.

[39] E. Morselli, G. Marino, M. V. Bennetzen et al., "Spermidine and resveratrol induce autophagy by distinct pathways converging on the acetylproteome," *The Journal of Cell Biology*, vol. 192, pp. 615–629, 2011.

[40] F. Pietrocola, S. Lachkar, D. P. Enot et al., "Spermidine induces autophagy by inhibiting the acetyltransferase EP300," *Cell Death and Differentiation*, vol. 22, pp. 509–516, 2015.

[41] I. H. Lee, L. Cao, R. Mostoslavsky et al., "A role for the NAD-dependent deacetylase Sirt1 in the regulation of autophagy," *Proceedings of the National Academy of Sciences of the United States of America*, vol. 105, pp. 3374–3379, 2008.

[42] I. H. Lee and T. Finkel, "Regulation of autophagy by the p 300 acetyltransferase," *The Journal of Biological Chemistry*, vol. 284, pp. 6322–6328, 2009.

[43] A. Prigione, B. Fauler, R. Lurz, H. Lehrach, and J. Adjaye, "The senescence-related mitochondrial/oxidative stress pathway is repressed in human induced pluripotent stem cells," *Stem Cells*, vol. 28, pp. 721–733, 2010.

[44] S. Rikka, M. N. Quinsay, R. L. Thomas et al., "Bnip3 impairs mitochondrial bioenergetics and stimulates mitochondrial turnover," *Cell Death and Differentiation*, vol. 18, pp. 721–731, 2011.

[45] S. Kume, T. Uzu, K. Horiike et al., "Calorie restriction enhances cell adaptation to hypoxia through Sirt1-dependent mitochondrial autophagy in mouse aged kidney," *The Journal of Clinical Investigation*, vol. 120, pp. 1043–1055, 2010.

[46] L. Ma, R. Fu, Z. Duan et al., "Sirt1 is essential for resveratrol enhancement of hypoxia-induced autophagy in the type 2 diabetic nephropathy rat," *Pathology, Research and Practice*, vol. 212, pp. 310–318, 2016.

[47] J. Zhou, W. Zhang, B. Liang et al., "PPARgamma activation induces autophagy in breast cancer cells," *The International Journal of Biochemistry & Cell Biology*, vol. 41, pp. 2334–2342, 2009.

[48] J. Krishnan, M. Suter, R. Windak et al., "Activation of a HIF1alpha-PPARgamma axis underlies the integration of glycolytic and lipid anabolic pathways in pathologic cardiac hypertrophy," *Cell Metabolism*, vol. 9, pp. 512–524, 2009.

[49] G. Bellot, R. Garcia-Medina, P. Gounon et al., "Hypoxia-induced autophagy is mediated through hypoxia-inducible factor induction of BNIP3 and BNIP3L via their BH3 domains," *Molecular and Cellular Biology*, vol. 29, pp. 2570–2581, 2009.

[50] K. E. Hawkins, S. Joy, J. M. Delhove et al., "NRF2 orchestrates the metabolic shift during induced pluripotent stem cell reprogramming," *Cell Reports*, vol. 14, pp. 1883–1891, 2016.

[51] D. Huangfu, R. Maehr, W. Guo et al., "Induction of pluripotent stem cells by defined factors is greatly improved by small-molecule compounds," *Nature Biotechnology*, vol. 26, pp. 795–797, 2008.

[52] X. Chen, Y. Zhai, D. Yu, J. Cui, J. F. Hu, and W. Li, "Valproic acid enhances iPSC induction from human bone marrow-derived cells through the suppression of reprogramming-induced senescence," *Journal of Cellular Physiology*, vol. 231, pp. 1719–1727, 2016.

[53] A. M. Elliott, M. P. de Miguel, V. I. Rebel, and P. J. Donovan, "Identifying genes differentially expressed between PGCs and ES cells reveals a role for CREB-binding protein in germ cell survival," *Developmental Biology*, vol. 311, pp. 347–358, 2007.

[54] J. Mathieu, W. Zhou, Y. Xing et al., "Hypoxia-inducible factors have distinct and stage-specific roles during reprogramming of human cells to pluripotency," *Cell Stem Cell*, vol. 14, pp. 592–605, 2014.

[55] C. E. Forristal, K. L. Wright, N. A. Hanley, R. O. Oreffo, and F. D. Houghton, "Hypoxia inducible factors regulate pluripotency and proliferation in human embryonic stem cells cultured at reduced oxygen tensions," *Reproduction*, vol. 139, pp. 85–97, 2010.

[56] K. L. Covello, J. Kehler, H. Yu et al., "HIF-2alpha regulates Oct-4: effects of hypoxia on stem cell function, embryonic development, and tumor growth," *Genes & Development*, vol. 20, pp. 557–570, 2006.

[57] V. Karwacki-Neisius, J. Goke, R. Osorno et al., "Reduced Oct4 expression directs a robust pluripotent state with distinct signaling activity and increased enhancer occupancy by Oct4 and Nanog," *Cell Stem Cell*, vol. 12, pp. 531–545, 2013.

[58] A. Radzisheuskaya, B. Chia Gle, R. L. dos Santos et al., "A defined Oct4 level governs cell state transitions of pluripotency entry and differentiation into all embryonic lineages," *Nature Cell Biology*, vol. 15, pp. 579–590, 2013.

[59] K. K-W. To, O. A. Sedelnikova, M. Samons, W. M. Bonner, and L. E. Huang, "The phosphorylation status of PAS-B distinguishes HIF-1alpha from HIF-2alpha in NBS1 repression," *The EMBO Journal*, vol. 25, pp. 4784–4794, 2006.

Hindawi
Oxidative Medicine and Cellular Longevity
Volume 2017, Article ID 9420539, 15 pages
https://doi.org/10.1155/2017/9420539

Review Article

NADPH Oxidases: Insights into Selected Functions and Mechanisms of Action in Cancer and Stem Cells

Magdalena Skonieczna,[1,2] Tomasz Hejmo,[3] Aleksandra Poterala-Hejmo,[1,2] Artur Cieslar-Pobuda,[1,4] and Rafal J. Buldak[3]

[1]*Institute of Automatic Control, Silesian University of Technology, Akademicka 16, 44-100 Gliwice, Poland*
[2]*Biotechnology Centre, Silesian University of Technology, Krzywoustego 8, 44-100 Gliwice, Poland*
[3]*Department of Biochemistry, School of Medicine with the Division of Dentistry, Medical University of Silesia, Jordana 19, 41-808 Zabrze, Poland*
[4]*Stem Cell Group, Nordic EMBL Partnership, Centre for Molecular Medicine Norway (NCMM), University of Oslo, P.O. Box 1137, Blindern, 0318 Oslo, Norway*

Correspondence should be addressed to Magdalena Skonieczna; magdalena.skonieczna@polsl.pl and Rafal J. Buldak; rbuldak@sum.edu.pl

Received 19 January 2017; Revised 7 April 2017; Accepted 20 April 2017; Published 23 May 2017

Academic Editor: Jacek Zielonka

NADPH oxidases (NOX) are reactive oxygen species- (ROS-) generating enzymes regulating numerous redox-dependent signaling pathways. NOX are important regulators of cell differentiation, growth, and proliferation and of mechanisms, important for a wide range of processes from embryonic development, through tissue regeneration to the development and spread of cancer. In this review, we discuss the roles of NOX and NOX-derived ROS in the functioning of stem cells and cancer stem cells and in selected aspects of cancer cell physiology. Understanding the functions and complex activities of NOX is important for the application of stem cells in tissue engineering, regenerative medicine, and development of new therapies toward invasive forms of cancers.

1. Introduction

Reactive oxygen species (ROS) are highly reactive oxygen-derived molecules that include free radicals such as superoxide or hydroxyl radicals, as well as nonradicals such as ozone or hydrogen peroxide. Depending on their level, ROS can play dual roles either as important mediators and signaling molecules required for proper cell functioning or as damaging factors leading to mutations, carcinogenesis, and cell death.

To keep the correct equilibrium between the production of ROS and their elimination, free radical scavengers, both endo- and exogenous, are needed. It has been commonly believed that antioxidants which neutralize ROS and thus protect biomolecules from damage should be beneficial in protection against cancer, but recent studies clearly show that antioxidants (in the form of dietary supplements) may actually promote tumor growth and cancer metastasis. In 2011, it was demonstrated, during a trial on over 30,000 men over 50 who were administrated high doses of vitamin E, that the risk of prostate cancer increased by 17% [1]. More recently, researchers from Sweden have shown that even relatively low doses of antioxidants may enhance the growth of lung tumors and melanomas in mice [2, 3]. Similar conclusions come from work which demonstrated that treating melanoma-bearing mice with antioxidants decreased oxidative stress in circulating cancer cells but increased their ability to metastasize [4]. No matter how puzzling or confusing these evidences are, it is undoubtedly important to understand better the biology of ROS and their sources to effectively treat various diseases and disorders.

The main sources of ROS in cells, beside the respiratory chain, are NADPH oxidases (NOX). The physiological functions of NADPH oxidases are very diverse: they play a role in

Table 1: Functions and mechanisms of action of NADPH oxidases in stem cells and cancer stem cells.

Process	Expression/activity of NOX	Effects/mechanism	Reference
Differentiation	↑ NOX2	Differentiation of stem cells/ROS-dependent Notch signaling pathway	[111]
	↓ NOX4	Myogenesis, C2C12 differentiation/↓ ERK1/2 phosphorylation, MAP kinases	[112]
	↑ NOX2 ↑ NOX4	Cardiac precursor cells (CPCs) → ↑ c-kit(+) cells/unknown mechanism	[114]
	↑ NOX4	Differentiation of endothelial cells into smooth muscle cells/TGFβ-1-dependent NOX4/H_2O_2 upregulation	[115]
	↑ NOX4	NOX4/H_2O_2 dependent (i) Neural crest stem cells (NCSCs) differentiation to neural cells (ii) 2T3 preosteoblast differentiation (iii) Renal progenitor cells differentiation to profibrotic cells	[116–118]
	↓ NOX4	Neural crest stem cells (NCSCs) death or retarded growth of PNS	[116]
Stem cell self-renewal	↑ NOX4	Proliferation of neural stem cells/superoxide dependent	[122]
	↑ NOX3	↑ proliferation of mouse spermatogonial stem cells/unknown mechanism	[123]
	↓ NOX4	↓ proliferation and migration of adipose-derived stem cells (ADSCs)/↓ ERK1/2, Akt, ↓ PDGFβ1	[124]
	↓ NOX	Proliferation of mesenchymal stem cells/↑ Nanog/Oct4 (TFs)	[125]
	NOX2 NOX4	↑ senescence of Ang. II-stimulated endothelial cells/unknown mechanism	[126]
Cancer stem cell growth and survival	NOX2	↑ proliferation of pancreatic cancer cells (SW1990 and BxPC-3)/NF-κB/STAT3 activation	[137]
	↑ NOX1	↑ enrichment of breast cancer stem-like cell population/RAS/Erk1/2/NOX1 activation	[138]
	↓ NOX2, NOX4, NOX5	↑ survival of prostate stem-like cells in vitro	[139]
Cancer stem cell drug resistance	↑ NOX2	↑ resistance of patient-derived glioblastoma stem cells and chronic myeloid leukemia stem cells to tyrosine kinase inhibitors/NOX2/Egr1/Fyn upregulation	[143]

cellular proliferation, serotonin biosynthesis, endothelial signaling, regulation of renal functions, and the immune response against microorganisms (as a source of the so called oxidative burst), but their overexpression is associated with various neurological diseases and cancer types [5–8].

The roles of NOX have been quite well established in many noncancerous cells, but the effects of NOX-generated ROS on functioning of cancer and stem cells are much less understood. Considering the role of ROS in cancer recurrence and chemo- and radiotherapy resistance, this seems to be one of the most important research areas in the current oxidative medicine [9]. Here, we review the importance of NOX and NOX-derived ROS in the functioning of stem cells, including cancer stem cells, and in cancer cells, focusing on their roles in differentiation, self-renewal, proliferation, angiogenesis, and metastasis (Table 1).

2. NADPH Oxidases

The NOX family is a group of transmembrane proteins able to transport electrons from NADPH and to reduce oxygen to the ROS superoxide anion ($O_2^{\cdot-}$) and hydrogen peroxide (H_2O_2) [10]. NOX and the mitochondrial electron transport chain are considered as the main sources of ROS in cells, although other potential sources such as cytochrome p450, xanthine oxidase (XO), or nitric oxide synthase (NOS) also contribute to the redox potential [11]. In mammals, seven proteins with NOX activity exist, NOX1 to NOX5 and Duox1 (dual oxidase 1) and Duox2; however, rats and mice lack NOX5 [12]. NADPH oxidases can be found not only within the plasma membrane (NOX1–5 and DUOX1-2) but also in the endoplasmic reticulum (NOX2, NOX4, and NOX5), mitochondrial membrane (NOX4), and nuclear membrane (NOX4 and NOX5), as well as in the specialized membrane microdomains caveoli and lipid rafts (NOX1), focal adhesions (NOX4), and invadopodia (NOX1 and NOX4) [13–19]. Every NOX family member is anchored to the membrane through six transmembrane helices binding two haem cofactors [20]. The C-terminal domain binds FAD/NADPH and allows electron transfer to the haem and further across the membrane to molecular oxygen [13, 21, 22]. DUOX1, DUOX2, and NOX5 also have calcium-binding regions at their N-terminus, which distinguish them from other NOX. Additionally, DUOX1 and 2 possess a domain with a structure similar to the active site of peroxidase (but do not show peroxidase or superoxide dismutase activity) [23, 24]. NOX1, NOX2, NOX3, and NOX5 produce $O_2^{\cdot-}$ while NOX4, DUOX1, and DUOX2 generate H_2O_2 (see Figure 1) [22].

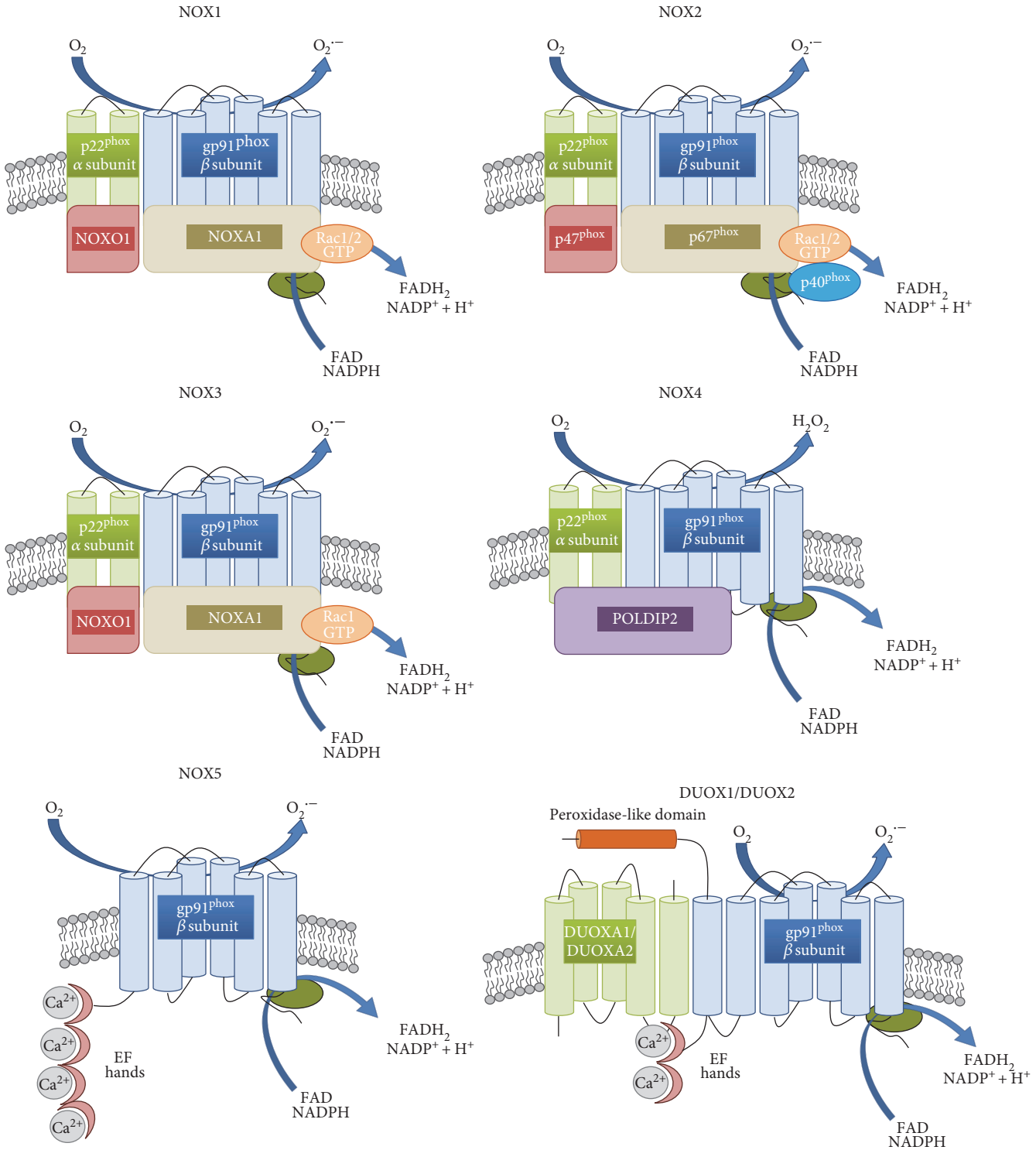

Figure 1: Structure of NOX isoforms. NOX1–4 are similar in their size and domain structure. Two NOX subunits, gp91phox and p22phox (also called β and α subunits, resp.), are integral membrane proteins that together comprise the large heterodimeric subunit flavocytochrome b558 (cyt b558). The cytoplasmic C-terminus contains flavin adenine dinucleotide (FAD) and NADPH-binding domains (shown in the picture as a green ellipse). NOX1 and NOX2 activation involves the phosphorylation of NOXO1 and p47phox, respectively, the translocation of the entire multidomain complex, including p40phox, p67Phox, and Rac from the cytosol to the membrane, and the transfer of electrons from the substrate to oxygen. Like NOX1 and NOX2, NOX3 is p22phox dependent, but it does not bind to Rac. NOX4 activation involves p22phox and POLDIP2. NOX5, DUOX1, and DUOX2 have calcium-binding regions (EF hands) at their N-terminus, which distinguish them from other NOX. DUOX1 and 2 have a domain with a structure similar to the active site of peroxidase but without peroxidase or superoxide dismutase activity.

To create an active NOX complex, stable complex NOX1–3 require binding to a membrane protein p22phox, cytosolic proteins p47phox, p67phox (or their homologues named NOXO1 and NOXA1, resp.), p40phox (only for NOX2), or the GTP-binding protein Rac1/2 [21, 25–28]. The main role of these subunits is to bring FAD and NADPH close together to facilitate the transport of electrons [29]. NOX4 interacts with p22phox but not with other proteins, and therefore, it is believed to be constitutively active and regulated at the level of transcript expression, or the activation may occur in a yet unknown way [30–32]. The activity of NOX4 may be enhanced by an interaction with DNA polymerase-δ-interacting protein 2 (POLDIP2) [33, 34]. DUOX1, DUOX2, and NOX5 activation is independent from cytosolic subunits—they contain EF-hands (helix-loop-helix motifs) that bind calcium ions for activation [12, 35, 36]. The mechanism of the activation of NOX family enzymes has been described in detail in [26, 30].

Once the active NOX complex is formed, electrons are transferred from NADPH to FAD, causing its reduction to $FADH_2$ [13]. As the NOX catalytic subunit can accept only one electron, a single electron is passed to the first inner haem and then used for the reduction of molecular oxygen bound by the second haem [10, 37]. Superoxide anion generated in this reaction often undergoes disproportionation reactions in which one molecule of $O_2^{\cdot}$ donates an electron to another, forming H_2O_2 and O_2 in a reaction termed dismutation (catalyzed by superoxide dismutase (SOD) or occurring spontaneously under low pH conditions) [38]. As described above, H_2O_2, rather than superoxide anion, has been identified as a product of NOX4, DUOX1, and DUOX2 but it is predicted that for thermodynamic reasons, this cannot be formed through haem-catalyzed two-electron reduction [13, 39]. More likely, some regions in NOX4, DUOX1, and DUOX2 serve as enhancers of spontaneous dismutation or as a proton donor, but this hypothesis has not been confirmed [13, 40].

ROS, including NOX-derived superoxide ($O_2^{\cdot}$) and H_2O_2, inhibit the activities of various biological molecules. At low levels, they serve as the second messengers for signal transduction, but higher concentrations cause oxidative damage to DNA, proteins, and lipids by direct oxidation or via the transition metal-driven Haber-Weiss reaction to the extremely reactive hydroxyl radical ($OH^{\cdot}$) (Figure 2) [41–44].

H_2O_2 induces apoptosis in many cancer cells in vitro via the activation of the caspase cascade. Many antitumor drugs, such as vinblastine, doxorubicin, or camptothecin, also exhibit antitumor activity via H_2O_2-dependent activation of apoptotic cell death, which suggests the potential use of H_2O_2 as an antitumor agent [45–48]. However, a biphasic effect of H_2O_2 and superdoxide has been demonstrated on cellular proliferation in which low levels (submicromolar concentrations) induce growth, but higher concentrations (>10–30 micromolar) induce apoptosis or necrosis. This phenomenon has been demonstrated for primary, immortalized and transformed cell types [38, 44].

This review highlights the relations between NOX proteins and several cellular processes which are of importance in medicine and hallmarks of cancer such as increased proliferation rate, avoidance of apoptosis, tumor invasiveness, tumor angiogenesis, differentiation, and self-renewal of stem cells, showing that several NOX may be considered as potential therapeutic targets. The expression of NOX, especially in cancer cells and solid tumors, has been a topic of several publications in the past few years (for details, see [11, 49]). Therefore, we concentrate here on selected processes in which NOX have been identified as important players, particularly proliferation, invasiveness, and metastasis, paying particular attention to potential mechanisms of action and regulation.

3. Roles of NOX in Cancer Cells

Increased expression of NOX1, NOX2, NOX4, and NOX5 or their regulatory components compared with normal controls has been described in many types of cultured cancer cell lines and in human tumors at early and late stages of tumorigenesis, indicating their importance in cancer development and progression [49–51].

Exogenous expression of NOX1 in NIH3T3 fibroblasts caused increased cell growth and the ability to form tumors in athymic mice [52]. Tenfold overexpression of NOX1 caused increased growth and transformation with only a < 2-fold increase in extracellular $O_2^{\cdot-}$ generation, showing that high levels of ROS are not required for these effects. Coexpression of catalase (CAT) reversed the transformed phenotype, indicating that H_2O_2 was the growth-promoting species [38, 52].

Studies of tumor and adjacent tissues from 123 patients with gastric cancer (*adenocarcinoma*) showed that in 47.2% of cases, the NOX2 level was detectable and was increased in the tumor compared to adjacent tissue. Patients in the NOX2-positive group presented a poor prognosis (5-year survival rates) [53].

The roles of NOX3, DUOX1, and DUOX2 in cancer and stem cells have not been very well established as yet. According to the current state of knowledge, NOX3 expression is generally limited to the cochlea and inner ear epithelial cells, where it plays a role in the perception of gravity and maintaining balance [54, 55]. DUOX promoters have been shown to be highly methylated in lung cancer [54, 56]. Recently, it has been also demonstrated that the loss of DUOX1 expression in lung cancer cell lines is strongly associated with the loss of the epithelial marker E-cadherin and that the silencing of DUOX1 promotes features of an epithelial-to-mesenchymal transition (EMT), an important feature of metastatic cancer [57]. Wu et al. [54] showed that DUOX2 is regulated by IFN-γ-mediated Stat1 binding to the Duox2 promoter in pancreatic tumor lines. At the same time, the authors demonstrated the upregulation of DUOX2 expression in vivo in pancreatic cancer xenografts and in patients with chronic pancreatitis. In another study by Wu et al. [58], IFN-γ-mediated DUOX2 overexpression resulted in H2O2-induced, ERK-associated upregulation of HIF-1α and VEGF-A in pancreatic cancer cells. Recently, DUOX enzymes were also found to constitutively maintain ROS levels in prostate cancer cells, and these ROS promote AKT signaling leading to increased resistance to apoptosis [59].

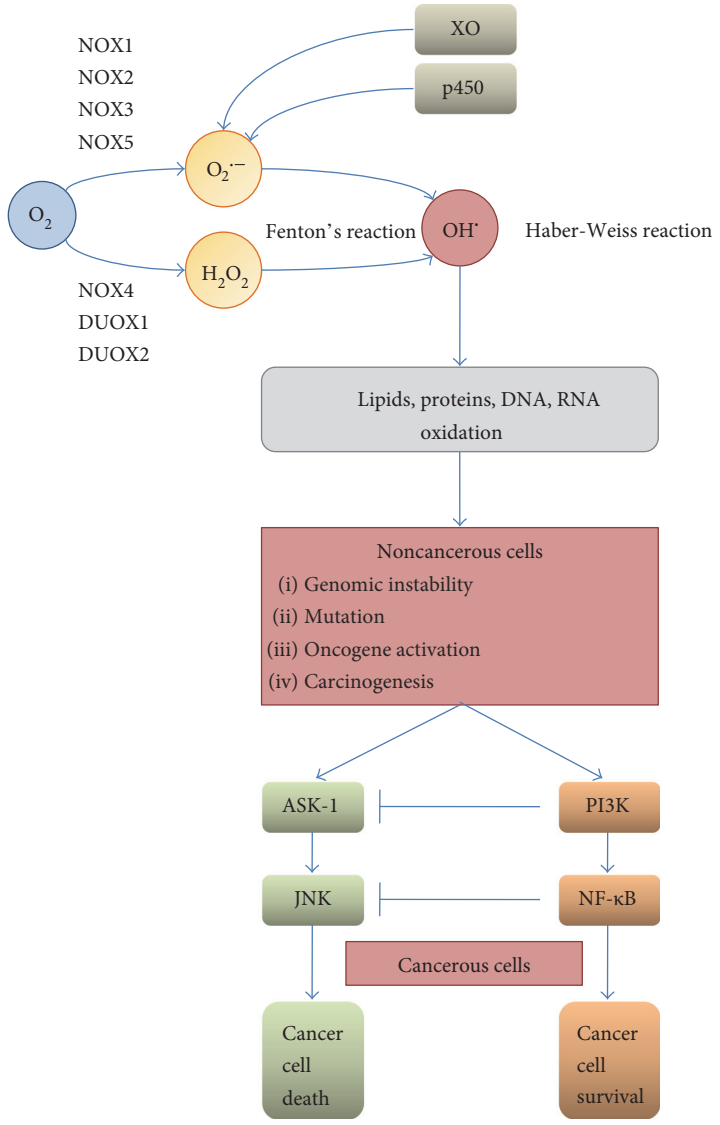

Figure 2: Endogenous sources and consequences of ROS overproduction. Overproduction of superoxide anion and H_2O_2 by NOX (NOX and Duox), cytochrome c oxidase, or xanthine oxidase (XO) and the subsequent increased level of hydroxyl radical (generated through the Fenton or Haber-Weiss reaction) are leading to lipids, proteins, and nucleic acid oxidation and, in consequence, to genomic instability, mutations, and carcinogenesis. Upon this conditions, cell survival or death is dependent on the activation of either ASK-1 or PI3K: high level of ROS tends to activate the ASK-1/JNK pathway leading to cell death, while lower or transient ROS production may result in the activation of PI3K kinase (accompanied by ASK-1/JNK inhibition) and NF-κB-mediated survival.

3.1. NOX in Tumor Development. Oxidative stress can result in genomic instability caused by direct modification and damage to nucleic acids and alteration of redox-sensitive proteins and signal transduction leading to tumor formation. The exact function of NOX-derived ROS in cellular transformation remains an open question.

ROS produced by NOX4 caused mitochondrial dysfunction and mitochondrial DNA damage [15, 60, 61]. As NOX4 can be found also in the nucleus, it could be responsible for direct oxidation of nuclear proteins and DNA as well [62]. Whether NOX play a role in ROS-induced genomic instability resulting in tumorigenesis is uncertain, as this would be an outcome of complex interactions between reactive species, antioxidants, and DNA repair pathways.

Besides, genomic instability NOX1 has been connected with the regulation of p53 activity. The corepressor HIPK2 which control the tumor suppressor p53 also upregulates NOX1, which in turn prevents deacetylation and inactivation of p53 by the stress-controlling protein sirtuin1 (SIRT1), therefore promoting tumorigenesis [63, 64].

Increased expression of NOX1 also accompanies activating mutations in K-RAS, a proto-oncogene with a key role in growth autonomy of tumor cells [65]. Overexpression of K-RAS enhances the transcription of NOX1 through RAF/MEK/ERK-dependent phosphorylation of the transcription factor GATA6 [66]. In RAS-transformed cells, NOX1 stimulates cell proliferation and anchorage-independent growth through the RAS/MEK and canonical WNT-β-catenin

pathways [67, 68]. NOX regulate several other phosphatases linked to cell survival, for example, the low molecular weight protein tyrosine phosphatases (LMW-PTP) and protein phosphatase 1 (PP1). In chronic myeloid leukemia, increased NOX4-mediated ROS production induced by Bcr-Abl (kinase generated from the Philadelphia chromosome) enhances survival signal transduction through the inhibition of PP1 which negatively regulates the PI3k/Akt pathway [69].

3.1.1. NOX in Proliferation, Invasiveness, and Metastasis. All cancer cells share some features known as the hallmarks of cancer which include insensitivity to growth-inhibitory signals, limitless replicative potential, self-sufficiency in growth signals, avoidance of apoptosis, sustained angiogenesis, tissue invasion, and metastasis [70, 71].

Recent studies on colon cancer show that NOX1 activity and ROS generation are modulated through a cascade of interactions between growth receptor-bound protein 2 (an adaptor involved in signal transduction), Cbl E3 ligase (an ubiquitin-protein ligase), NOXA1 (an activator of the NOX complex), epidermal growth factor, and NOXO1 (an organizer of the NOX complex). NOX1 can modulate the canonical Wnt-β-catenin signaling pathway which is crucial for the proliferation and fate of both malignant and normal cells, and on the other hand, Wnt can induce NOX1-derived ROS production [67]. Thus, the connections between NOX activity and cancer cell growth, proliferation, and tumor formation involve complex signaling pathways and interactions.

Cancer cells can be transferred to and proliferate in different regions of the same organ or in very distant sites. This spreading, termed metastasis, is a multistep process involving the invasion of tumor cells into the extracellular matrix, the migration through the endothelium into vessels (intravasation) and then out of them (extravasation), and finally, the colonization and proliferation leading to growth of the secondary tumors [72, 73]. The steps of extracellular matrix degradation and extravasation are mediated by invadopodia, actin-rich structures in the plasma membrane which contain integrins, matrix metalloproteinases, NOX, and other transmembrane proteins. The formation of invadopodia is dependent on NOX-mediated production of ROS [17, 74, 75]. Two proteins found only invadopodia, named Tks4 and Tks5, show homology to p47phox (as well as some structural similarities to p40phox and NOXO1 and associate with and activate NOX1 and NOX3, even when no other organizers were present [76, 77]. This suggest that ROS-dependent invadopodia formation may be dependent on a NOX-Tks protein complex, formed exclusively at invadopodia membranes [17, 78].

Higher metastatic potential is correlated with elevated matrix metalloproteinase-7 (MMP-7) expression in human colon cancer cells; less invasive colon cancer cells, such as Caco2 and HT29 cell line, present low MMP-7 expression level and high NOX1 and AMPK phosphorylation levels. AMPK is an energy-sensing kinase, activated by changes of the AMP/ATP ratio caused by insufficient amount of nutrients and required for rapid cell proliferation and hypoxic conditions. Pharmacological activation of AMPK by adding 5-aminoimidazole-4-carboxamide riboside (AICAR) and D942 leads to reduced NOX4 expression and NOX4-dependent ROS generation. NOX may be linked to inflammation-induced metastasis in renal cell carcinoma (RCC), where cell invasion is based on NOX4-mediated hypoxic-induced production of interleukin-6 and interleukin-8 (IL-6 and IL-8) [79]. IL-6 and IL-8 induce metastasis in RCC, but their NOX-dependent production can be reduced through the activation of AMPK (previously shown to decrease tumor growth in a xenograft model and in vitro) [79, 80].

The induction of an invasive phenotype by TPA (12-O-tetradecanoylphorbol-13-acetate) results in increased NOX2 and MMP-7 expression which leads to higher ROS production and decreased AMPK phosphorylation [81]. In colon cancer cells, this molecular switch from NOX1 to NOX2, together with NOX2-derived ROS, increases MMP-7 expression by the deactivation of AMPK, and the TPA-induced phenotype can be reverted by NOX2 but not NOX1-targeting siRNA, suggesting that NOX2 activity induces an invasive phenotype [81]. In contrast, in melanoma cells, the role of a switch-deciding transformation from a noninvasive to an invasive phenotype is played by the Akt protein, a kinase that plays a key role in proliferation, cell migration, and apoptosis, which induces NOX4-derived ROS [82].

The inhibition of NOX by siRNA or a pharmacologic inhibitor leads to significantly reduced lung cancer formation in vivo and lung cancer cell invasion in vitro, as shown by a meta-analysis [83]. NOX1-derived ROS are crucial for the regulation of metastasis through the toll-like receptor 4 (TLR4) in non-small lung cancer cells (NSCLC) [84], and it is possible that TLR4 signaling enhances the expression of NOX1 which subsequently regulates MMP-9 and increases metastasis in these cells [84, 85]. O'Leary described the role of TLR-4-dependent NOX1 activity in accelerating adherence of lipopolysaccharide- (LPS-) stimulated colon cancer cells (SW480, SW620, and CT-26 cell lines) and proposed a mechanism in which TLR-4-mediated activation of NF-κB leads to increased activation of NOX and in consequence to a higher level of ROS and phosphorylation of Akt [86]. The PI3K/Akt signaling pathway mediates TG-interacting factor-(TGIF-) induced NOX2 activation and ROS production, which stimulate PI3K/Akt to promote the invasiveness of urothelial *carcinoma* [87]. TGIF acts as a transcriptional repressor/corepressor regulated by TGF-β and associated with the protein SMAD [88]. TGF-β/SMAD3-induced NOX4 activity affects cell migration and expression of fibronectin, a marker of TGF-β-induced epithelial-to-mesenchymal transition (EMT), in normal and metastatic breast epithelial cells [89, 90].

There is growing body of evidence that microRNAs are involved in NOX-dependent regulation of tumor growth, invasiveness, and metastasis [91–93]. miR-21 has been reported to promote growth, metastasis, and chemo- and radioresistance in non-small lung cancer cells by targeting PTEN, the product of a tumor suppressor that is mutated in many cancers [93]. The inhibition of NOX activity in human lung cancer cells decreases their invasive potential in vitro, lowers the level of miR-21 and MMP-9, and also increases expression of PTEN. The expression of miR-21 and of the NOX subunit p47phox was significantly higher

in poorly differentiated tumor cells. An increased level of miR-21 also compensates for the effect of NOX inhibitors on metastasis [92]. Consistent with the results for prostate cancer cells in which NOX-derived ROS are known to regulate invasiveness and metastasis in vivo, the depletion of p47phox subunit using siRNA reduced tumor metastasis in a xenograft model of prostate cancer [94]. The regulation of miR-21 by NOX-derived ROS probably occurs by the activation of Akt, but understanding of this axis requires further studies [94, 95]. miRNAs can also affect the NOX4-MCP-1 axis critical for *hemangioendothelioma*; silencing of the enzyme required for miRNA maturation (Dicer) prevented formation of tumors in vivo, accompanied by the upregulation of miR-21a-3p activity targeting the 3′UTR of the NOX4 transcript [96]. A lower level of NOX4-derived ROS resulted in decreased production of the oxidant-inducible monocyte chemoattractant protein-1 (MCP-1) which is critical for endothelial cell tumor formation [96, 97].

The role of NOX5 is less understood than those of NOX1, 2, and 4, but it is also reported to play a significant function in cancer. Its silencing results in a lower proliferation rate of prostate cancer PC-3 cells and increased apoptosis caused by enhanced activity of caspases 3 and 7 [51], and therefore, NOX5-derived ROS are suggested to be important for the regulation of proliferation and survival of prostate cancer cells [51]. Lower expression of NOX5 resulted in a decreased level of phosphorylation of c-Jun N-terminal kinase 1/3 (JNK1/3) and a reduced level of PKC-ζ protein, which is known to promote an aggressive phenotype of human prostate cancer cells [51, 98].

3.1.2. NOX and Angiogenesis. Cell function and survival and, in the case of cancer cells, also the ability to spread to adjacent and distant tissues are dependent on the oxygen and nutrients provided by the vasculature [99]. Angiogenesis is a critical step for the development of tumors with a diameter higher than ~2 mm as it allows the delivery of nutrients into the solid tumor [13, 99]. New blood vessel formation from existing vasculature is regulated by growth factors such as vascular endothelial growth factor (VEGF) which activates matrix metaloproteinases (MMPs) and can be regulated by inhibitors (i.e., angiostatin) [100]. Another key element of angiogenesis in tumors is the transcription factor hypoxia-inducible factor 1 (HIF-1) which under hypoxic condition characteristic for the center of tumor, increases the transcription of VEGF, and furthermore, both HIF-1α and VEGF expression can be stimulated by ROS [100, 101].

In ovarian cancer cells, NOX4-derived ROS together with mitochondrial-derived ROS are necessary for tumor-induced angiogenesis and regulation of VEGF level through HIF-1α expression [13, 102]. NOX1- and NOX4-derived ROS promote HIF-dependent vascularization in prostate cancer and malignant melanomas; however, several reports indicate that ROS-mediated angiogenesis can also occur through an HIF-independent mechanism [13, 82, 103]. Garrido-Urbani et al. reported increased expression and activity of NOX1 during angiogenesis and impaired angiogenesis in NOX1-deficient mice, indicating its role in endothelial cell migration and tumor progression [104]. NOX1 downregulates expression and activity of the antiangiogenic receptor PPARα (peroxisome proliferator-activated receptor α) which is known to inhibit the transcription factor NF-κB (see Figure 3) and VEGF [104, 105]. Another mechanism has been reported for serotonin-induced angiogenesis: serotonin (5-HT, 5-hydroxytryptamine) activates NOX and induces ROS production, which is probably mediated through the activation of the 5-HT1 receptor-linked Src/PI3K pathway [106]. However, it is not clear if HIF-1 plays a role in this mechanism because the PI3K pathway can increase VEGF production by tumor cells in both an HIF-1-dependent and HIF-1-independent manner [106, 107].

4. NOX in Stem Cells

Stem cells play important roles in many stages of development, from progenitors of all cells, pluripotent stem cells, in early embryonic stages, to tissue-restricted cells—giving rise to cells with highly specialized functions [108]. Numerous studies have demonstrated the potential of stem cells in therapies [109]. Redox states have been reported to play important role in both maintaining stemness and mediating differentiation of several precursor cell types [110].

4.1. NOX and Differentiation. NOX2 regulates the differentiation of mouse induced-pluripotent stem cells (miPCs) into arterial endothelial cells (miPSC-ECs) via the Notch signaling pathway [111]. The expression of arterial endothelial markers such as EphrinB2, neuropilin 1 (Nrp1), and activin receptor-like kinase 1 (ALK1), as well as the expression of Notch-pathway components, was significantly decreased (at the mRNA and protein levels) in NOX2$^{-/-}$ miPSCs. However, the transfection with an adenovirus vector coding for NOX2 resulted in a significant increase of arterial endothelial markers and Notch1 expression, and the same effect was obtained by the upregulation of Notch activity. In both cases, the effect of this increase can be reversed either by DPI-induced inhibition of ROS generation or by silencing of Notch1 expression [111]. NOX2 deficiency has been shown to significantly lower the potency of miPSC-ECs for vascular repair in mouse ischemic limbs, tube formation, cell proliferation, cell migration, and uptake of Ac-LDL (acetylated low-density lipoprotein) and to increase sensitivity to oxidative stress [111].

NOX4 has been reported to regulate *myogenesis*, the process in which muscle stem cells first proliferate and then differentiate. In myogenic C2C12, cell changes in NOX4 expression level correlate with the changes in the level of the differentiation markers myogenin, MyoD1, Pax7, and Myf5 which can be further linked to the changes in MAPK signaling pathways. Both overexpression and depletion of NOX4 caused reduction of ERK1/2 phosphorylation during the differentiation [112]. The MAPK family consists of extracellular regulated kinases (ERK1/2), Jun N-terminal kinase (JNK), p38 kinase, ERK3/4, and the mitogen-activated protein kinase 1 (BMK1/ERK5) pathways. The JNK and p38 kinase pathways are sometimes grouped together and referred to as the stress-activated protein kinases (SAPKs)

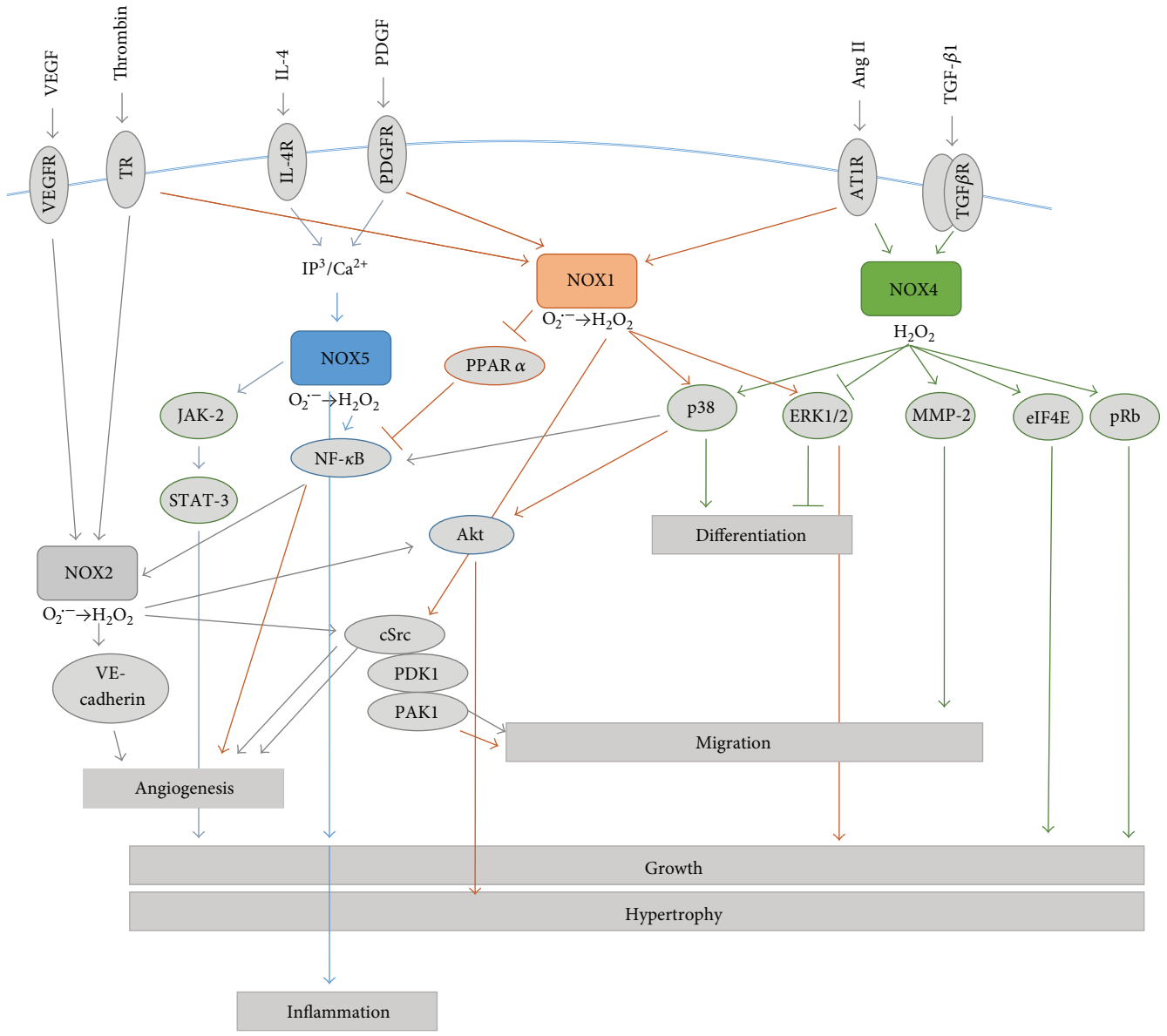

Figure 3: Examples of NOX signal transduction. NOX1-derived ROS can affect the following: differentiation through the p38 and ERK1/2 pathway, hypertrophy via p38-mediated activation of Akt, cell migration by the activation of cSrc protein, and cellular growth by the activation of ERK1/2; and subsequent activation of transcription factor Ets-1 and upregulation of cyclin *D*. *nox*1 also downregulates the expression and activity of the antiangiogenic receptor PPARα, known to inhibit the transcription factor NF-κB and, therefore, affects angiogenesis. NOX1 can be activated by thrombin, PDGF, or Ang II; activated by TNFα, thrombin or NF-κB NOX2-generated ROS promote migration and angiogenesis through the Akt and cSrc pathways. NOX2-mediated regulation of angiogenesis also occurs via VE-cadherin; via the activation of p38 or the inhibition of ERK1/2 NOX4-derived ROS promotion; via the activation of p38 or the inhibition of ERK1/2 differentiation, which regulates growth, by eiF4E and pRB pathways, and migration (through the activation of MMP2). NOX4 expression and activity can be increased by TGF-β1 or Ang II; NOX5 promotes growth and inflammation, respectively, through JAK-2/STAT3 and NF-κB signaling pathways. ROS production by NOX5 can be activated by IL4 or PDGF; there will be always some omitted proteins, no matter how detailed is the scheme.

[113]. NOX are also implicated in the differentiation of cardiac cells into cardiac muscle, endothelial, and smooth muscle cells. Cardiac precursor cells (CPCs) marked by type III receptor tyrosine kinase c-kit (c-kit$^+$) with silenced *Nox2* and *Nox4* genes showed increased expression of the CPC stemness markers c-kit and Flk1 (receptor for vascular endothelial growth factor), while cells with overexpression of NOX2 and NOX4 presented decreased c-kit level [114].

These changes were accompanied by changes in the level of Gata6, Gata4, and cytokine-transforming growth factor β1 (TGF-β1) required for cardiac lineage specification, as well as an altered level of the differentiation markers α-smooth muscle actin (α-SMA) and cardiac troponin T (cTnT). The upregulation of NOX2 and NOX4 during the differentiation of early postnatal c-kit$^+$ cells suggests that they are responsible for maintaining "the balance between precursors and

differentiation status" [114]. NOX4 has also been described as a mediator of the differentiation of mouse embryonic stem cells into smooth muscle cells (SMC) with a positive correlation between the expression of NOX4 and SMC-specific genes (*SMαA*, *SM22α*, *h1-colponin*, and *SM-myh11*) and transcription factors essential for the differentiation (serum response factor and myocardin), expression, and activation of NOX4 (which can occur through TGF-β1) driving the differentiation (and maintenance of phenotype) of functional SMC from EC through H_2O_2 generation [115].

NOX4 activity is essential for BMP-induced neuronal differentiation of neural crest stem cells (NCSCs) [116], differentiation of osteoblasts from murine 2T3 preosteoblast cells [117], and profibrotic cell differentiation from adult renal progenitor cells [118]. The silencing of NOX4 in primary NCSCs leads to cell death; however, in NOX4$^{-/-}$ knockout mice, the development of the neural crest-derived peripheral nervous system occurred normally (although embryos showed retarded growth). As NOX4 is the only NOX expressed in NCSCs at a detectable level, it is suggested that other NOX proteins from surrounding cells and tissues may provide ROS for NCSCs during embryogenesis [116]. It seems also that NOX levels and functions are dynamically regulated during mouse embryonic stem cell differentiation, as p67phox subunit expression is significantly increased in 2-3-day-old embryoid bodies compared to those 11-12-day old [119, 120].

4.2. NOX and Stem Cells Self-Renewal. There are two key characteristics of stemness: one is potency, understood as an ability to differentiate, and the other is self-renewal, an ability to maintain a pool of undifferentiated stem cells through symmetric and asymmetric cell divisions [121]. The stimulation of NOX4-derived superoxide production by angiotensin II (Ang II) in neural stem cells significantly increases their proliferation [122], leading to the suggestion that NOX4 level regulates stem cell self-renewal and, therefore, may be an important player in neurodegenerative processes such as Alzhaimer's disease, Parkinson's disease, or multiple sclerosis [122]. A function of NOX in self-renewal has also been reported by Morimoto et al. who described a connection between the self-renewal potential of mouse spermatogonial stem cells (SSCs) and NOX3 and presented the hypothesis that renewal of SSCs is in fact regulated by sequential activation of different NOX genes and may or may not occur through the PIK3-AKT and MAP2K1 pathways [123]. Similar results were obtained for adipose-derived stem cells (ASCs) in which the silencing of NOX4 leads to reduced proliferation and cell migration, as well as decreased expression of Oct4 and Rex1 and a lower level of phosphorylation of PDGFR-β, AKT, and ERK1/2 [124].

In contrast, another study suggests that the suppression of NOX using apocynin can reverse the aging process in mesenchymal stem cells and increases the expression of the transcription factors Nanog and Oct-4—which are important in the self-renewal of stem cells [125]. Increased expression of NOX2 and NOX4 has been reported to accelerate senescence of Ang II-stimulated endothelial progenitor cells [126].

ROS generated by NOX (and other sources) can act as an enhancer of stem cell signaling but also as damaging molecules, and therefore, more studies are still required as the threshold is not clearly defined [9]. Additionally, it should be noted that the idea of NOX-mediating differentiation, aging, and senescence of stem cells interferes with data on their role in undifferentiated and not senescent cancer cells. Unfortunately, there is not enough data to draw precise conclusions.

4.3. NOX and Cancer Stem Cells. Several reports indicate that the growth of some solid tumors and their high resistance to chemotherapy are dependent on small population of cells called cancer stem cells (CSCs) [127].

CSCs are subgroup of cancer cells having the ability of self-renewal and capability to initiate tumor formation and metastasis [59]. So far, these tumor-initiating cells have been found in many types of cancer, breast, brain, skin, head and neck, thyroid, cervix, retina, and lung and from leukemia and lymphoma [128–131]. The origin of CSCs remains still unclear, and it is debated if they are formed in a process similar to reprogramming (dedifferentiation) from cells that have acquired a more stem cell-like phenotype or if they are stem cells which have accumulated the sufficient number of mutations required for carcinogenic transformation. It is also possible that they are a result of a combination of both these processes. The issue of the origin of these cells raises numerous discussions, and to highlight this uncertainty, they are often referred as cancer stem-like cells or tumor-initiating cells.

CSCs reside preferentially in special microenvironmental niches within tumor tissue, where cells have a limited access to oxygen. The features of these hypoxic niches are of crucial importance for CSC self-renewal, metastatic potential, and therapy resistance. CSCs express increased levels of antiapoptotic proteins in comparison to mature cell types from the same tissue, which could explain their resistance to cytotoxic drugs [132, 133].

The presence of CSCs might also explain why cancer may reoccur after treatment; most chemotherapeutic drugs act only on mature cancer cells, and CSCs have elevated levels of an ATP-binding cassette which promotes drug resistance [134]. In glioma cells, CSCs preferentially activate DNA-damage checkpoints, so the cells can repair the damage faster and escape radiation-mediated cell death [135]. In breast cancers, CSCs express a low level of ROS due to higher expression of free radical scavengers, which ultimately causes resistant to radiation therapy [136].

Recently, NOX-mediated production of ROS has been recognized as an important factor involved in cancer stem cell regulation and chemotherapy resistance [137]. Enrichment of a population of breast cancer stem-like cell population, induced by exposure to low concentrations of combined carcinogens, correlates with the activation of the RAS-Erk1/2-NOX1 pathway which plays an important role in maintaining increased cell proliferation [138]. The opposite result was observed for stem-like holoclones derived from the PC3 human prostate cancer cell line, which showed reduced expression of NOX2, NOX4, and

NOX5, and their upregulation significantly lowered cell survival in vitro [139].

Gemcitabine, a chemotherapeutic drug used in advanced pancreatic cancer, is characterized by low efficiency and causes rapid development of chemoresistance [137, 140, 141]. New data show that the pancreatic cancer stem cell phenotype (characterized by $CD44^+$, $CD24^+$, and $CD133^+$ markers) can be actually induced by gemcitabine itself [142]. Gemcitabine activates the NF-κB/STAT3 signaling cascade through NOX-mediated production of ROS [137], and pancreatic cell lines incubated with the NOX inhibitor apocynin show not only a decrease in ROS and p-STAT3 levels but also an abolished expression of Nanog, Sox2, and Bmi1, genes associated with self-renewal and maintaining pluripotency [137].

NOX2 has been suggested as a potential target in the development of a therapy against chronic myeloid leukemia (CML) and glioblastoma, as the resistance of CML stem cells and patient-derived glioblastoma stem cells to tyrosine kinase inhibitors seem to be mediated through the NOX2/Egr1/Fyn axis [143]. Chemotherapy may induce the overproduction of ROS which leads to NF-κB-mediated release of inflammatory cytokines, including IL-6 and IL-8, and drive cancer progression through inflammation. Additionally, interleukin-6 is known to induce resistance of myeloma cells to chemo- and radiotherapy by NF-κB-dependent increase of manganese superoxide dismutase expression (MnSOD) [144]. Unfortunately, there is not enough data to confirm whether such re-establishing of redox homeostasis exist in cancer stem cells [144].

The role of NOX-generated ROS in the functioning of cancer stem cells is not well understood yet, but considering their role in cancer recurrence and chemo- and radiotherapy resistance, this seems to be one of the most important research areas in current oxidative medicine [9].

5. Summary

NOX are the only enzymes for which the production of ROS is main physiological function. They play roles in many processes required for functioning of cells and organisms, including wound healing, host defense, cell differentiation during embryogenesis, proliferation, and regulation of gene expression. However, their pathologically altered expression and activity are connected with several neurodegenerative and inflammatory diseases, as well as the development and progression of cancer [145].

NOX can modulate proliferation and differentiation of stem cells which make them a potential tool and target in stem cell therapies, tissue engineering, and regenerative medicine. Studies aimed at growing functional cardiac tissue from stem cells (neonatal rat cardiomyocytes) have already shown NOX-mediated redox signaling to be crucial for neovascularization in vivo which is necessary for the generation of functional tissues [119, 146].

Altered expression of NOX has been observed in many types of cancers [147]. As recent research has brought some light into the mechanisms of NOX-derived ROS action and effects on proliferation, invasiveness, metastasis, and angiogenesis of cancer cells, NOX have been proposed as targets in therapy of lung, colon, thyroid, and prostate cancer [51, 147, 148]. Especially, the ability to prevent metastasis through the modulation of cancer stem cell growth and proliferation would bring enormous benefits for patients. However, this approach is currently limited by the lack of highly specific and validated inhibitors for different NOX enzymes which would not affect other sources of ROS. The development of specific inhibitors seems to be even more important given the poor results of therapies based on antioxidants aimed at scavenging ROS [149]. As NOX are not the only origin of ROS in cells, it is important to understand the mutual interactions between these enzymes and other ROS sources, especially the respiratory chain, to effectively regulate redox potential for therapeutic purposes.

NOX have been intensively studied over the past decade, and the results obtained have significantly increased our knowledge about their activation and the signaling pathways which they influence; however, much more research is still required, especially in vivo using animal models.

Abbreviations

AMPK: 5'AMP-activated protein kinase
BMP-2: Bone morphogenetic protein-2
CPCs: Cardiac precursor cells
CSCs: Cancer stem cells
DPI: Diphenyleiodonium
Egr-1: Early growth response 1
FAD: Flavin adenine dinucleotide
NADPH: Nicotinamide adenine dinucleotide phosphate
NOXA1: NADPH oxidase activator 1
NOXO1: NADPH oxidase organizer 1
PDGFR-β: Platelet-derived growth factor receptor-β
ROS: Reactive oxygen species
Vav2: Guanine nucleotide exchange factor 2.

Conflicts of Interest

The authors declare that there is no conflict of interest regarding the publication of this paper.

Acknowledgments

This work was supported by a grant from the Medical University of Silesia, Project no. KNW-1-101/N/6/I (Rafal J. Buldak), and by the National Science Center Grant nos. DEC-2012/07/B/NZ1/00008 (Magdalena Skonieczna) and SUT-BKM/506/Rau1/2016t.23 (Aleksandra Poterala-Hejmo). Ronald Hancock (Laval University, QC, Canada) is acknowledged for critically reading and editing the manuscript.

References

[1] E. A. Klein, I. M. Thompson, C. M. Tangen et al., "Vitamin E and the risk of prostate cancer: the Selenium and Vitamin E Cancer Prevention Trial (SELECT)," *Jama*, vol. 306, no. 14, pp. 1549–1556, 2011.

[2] V. I. Sayin, M. X. Ibrahim, E. Larsson, J. A. Nilsson, P. Lindahl, and M. O. Bergo, "Antioxidants accelerate lung cancer progression in mice," *Science Translational Medicine*, vol. 6, no. 221, 2014.

[3] K. Le Gal, M. X. Ibrahim, C. Wiel et al., "Antioxidants can increase melanoma metastasis in mice," *Science Translational Medicine*, vol. 7, no. 308, 2015.

[4] E. Piskounova, M. Agathocleous, M. M. Murphy et al., "Oxidative stress inhibits distant metastasis by human melanoma cells," *Nature*, vol. 527, no. 7577, pp. 186–191, 2015.

[5] C. Angeloni, C. Prata, F. Vieceli Dalla Sega, R. Piperno, and S. Hrelia, "Traumatic brain injury and NADPH oxidase: a deep relationship," *Oxidative Medicine and Cellular Longevity*, vol. 2015, Article ID 370312, p. 10, 2015.

[6] A. C. Loureiro, I. C. Rêgo-Monteiro, R. A. Louzada et al., "Differential expression of NADPH oxidases depends on skeletal muscle fiber type in rats," *Oxidative Medicine and Cellular Longevity*, vol. 2016, Article ID 6738701, p. 10, 2016.

[7] D. Burger, M. Turner, M. N. Munkonda, and R. M. Touyz, "Endothelial microparticle-derived reactive oxygen species: role in endothelial signaling and vascular function," *Oxidative Medicine and Cellular Longevity*, vol. 2016, Article ID 5047954, pp. 1–10, 2016.

[8] A. Panday, M. K. Sahoo, D. Osorio, and S. Batra, "NADPH oxidases: an overview from structure to innate immunity-associated pathologies," *Cellular & Molecular Immunology*, vol. 12, no. 1, pp. 5–23, 2015.

[9] T. Maraldi, C. Angeloni, E. Giannoni, and C. Sell, "Reactive oxygen species in stem cells," *Oxidative Medicine and Cellular Longevity*, vol. 2015, Article ID 159080, p. 2, 2015.

[10] K. Bedard and K. H. Krause, "The NOX family of ROS-generating NADPH oxidases: physiology and pathophysiology," *Physiological Reviews*, vol. 87, no. 1, pp. 245–313, 2007.

[11] K. Roy, Y. Wu, J. L. Meitzler et al., "NADPH oxidases and cancer," *Clinical Science*, vol. 128, no. 12, pp. 863–875, 2015.

[12] C. E. Holterman, J. F. Thibodeau, C. Towaij et al., "Nephropathy and elevated BP in mice with podocyte-specific NADPH oxidase 5 expression," *Journal of the American Society of Nephrology*, vol. 25, no. 4, pp. 784–797, 2014.

[13] K. Block and Y. Gorin, "Aiding and abetting roles of NOX oxidases in cellular transformation," *Nature Reviews. Cancer*, vol. 12, no. 9, pp. 627–637, 2012.

[14] J. V. Buul, M. Fernandez-Borja, E. C. Anthony, and P. L. Hordijk, "Expression and localization of NOX2 and NOX4 in primary human endothelial cells," *Antioxidants & Redox Signaling*, vol. 7, no. 3-4, pp. 308–317, 2005.

[15] K. A. Graham, M. Kulawiec, K. M. Owens et al., "NADPH oxidase 4 is an oncoprotein localized to mitochondria," *Cancer Biology & Therapy*, vol. 10, no. 3, pp. 223–231, 2010.

[16] L. L. Hilenski, R. E. Clempus, M. T. Quinn, J. D. Lambeth, and K. K. Griendling, "Distinct subcellular localizations of Nox1 and Nox4 in vascular smooth muscle cells," *Arteriosclerosis, Thrombosis, and Vascular Biology*, vol. 24, no. 4, pp. 677–683, 2004.

[17] B. Diaz, G. Shani, I. Pass, D. Anderson, M. Quintavalle, and S. A. Courtneidge, "Tks5-dependent, Nox-mediated generation of reactive oxygen species is necessary for invadopodia formation," *Science Signaling*, vol. 2, no. 88, 2009.

[18] L. Ahmarani, L. Avedanian, J. Al-Khoury, C. Perreault, D. Jacques, and G. Bkaily, "Whole-cell and nuclear NADPH oxidases levels and distribution in human endocardial endothelial, vascular smooth muscle, and vascular endothelial cells," *Canadian Journal of Physiology and Pharmacology*, vol. 91, no. 1, pp. 71–79, 2013.

[19] B. A. RS, T. Djordjevic, A. Petry et al., "NOX5 variants are functionally active in endothelial cells," *Free Radical Biology & Medicine*, vol. 42, no. 4, pp. 446–459, 2007.

[20] J. L. Meitzler, R. Brandman, and P. R. Ortiz de Montellano, "Perturbed heme binding is responsible for the blistering phenotype associated with mutations in the *Caenorhabditis elegans* dual oxidase 1 (DUOX1) peroxidase domain," *The Journal of Biological Chemistry*, vol. 285, no. 52, pp. 40991–40100, 2010.

[21] H. M. Jackson, T. Kawahara, Y. Nisimoto, S. M. Smith, and J. D. Lambeth, "Nox4 B-loop creates an interface between the transmembrane and dehydrogenase domains," *The Journal of Biological Chemistry*, vol. 285, no. 14, pp. 10281–10290, 2010.

[22] D. I. Brown and K. K. Griendling, "Nox proteins in signal transduction David," *Free Radical Biology & Medicine*, vol. 47, no. 9, pp. 1239–1253, 2009.

[23] J. L. Meitzler and P. R. Ortiz De Montellano, "*Caenorhabditis elegans* and human dual oxidase 1 (DUOX1) "peroxidase" domains: insights into heme binding and catalytic activity," *The Journal of Biological Chemistry*, vol. 284, no. 28, pp. 18634–18643, 2009.

[24] A. C. Gandara, A. Torres, A. C. Bahia, P. L. Oliveira, and R. Schama, "Evolutionary origin and function of NOX4-art, an arthropod specific NADPH oxidase," *BMC Evolutionary Biology*, vol. 17, no. 92, 2017.

[25] I. Dahan, S. M. E. Smith, and E. Pick, "A Cys-Gly-Cys triad in the dehydrogenase region of Nox2 plays a key role in the interaction with p67phox," *Journal of Leukocyte Biology*, vol. 98, no. 5, pp. 850–874, 2015.

[26] A. Petry, M. Weitnauer, and A. Görlach, "Receptor activation of NADPH oxidases," *Antioxidants & Redox Signaling*, vol. 13, no. 4, pp. 467–487, 2010.

[27] J. D. Lambeth, T. Kawahara, and B. Diebold, "Regulation of Nox and Duox enzymatic activity and expression," *Free Radical Biology & Medicine*, vol. 43, no. 3, pp. 319–331, 2007.

[28] M. Geiszt, "NADPH oxidases: new kids on the block," *Cardiovascular Research*, vol. 71, no. 2, pp. 289–299, 2006.

[29] S. R. Coughlin, "Protease-activated receptors in hemostasis, thrombosis and vascular biology," *Journal of Thrombosis and Haemostasis*, vol. 3, no. 8, pp. 1800–1814, 2005.

[30] R. P. Brandes, N. Weissmann, and K. Schröder, "Nox family NADPH oxidases: molecular mechanisms of activation," *Free Radical Biology & Medicine*, vol. 76 no. 2014, pp. 208–226, 2014.

[31] K. D. Martyn, L. M. Frederick, K. von Loehneysen, M. C. Dinauer, and U. G. Knaus, "Functional analysis of Nox4 reveals unique characteristics compared to other NADPH oxidases," *Cellular Signalling*, vol. 18, no. 1, pp. 69–82, 2006.

[32] R. K. Ambasta, P. Kumar, K. K. Griendling, H. H. Schmidt, R. Busse, and R. P. Brandes, "Direct interaction of the novel Nox proteins with p22phox is required for the formation of a functionally active NADPH oxidase," *The Journal of Biological Chemistry*, vol. 279, no. 44, pp. 45935–45941, 2004.

[33] S. Morand, T. Ueyama, S. Tsujibe, N. Saito, A. Korzeniowska, and T. L. Leto, "Duox maturation factors form cell surface

complexes with Duox affecting the specificity of reactive oxygen species generation," *The FASEB Journal*, vol. 23, no. 4, pp. 1205–1218, 2009.

[34] A. N. Lyle, N. N. Deshpande, Y. Taniyama, B. Seidel-Rogol, L. Pounkova, and P. Du, "Poldip2, a novel regulator of Nox4 and cytoskeletal integrity in vascular smooth muscle cells," *Circulation Research*, vol. 105, no. 3, pp. 249–259, 2009.

[35] F. Rizvi, T. Heimann, and W. J. O'Brien, "Expression of NADPH oxidase (NOX) 5 in rabbit corneal stromal cells," *PLoS One*, vol. 7, no. 4, 2012.

[36] X. Zhang, K.-H. Krause, and I. Xenarios, "Evolution of the ferric reductase domain (FRD) superfamily: modularity, functional diversification, and signature motifs," *PLoS One*, vol. 8, no. 3, 2013.

[37] C. Juillan-Binard, A. Picciocchi, J. P. Andrieu et al., "Two-component NOX-like system in bacteria is involved in the electron transfer chain to the methionine sulfoxide reductase MsrP," *The Journal of Biological Chemistry*, vol. 292, no. 6, pp. 2485–2494, 2017.

[38] R. Day and Y. Suzuki, "Cell proliferation, reactive oxygen and cellular glutathione," *Dose-Response*, vol. 3, no. 3, pp. 425–442, 2005.

[39] M. Milenkovic, X. De Deken, L. Jin et al., "Duox expression and related H2O2 measurement in mouse thyroid: onset in embryonic development and regulation by TSH in adult," *The Journal of Endocrinology*, vol. 192, no. 3, pp. 615–626, 2007.

[40] I. Takac, K. Schröder, L. Zhang et al., "The E-loop is involved in hydrogen peroxide formation by the NADPH oxidase Nox4," *The Journal of Biological Chemistry*, vol. 286, no. 15, pp. 13304–13313, 2011.

[41] B. Halliwell and J. M. Gutteridge, "Free radicals, lipid peroxidation, and cell damage," *Lancet*, vol. 2, no. 8411, p. 1095, 1984.

[42] K. B. Beckman and B. N. Ames, "Oxidative decay of DNA," *The Journal of Biological Chemistry*, vol. 272, no. 32, pp. 19633–19636, 1997.

[43] B. S. Berlett, "Protein oxidation in aging, disease, and oxidative stress," *The Journal of Biological Chemistry*, vol. 272, no. 33, pp. 20313–20316, 1997.

[44] J. Fang, T. Sawa, T. Akaike, and H. Maeda, "Tumor-targeted delivery of polyethylene glycol-conjugated D-amino acid oxidase for antitumor therapy via enzymatic generation of hydrogen peroxide," *Cancer Research*, vol. 62, no. 11, pp. 3138–3143, 2002.

[45] J. G. Ren, H. L. Xia, T. Just, and Y. R. Dai, "Hydroxyl radical-induced apoptosis in human tumor cells is associated with telomere shortening but not telomerase inhibition and caspase activation," *FEBS Letters*, vol. 488, no. 3, pp. 123–132, 2001.

[46] T. Matsura, M. Kai, Y. Fujii, H. Ito, and K. Yamada, "Hydrogen peroxide-induced apoptosis in HL-60 cells requires caspase-3 activation," *Free Radical Research*, vol. 30, no. 1, pp. 73–83, 1999.

[47] H. Yamakawa, Y. Ito, T. Naganawa et al., "Activation of caspase-9 and -3 during H2O2-induced apoptosis of PC12 cells independent of ceramide formation," *Neurological Research*, vol. 22, no. 6, 2000.

[48] S. Simizu, M. Takada, K. Umezawa, and M. Imoto, "Requirement of caspase-3 (–like) protease-mediated hydrogen peroxide production for apoptosis induced by various anticancer drugs," vol. 273, no. 41, pp. 26900–26907, 1998.

[49] J. L. Meitzler, S. Antony, Y. Wu et al., "NADPH oxidases: a perspective on reactive oxygen species production in tumor biology," *Antioxidants & Redox Signaling*, vol. 20, no. 17, pp. 2873–2889, 2014.

[50] A. Juhasz, Y. Ge, S. Markel et al., "Expression of NADPH oxidase homologues and accessory genes in human cancer cell lines, tumours and adjacent normal tissues," *Free Radical Research*, vol. 43, no. 6, pp. 523–532, 2010.

[51] M. Höll, R. Koziel, G. Schäfer et al., "ROS signaling by NADPH oxidase 5 modulates the proliferation and survival of prostate carcinoma cells," *Molecular Carcinogenesis*, vol. 55, no. 1, pp. 27–39, 2016.

[52] R. S. Arnold, J. Shi, E. Murad et al., "Hydrogen peroxide mediates the cell growth and transformation caused by the mitogenic oxidase Nox1," in *Edited by Irwin Fridovich, Duke University Medical Center*, vol 98, no. 10, pp. 5550–5555, Durham, NC, USA, 2001.

[53] P. Wang, Q. Shi, W. H. Deng et al., "Relationship between expression of NADPH oxidase 2 and invasion and prognosis of human gastric cancer," *World Journal of Gastroenterology*, vol. 21, no. 20, p. 6271, 2015.

[54] Y. Wu, J. Lu, S. Antony et al., "Activation of TLR4 is required for the synergistic induction of dual oxidase 2 and dual oxidase A2 by IFN-gamma and lipopolysaccharide in human pancreatic cancer cell lines," *Journal of Immunology*, vol. 190, no. 4, pp. 1859–1872, 2013.

[55] N. Ueno, R. Takeya, K. Miyano, H. Kikuchi, and H. Sumimoto, "The NADPH oxidase Nox3 constitutively produces superoxide in a p22 phox-dependent manner: its regulation by oxidase organizers and activators," *The Journal of Biological Chemistry*, vol. 280, no. 24, pp. 23328–23339, 2005.

[56] S. Luxen, S. A. Belinsky, and U. G. Knaus, "Silencing of DUOX NADPH oxidases by promoter hypermethylation in lung cancer," *Cancer Research*, vol. 68, no. 4, pp. 1037–1045, 2008.

[57] A. C. Little, D. Sham, M. Hristova et al., "DUOX1 silencing in lung cancer promotes EMT, cancer stem cell characteristics and invasive properties," *Oncogene*, vol. 5, no. 10, 2016.

[58] Y. Wu, J. L. Meitzler, S. Antony et al., "Dual oxidase 2 and pancreatic adenocarcinoma: IFN-gamma-mediated dual oxidase 2 overexpression results in H2O2-induced, ERK-associated up-regulation of HIF-1alpha and VEGF-A," *Oncotarget*, vol. 7, no. 42, pp. 68412–68433, 2016.

[59] T. Reya, S. J. Morrison, M. F. Clarke, and I. L. Weissman, "Stem cells, cancer, and cancer stem cells," *Nature*, vol. 414, no. 6859, pp. 105–111, 2001.

[60] T. Ago, J. Kuroda, J. Pain, C. Fu, H. Li, and J. Sadoshima, "Upregulation of Nox4 by hypertrophic stimuli promotes apoptosis and mitochondrial dysfunction in cardiac myocytes," *Circulation Research*, vol. 106, no. 7, pp. 1253–1264, 2010.

[61] G. K. Kartha, K. S. Moshal, U. Sen et al., "Renal mitochondrial damage and protein modification in type-2 diabetes," *Acta Diabetologica*, vol. 45, no. 2, pp. 75–81, 2008.

[62] N. Y. Spencer, Z. Yan, R. L. Boudreau et al., "Control of hepatic nuclear superoxide production by glucose 6-phosphate dehydrogenase and NADPH oxidase-4," *The Journal of Biological Chemistry*, vol. 286, no. 11, pp. 8977–8987, 2011.

[63] H. Vaziri, S. K. Dessain, E. N. Eaton et al., "hSIR2(SIRT1) functions as an NAD-dependent p53 deacetylase," *Cell*, vol. 107, no. 2, pp. 149–159, 2001.

[64] J. Barretina, G. Caponigro, N. Stransky et al., "The Cancer-Cell Line Encyclopedia enables predictive modelling of anticancer drug sensitivity," *Nature*, vol. 483, no. 7391, pp. 603–607, 2012.

[65] Y. A. Suh, R. S. Arnold, B. Lassegue et al., "Cell transformation by the superoxide generating oxidase Mox1," *Nature*, vol. 401, no. 6748, pp. 79–82, 1999.

[66] Y. Adachi, Y. Shibai, J. Mitsushita, W. H. Shang, K. Hirose, and T. Kamata, "Oncogenic Ras upregulates NADPH oxidase 1 gene expression through MEK-ERK-dependent phosphorylation of GATA-6," *Oncogene*, vol. 27, no. 36, pp. 4921–4932, 2008.

[67] S. Kajla, A. S. Mondol, A. Nagasawa et al., "A crucial role for Nox 1 in redox-dependent regulation of Wnt-β-catenin signaling," *The FASEB Journal*, vol. 26, no. 5, pp. 2049–2059, 2012.

[68] R. A. Rimerman, A. Gellert-Randleman, and J. A. Diehl, "Wnt1 and MEK1 cooperate to promote cyclin D1 accumulation and cellular transformation," *The Journal of Biological Chemistry*, vol. 275, no. 19, pp. 14736–14742, 2000.

[69] R. Naughton, C. Quiney, S. D. Turner, and T. G. Cotter, "Bcr-Abl-mediated redox regulation of the PI3K/AKT pathway," *Leukemia*, vol. 23, no. 8, pp. 1432–1440, 2009.

[70] D. Hanahan and R. A. Weinberg, "The hallmarks of cancer," *Cell*, vol. 100, no. 1, pp. 57–70, 2000.

[71] D. Hanahan and R. A. Weinberg, "Hallmarks of cancer: the next generation," *Cell*, vol. 144, no. 5, pp. 646–674, 2011.

[72] J. P. Thiery, "Epithelial-mesenchymal transitions in development and pathologies," *Current Opinion in Cell Biology*, vol. 15, no. 6, pp. 740–746, 2003.

[73] H. S. Leong, A. E. Robertson, K. Stoletov et al., "Invadopodia are required for cancer cell extravasation and are a therapeutic target for metastasis," *Cell Reports*, vol. 8, no. 5, pp. 1558–1570, 2014.

[74] F. van Zijl, G. Krupitza, and W. Mikulits, "Initial steps of metastasis: cell invasion and endothelial transmigration," *Mutation Research*, vol. 728, no. 1-2, pp. 23–34, 2011.

[75] H. Paz, N. Pathak, and J. Yang, "Invading one step at a time: the role of invadopodia in tumor metastasis," *Oncogene*, vol. 33, no. 33, pp. 4193–4202, 2014.

[76] H. S. Leong, A. E. Robertson, K. Stoletov et al., "Novel p47(phox)-related organizers regulate localized NADPH oxidase 1 (Nox1) activity," *Science Signaling*, vol. 2, no. 88, 2009.

[77] P. Lock, C. L. Abram, T. Gibson, and S. A. Courtneidge, "A new method for isolating tyrosine kinase substrates used to identify fish, an SH3 and PX domain-containing protein, and Src substrate," *The EMBO Journal*, vol. 17, no. 15, pp. 4346–4357, 1998.

[78] D. F. Seals, E. F. Azucena, I. Pass et al., "The adaptor protein Tks5/fish is required for podosome formation and function, and for the protease-driven invasion of cancer cells," *Cancer Cell*, vol. 7, no. 2, pp. 155–165, 2005.

[79] J. P. Fitzgerald, B. Nayak, K. Shanmugasundaram et al., "Nox4 mediates renal cell carcinoma cell invasion through hypoxia-induced interleukin 6- and 8- production," *PLoS One*, vol. 7, no. 1, pp. 1–9, 2012.

[80] J. Woodard, S. Joshi, B. Viollet, N. Hay, and L. C. Platanias, "AMPK as a therapeutic target in renal cell carcinoma," *Cancer Biology & Therapy*, vol. 10, no. 11, pp. 1168–1177, 2010.

[81] S. Banskota, S. C. Regmi, and J.-A. Kim, "NOX1 to NOX2 switch deactivates AMPK and induces invasive phenotype in colon cancer cells through overexpression of MMP-7," *Molecular Cancer*, vol. 14, no. 1, p. 123, 2015.

[82] B. Govindarajan, J. E. Sligh, B. J. Vincent et al., "Overexpression of Akt converts radial growth melanoma to vertical growth melanoma," *The Journal of Clinical Investigation*, vol. 117, no. 3, pp. 719–729, 2007.

[83] M. Han, T. Zhang, L. Yang, Z. Wang, J. Ruan, and X. Chang, "Association between NADPH oxidase (NOX) and lung cancer: a systematic review and meta-analysis," *J. Thorac. Dis.*, vol. 8, no. 7, pp. 1704–1711, 2016.

[84] X. Liu, C. Pei, S. Yan et al., "NADPH oxidase 1-dependent ROS is crucial for TLR4 signaling to promote tumor metastasis of non-small cell lung cancer," *Tumor Biology*, vol. 36, no. 3, pp. 1493–1502, 2015.

[85] J. Pei, Y. Lou, R. Zhong, and B. Han, "MMP9 activation triggered by epidermal growth factor induced FoxO1 nuclear exclusion in non-small cell lung cancer," *Tumor Biology*, vol. 35, no. 7, pp. 6673–6678, 2014.

[86] D. P. O'Leary, L. Bhatt, J. F. Woolley et al., "TLR-4 signalling accelerates colon cancer cell adhesion via NF-κB mediated transcriptional up-regulation of Nox-1," *PLoS One*, vol. 7, no. 10, 2012.

[87] H. S. Huang, Z. M. Liu, P. C. Chen, H. Y. Tseng, and B. W. Yeh, "TG-interacting factor-induced superoxide production from NADPH oxidase contributes to the migration/invasion of urothelial carcinoma," *Free Radical Biology & Medicine*, vol. 53, no. 4, pp. 769–778, 2012.

[88] D. Wotton, R. S. Lo, S. Lee, and J. Massagué, "A Smad transcriptional corepressor," *Cell*, vol. 97, no. 1, pp. 29–39, 1999.

[89] H. E. Boudreau, B. W. Casterline, D. J. Burke, and T. L. Leto, "Wild-type and mutant p53 differentially regulate NADPH oxidase 4 in TGF-β-mediated migration of human lung and breast epithelial cells," *British Journal of Cancer*, vol. 110, no. 10, pp. 2569–2582, 2014.

[90] H. E. Boudreau, B. W. Casterline, B. Rada, A. Korzeniowska, and T. L. Leto, "Nox4 involvement in TGF-beta and SMAD3-driven induction of the epithelial-to-mesenchymal transition and migration of breast epithelial cells," *Free Radical Biology & Medicine*, vol. 53, no. 7, pp. 1489–1499, 2012.

[91] L. S. Wang, C. T. Kuo, Y. W. Huang, G. D. Stoner, and J. F. Lechner, "Gene-diet interactions on colorectal cancer risk," *Current nutrition reports*, vol. 1, no. 3, pp. 132–141, 2012.

[92] S. Yan, G. Liu, C. Pei et al., "Inhibition of NADPH oxidase protects against metastasis of human lung cancer by decreasing microRNA-21," *Anti-Cancer Drugs*, vol. 26, no. 4, pp. 388–398, 2015.

[93] Z. L. Liu, H. Wang, J. Liu, and Z. X. Wang, "MicroRNA-21 (miR-21) expression promotes growth, metastasis, and chemo- or radioresistance in non-small cell lung cancer cells by targeting PTEN," *Molecular and Cellular Biochemistry*, vol. 372, no. 1-2, pp. 35–45, 2013.

[94] S. Jajoo, D. Mukherjea, T. Kaur et al., "Essential role of NADPH oxidase-dependent reactive oxygen species generation in regulating microRNA-21 expression and function in prostate cancer," *Antioxidants & Redox Signaling*, vol. 19, no. 16, pp. 1863–1876, 2013.

[95] S. Sheth, S. Jajoo, T. Kaur et al., "Resveratrol reduces prostate cancer growth and metastasis by inhibiting the Akt/microRNA-21 pathway," *PLoS One*, vol. 7, no. 12, 2012.

[96] G. M. Gordillo, A. Biswas, S. Khanna et al., "Dicer knockdown inhibits endothelial cell tumor growth via microRNA

21a-3p targeting of nox-4," *The Journal of Biological Chemistry*, vol. 289, no. 13, pp. 9027–9038, 2014.

[97] G. Gordillo, H. Fang, H. Park, and S. Roy, "Nox-4—dependent nuclear H2O2 drives DNA oxidation resulting in 8-OHdG as urinary biomarker," *Antioxidants & Redox Signaling*, vol. 12, no. 8, pp. 933–943, 2010.

[98] S. Yao, A. Bee, D. Brewer et al., "PRKC-ζ expression promotes the aggressive phenotype of human prostate cancer cells and is a novel target for therapeutic intervention," *Genes & Cancer*, vol. 1, no. 5, pp. 444–464, 2010.

[99] N. Nishida, H. Yano, T. Nishida, T. Kamura, and M. Kojiro, "Angiogenesis in cancer," *Vascular Health and Risk Management*, vol. 2, no. 3, pp. 213–219, 2006.

[100] V. Helfinger, N. Henke, S. Harenkamp et al., "The NADPH oxidase Nox4 mediates tumour angiogenesis," *Acta Physiologica*, vol. 216, no. 4, pp. 435–446, 2016.

[101] S. N. Jung, W. K. Yang, J. Kim et al., "Reactive oxygen species stabilize hypoxia-inducible factor-1 alpha protein and stimulate transcriptional activity via AMP-activated protein kinase in DU145 human prostate cancer cells," *Carcinogenesis*, vol. 29, no. 4, pp. 713–721, 2008.

[102] C. Xia, Q. Meng, L. Z. Liu, Y. Rojanasakul, X. R. Wang, and B. H. Jiang, "Reactive oxygen species regulate angiogenesis and tumor growth through vascular endothelial growth factor," *Cancer Research*, vol. 67, no. 22, pp. 10823–10830, 2007.

[103] J. L. Arbiser, J. Petros, R. Klafter et al., "Reactive oxygen generated by Nox1 triggers the angiogenic switch," *Proceedings of the National Academy of Sciences of the United States of America*, vol. 99, no. 2, pp. 715–720, 2002.

[104] S. Garrido-Urbani, S. Jemelin, C. Deffert et al., "Targeting vascular NADPH oxidase 1 blocks tumor angiogenesis through a PPARα mediated mechanism," *PLoS One*, vol. 6, no. 2, 2011.

[105] A. Pozzi, M. R. Ibanez, A. E. Gatica et al., "Peroxisomal proliferator-activated receptor-α-dependent inhibition of endothelial cell proliferation and tumorigenesis," *The Journal of Biological Chemistry*, vol. 282, no. 24, pp. 17685–17695, 2007.

[106] S. Banskota, J. Gautam, S. C. Regmi et al., "BJ-1108, a 6-amino-2,4,5-trimethylpyridin-3-ol analog, inhibits serotonin-induced angiogenesis and tumor growth through PI3K/NOX pathway," *PLoS One*, vol. 11, no. 1, pp. 1–16, 2016.

[107] J. Karar and A. Maity, "PI3K/AKT/mTOR pathway in angiogenesis," *Frontiers in Molecular Neuroscience*, vol. 4, p. 51, 2011.

[108] G. Q. Daley, "Stem cells and the evolving notion of cellular identity," *Philosophical Transactions of the Royal Society of London. Series B, Biological Sciences*, vol. 370, no. 1680, 2015.

[109] P. T. Yin, E. Han, and K. B. Lee, "Engineering stem cells for biomedical applications," *Advanced Healthcare Materials*, vol. 5, no. 1, pp. 10–55, 2016.

[110] S. Pervaiz, R. Taneja, and S. Ghaffari, "Oxidative stress regulation of stem and progenitor cells," *Antioxidants & Redox Signaling*, vol. 11, no. 11, pp. 2777–2789, 2009.

[111] X. Kang, X. Wei, X. Wang et al., "Nox2 contributes to the arterial endothelial specification of mouse induced pluripotent stem cells by upregulating Notch signaling," *Scientific Reports*, vol. 6, 2016.

[112] S. Acharya, A. M. Peters, A. S. Norton, G. K. Murdoch, and R. A. Hill, "Change in Nox4 expression is accompanied by changes in myogenic marker expression in differentiating C2C12 myoblasts," *Pflügers Archiv - European Journal of Physiology*, vol. 465, no. 8, pp. 1181–1196, 2013.

[113] D. Trachootham, W. Lu, M. A. Ogasawara, N. R. Valle, and P. Huang, "Redox regulation of cell survival," *Antioxidants & Redox Signaling*, vol. 10, no. 8, pp. 1343–1374, 2008.

[114] A. S. Nadworny, M. R. Guruju, D. Poor et al., "Nox2 and Nox4 influence neonatal c-kit(+) cardiac precursor cell status and differentiation," *American Journal of Physiology. Heart and Circulatory Physiology*, vol. 305, no. 6, 2013.

[115] Q. Xiao, Z. Luo, A. E. Pepe, A. Margariti, L. Zeng, and Q. Xu, "Embryonic stem cell differentiation into smooth muscle cells is mediated by Nox4-produced H2O2," *American Journal of Physiology. Cell Physiology*, vol. 296, no. 4, pp. 711–723, 2009.

[116] J. E. Lee, K. E. Cho, K. E. Lee, J. Kim, and Y. S. Bae, "Nox4-mediated cell signaling regulates differentiation and survival of neural crest stem cells," *Molecules and Cells*, vol. 37, no. 12, pp. 907–911, 2014.

[117] C. C. Mandal, S. Ganapathy, Y. Gorin et al., "Reactive oxygen species derived from Nox4 mediate BMP2 gene transcription and osteoblast differentiation," *The Biochemical Journal*, vol. 433, no. 2, pp. 393–402, 2011.

[118] S. Simone, C. Cosola, A. Loverre et al., "BMP-2 induces a profibrotic phenotype in adult renal progenitor cells through Nox4 activation," *American Journal of Physiology-Renal Physiology*, vol. 303, no. 1, 2012.

[119] E. C. Chan, F. Jiang, H. M. Peshavariya, and G. J. Dusting, "Regulation of cell proliferation by NADPH oxidase-mediated signaling: potential roles in tissue repair, regenerative medicine and tissue engineering," *Pharmacology & Therapeutics*, vol. 122, no. 2, pp. 97–108, 2009.

[120] H. Sauer, G. Rahimi, J. Hescheler, and M. Wartenberg, "Role of reactive oxygen species and phosphatidylinositol 3-kinase in cardiomyocyte differentiation of embryonic stem cells," *FEBS Letters*, vol. 476, no. 3, pp. 218–223, 2000.

[121] T. Bergström and K. Forsberg-Nilsson, "Neural stem cells: brain building blocks and beyond," *Upsala Journal of Medical Sciences*, vol. 117, no. 2, pp. 132–142, 2012.

[122] E. Topchiy, E. Panzhinskiy, W. S. Griffin, S. W. Barger, M. Das, and W. M. Zawada, "Nox4-generated superoxide drives angiotensin II-induced neural stem cell proliferation," *Developmental Neuroscience*, vol. 35, no. 4, pp. 293–305, 2013.

[123] H. Morimoto, M. Kanatsu-Shinohara, and T. Shinohara, "ROS-generating oxidase Nox3 regulates the self-renewal of mouse spermatogonial stem cells," *Biology of Reproduction*, vol. 92, no. 6, p. 147, 2015.

[124] J. H. Kim, S. Y. Song, S. G. Park, S. U. Song, Y. Xia, and J. H. Sung, "Primary involvement of NADPH oxidase 4 in hypoxia-induced generation of reactive oxygen species in adipose-derived stem cells," *Stem Cells and Development*, vol. 21, no. 12, pp. 2212–2221, 2012.

[125] J. Sun, L. Ming, F. Shang, L. Shen, J. Chen, and Y. Jin, "Apocynin suppression of NADPH oxidase reverses the aging process in mesenchymal stem cells to promote osteogenesis and increase bone mass," *Nature Publishing Group*, no. 5, pp. 1–11, 2015.

[126] H. Li, Q. Liu, N. Wang, and J. Xu, "Correlation of different NADPH oxidase homologues with late endothelial progenitor cell senescence induced by angiotensin II: effect of telmisartan," *Internal Medicine*, vol. 50, no. 16, pp. 1631–1642, 2011.

[127] M. Zaccarin, V. Bosello-Travain, M. L. Di Paolo et al., "Redox status in a model of cancer stem cells," *Archives of Biochemistry and Biophysics*, vol. 617 no. 2017, pp. 120–128, 2017.

[128] T. Klonisch, E. Wiechec, S. Hombach-Klonisch et al., "Cancer stem cell markers in common cancers - therapeutic implications," *Trends in Molecular Medicine*, vol. 14, no. 10, pp. 450–460, 2008.

[129] S. Hombach-Klonisch, T. Paranjothy, E. Wiechec et al., "Cancer stem cells as targets for cancer therapy: selected cancers as examples," *Archivum Immunologiae et Therapiae Experimentalis (Warsz)*, vol. 56, no. 3, pp. 165–180, 2008.

[130] A. M. Wasik, J. Grabarek, A. Pantovic et al., "Reprogramming and carcinogenesis - parallels and distinctions," *International Review of Cell and Molecular Biology*, vol. 308 no. 2014, pp. 167–203, 2014.

[131] E. Farahani, H. K. Patra, J. R. Jangamreddy et al., "Cell adhesion molecules and their relation to (cancer) cell stemness," *Carcinogenesis*, vol. 35, no. 4, pp. 747–759, 2014.

[132] N. Bitarte, E. Bandres, V. Boni et al., "MicroRNA-451 is involved in the self-renewal, tumorigenicity, and chemoresistance of colorectal cancer stem cells," *Stem Cells*, vol. 29, no. 11, pp. 1661–1671, 2011.

[133] D. Ribatti, "Cancer stem cells and tumor angiogenesis," *Cancer Letters*, vol. 321, no. 1, pp. 13–17, 2012.

[134] M. M. Gottesman, T. Fojo, and S. E. Bates, "Multidrug resistance in cancer: role of ATP-dependent transporters," *Nature Reviews. Cancer*, vol. 2, no. 1, pp. 48–58, 2002.

[135] S. Bao, Q. Wu, M. L. RE et al., "Glioma stem cells promote radioresistance by preferential activation of the DNA damage response," *Nature*, vol. 444, no. 7120, pp. 756–760, 2006.

[136] M. Diehn, R. W. Cho, N. A. Lobo et al., "Association of reactive oxygen species levels and radioresistance in cancer stem cells," *Nature*, vol. 458, no. 7239, pp. 780–783, 2009.

[137] Z. Zhang, Q. Duan, H. Zhao et al., "Gemcitabine treatment promotes pancreatic cancer stemness through the Nox/ROS/NF-κB/STAT3 signaling cascade," *Cancer Letters*, vol. 382, no. 1, pp. 53–63, 2016.

[138] L. A. Pluchino and H. C. R. Wang, "Chronic exposure to combined carcinogens enhances breast cell carcinogenesis with mesenchymal and stemlike cell properties," *PLoS One*, vol. 9, no. 11, pp. 1–11, 2014.

[139] K. Shimada, S. Anai, T. Fujii, N. Tanaka, K. Fujimoto, and N. Konishi, "Syndecan-1 (CD138) contributes to prostate cancer progression by stabilizing tumour-initiating cells," *The Journal of Pathology*, vol. 231, no. 4, pp. 495–504, 2013.

[140] L. De Sousa Cavalcante and G. Monteiro, "Gemcitabine: metabolism and molecular mechanisms of action, sensitivity and chemoresistance in pancreatic cancer," *European Journal of Pharmacology*, vol. 741, pp. 8–16, 2014.

[141] R. Warsame and A. Grothey, "Treatment options for advanced pancreatic cancer: a review," *Expert Review of Anticancer Therapy*, vol. 12, no. 10, pp. 1327–1336, 2012.

[142] K. Quint, M. Tonigold, P. Di Fazio et al., "Pancreatic cancer cells surviving gemcitabine treatment express markers of stem cell differentiation and epithelial-mesenchymal transition," *International Journal of Oncology*, vol. 41, no. 6, pp. 2093–2102, 2012.

[143] M. E. Irwin, B. P. Johnson, R. Manshouri, H. M. Amin, and J. Chandra, "A NOX2/Egr-1/Fyn pathway delineates new targets for TKI-resistant malignancies," *Oncotarget*, vol. 6, no. 27, pp. 23631–23646, 2015.

[144] C. O. Brown, K. Salem, B. A. Wagner et al., "Interleukin-6 counteracts therapy-induced cellular oxidative stress in multiple myeloma by up-regulating manganese superoxide dismutase," *The Biochemical Journal*, vol. 444, no. 3, pp. 515–527, 2012.

[145] T. Maraldi, "Natural compounds as modulators of NADPH oxidases," *Oxidative Medicine and Cellular Longevity*, vol. 2013, Article ID 271602, 2013.

[146] F. Jiang, G. Zhang, I. Hashimoto et al., "Neovascularization in an arterio-venous loop-containing tissue engineering chamber: role of NADPH oxidase," *Journal of Cellular and Molecular Medicine*, vol. 12, no. 5B, pp. 2062–2072, 2008.

[147] U. Weyemi, C. E. Redon, P. R. Parekh, C. Dupuy, and W. M. Bonner, "NADPH oxidases NOXs and DUOXs as putative targets for cancer therapy," *Anti-Cancer Agents in Medicinal Chemistry*, vol. 13, no. 3, pp. 502–514, 2013.

[148] Z. Fan, X. Duan, H. Cai et al., "Curcumin inhibits the invasion of lung cancer cells by modulating the PKCα/Nox-2/ROS/ATF-2/MMP-9 signaling pathway," *Oncology Reports*, vol. 34, no. 2, pp. 691–698, Jun. 2015.

[149] G. Bjelakovic, D. Nikolova, L. L. Gluud, R. G. Simonetti, and C. Gluud, "Mortality in randomized trials of antioxidant supplements for primary and secondary prevention: systematic review and meta-analysis," *JAMA*, no. 297, pp. 842–857, 2007.

Hindawi
Oxidative Medicine and Cellular Longevity
Volume 2017, Article ID 5691215, 22 pages
https://doi.org/10.1155/2017/5691215

Research Article

Mitochondrial Transfer from Wharton's Jelly Mesenchymal Stem Cell to MERRF Cybrid Reduces Oxidative Stress and Improves Mitochondrial Bioenergetics

Yao-Chung Chuang,[1,2,3,4,5] Chia-Wei Liou,[1,6] Shang-Der Chen,[1] Pei-Wen Wang,[6,7] Jiin-Haur Chuang,[6,8] Mao-Meng Tiao,[6,9] Te-Yao Hsu,[10] Hung-Yu Lin,[6,7] and Tsu-Kung Lin[1,2,6]

[1]*Department of Neurology, Kaohsiung Chang Gung Memorial Hospital and Chang Gung University College of Medicine, Kaohsiung 833, Taiwan*
[2]*Center of Parkinson's Disease, Kaohsiung Chang Gung Memorial Hospital and Chang Gung University College of Medicine, Kaohsiung 833, Taiwan*
[3]*Faculty of Medicine, College of Medicine, Kaohsiung Medical University, Kaohsiung 833, Taiwan*
[4]*Center for Translational Research in Biomedical Sciences, Kaohsiung Chang Gung Memorial Hospital, Kaohsiung 833, Taiwan*
[5]*Department of Biological Science, National Sun Yat-Sen University, Kaohsiung 833, Taiwan*
[6]*Mitochondrial Research Unit, Kaohsiung Chang Gung Memorial Hospital and Chang Gung University College of Medicine, Kaohsiung 833, Taiwan*
[7]*Department of Internal Medicine, Kaohsiung Chang Gung Memorial Hospital and Chang Gung University College of Medicine, Kaohsiung 833, Taiwan*
[8]*Department of Pediatric Surgery, Kaohsiung Chang Gung Memorial Hospital and Chang Gung University College of Medicine, Kaohsiung 833, Taiwan*
[9]*Department of Pediatrics, Kaohsiung Chang Gung Memorial Hospital and Chang Gung University College of Medicine, Kaohsiung 833, Taiwan*
[10]*Department of Obstetrics and Gynecology, Kaohsiung Chang Gung Memorial Hospital and Chang Gung University College of Medicine, Kaohsiung 833, Taiwan*

Correspondence should be addressed to Hung-Yu Lin; linhungyu700218@gmail.com and Tsu-Kung Lin; tklin@cgmh.org.tw

Received 20 January 2017; Accepted 13 March 2017; Published 4 May 2017

Academic Editor: Jianbo Yue

Myoclonus epilepsy associated with ragged-red fibers (MERRF) is a maternally inherited mitochondrial disease affecting neuromuscular functions. Mt.8344A>G mutation in mitochondrial DNA (mtDNA) is the most common cause of MERRF syndrome and has been linked to an increase in reactive oxygen species (ROS) level and oxidative stress, as well as impaired mitochondrial bioenergetics. Here, we tested whether WJMSC has therapeutic potential for the treatment of MERRF syndrome through the transfer of mitochondria. The MERRF cybrid cells exhibited a high mt.8344A>G mutation ratio, enhanced ROS level and oxidative damage, impaired mitochondrial bioenergetics, defected mitochondria-dependent viability, exhibited an imbalance of mitochondrial dynamics, and are susceptible to apoptotic stress. Coculture experiments revealed that mitochondria were intercellularly conducted from the WJMSC to the MERRF cybrid. Furthermore, WJMSC transferred mitochondria exclusively to cells with defective mitochondria but not to cells with normal mitochondria. MERRF cybrid following WJMSC coculture (MF+WJ) demonstrated improvement of mt.8344A>G mutation ratio, ROS level, oxidative damage, mitochondrial bioenergetics, mitochondria-dependent viability, balance of mitochondrial dynamics, and resistance against apoptotic stress. WJMSC-derived mitochondrial transfer and its therapeutic effect were noted to be blocked by F-actin depolymerizing agent cytochalasin B. Collectively, the WJMSC ability to rescue cells with defective mitochondrial function through donating healthy mitochondria may lead to new insights into the development of more efficient strategies to treat diseases related to mitochondrial dysfunction.

1. Introduction

Mitochondria play crucial roles in oxidative phosphorylation (OXPHOS), ATP production, and diverse cell signaling events. The human mitochondrial genome (mtDNA) is 16,568 bp and encodes a limited number of mitochondria-specific proteins, rRNAs, and tRNAs [1]. Mitochondria are also the major source of intracellular ROS. The electron transport chain (ETC) in the mitochondrial inner membrane is critically involved in the generation of energy, where oxygen acts as an electron acceptor. Mitochondrial ROS is generated in the form of superoxide as a byproduct of inefficient transfer of electrons across the ETC [2]. Accumulated ROS, in a form such as hydrogen peroxide (H_2O_2), when built up to a toxic level within cells can result in oxidative stress and oxidative damage [3]. Mitochondria are highly dynamic organelles, able to divide and combine through the processes of fission and fusion, allowing them to adjust their size, shape, and organization inside the cell [4]. Mitochondria dynamic processes are crucial for cell apoptosis, mitochondrial biogenesis, and mtDNA integrity maintenance [5] and are implicated in the aging process [6]. It has been well documented that changes in mitochondrial metabolism affect mitochondrial morphology and network within the cell. Pharmacological inhibition of respiratory chain complexes alters organization of the mitochondrial network, mitochondrial membrane potential, and usually increases ROS production [7, 8]. Increased ROS production triggers dynamic changes in the morphology of the organelles by mitochondrial fragmentation [9]. An intact mitochondrial membrane potential was found to be crucial for mitochondrial dynamics and morphological changes [10]. In mammalian cells, dynamin 1-like (DNM1L or DRP1), mitochondrial fission factor (MFF), and fission 1 (FIS1) are involved in the fission process, while optic atrophy 1 (OPA1) and mitofusin 1 and 2 (MFN1 and MFN2) participate in the fusion process [11].

Mitochondrial DNA (mtDNA) mutations are critical causes of rare human diseases, characterized by mitochondrial dysfunction [12]. Myoclonus epilepsy with ragged-red fiber (MERRF) is associated with specific point mutations of mtDNA, mainly the mt.8344A>G transition in the mitochondrial $tRNA^{Lys}$ coding gene [13], which is associated with severe defects in protein synthesis, leading to impaired OXPHOS [14]. MtDNA mutation-elicited oxidative stress, oxidative damage, and altered gene expression are involved in the pathogenesis and progression of MERRF syndrome [15, 16]. The heteroplasmy ratio of mutated and wild-type mtDNA deteriorates the development and the severity of this syndrome. Clinically, the MERRF syndrome is maternally inherited and is a neurodegenerative disease characterized by myoclonus, mitochondrial myopathy, cerebellar ataxia, and generalized epilepsy. Histologically, Gomori's trichrome staining of MERRF patients' muscle biopsies revealed the presence of ragged-red fibers, due to the subsarcolemmal accumulation of mitochondria [13]. The mt.8344A>G mutation results not only in inefficient bioenergetics but also in intracellular oxidative stress as indicated by an increased expression of ROS and manganese-superoxide dismutase [15]. In addition, cells harboring the mt.8344A>G mutation presented fragmentation of mitochondria, which is correlated with altered processing of the profusion protein optic atrophy type 1 (OPA1, [17]).

More recently, several studies have shown that mitochondrial transfer from stem cells can rescue aerobic respiration of mtDNA-defective cells [18–20] and stressed cells [21–23]. In 2006, Spees et al. first demonstrated that in mtDNA-devoid A549human lung carcinoma cells (ρ^0-A549 cells), cocultured with human bone marrow mesenchymal stem cells (BMMSC), mitochondria moved from BMMSC to ρ^0-A549 cells [18]. Transferred mtDNA from MSC was identified and defective mitochondrial respiration and ATP production of ρ^0-A549 cells were restored [18]. Islam et al. demonstrated that lipopolysaccharide- (LPS-) damaged lung alveoli in vivo received mitochondrial transfer from BMMSC and presented increased ATP restoration, as well as an improved survival rate [21]. In addition, Wang and Gerdes showed that DNA-damaging UV light induced formation of tunneling nanotubes, which facilitate intercellular mitochondrial transfer from healthy cells to damaged cells [23]. Thus, mitochondrial transfer provides a therapeutic opportunity for disorders related to mtDNA defects and mitochondrial dysfunction. Recently, we have shown that human umbilical cord Wharton's jelly mesenchymal stem cells (WJMSC) demonstrate the capability to conduct mitochondrial transfer [23]. ρ^0 cells receiving mitochondria from WJMSC retained the donated mtDNA long term and exhibited restoration of mitochondrial protein synthesis, electron transport chain (ETC) activity, respiratory function, ATP production, mitochondria-dependent growth, and cellular motility [20]. Herein, we report that mitochondrial transfer from WJMSC to MERRF cybrid is able to partly reduce mtDNA mutation load, decrease oxidative stress, and improve mitochondrial bioenergetics. Furthermore, the effect is concomitant with restoration of mitochondrial dynamics and antiapoptosis resistance.

2. Materials and Methods

2.1. Cell Culture and Cybrid Production. Human 143B osteosarcoma cells were grown in Dulbecco's modified Eagle's medium (DMEM, high glucose, Gibco, Carlsbad, CA, USA) supplemented with 10% heat-inactivated fetal bovine serum (FBS; Gibco, Carlsbad, CA, USA) at 37°C in 5% CO_2. The FBS was thawed at 37°C and then heated to 56°C for 30 minutes for heat inactivation. Cybrids were generated by fusing 143B-ρ^0 cells with human platelets in the absence of pyruvate and uridine as previously described [24]. Briefly, platelets from healthy volunteers were isolated and fused with ρ^0 cells in the presence of polyethylene glycol 1500 (50% *w*/*v*; Roche, Nutley, NJ, USA). After 1 week of recovery, the cells were placed on a 96-well plate in a 1 : 2 limited dilution in pyruvate/uridine-free medium. After 14 days, the cybrid populations forming single colonies were screened and transferred to a 35 mm dish. With continuing growth, the cybrids were transferred to a 100 mm dish for a further 20 generations of culture in order to ensure that nuclear-encoded mitochondrial proteins were incorporated into the

newly introduced mitochondria. Control subject or MERRF patient-donated blood were used for experimentation only after written informed consent had been obtained. This study protocol and written informed content were reviewed and approved by the Institutional Review Board of Chang Gung Memorial Hospital (CGMH; IRB number 101-1620A3).

2.2. Isolation, Cultivation, and Identification of WJMSCs. Human WJMSCs were prepared from fresh human umbilical cords obtained during normal spontaneous deliveries after written informed consent had been obtained. The preparation of human WJMSC has previously been described [20]. Briefly, human umbilical cords were placed in Hanks' balanced salt solution (Gibco, Carlsbad, CA, USA) before harvesting of the WJMSC. After the arteries and veins had been removed, the remaining cord was diced into small pieces and transferred to 10 cm dishes containing DMEM in a 37°C incubator at 5% CO_2. Upon reaching 100% confluence, cells were detached using 0.25% trypsin-EDTA (Gibco, Carlsbad, CA, USA). The WJMSC had a typical spindle-shaped appearance and were found to be positive for CD73, CD90, and CD105 and negative for CD31, CD34, and CD45 in flow cytometric analysis. The WJMSCs used for the experiments were within five passages. Likewise, this study protocol and written informed consent were reviewed and approved by the Institutional Review Board of Chang Gung Memorial Hospital (CGMH; IRB number 101-1620A3).

2.3. Mt.8344A>G Mutation Load. To determine the amount of mtDNA containing the mt.8344A>G mutation of MERRF, PCR/RFLP analysis was performed [25]. The primers used were Primer L8150 (8150-8169): 5′-CCGGGGGTATACTA CGGTCA-3′ and Primer MR28 (8372-8345): 5′-GGGGCAT TTCACTGTAAAGAGGTGCCGG-3′. The amplified PCR products (223 bp) were subjected to restriction digestion by *Nae I* (Thermo Scientific), which can recognize the restriction site (5′-GCCGGC-3′) created by the mt.8344A>G mutation to form a 197 bp and a 26 bp fragment. The PCR products were loaded onto 1.2% agarose gel in Tris-acetate-EDTA (TAE) buffer containing 0.01% of SYBR safe DNA Gen Stain (Invitrogen, Carlsbad, CA, USA). After electrophoresis, the gels were photographed under ultraviolet light. The heteroplasmy of mt.8344A>G was quantified by determining the ratio of 223 bp and 197 bp band intensity using ImageJ.

2.4. ROS Expression and Protein Oxidative Damage. Intracellular ROS generation was determined by flow cytometry, following cell staining with a 6-carboxy-2,7-dichlorodihydrofluorescein diacetate (DCFDA) (Sigma) fluorescent probe. DCFDA was converted by oxidation to highly fluorescent 2′,7′-dichlorodihydrofluorescein (DCF), which was detected at an emission wavelength of 530 nm with excitation at 485 nm. Cells were washed twice with PBS and stained with 5 μM DCFDA for 30 min at 37°C. Cell pellets were collected, washed twice with PBS, and then resuspended in PBS. Fluorescence was detected using a FACSCalibur flow cytometer (BD Biosciences, San Jose, CA, USA) and analyzed using CellQuest software (Becton Dickinson, San Jose, CA, USA). For protein oxidative damage, immunoblot-based detection of carbonyl groups, which are introduced into proteins by oxidative reactions with ozone or oxides of nitrogen or by metal-catalyzed oxidation, were detected using Protein Oxidation Detection Kit (OxyBlot™, Millipore).

2.5. Western Blot. Cells were lysed in RIPA lysis buffer (50 mM Tris, pH 7.4; 150 mM NaCl; 1 mM phenylmethanesulfonyl fluoride; 1 mM ethylenediaminetetraacetic acid (EDTA); 1% Triton X-100; 1% sodium deoxycholate; and 0.1% SDS) with the addition of Protease Inhibitor Cocktail (Roche Diagnostics, Penzberg, Germany) and Phosphatase Inhibitor Cocktail I (Sigma, St. Louis, MO, USA). The antibodies used included anti-COX2 (Abcam, Cambridge, UK), anti-β-actin (Cell Signaling, Danvers, MA), anti-OPA1 (Santa Cruz Biotechnology), anti-MFN2 (Santa Cruz Biotechnology), anti-DRP1 (Santa Cruz Biotechnology), anti-FIS1 (Santa Cruz Biotechnology), and peroxidase-labeled anti-rabbit IgG (H + L) secondary antibody (Abcam, Cambridge, UK). The signals were developed using ECL plus (GE Healthcare Bio-Sciences AB, Uppsala, Sweden) using X-ray films.

2.6. Mitochondrial Membrane Potential. Cationic fluorescent dye tetramethylrhodamine ethyl ester (TMRE; Sigma, St. Louis, MO, USA) was used to assess mitochondrial membrane potential as previously described [24]. Cells were incubated in 100 nM TMRE for 30 min at 37°C. They were then washed twice with 1x PBS and fluorescence signal was examined and photographed by fluorescence microscope. Fluorescent intensity of the image was exhibited by HeatMap Histogram, a plugin for ImageJ. For quantitative measurement, cells stained by TMRE or JC-1 (T-3168; Thermo Fisher Scientific) were analyzed using flow cytometry.

2.7. Oxygen Consumption Rate (OCR). OCR was monitored with a Clark electrode (Mitocell S200 micro respirometry system; Strathkelvin Instruments, Motherwell, UK) as previously described [20]. Cells (100 μl at 5×10^6 cells/ml) in KCl medium (100 mM KCl, 3 mM $MgCl_2$, 20 mM HEPES, 1 mM EDTA, 5 mM KH_2PO_4, pH 7.4) were permeabilized by digitonin (optimal concentration of 32.5 μg/ml determined by trypan blue staining) and loaded into a 200 μl MT200 Respirometer Chamber, suspended by a fixed speed solid-state magnetic stirrer inside the chamber, and maintained at 37°C using a circulating water bath. Basal, ADP-activated, ATP synthase-inhibited, and maximal OCR were determined by adding 10 mM glutamate and 10 mM malate, 0.2 mM ADP, 1 μM oligomycin, 1 μM carbonyl cyanide-4-(trifluoromethoxy)phenylhydrazone (FCCP), and rotenone.

2.8. ATP Assay. 7.5×10^4 cells were trypsinized, washed, and resuspended in DPBS (Invitrogen, Carlsbad, CA, USA); supplemented with 2% FBS; and incubated in the presence of DMSO or oligomycin (Sigma, St. Louis, MO, USA) at37°C for 2 h. Cells were then collected to determine ATP level (ATP Assay Kit #K354-100, BioVision, Palo Alto, CA, USA) according to the manufacturers' instructions.

2.9. Mitochondria-Dependent Viability Assay. 2×10^4 cells were seeded in a 24-well plate with glucose-free DMEM supplemented with 10 mM galactose and 10% FBS at day 0. Bright field cellular morphology was observed under a microscope (Leica, Wetzlar, Germany) at days 1 and 2. Viable cell number was counted by trypan blue assay. For general proliferative rate, cells were seeded in high-glucose DMEM (Gibco, Carlsbad, CA, USA) and trypan blue assay was wielded at days 1 and 2.

2.10. Experimental Procedures for Coculturing and Imaging. Prior to coculture, mitochondria of WJMSC and cybrid were traced by 500 nM Mitotracker Red FM (Invitrogen, Carlsbad, CA, USA) and 100 nM Mitotracker Green FM (Invitrogen, Carlsbad, CA, USA), respectively, for 45 min at 37°C. After washing three times with PBS, the cells were trypsinized and cocultured on glass coverslips for 24 h. The cocultured cells were then fixed with absolute methanol for 10 min on ice, followed by nuclear staining using 1 μg/ml Hoechst 33342 (Invitrogen, Carlsbad, CA, USA) for 5 min at room temperature, and finally mounting on glass slides for analysis using a fluorescence microscope (Leica, Wetzlar, Germany). In an additional experiment using mitochondria-targeted fluorescent protein, Cox4-DsRed and Su9-EGFP constructed plasmids were, respectively, transfected into WJMSC and MERRF cybrids using Lipofectamine3000 Transfection Reagent (Invitrogen, Carlsbad, CA, USA).

For contact coculture, MERRF cybrid and WJMSC (5×10^3 cells each) were mixed and grown onto a glass coverslip in a 35 mm dish. For separated coculture, WJMSC (upper well) and cybrid (lower well) were separated by 3 μm pore transwell insert system (SPL Lifescience, Pocheon, Korea). After 24 h, the upper insert was removed and cybrid in the lower well was analyzed for image, genotyping, and functions.

2.11. Quantification of Mitochondrial Transfer. The interaction of Cox4-DsRed-expressing WJMSCs and Su9-EGFP-expressing ρ^0/cybrid cells were facilitated by direct cocultured. After 24 h, mixed cell population was assayed by flow cytometry. Percentage of mitochondrial transfer was determined by calculating events using the equation below: upper right/(upper right + upper left + lower right) × 100%.

2.12. Mitochondrial Morphology. To observe mitochondrial morphology, cells expressing Cox4-DsRed were seeded onto a 35 mm glass bottom dish. Images were taken under a confocal microscope (FluoView FV10i, Olympus). A cell containing only spherical mitochondria was defined as fragmented. A cell with mitochondrial length less than 5 μm was defined as short tubular. A cell with mitochondria more than 5 μm was indicated as long tubular. 50–100 cells were counted for each cell type. The basis for analyzing mitochondrial aspect ratio, elongation, and interconnectivity using ImageJ macro was previously described by Dagda et al. [26]. Aspect ratio calculated by major/minor axis ratio was used to determine the roundness of mitochondria. Mitochondrial elongation was measured by inverse of circularity. Mitochondrial interconnectivity was estimated by area/perimeter ratio.

2.13. Determination of Cell Apoptosis. Annexin V fluorescent staining was utilized to determine cell apoptosis. Cells were cultured in medium in the presence of 500 nM staurosporine (Sigma, St. Louis, MO, USA). After 6 h of treatment, cells were washed twice with 0.01 M PBS and once with 1x Annexin V Binding Buffer. Cells were then incubated with Annexin V-FITC diluted 1 : 10 in 1x Annexin V Binding Buffer for 15 min at RT. Annexin V-FITC fluorescence was immediately observed under a fluorescence microscope (Leica, Wetzlar, Germany).

For quantitative determination of apoptosis, cells were harvested with trypsinization at the 90% confluent after indicated treatment, stained by Annexin V-FITC, and then assessed for cell apoptosis by flow cytometry (Beckman Coulter, CA, USA).

2.14. Statistical Analysis. Data collected from at least three independent experiments are expressed as the mean ± SEM. Differences between two data sets were evaluated by two tailed unpaired Student's *t*-test. Statistical tests between multiple data sets were analyzed using a one-way analysis of variance (ANOVA) followed by post hoc Bonferroni's test. A p value < 0.05 was considered statistically significant.

3. Results

3.1. MERRF Cybrid Presents High Level of mtDNA Mutation Load, ROS Expression and Oxidative Damage, and Reduced Mitochondrial Bioenergetics. The cytoplasmic hybrid (cybrid) is generated by fusing cytoplast or isolated platelet with an mtDNA-depleted ρ^0 cell, permitting the study of the impact of a particular mitochondrial genome on cellular physiology [27]. Our previous study has demonstrated the successful development of a stable mtDNA-depleted ρ^0 cell and the creation of a cybrid cell line [24]. To establish a cybrid cell model harboring either control subjects or MERRF patients, we introduced mitochondria from control subjects and MERRF patients into mtDNA-depleted ρ^0 cells (Figure 1(a)). Compared to 0% mutation of the control cybrid, the MERRF cybrid harbored more than 90% mutation of mt.8344A>G (Figures 1(b) and 1(c)). The MERRF cybrid presented increased intracellular and mitochondrial ROS expression (Figures 1(d), 1(e), and 1(f)) and a higher abundance of protein carbonylation (Figures 1(g) and 1(h)), indicating mt.8344A>G and resulting in higher cellular oxidative stress and damage. As the mitochondrial membrane potential ($\Delta\Psi$m) resulting from proton gradient drives the F_oF_1-ATP synthase to synthesize ATP, its status regulates the balance of mitochondrial bioenergetics. To assess mitochondrial membrane potential, we used fluorescent dye TMRE that is cell permeant, and it specifically accumulates in mitochondria with membrane potential. In addition, fluorescent dye JC-1 normally presenting green fluorescent forms red fluorescent aggregates when concentrated in active mitochondria and is able to probe change of mitochondrial membrane potential. The MERRF cybrid

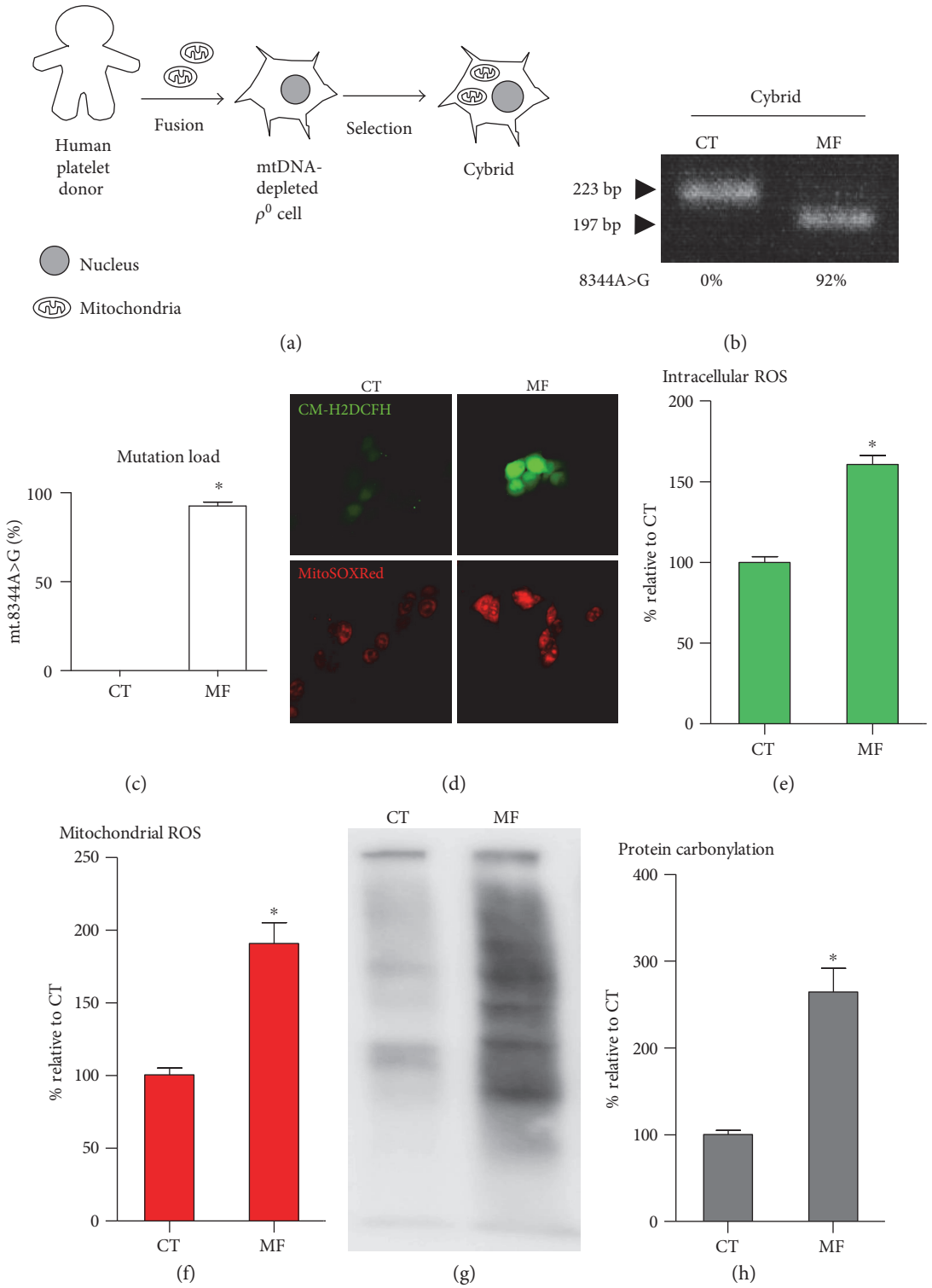

Figure 1: MERRF cybrid with high rate of mt.8344A>G presented higher level of ROS expression and oxidative damage. (a) Schematic drawing shows that cybrid is generated by introducing mitochondria-containing human platelet into mtDNA-depleted ρ^0 cell. (b-c) Mt.8344A>G heteroplasmic rate was examined using PCR-RFLP. PCR fragment containing normal mt.8344A was not digested by *Nae I* and showed a 223 bp band. Mt.8344A>G mutation was *Nae I*-cleaved into 197 bp and 26 bp (not shown in gel). The proportion (%) of mt.8344A>G was quantified using ImageJ. Quantified histogram of mt.8344A>G was obtained by three independent clones. (d–f) Intracellular and mitochondrial ROS expression probed, respectively, by CM-H2DCFH and MitoSOXRed were imaged by fluorescent microscope and quantified by flow cytometry. (g) Protein carbonylation was determined using OxyBlot method. $^*p < 0.05$.

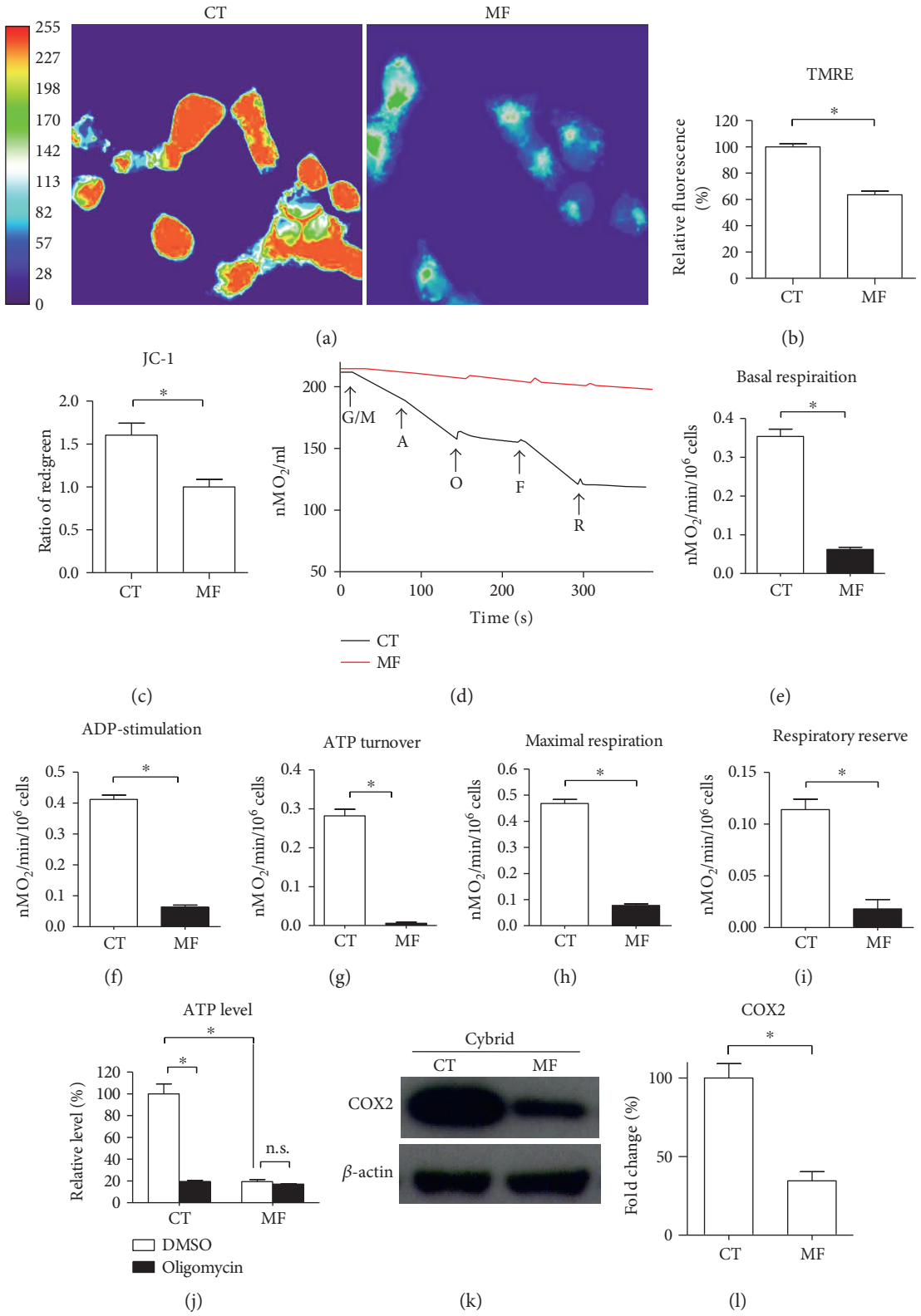

Figure 2: Continued.

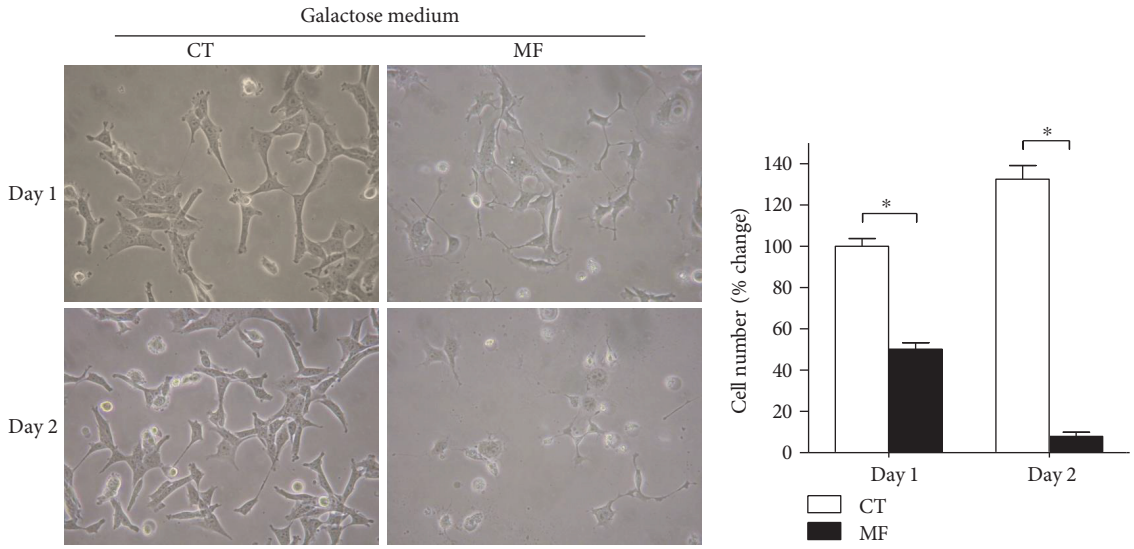

Figure 2: MERRF cybrid demonstrated defective mitochondrial bioenergetics. (a) Mitochondrial membrane potential probed with TMRE was imaged using a fluorescence microscope. Heat map reflecting the fluorescent intensity was analyzed using ImageJ. (b) Quantitative TMRE fluorescence was analyzed using flow cytometer. (c) Mitochondrial membrane potential probed with JC-1 was analyzed using flow cytometer. (d) Representative polarography of OCR measurement. Substrates and inhibitors were sequentially added to cell-containing oximeter chamber, including glutamate/malate (G/M), ADP (A), oligomycin (O), FCCP (F), and rotenone (R). (e) Basal respiration was calculated by OCR in the presence of G/M. (f) ADP-stimulated respiration was calculated by OCR in the presence of ADP. (g) Respiration related to ATP turnover was determined by the difference between ADP-stimulated OCR and oligomycin-suppressed OCR. (h) Maximal respiration was calculated by OCR in the presence of FCCP. (i) Respiratory reserve was determined by the difference between maximal and basal OCR. (j) ATP level was measured in the presence of DMSO or oligomycin. (k-l) Cytochrome c oxidase subunit 2 (COX2) expression level was determined using immunoblotting. β-Actin as a loading control. (m-n) Mitochondria-dependent cellular viability was examined by growing cells in galactose medium. Viable cells were observed under microscope and counted by trypan blue assay. $^{*}p < 0.05$, significantly different when compared to indicated group. CT, control. MF, MERRF.

displayed significantly abated mitochondrial membrane potential compared to the control cybrid by heat map demonstration (Figure 2(a)), as well as cytometric quantitative determination (Figures 2(b) and 2(c)). To examine respiratory capacity, cellular oxygen consumption rate (OCR) was examined using oxygen electrode chamber. Glutamate/malate, ADP, oligomycin, FCCP, and rotenone were sequentially added to cell suspension in respirometer chamber. The presence of digitonin causes the cell membrane to be permeabilized and facilitate entry of water-soluble substrates. Complex I substrate glutamate/malate is used to support basal respiration. Complex V substrate ADP is used to drive oxidative phosphorylation (OXPHOS). As ATP synthase inhibitor oligomycin specifically inhibits F_o portion of mitochondrial ATP synthase (complex V), the OCR suppressed by oligomycin reflects mitochondria-derived ATP turnover. Maximal respiration can be stimulated by the mitochondrial uncoupler FCCP that uncouples OXPHOS and dissipates the mitochondrial membrane potential [28]. Respiratory reserve can be accordingly determined by the difference between maximal and basal respiration. Polarography of oxygen consumption showed that the control cybrid normally consumed oxygen with an expected pattern in response to each added reagent, whereas the MERRF cybrid had a greatly diminished oxygen consumption capacity and did not respond to the presence of reagents (Figure 2(d)). Accordingly, OCR related to basal, ADP-stimulated, ATP turnover, and maximal respiration and respiratory reserve were significantly reduced in MERRF cybrids compared to that in controls (Figures 2(e), 2(f), 2(g), 2(h), and 2(i)). In addition, total ATP level of MERRF cybrids decreased approximately 80% compared to control (Figure 2(j)). The presence of oligomycin caused 80% ATP reduction in control cybrids but has no effect on MERRF cybrids (Figure 2(j)), suggesting that the MERRF cybrid loses mitochondria-derived ATP production. As MERRF mt.8344A>G affects the *MT-TK* gene that encodes mitochondrial $tRNA^{lys}$ [13], we examined mitochondrial translation of the MERRF cybrid by analyzing the expression of mtDNA-encoded cytochrome c oxidase subunit 2 (COX2). The MERRF cybrid had a ~65% decrease in mtDNA-encoded COX2 level compared to the control cybrid, suggesting insufficient protein translation from mitochondrial genome (Figures 2(k) and 2(l)). To examine mitochondria-dependent viability, we employed glucose-free galactose medium in which cells are not able to conduct glycolysis for energy production but exclusively rely on functional mitochondria to generate energy [29]. Compared to control cybrids, MERRF cybrids showed an inability to maintain viability in a glucose-free galactose medium (Figures 2(m) and 2(n)), indicating mt8344A>G, resulting in mitochondrial dysfunction.

3.2. Mitochondria Transfer from WJMSC to Cells with Defective Mitochondria. Our previous work has revealed that

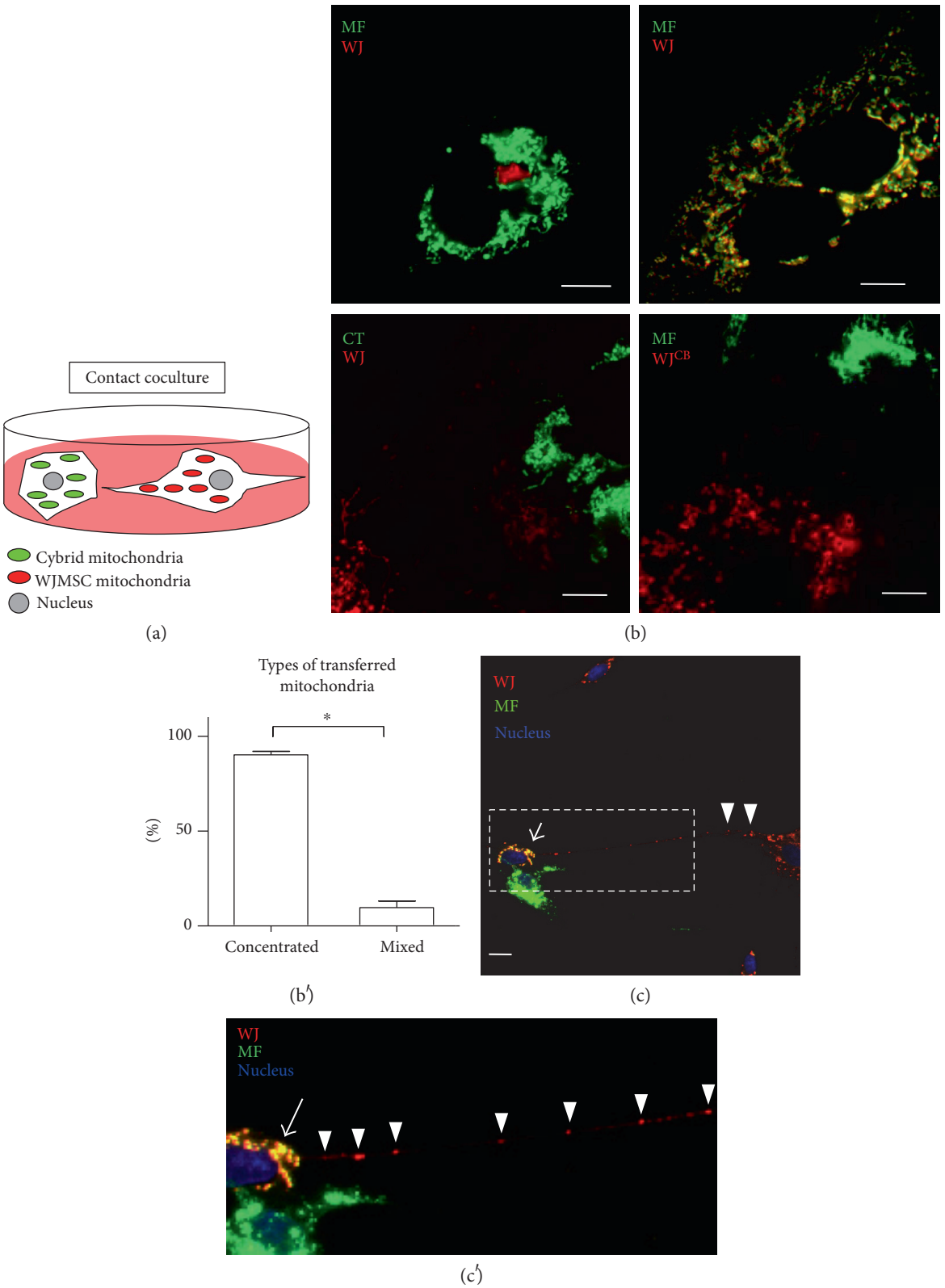

Figure 3: Continued.

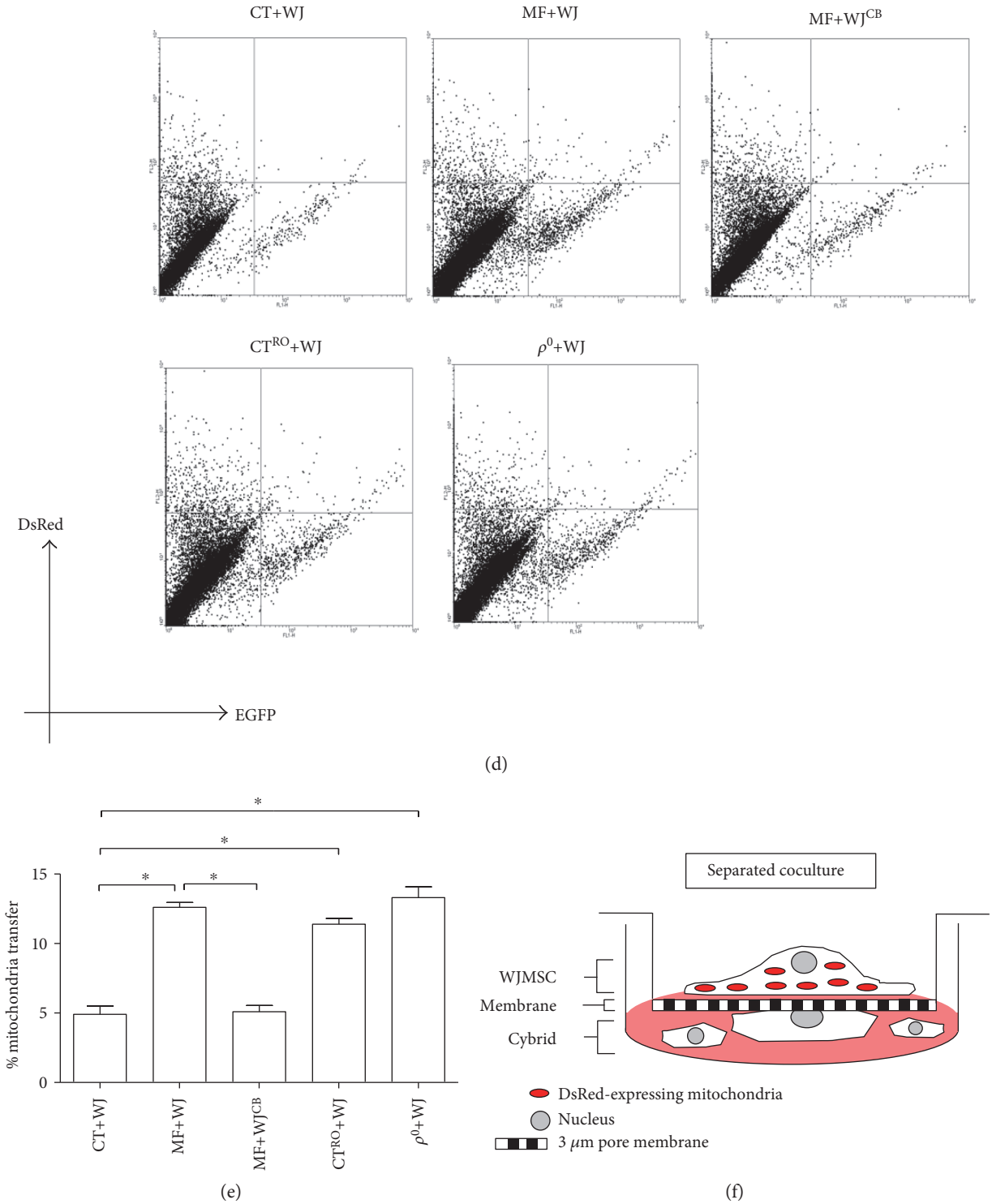

Figure 3: Continued.

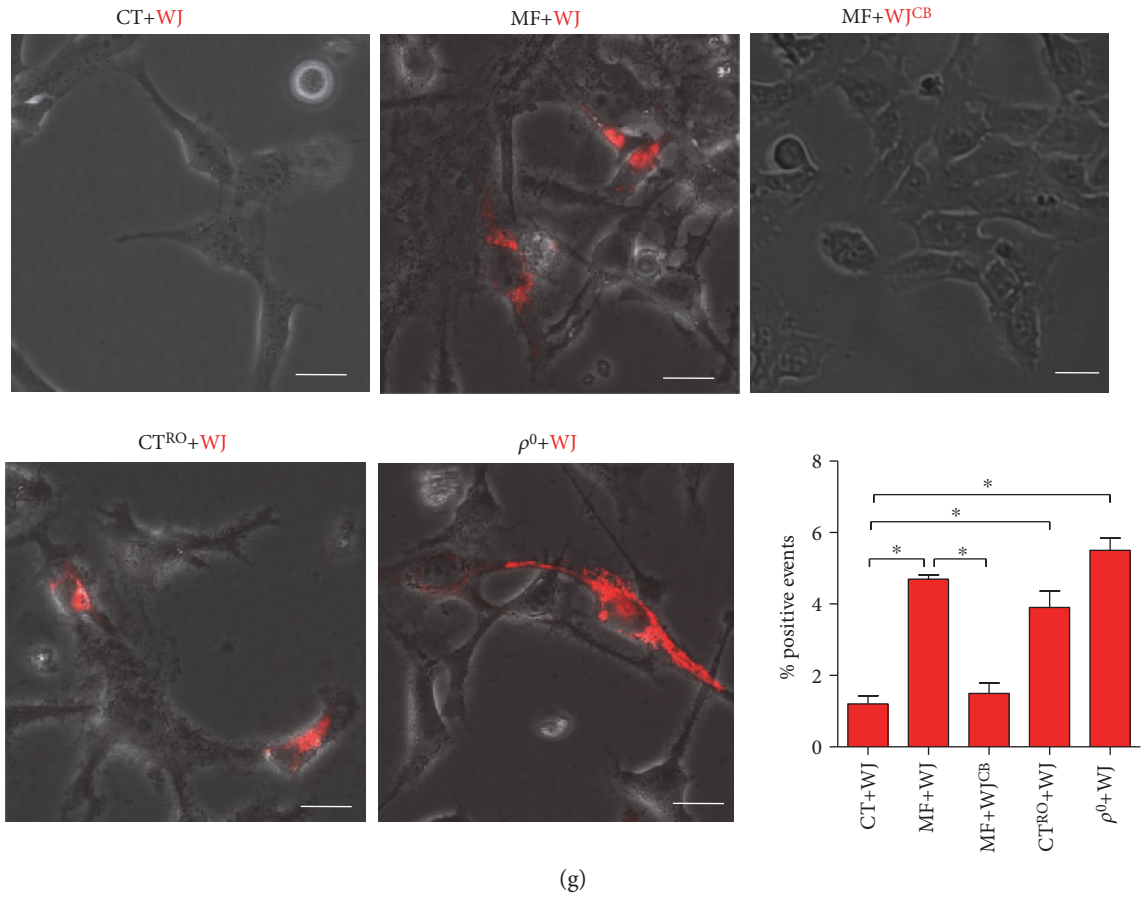

Figure 3: WJMSC transferred mitochondria to MERRF cybrid through a protruded tubular structure. (a) Schematic of contact coculture in which WJMSC and cybrid cell were transfected, respectively, with Cox4-DsRed and Su9-EGFP to tracking mitochondria. (b) After 24 h of coculture, images were photographed under fluorescent microscope. Scale bar, 5 μm. (b′) Types of transferred mitochondria. MERRF cybrids with transferred mitochondria from WJMSC were categorized into concentrated or mixed type. Histogram data are from three experiments, with 50–100 cells counted per experiment. (c) Mitochondria of WJMSC was transferred via a protruded tubular structure to MERRF cybrid. Arrow indicates intercellular mitochondrial fusion with yellow signal. Rectangular dotted line was enlarged in (c′). (c′) Arrowheads indicate that mitochondria of WJMSC was transported along a protruded tubular structure. (d and e) Dot plot of both channels of FACS revealed percentage of mitochondrial transfer in the upper-right quadrant. (f) Schematic of separate coculture in which a 3 μm pore membrane divides Cox4-DsRed-expressing WJMSC from cybrid. (g) Mitochondria from WJMSC transmitted through membrane pore was examined under fluorescence microscope after the upper chamber was offloaded. Percentage of fluorescence-positive events were counted from 25 to 40 view fields of at least three experiments. CT, control cybrid; CT^{RO}, control cybrid pretreated with 500 nM rotenone for 24 h; WJ, WJMSC; MF, MERRF cybrid; MF+WJ, MERRF cybrid-plus-WJMSC; WJ^{CB}, WJMSC pretreated with 350 nM cytochalasin B for 24 h.

WJMSC is capable of transferring healthy mitochondria to mtDNA-depleted ρ^0 cells and rescues impaired mitochondrial function [20]. In light of this finding, we therefore tested whether the mitochondria of WJMSC can be transferred to the MERRF cybrid. To this end, we employed a contact coculture system in which mitochondria of both WJMSC and cybrids were individually traced by red and green fluorescent proteins (Figure 3(a)). Mitochondria-targeted fusion protein Cox4-DsRed and Su9-EGFP were, respectively, transfected into WJMSC and cybrids, followed by coculture (Figure 3(a)). After 24 h, mitochondria distribution was examined and photographed. As shown in Figure 3(b), the MERRF cybrid was noted as having received mitochondria from WJMSC (concentrated mitochondria, upper left panel, Figure 3(b)), mitochondrial mixture was shown by red-green-merged yellow signal (mixed mitochondria, upper right panel, Figure 3(b)). Although the concentrated and mixed mitochondria were simultaneously observed after 24 h coculture, the concentrated type accounted for the majority of cases of identified mitochondrial transfer (Figure 3(b′)). This phenomenon of intercellular mitochondrial transfer was not seen between WJMSC and the control cybrid (lower left panel, Figure 3(b)). Specifically, mitochondrial transfer mediated through protruded tubular structure was presented (Figures 3(c) and 3(c′)). As F-actin-composed structure can facilitate intercellular transfer of organelle, vesicles, and proteins [23, 30], we then investigated its role in WJMSC-derived mitochondrial transfer. To this end, an F-actin-depolymerizing agent cytochalasin B was used to treat WJMSC 24 h prior to coculture. As shown in

Figure 3(b), mitochondrial transfer did not occur from cytochalasin B-treated WJMSC to the MERRF cybrid (lower right panel, Figure 3(b)). Furthermore, we quantitatively measured mitochondrial transfer using flow cytometry. EGFP and DsRed signal were detected using FL1 and FL2 channel. The overlapping signal in the upper right region of FL1/FL2 dot plot was defined as occurrence of intercellular mitochondrial transfer (Figure 3(d)). In like manner, WJMSC-plus-MERRF coculture had a significantly higher percentage of mitochondrial transfer than WJMSC-plus-control coculture (Figures 3(d) and 3(e)). Also, the percentage of intercellular mitochondrial transfer between WJMSC and MERRF cybrids in the presence of cytochalasin B was also abolished (Figures 3(d) and 3(e)). As the MERRF cybrids in our model demonstrated impaired mitochondrial respiration, we thus tested if suppressed mitochondrial respiration plays a role in WJMSC-derived mitochondrial transfer. To achieve this, we individually utilized rotenone and mtDNA depletion to induce mitochondrial dysfunction. Treatment of mitochondrial complex I inhibitor rotenone and mtDNA-depleted ρ^0 cell were shown to cause mitochondrial dysfunction [20, 24]. As expected, the percentage of mitochondrial transfer of rotenone-treated control cybrids and ρ^0 cells significantly increased compared to untreated control cybrids in coculture system with WJMSC (Figures 3(d) and 3(e)). To further confirm that WJMSC transfers mitochondria through intercellular connection but not cellular fusion, we designed a separate coculture system with a 3 μm pore membrane that can permit intercellular interaction by tubular structure. As shown in Figure 3(f), WJMSC transfected with Cox4-DsRed was seeded on the upper chamber with the MERRF cybrid seeded on the bottom chamber (Figure 3(f)). The MERRF cybrid, but not the control cybrid, received mitochondria from WJMSC (Figure 3(g)). WJMSC treated with cytochalasin B was not able to transport mitochondria to the MERRF cybrid via a 3 μm pore membrane (Figure 3(g)), indicating that mitochondrial transfer is dependent on F-actin-composed structure. Likewise, the control cybrid treated with rotenone and the ρ^0 cell presented mitochondria transferred from WJMSC (Figure 3(g)). This result suggests that impaired mitochondrial functions, such as the status seen in mt.8344A>G, complex I inhibition, and mtDNA depletion, play a role in mitochondrial transfer from WJMSC.

3.3. Partly Reduced mtDNA Mutation Load by Mitochondrial Transfer Is Sufficient to Mitigate ROS Expression and Oxidative Damage and Improve Bioenergetics. To inspect mitochondrial function and cellular performance of the MERRF cybrid following mitochondrial transfer from WJMSC, we employed BrdU to remove WJMSC and preserve the MERRF cybrids in coculture system, as WJMSC could not survive with the presence of BrdU. As described in our previous work, cybrids with nuclear background of 143B osteosarcoma have defective activity of thymidine kinase (TK^-) and hence present resistance against BrdU [20]. Then, we cocultured the MERRF cybrid (MF) with WJMSC (WJ) for seven days, followed by 14 days of BrdU selection to remove WJMSC. The remaining cells (MF+WJ cells) should contain normal functional mitochondria and 143B nucleus background which further demonstrates that after coculture MERRF cybrids received mitochondrial transfer from WJMSC (Figure 4(a)). MF+WJ cells demonstrated a partly reduced mtDNA mutation load, whereas WJMSC pretreated with cytochalasin B did not show mitochondrial transfer to affect mtDNA mutation load (Figures 4(b) and 4(c)). The expression of intracellular and mitochondrial ROS (Figures 4(d), 4(e), and 4(f)) and abundance of protein oxidation (Figures 4(g) and 4(h)) were suppressed by the reduction of mtDNA mutation load. Furthermore, mitochondrial membrane potential of MF+WJ cells was partly recovered (Figures 5(a), 5(b), and 5(c)). OCR of basal status, ADP-stimulated, ATP turnover, maximal activity, and respiration reserve of MF+WJ cells were recaptured (Figures 5(d), 5(e), 5(f), 5(g), 5(h), 5(i), 5(j), and 5(k)). ATP level of MF+WJ cells was significantly recovered and mitochondrial ATPase inhibitor oligomycin caused ATP level to plummet (Figure 5(l)). MtDNA-encoded COX2 expression of MF+WJ cells was reversed (Figures 5(m) and 5(n)). In contrast to the inability of the MERRF cell to survive the galactose medium, the MF+WJ cell was able to expand in a glucose-free condition (Figures 5(o) and 5(p)). Moreover, we demonstrated that three lines of WJMSC from different donors were able to rescue mitochondria-dependent viability of MERRF cells (Figures 5(o) and 5(p)). Notably, the recaptured mitochondria-dependent viability persisted for a further 60 days of cultivation, more than 20 passages (Figures 5(q) and 5(r)). These results indicated that a partly reduced mtDNA mutation load by mitochondrial transfer is sufficient to mitigate ROS expression and oxidative damage and improve bioenergetics.

3.4. Improvement of Mitochondrial Bioenergetics and Oxidative Stress Contributes to Recapture of Mitochondrial Network and Apoptotic Tolerance. To analyze mitochondrial network and dynamics, cells were transfected with mitochondrial Cox4-DsRed to display mitochondria. Compared to that of the control cybrid, the MERRF cybrid predominantly presented fragmentation of mitochondria (Figures 6(a), 6(b), 6(c), 6(d), and 6(e)). In line with the fragmented shape of mitochondria, the MERRF cybrid presented decreased OPA1 and increased FIS1 but no change in MFN2 and DRP1 (Figures 6(f), 6(g), 6(h), 6(i), and 6(j)). Also, the MERRF cybrid was more susceptible to apoptosis inducer staurosporine (STS) than the control cybrid (Figures 6(k) and 6(l)). Moreover, mitochondrial network, fusion/fission protein expression pattern, and STS susceptibility were recaptured in MF+WJ cells (Figure 6), suggesting that improvement of mitochondrial bioenergetics and oxidative stress by mitochondrial transfer contributes to modifications in mitochondrial dynamics and apoptotic tolerance.

4. Discussion

Although it has been established that mtDNA mutation causes MERRF, the MERRF cybrid model was constructed to confirm the causal relationship between mutation and mitochondrial dysfunction; a feasible strategy to rescue disease progression remains wanting. Here, we visualized and

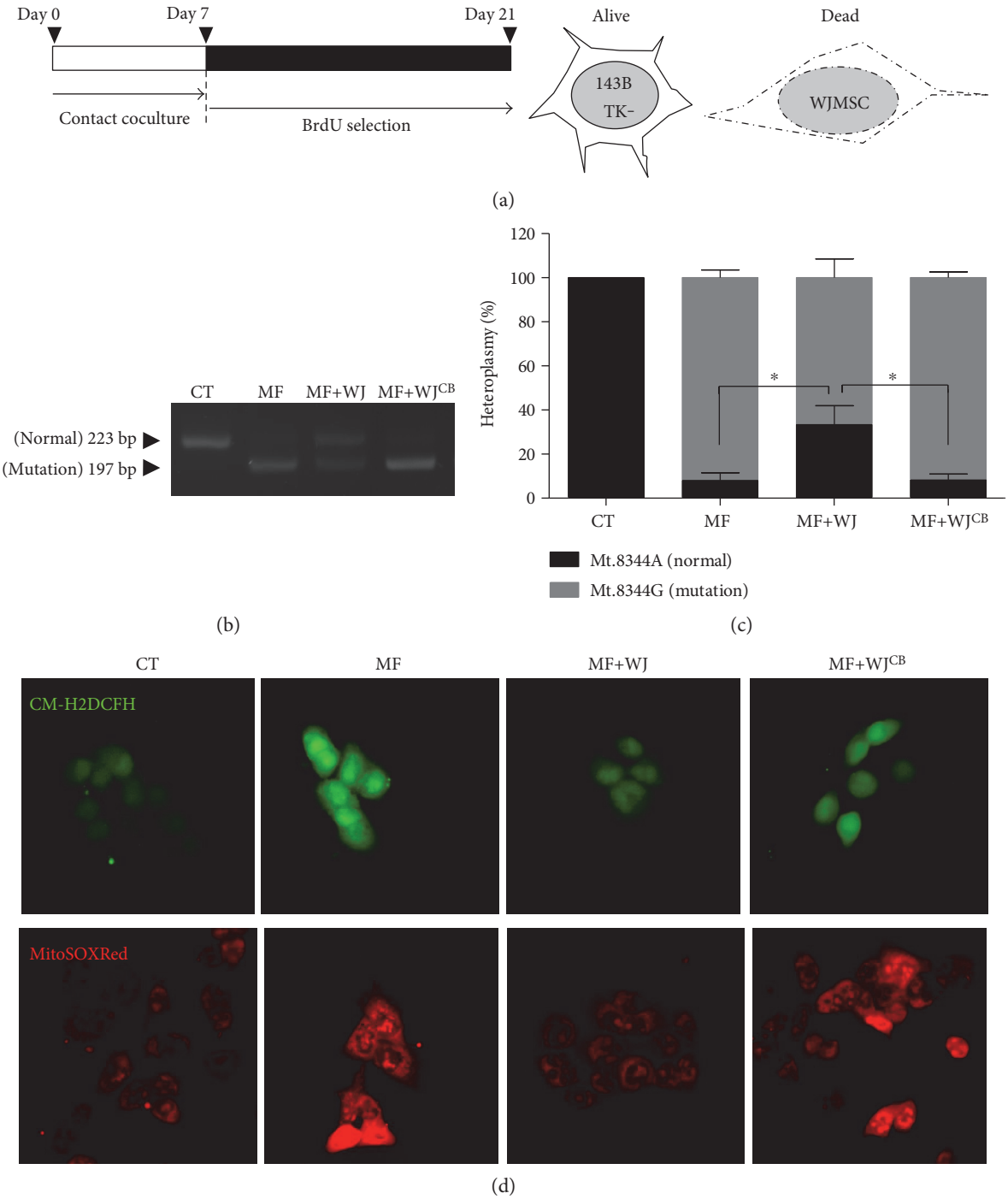

Figure 4: Continued.

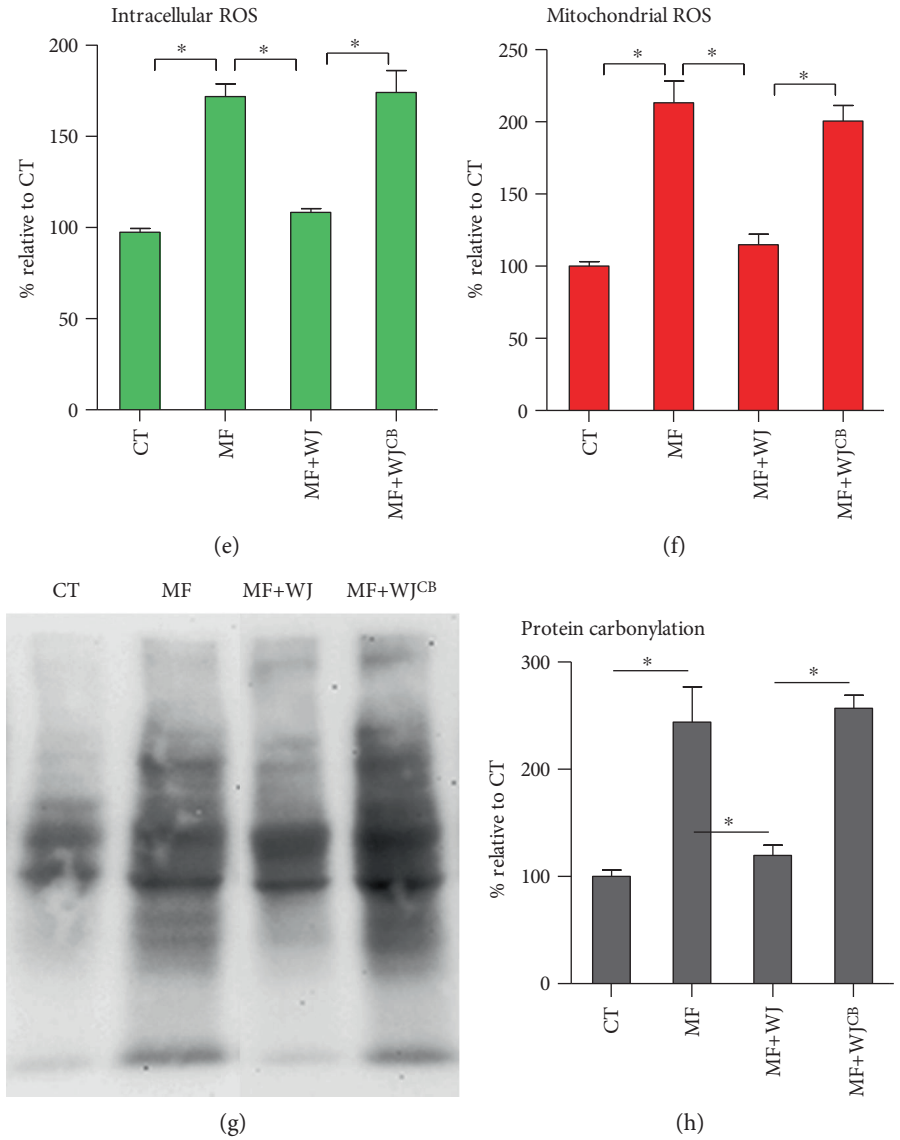

Figure 4: Partly reduced mtDNA mutation load by mitochondrial transfer is sufficient to mitigate ROS expression and oxidative damage. (a) Time course of coculture in which WJMSC and MERRF cybrid interacted for 7 days. Then, WJMSC was eliminated while MERRF cybrid was preserved in the presence of BrdU for another 14 days. Only cells with defective activity of thymidine kinase (TK^-) can survive. (b-c) Mitochondrial transfer partly altered mt.8344A>G mutation rate, whereas cytochalasin B (CB) blocked the effect. (d–f) Intracellular and mitochondrial ROS expression probed, respectively, by CM-H2DCFH and MitoSOXRed were imaged with fluorescent microscope and quantified by flow cytometry. (g-h) Protein carbonylation was determined using OxyBlot method. $^*p < 0.05$. CT, control cybrid; WJ, WJMSC; MF, MERRF cybrid; MF+WJ, MERRF cybrid-plus-WJMSC; WJ^{CB}, WJMSC pretreated with 350 nM cytochalasin B for 24 h.

quantified that WJMSC is able to conduct mitochondrial transfer along with wild-type mtDNA into the mt.8344A>G harboring the MERRF cybrid, resulting in a partial reduction of mtDNA mutation load, oxidative stress, and mitochondrial bioenergetics. Following improved mitochondrial function, the MERRF cybrid presents amelioration in mitochondria-dependent cellular viability, mitochondrial networks and dynamics, and antiapoptosis resistance. These results indicate a possible therapeutic strategy for managing MERRF syndrome.

There is some evidence revealing that exogenous donation of normal mitochondria is able to improve mitochondrial disorders that are caused by either mtDNA mutation or stress. Peptide-mediated mitochondrial delivery has been shown to be effectively transferred into human cells harboring mt.8344A>G in vitro and to improve mitochondrial protein synthesis, bioenergetics, biogenesis, dynamics and calcium homeostasis, while reducing ROS generation [31, 32]. Intercellular mitochondrial transfer via tunneling nanotubes is able to rescue UV-damaged rat pheochromocytoma cells from apoptosis in vitro. In addition, mitochondrial transfer from BMMSC to LPS-damaged lung alveolar epithelia in vivo significantly reduces acute lung injury and increases alveolar

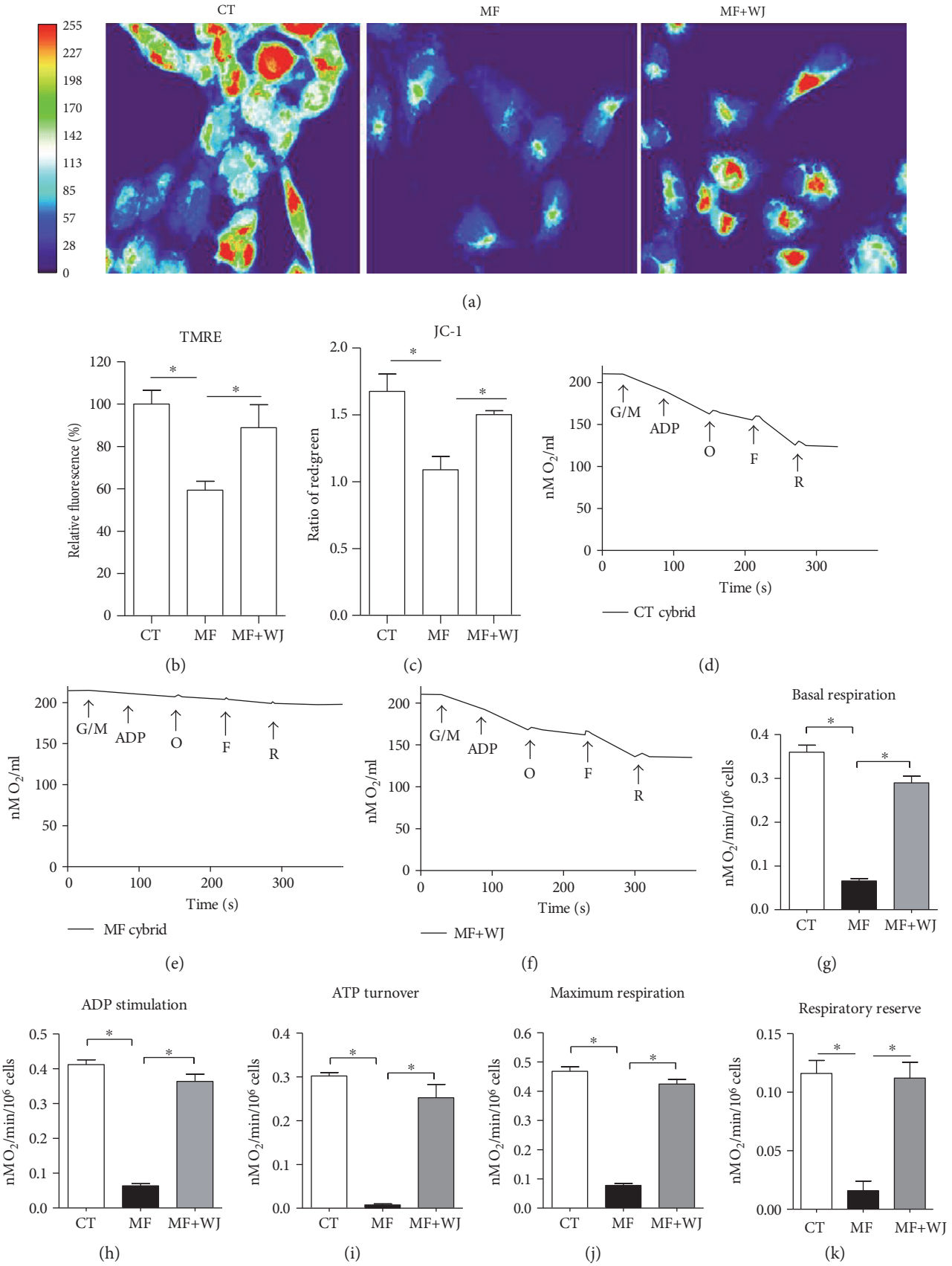

Figure 5: Continued.

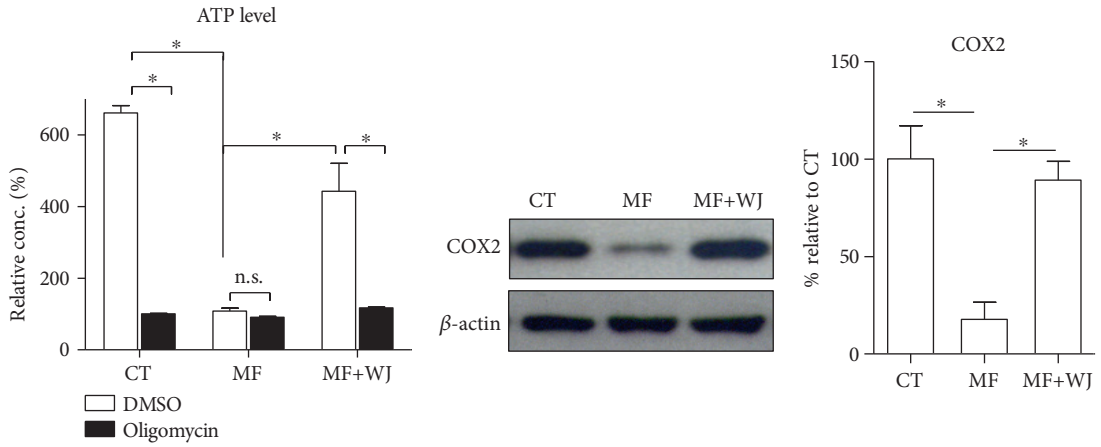

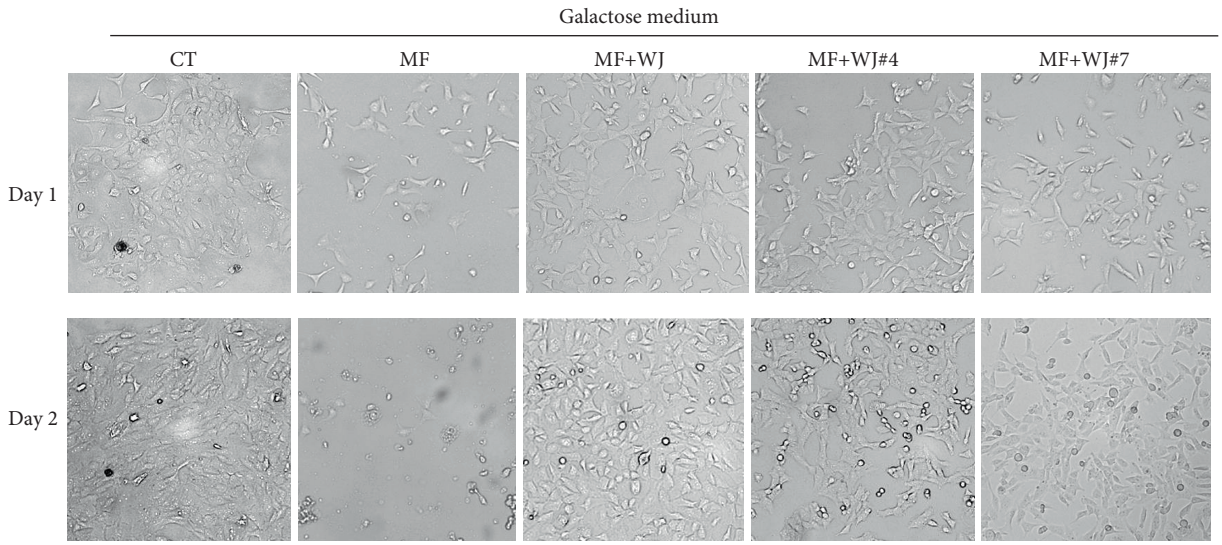

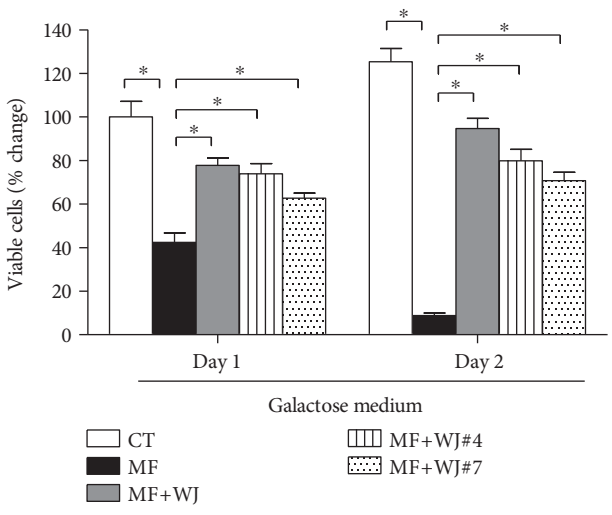

Figure 5: Continued.

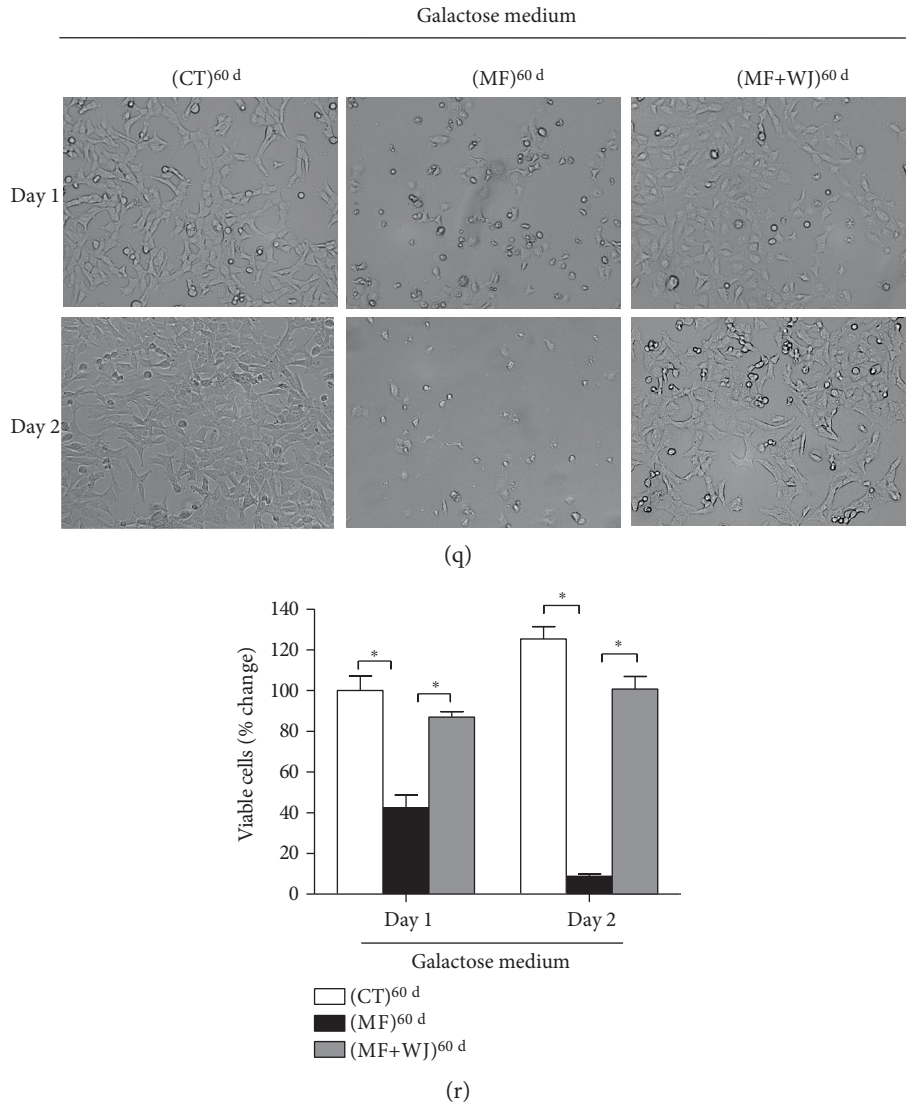

Figure 5: Partly reduced mtDNA mutation load by mitochondrial transfer is sufficient to improve mitochondrial bioenergetics long term. (a) Mitochondrial membrane potential probed with TMRE was imaged using a fluorescence microscope. Heat map reflecting the fluorescent intensity was analyzed using ImageJ. (b) Quantitative TMRE fluorescence was analyzed using flow cytometer. (c) Mitochondrial membrane potential probed with JC-1 was analyzed using flow cytometer. (d–f) representative polarography of OCR measurement. Substrates and inhibitors were sequentially added to a cell-containing oximeter chamber, including glutamate/malate (G/M), ADP (A), oligomycin (O), FCCP (F), and rotenone (R). (g) Basal respiration was calculated by OCR in the presence of G/M. (h) ADP-stimulated respiration was calculated by OCR in the presence of ADP. (i) Respiration related to ATP turnover was determined by the difference between ADP-stimulated OCR and oligomycin-suppressed OCR. (j) Maximal respiration was calculated by OCR in the presence of FCCP. (k) Respiratory reserve was determined by the difference between maximal and basal OCR. (l) ATP level was measured in the presence of DMSO or oligomycin. (m-n) Cytochrome c oxidase subunit 2 (COX2) expression level was determined using immunoblotting. β-Actin as a loading control. (o–r) Mitochondria-dependent cellular viability was examined by growing cell in galactose medium. Viable cells were observed under microscope and counted by trypan blue assay. $^*p < 0.05$, significantly different when compared to indicated group. CT, control; MF, MERRF; MF+WJ, MERRF cybrid-plus-WJMSC.

bioenergetics, as well as improves survival rate [21]. Recently, we also found that human WJMSC demonstrates the capability to transfer mitochondria to mtDNA-devoid cells and recapture mitochondrial protein synthesis and bioenergetics. In this study, we observed the transfer of mitochondria from WJMSC to MERRF cybrids which mitigated mtDNA mutation load, oxidative stress, and mitochondrial bioenergetics. Thus, our study provides further support for the notion that successful delivery of normal mitochondria along with mtDNA can rescue mitochondrial dysfunction.

MtDNA heteroplasmy is a critical contributor to the severity of mitochondrial diseases. Our results demonstrate that mitochondrial transfer was coupled with mtDNA transfer, which partly reduced mt.8344A>G mutation load. This reduced mtDNA mutation burden may contribute to the enhancement of translation of mtDNA-encoded protein.

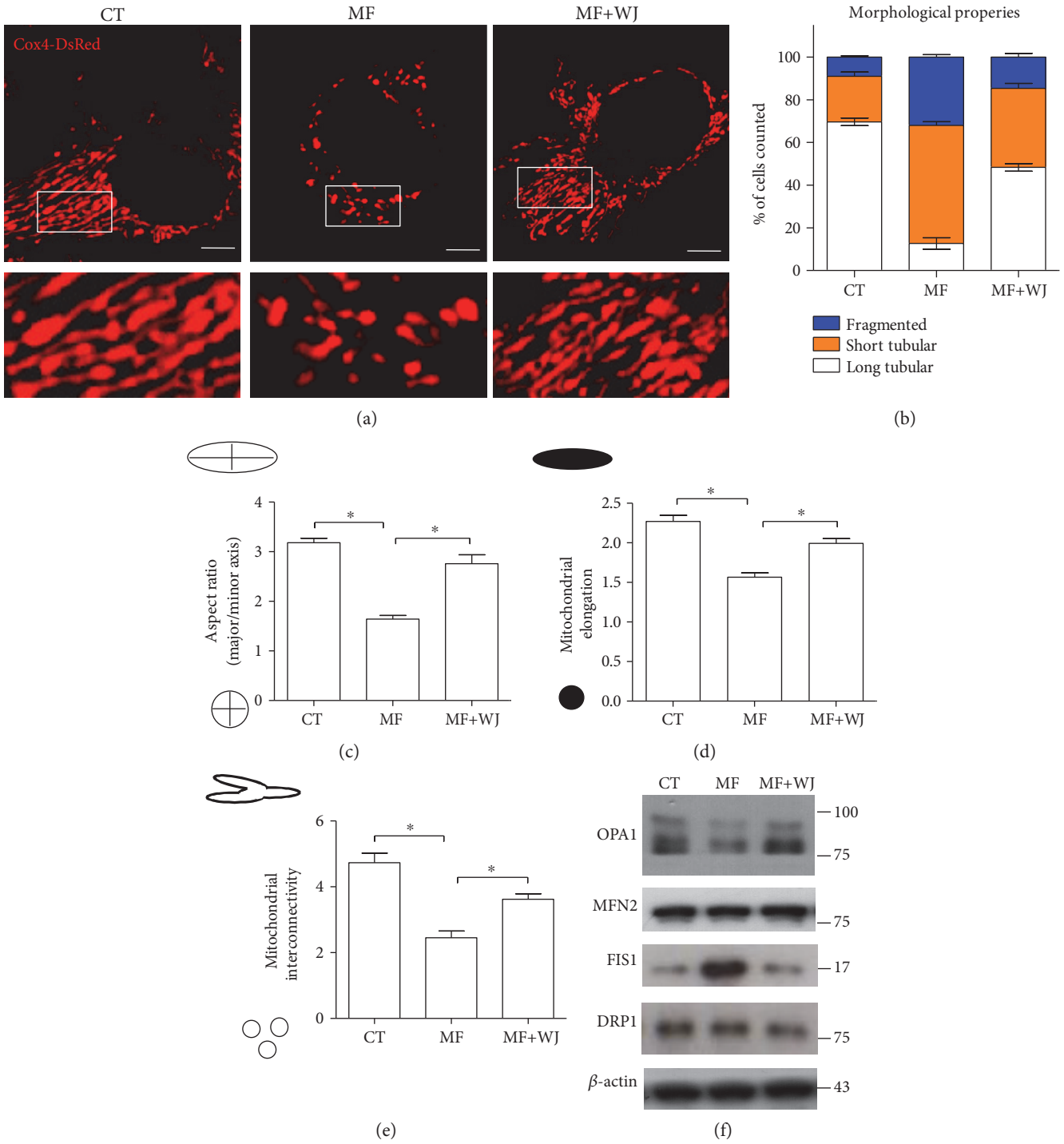

Figure 6: Continued.

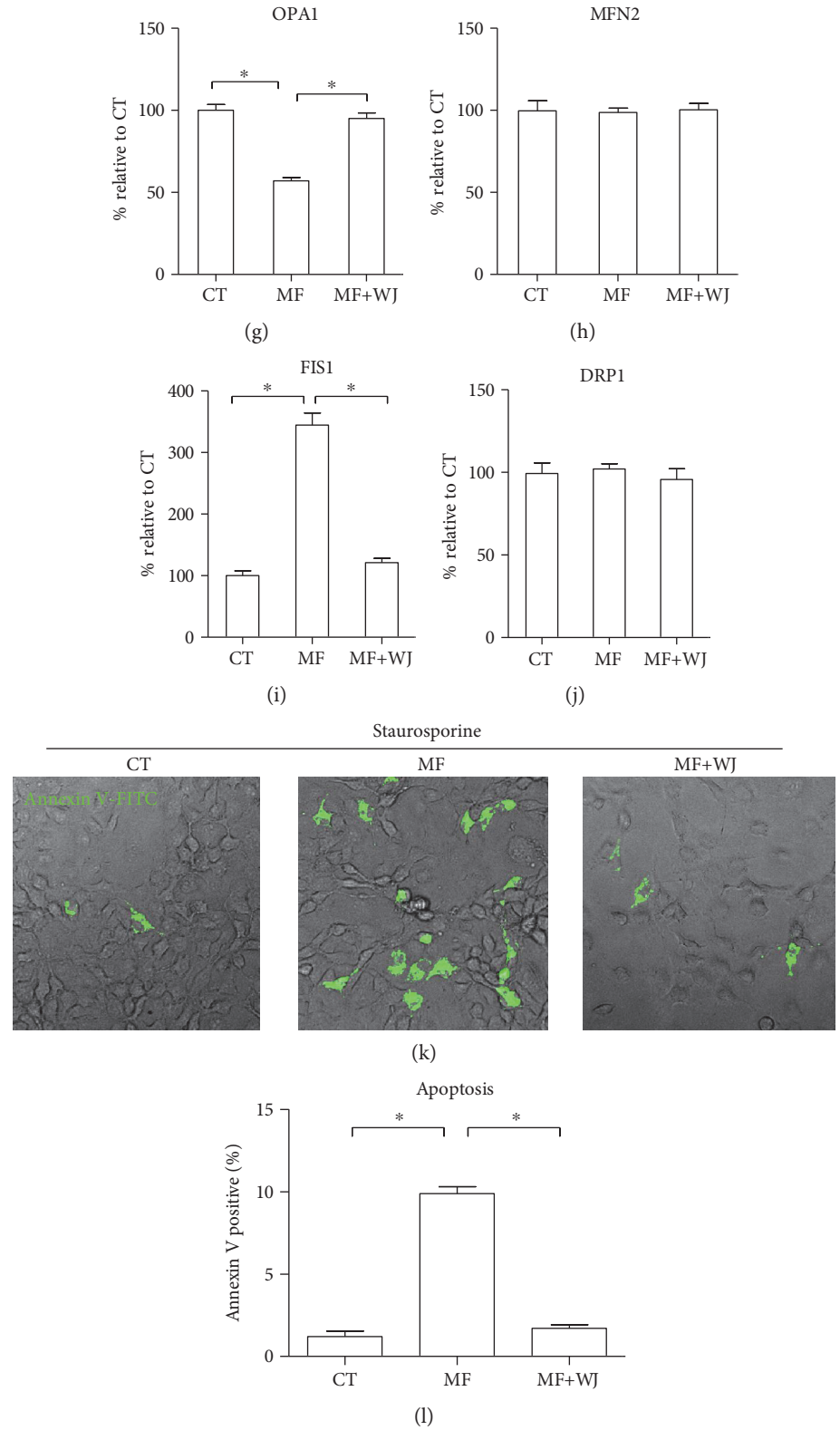

Figure 6: Improvement of mitochondrial bioenergetics and oxidative stress is associated with recapture of mitochondrial network and antiapoptosis resistance. (a) Cells expressed mitochondrial Cox4-DsRed to display mitochondrial morphology under confocal microscope. Scale bar, 5 μm. (b) 50–100 cells were counted for each cell type. (c–e) Mitochondrial morphology was analyzed using Dagda's method [26], as described in Materials and Methods. (f–j) Expression level of mitochondrial fusion protein (OPA1 and MFN2) and fission protein (FIS1 and DRP1). (k-l) Cellular apoptosis was induced by 6 h exposure of 500 nM staurosporine. Apoptosis was detected by Annexin V-FITC. $^*p < 0.05$, significantly different when compared to indicated group. CT, control; MF, MERRF; MF+WJ, MERRF cybrid-plus-WJMSC.

We reason that corrected mitochondrial translation assists respiratory enzyme complex to perform mitochondrial bioenergetics, such as facilitating electron transport, generating mitochondrial membrane potential, oxygen consumption, and ATP production through oxidative phosphorylation. Accordingly, the clinical application of WJMSC for MERRF and other mitochondrial disease patients may offer potential for the development of therapeutic treatment. Besides cells harboring mt.8344A>G, we also demonstrated that WJMSC transfers mitochondria to cells exposed to mitochondrial complex I inhibitor rotenone, as well as those with depleted mtDNA. That may raise the prospect that WJMSC possesses therapeutic potential for other diseases associated with mitochondrial disorders, such as Parkinson disease, Huntington disease, and metabolic diseases.

Whether the effect of mitochondrial transfer can persist for the long term may be a critical issue for the development of future clinical applications. Chang and colleagues showed that the effect of peptide-mediated mitochondria delivery to MERRF cells can be maintained for at least 21 days [32]. Here, we demonstrated that mitochondrial transfer from WJMSC to the MERRF cell sustains for at least 60 days, and aerobic viability of rescued MERRF cells still remains intact. These findings imply that the MERRF cell is likely to preserve transferred mtDNA without immediately removing exogenous mtDNA. Interestingly, Cho et al. demonstrated that bone marrow mesenchymal stem cells can transfer mitochondria to ρ^0 cells but not to cybrid cells harboring the pathogenic mutation of mt.3243A>G and 4977 bp deletion. Although the issue of whether bone marrow mesenchymal stem cells can transfer mitochondria to MERRF cells is not investigated in Cho's study, the mechanism receiving exogenous mitochondria may be different between mt.8344A>G and mt.3243A>G/4977 bp deletion. On the other hand, the possibility that WJMSC may possess a superior ability to transfer mitochondria cannot be ignored. In this regard, Lund et al. have shown that WJMSCs exhibited superior efficacy than bone marrow mesenchymal stem cells in rescuing the photoreceptor after transplantation into the rodent's eyes [33]. More studies are required to determine the efficiency and rescue effect of WJMSC compared to those of other cell sources.

Mitochondrial matrix-localized fluorescent protein facilitates the surveillance of mitochondrial transfer, as well as fusion status of mitochondria from two cellular origins. We employed matrix-localized Cox4-DsRed and Su9-EGFP to demonstrate not only intercellular mitochondrial transfer but also the integrating status of both mitochondria (Figure 3). We observed two distinct patterns of transferred mitochondria, concentrated and mixed mitochondria, which take place simultaneously, with the concentrated pattern as the majority (Figures 3(b) and 3(b′)). In this regard, concentrated and mixed presentations indicate incomplete and full fusion of both mitochondria, respectively. We reason that transferred mitochondria from WJMSC in an earlier phase are yet to fuse with MERRF cybrid's mitochondria, demonstrating a concentrated appearance; whereas in a later phase, both mitochondria undergo full fusion, resulting in a mixed appearance. As a result, the reciprocal fusion may allow modification of mtDNA heteroplasmy. Accordingly, the reduction of mtDNA mutation load in MERRF cybrid receiving mitochondrial transfer verifies the sustainability of WJMSC mtDNA (Figures 4(b) and 4(c)).

WJMSC exhibits similar basic hallmarks of adult MSCs, such as surface markers, morphology, and multipotency to differentiation [34]. Adult MSCs, such as bone marrow MSC and adipocyte-derived MSC, have been shown to conduct mitochondrial transfer to restore cellular viability [21, 35, 36]. However, the procedure to obtain adult MSC is highly invasive and not frequently acceptable for healthy donors. Unlike adult MSC, WJMSC is derived from the umbilical cord, which is a natural form of waste resulting after birth and free from additional invasive procedures. This makes WJMSC a more accessible source of stem cells for use in clinical and experimental applications. Harvesting WJMSC allows for a rapid initial isolation of larger cell numbers and growth of WJMSC demonstrates shorter doubling time compared to BMMSCs [37, 38]. Of note, the immunomodulatory properties of WJMSC that avoids graft-versus-host disease and permits transplanted cells to survive long term [39] allow for possible immunosuppressant-free management following xenograft transplantation. Additionally, the inability of WJMSC to perform attachment-free colony formation and invasiveness in vitro implies that it is devoid of tumorigenic potential [20]. These advantages thus facilitate the further development of WJMSC-based therapy and may pave the way for future clinical application.

With reference to the mechanisms accounting for mitochondrial transfer, previous studies have suggested that the induction of mitochondrial dysfunction and the formation of F-actin-containing tunneling nanotubes may play a role. In this regard, Ahmad et al. demonstrated that mitochondrial dysfunction in epithelial cell injury induced by mitochondrial complex I inhibitor rotenone can be rescued by BMMSC-derived mitochondrial transfer via intercellular F-actin-containing tubular structure [22]. Knockdown tunneling nanotube-formatting protein TNFAIP2 abolished mitochondrial transfer and lead to a substantial reduction of therapeutic effect [22]. On the other hand, Wang and Gerdes have shown that UV light-stressed pheochromocytoma cells form tunneling nanotubes that communicate with healthy cells and facilitate mitochondrial transfer to prevent UV stress-induced apoptosis [23]. F-actin-depolymerizing agent cytochalasin B abolished intercellular formation of tunneling nanotubes and accordingly blocked mitochondrial transfer and antiapoptosis effect [23]. In our study, mitochondrial transfer from WJMSC is able to rescue mitochondrial dysfunction caused by the mt.8344A>G mutation in MERRF cells. We demonstrated the occurrence of mitochondrial transfer by observing and quantifying fluorescence mitochondria in a contact coculture system, as well as a separated coculture system which permits tubular structure-mediated communication without cell-cell contact. In addition, mitochondrial transfer from WJMSC occurred when cocultured with cells stressed with rotenone and those devoid of mtDNA but not cells with functional mitochondria. Moreover, cytochalasin B pretreatment to WJMSC abolished the mitochondrial transfer and subsequent rescue

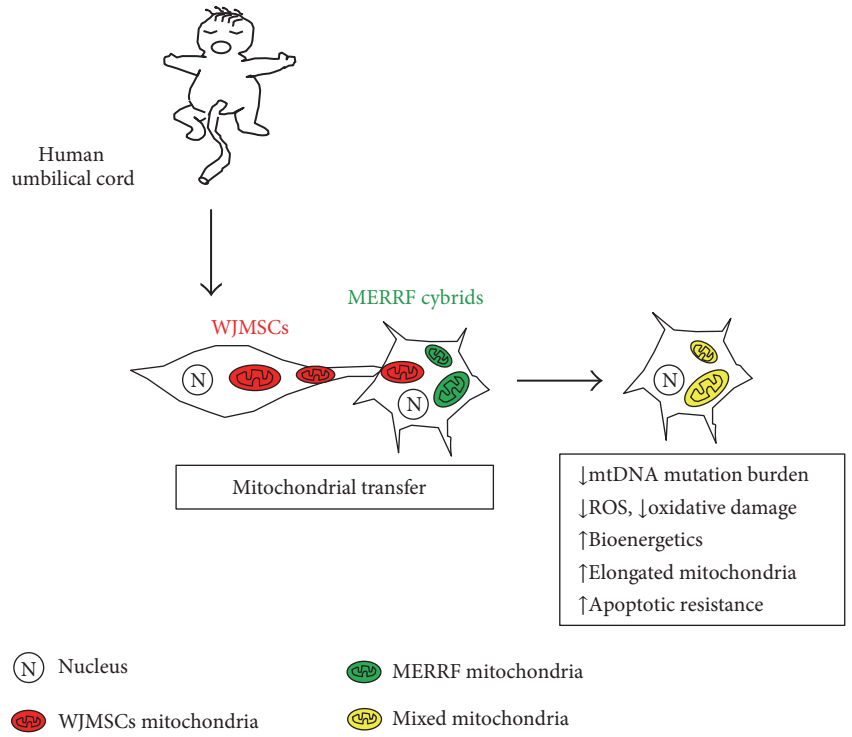

Figure 7: Graphic summary: WJMSC is capable of transferring healthy mitochondria to MERRF cybrid and reduces mtDNA mutation burden. Improved mtDNA mutation burden leads to amelioration in ROS generation, oxidative damage, and mitochondrial bioenergetics. The therapeutic effect of mitochondrial transfer also contributes to elongated network of mitochondria and apoptotic resistance.

effect. These results support the notion that induction of mitochondrial dysfunction and the formation of F-actin-containing tunneling nanotubes play a role in the process of mitochondrial transfer.

In addition to bioenergetics, the mt.8344A>G mutation in MERRF cells also leads to higher oxidative stress. MERRF cybrids and fibroblasts were reported to present increased intracellular H_2O_2 and oxidation-related markers [15]. Higher oxidative stress may render the MERRF cell more sensitive to the apoptotic inducer staurosporine, as shown in our study. In this regard, perturbed calcium homeostasis induced by mt.8344A>G-associated mitochondrial dysfunction and subsequent altered activity of calpain protease play a role in the hypersensitivity of MERRF cells to staurosporine [40]. As well, induced oxidative stress caused mitochondrial fragmentation [41], whereas OPA1 overexpression reduces intracellular oxidative stress and cellular apoptosis [42], suggesting the existence of mutual regulation between mitochondrial dynamics and oxidative stress. Our study reveals that the MERRF cybrid receiving WJMSC-derived mitochondrial transfer exhibited a reduced ROS level, increased mitochondrial fusion-network and profusion manner of dynamic protein, and enhanced resistance against apoptotic stress. We reason that improved mitochondrial bioenergetics through the reduction of heteroplasmic mtDNA mutation load following mitochondrial transfer plays a role in remodeling the elongated morphology of mitochondria. Indeed, OPA1-mediated mitochondrial fusion required functional OXPHOS [43]. We show that the MERRF cybrid with impaired OXPHOS presents reduced OPA1 and increased FIS1 expression along with fragmented mitochondria. After mitochondrial transfer, the corrected OXPHOS activity of the MERRF cybrid may contribute to a recovered OPA1/FIS expression pattern, which is then responsible for elongated morphology of mitochondria. Consistent with our data, Chang et al. have demonstrated that fragmentation of mitochondria network and decreased OPA1/increased FIS1 expression were caused by the mt.8344A>G mutation in MERRF cybrids, while mitochondrial transfer conducted by peptide-mediated mitochondrial delivery restored the network morphology and OPA1/FIS expression [31].

This study provides evidence for successful mitochondrial transfer from WJMSC to MERRF cybrids and its subsequent rescue effect in the changes to mtDNA mutation load, oxidative stress, bioenergetics, mitochondrial dynamics, and antiapoptotic resistance (Figure 7). We propose a new stem cell-based mitochondrial transfer resource for rescuing cells with mitochondrial disorders, which offers promise for the further development of treatment for mitochondrial diseases.

Conflicts of Interest

The authors declare that they have no conflicts of interest.

Authors' Contributions

Yao-Chung Chuang and Tsu-Kung Lin contributed equally to this work.

Acknowledgments

This work was supported by grants from Chang Gung Memorial Hospital (CMRPG8E0291; CMRPG8E0292) and the Ministry of Science and Technology, Taiwan (MOST 105-2314-B-182A-010). The authors acknowledge the kind gifts, Cox4-DsRed and Su9-EGFP plasmids, from Dr. David Chan (California Institute of Technology, Pasadena, CA 91125, USA). The authors thank the Stem Cell Research Core Laboratory Facilities at Kaohsiung Chang Gung Memorial Hospital for the technical support.

References

[1] M. C. Brandon, M. T. Lott, K. C. Nguyen et al., "MITOMAP: a human mitochondrial genome database—2004 update," *Nucleic Acids Research*, vol. 33, no. Database issue, pp. D611–D613, 2005.

[2] C. L. Quinlan, I. V. Perevoshchikova, M. Hey-Mogensen, A. L. Orr, and M. D. Brand, "Sites of reactive oxygen species generation by mitochondria oxidizing different substrates," *Redox Biology*, vol. 1, no. 1, pp. 304–312, 2013.

[3] R. S. Balaban, S. Nemoto, and T. Finkel, "Mitochondria, oxidants, and aging," *Cell*, vol. 120, no. 4, pp. 483–495, 2005.

[4] D. C. Chan, "Mitochondrial fusion and fission in mammals," *Annual Review of Cell and Developmental Biology*, vol. 22, pp. 79–99, 2006.

[5] S. A. Detmer and D. C. Chan, "Functions and dysfunctions of mitochondrial dynamics," *Nature Reviews Molecular Cell Biology*, vol. 8, no. 11, pp. 870–879, 2007.

[6] A. Y. Seo, A. M. Joseph, D. Dutta, J. C. Hwang, J. P. Aris, and C. Leeuwenburgh, "New insights into the role of mitochondria in aging: mitochondrial dynamics and more," *Journal of Cell Science*, vol. 123, Part 15, pp. 2533–2542, 2010.

[7] G. Benard, N. Bellance, D. James et al., "Mitochondrial bioenergetics and structural network organization," *Journal of Cell Science*, vol. 120, Part 5, pp. 838–848, 2007.

[8] G. Benard, N. Bellance, C. Jose, S. Melser, K. Nouette-Gaulain, and R. Rossignol, "Multi-site control and regulation of mitochondrial energy production," *Biochimica et Biophysica Acta*, vol. 1797, no. 6-7, pp. 698–709, 2010.

[9] T. Yu, J. L. Robotham, and Y. Yoon, "Increased production of reactive oxygen species in hyperglycemic conditions requires dynamic change of mitochondrial morphology," *Proceedings of the National Academy of Sciences of the United States of America*, vol. 103, no. 8, pp. 2653–2658, 2006.

[10] F. Legros, A. Lombes, P. Frachon, and M. Rojo, "Mitochondrial fusion in human cells is efficient, requires the inner membrane potential, and is mediated by mitofusins," *Molecular Biology of the Cell*, vol. 13, no. 12, pp. 4343–4354, 2002.

[11] D. C. Chan, "Fusion and fission: interlinked processes critical for mitochondrial health," *Annual Review of Genetics*, vol. 46, pp. 265–287, 2012.

[12] F. Reinecke, J. A. Smeitink, and F. H. van der Westhuizen, "OXPHOS gene expression and control in mitochondrial disorders," *Biochimica et Biophysica Acta*, vol. 1792, no. 12, pp. 1113–1121, 2009.

[13] H. A. Tuppen, E. L. Blakely, D. M. Turnbull, and R. W. Taylor, "Mitochondrial DNA mutations and human disease," *Biochimica et Biophysica Acta*, vol. 1797, no. 2, pp. 113–128, 2010.

[14] A. S. Noer, H. Sudoyo, P. Lertrit et al., "A tRNA(Lys) mutation in the mtDNA is the causal genetic lesion underlying myoclonic epilepsy and ragged-red fiber (MERRF) syndrome," *American Journal of Human Genetics*, vol. 49, no. 4, pp. 715–722, 1991.

[15] S. B. Wu, Y. S. Ma, Y. T. Wu, Y. C. Chen, and Y. H. Wei, "Mitochondrial DNA mutation-elicited oxidative stress, oxidative damage, and altered gene expression in cultured cells of patients with MERRF syndrome," *Molecular Neurobiology*, vol. 41, no. 2-3, pp. 256–266, 2010.

[16] C. Vives-Bauza, R. Gonzalo, G. Manfredi, E. Garcia-Arumi, and A. L. Andreu, "Enhanced ROS production and antioxidant defenses in cybrids harbouring mutations in mtDNA," *Neuroscience Letters*, vol. 391, no. 3, pp. 136–141, 2006.

[17] S. Duvezin-Caubet, R. Jagasia, J. Wagener et al., "Proteolytic processing of OPA1 links mitochondrial dysfunction to alterations in mitochondrial morphology," *The Journal of Biological Chemistry*, vol. 281, no. 49, pp. 37972–37979, 2006.

[18] J. L. Spees, S. D. Olson, M. J. Whitney, and D. J. Prockop, "Mitochondrial transfer between cells can rescue aerobic respiration," *Proceedings of the National Academy of Sciences of the United States of America*, vol. 103, no. 5, pp. 1283–1288, 2006.

[19] Y. M. Cho, J. H. Kim, M. Kim et al., "Mesenchymal stem cells transfer mitochondria to the cells with virtually no mitochondrial function but not with pathogenic mtDNA mutations," *PloS One*, vol. 7, no. 3, article e32778, 2012.

[20] H. Y. Lin, C. W. Liou, S. D. Chen et al., "Mitochondrial transfer from Wharton's jelly-derived mesenchymal stem cells to mitochondria-defective cells recaptures impaired mitochondrial function," *Mitochondrion*, vol. 22, pp. 31–44, 2015.

[21] M. N. Islam, S. R. Das, M. T. Emin et al., "Mitochondrial transfer from bone-marrow-derived stromal cells to pulmonary alveoli protects against acute lung injury," *Nature Medicine*, vol. 18, no. 5, pp. 759–765, 2012.

[22] T. Ahmad, S. Mukherjee, B. Pattnaik et al., "Miro1 regulates intercellular mitochondrial transport & enhances mesenchymal stem cell rescue efficacy," *The EMBO Journal*, vol. 33, no. 9, pp. 994–1010, 2014.

[23] X. Wang and H. H. Gerdes, "Transfer of mitochondria via tunneling nanotubes rescues apoptotic PC12 cells," *Cell Death and Differentiation*, vol. 22, no. 7, pp. 1181–1191, 2015.

[24] T. K. Lin, H. Y. Lin, S. D. Chen et al., "The creation of cybrids harboring mitochondrial haplogroups in the Taiwanese population of ethnic Chinese background: an extensive in vitro tool for the study of mitochondrial genomic variations," *Oxidative Medicine and Cellular Longevity*, vol. 2012, Article ID 824275, 2012.

[25] K. D. Shih, T. C. Yen, C. Y. Pang, and Y. H. Wei, "Mitochondrial DNA mutation in a Chinese family with myoclonic epilepsy and ragged-red fiber disease," *Biochemical and Biophysical Research Communications*, vol. 174, no. 3, pp. 1109–1116, 1991.

[26] R. K. Dagda, S. J. Cherra 3rd, S. M. Kulich, A. Tandon, D. Park, and C. T. Chu, "Loss of PINK1 function promotes mitophagy through effects on oxidative stress and mitochondrial fission," *The Journal of Biological Chemistry*, vol. 284, no. 20, pp. 13843–13855, 2009.

[27] H. M. Wilkins, S. M. Carl, and R. H. Swerdlow, "Cytoplasmic hybrid (cybrid) cell lines as a practical model for mitochondriopathies," *Redox Biology*, vol. 2C, pp. 619–631, 2014.

[28] P. G. Heytler, "Uncouplers of oxidative phosphorylation," *Methods in Enzymology*, vol. 55, pp. 462–442, 1979.

[29] V. M. Gohil, S. A. Sheth, R. Nilsson et al., "Nutrient-sensitized screening for drugs that shift energy metabolism from mitochondrial respiration to glycolysis," *Nature Biotechnology*, vol. 28, no. 3, pp. 249–255, 2010.

[30] A. Rustom, R. Saffrich, I. Markovic, P. Walther, and H. H. Gerdes, "Nanotubular highways for intercellular organelle transport," *Science*, vol. 303, no. 5660, pp. 1007–1010, 2004.

[31] J. C. Chang, K. H. Liu, Y. C. Li et al., "Functional recovery of human cells harbouring the mitochondrial DNA mutation MERRF A8344G via peptide-mediated mitochondrial delivery," *Neuro-Signals*, vol. 21, no. 3-4, pp. 160–173, 2013.

[32] J. C. Chang, K. H. Liu, C. S. Chuang et al., "Treatment of human cells derived from MERRF syndrome by peptide-mediated mitochondrial delivery," *Cytotherapy*, vol. 15, no. 12, pp. 1580–1596, 2013.

[33] R. D. Lund, S. Wang, B. Lu et al., "Cells isolated from umbilical cord tissue rescue photoreceptors and visual functions in a rodent model of retinal disease," *Stem Cells*, vol. 25, no. 3, pp. 602–611, 2007.

[34] H. S. Wang, S. C. Hung, S. T. Peng et al., "Mesenchymal stem cells in the Wharton's jelly of the human umbilical cord," *Stem Cells*, vol. 22, no. 7, pp. 1330–1337, 2004.

[35] F. Figeac, P. F. Lesault, O. Coz et al., "Nanotubular crosstalk with distressed cardiomyocytes stimulates the paracrine repair function of mesenchymal stem cells," *Stem Cells*, vol. 32, no. 1, pp. 216–230, 2014.

[36] A. Acquistapace, T. Bru, P. F. Lesault et al., "Human mesenchymal stem cells reprogram adult cardiomyocytes toward a progenitor-like state through partial cell fusion and mitochondria transfer," *Stem Cells*, vol. 29, no. 5, pp. 812–824, 2011.

[37] D. Baksh, R. Yao, and R. S. Tuan, "Comparison of proliferative and multilineage differentiation potential of human mesenchymal stem cells derived from umbilical cord and bone marrow," *Stem Cells*, vol. 25, no. 6, pp. 1384–1392, 2007.

[38] M. Y. Chen, P. C. Lie, Z. L. Li, and X. Wei, "Endothelial differentiation of Wharton's jelly-derived mesenchymal stem cells in comparison with bone marrow-derived mesenchymal stem cells," *Experimental Hematology*, vol. 37, no. 5, pp. 629–640, 2009.

[39] P. Hematti, "Role of mesenchymal stromal cells in solid organ transplantation," *Transplantation Reviews (Orlando, Fla.)*, vol. 22, no. 4, pp. 262–273, 2008.

[40] G. Rommelaere, S. Michel, J. Malaisse, S. Charlier, T. Arnould, and P. Renard, "Hypersensitivity of A8344G MERRF mutated cybrid cells to staurosporine-induced cell death is mediated by calcium-dependent activation of calpains," *The International Journal of Biochemistry & Cell Biology*, vol. 44, no. 1, pp. 139–149, 2012.

[41] D. Nguyen, M. V. Alavi, K. Y. Kim et al., "A new vicious cycle involving glutamate excitotoxicity, oxidative stress and mitochondrial dynamics," *Cell Death & Disease*, vol. 2, no. 12, article e240, 2011.

[42] T. Varanita, M. E. Soriano, V. Romanello et al., "The OPA1-dependent mitochondrial cristae remodeling pathway controls atrophic, apoptotic, and ischemic tissue damage," *Cell Metabolism*, vol. 21, no. 6, pp. 834–844, 2015.

[43] P. Mishra, V. Carelli, G. Manfredi, and D. C. Chan, "Proteolytic cleavage of Opa1 stimulates mitochondrial inner membrane fusion and couples fusion to oxidative phosphorylation," *Cell Metabolism*, vol. 19, no. 4, pp. 630–641, 2014.

Hindawi
Oxidative Medicine and Cellular Longevity
Volume 2017, Article ID 8510805, 13 pages
https://doi.org/10.1155/2017/8510805

Research Article

Enhancement of Mitochondrial Transfer by Antioxidants in Human Mesenchymal Stem Cells

Chia-Jung Li,[1,2] Po-Kong Chen,[3] Li-Yi Sun,[3] and Cheng-Yoong Pang[1,3]

[1]*Institute of Medical Sciences, Tzu Chi University, Hualien, Taiwan*
[2]*Research Assistant Center, Show Chwan Memorial Hospital, Changhua, Taiwan*
[3]*Department of Medical Research, Buddhist Tzu Chi General Hospital, Hualien, Taiwan*

Correspondence should be addressed to Cheng-Yoong Pang; cypang@mail.tcu.edu.tw

Received 19 January 2017; Accepted 23 March 2017; Published 17 May 2017

Academic Editor: Hsin-Chen Lee

Excessive reactive oxygen species is the major component of a harsh microenvironment after ischemia/reperfusion injury in human tissues. Combined treatment of N-acetyl-L-cysteine (NAC) and L-ascorbic acid 2-phosphate (AAP) promoted the growth of human mesenchymal stem cells (hMSCs) and suppressed oxidative stress-induced cell death by enhancing mitochondrial integrity and function in vitro. In this study, we aimed to determine whether NAC and AAP (termed MCA) could enhance the therapeutic potential of hMSCs. We established a coculture system consisting of MCA-treated and H_2O_2-treated hMSCs and investigated the role of tunneling nanotubes (TNTs) in the exchange of mitochondria between the 2 cell populations. The consequences of mitochondria exchange were assessed by fluorescence confocal microscopy and flow cytometry. The results showed that MCA could increase the mitochondrial mass, respiratory capacity, and numbers of TNTs in hMSCs. The "energized" mitochondria were transferred to the injured hMSCs via TNTs, the oxidative stress was decreased, and the mitochondrial membrane potential of the H_2O_2-treated hMSCs was stabilized. The transfer of mitochondria decreased the expression of S616-phosphorylated dynamin-related protein 1, a protein that dictates the fragmentation/fission of mitochondria. Concurrently, MCA also enhanced mitophagy in the coculture system, implicating that damaged mitochondria were eliminated in order to maintain cell physiology.

1. Introduction

Human mesenchymal stem cells (hMSCs) are multipotent cells isolated from adult tissues and possess the potential to differentiate into various cell types [1–3]. Recently, hMSCs have been tested in rescuing tissue injuries, including ischemia/reperfusion injuries of the heart, kidney, and brain [4, 5]. Ischemia/reperfusion injuries caused complex pathology in these tissues. Among them, overproduction of reactive oxygen species (ROS) in the injured tissues usually decrease the viability of engrafted MSCs after transplantation [6]. ROS are highly reactive molecules and are derived from the metabolism of oxygen. Mitochondria are the primary sources of ROS in eukaryotic cells, and excessive ROS in mitochondria usually cause damages to mitochondria and subsequently trigger mitochondrion-mediated cell death [7, 8]. It is thus important to increase the viability of hMSCs when transplanting them into injured tissues.

Recently, a tubular and thin membranous structure named tunneling nanotubes (TNTs) have been described to serve as channels transporting intracellular components between connected cells in vitro and in vivo [9]. These cellular components range from cytoplasm, ions, lipid droplet, viral and bacterial pathogens, and organelles (including mitochondria and lysosomes as well) [10–12]. TNTs can be found in various cell types, such as vascular smooth muscle cells, endothelial cells, and MSCs and cancer cells, and have been implicated to be beneficial in the repair of injured cells/tissues by exchange of functional mitochondria through TNTs after cell therapy [9, 13, 14].

In our previous studies, we demonstrated that combined treatment of N-acetyl-L-cysteine (NAC) and L-ascorbic acid 2-phosphate (AAP) offered several advantages in human adipose-derived MSCs: (1) NAC and AAP-pretreatment promotes hMSCs proliferation and maintains its stemness; (2) NAC and AAP-pretreatment suppresses oxidative stress-induced cell death by enhancing mitochondrial integrity and functions [15, 16]. In this study, we aimed to determine whether NAC and AAP-pretreatment could enhance the therapeutic potential of hMSCs. The medium that contained both antioxidants was named mesenchymal stem cell adjuvant (MCA). We established a coculture system that consisted of MCA-treated and H_2O_2-treated hMSCs and investigated the formation of TNTs and the exchange of mitochondria between the 2 cell populations. The consequences of mitochondria exchange were assessed by fluorescence confocal microscopy and flow cytometry after staining the cells with mitochondrion-specific fluorescent dyes.

2. Materials and Methods

2.1. Isolation and Maintenance of Human Adipose Tissue-Derived MSCs. Adipose tissue was procured from a donor who underwent liposuction with written informed consent (Buddhist Tzu Chi General Hospital Internal Review Board# IRB102-130). The human adipocyte-derived MSCs were isolated using our previously published method [15]. The hMSCs were cultured in a medium that consisted of Iscove's modified Dulbecco's medium (IMDM; GIBCO-Invitrogen Co.), 10% FBS (MSC-Qualified, GIBCO-Invitrogen Co.), 10 ng/mL FGF-2 (R&D Systems), and 2 mM L-glutamine and adjusted to contain 0.1 M sodium bicarbonate at 37°C in a humidified incubator containing 5% CO_2 and 95% air. All experiments were performed using hMSCs cultured between passages 3 to 6.

2.2. Oxygen Uptake Measurement. Mitochondrial oxygen consumption was measured using Oxygraph-2k according to the manual provided by the manufacturer (Oroboros Instruments Corp., Austria, http://wiki.oroboros.at/index.php/O2k-Protocols:_MitoPathways). The electrode was calibrated between 0 and 100% saturation with atmospheric oxygen at 37°C. In brief, respiration was measured at 37°C in 2 mL glass chambers. Cells were harvested by trypsinization, followed by centrifugation, and the cell pellet was resuspended in PBS for analysis. Maximal oxidative capacities (state 3) were determined in the presence of oxygen content of room air (21%). Respiration rates were calculated as the time derivative of oxygen measured in the closed respirometer and expressed per million viable cells. The amplified signal was recorded in a computer with online display of the calibrated oxygen concentration and oxygen flux (DatLab software for data acquisition and analysis; Oroboros Instruments, Innsbruck, Austria). Oxygen consumption is expressed as pmol O_2/s/mg of mitochondrial protein. The reaction chamber was filled with $\sim 1 \times 10^6$ indicated cells, and the oxygen consumption rate (OCR) of each respiratory complex was measured after addition of appropriate substrates, respiratory inhibitors (2 μM rotenone, 2 μM antimycin A, 0.5 μM oligomycin), and mitochondrial uncoupler FCCP (2 μM).

2.3. Mitochondrial Dehydrogenase Activity Assay. Mitochondrial dehydrogenase activity was analyzed using WST-8 (2-(2-methoxy-4-nitrophenyl)-3-(4-nitrophenyl)-5-(2,4-disulfophenyl)-2H-tetrazolium; CCK-8 Cell Counting Kit-8, Enzo Sci. Inc., US) that produces a highly water soluble formazan dye upon biochemical reduction at the presence of an electron carrier, 1-methoxy-PMS. At the end of various treatments, 10 μL of the CCK-8 reagent was added to each well and incubated at 37°C for additional 4 h. Absorbance at 450 nm was recorded by an ELISA microplate reader.

2.4. Cell Treatments. The MCA consisted of 2 mM NAC (Sigma) and 0.2 mM AAP (L-ascorbic acid 2-phosphate sesquimagnesium salt hydrate, Sigma). The cells cultured in medium without NAC and AAP were used as the normal control. Generally, for MCA protection experiments, the hMSCs were treated with MCA for 24 h and H_2O_2 (Sigma) for 4 h.

2.5. Detecting Mitochondria Transfer in Coculture System. The mitochondria of the healthy hMSCs were labeled with MitoTracker Red (Molecular Probes), and the mitochondria of the H_2O_2-treated hMSCs were labeled with Mitotracker Green (Molecular Probes) according to the manufacturer's instructions. To induce mitochondrial dysfunction, hMSCs were treated with 0.5 mM H_2O_2 for 4 h, while the healthy cells were cultured in control medium or MCA medium for 24 h. The injured cells were then cocultured at a 1 : 1 ratio with the control or MCA-treated hMSCs, respectively. Cells were observed under confocal microscopy (LSM510 Meta, Carl Zeiss) at an indicated time after coculture.

2.6. Quantification of Mitochondria Transfer. Healthy cells were labeled with 5-carboxyfluorescein diacetate (CFDA, Thermo Fisher Scientific) before 1 : 1 coculture with H_2O_2-treated hMSCs. The mitochondria of the control or MCA-treated hMSCs were stained with MitoTracker Red before 1 : 1 coculture. After 24 h coculture, all cells were harvested and subjected to flow cytometric analysis (BD FACSCalibur, US). The transfer of mitochondria was quantitated in the R2-gated CFDA-free cells. The appearance of MitoTracker Red fluorescence in the gated cells were supposed to be transferred from the control or MCA-treated hMSCs.

2.7. Determination of Mitochondrial Membrane Potential ($\Delta\Psi m$), ROS, and Mass. Cells from each experimental condition were stained with JC-1 reagent (for $\Delta\Psi$m, 5 μM), MitoSOX Red (for mitochondrial ROS, 5 μM), and MitoTracker Green (for mitochondrial mass, 0.1 μM) (all purchased from Molecular Probes), at 37°C for 30 min. Cells were washed twice with PBS, harvested, resuspended in PBS, and subjected to cytometric analysis (BD FACSCalibur, US).

2.8. Western Blotting Analysis. Cells were harvested after various treatments, and the expressions of each indicated proteins were densitometrically quantitated after SDS-PAGE and immunoblotting [16].

2.9. Quantification of TNTs. Fluorescent staining of actin was done with phalloidin 633 (4 units/mL, Molecular Probes) in culture medium containing 0.05% Triton X. The staining was performed on live cells with 15 min incubation at 37°C prior to fixation. The number of TNTs in the actin-labelled populations was counted and expressed as the number of TNTs per 100 cells.

2.10. Antibodies and Inhibitors. Anti-dynamin-related protein 1 (Drp-1, #5931), anti-phospho-Drp-1 Ser616 (#53455) were purchased from Cell Signaling Technology (MA, US). The antimitofusin-2 (Mfn2) was from GeneTex (GTX102055, GeneTex Inc., US). Anti-β-actin (A5411) was purchased from Sigma. To inhibit gap junctions as well as microtubule polymerization, the coculture medium was loaded with 50 μM nocodazole (M1404, Sigma).

2.11. Statistical Analysis. The intensity of bands in Western blots or fluorescence in fluorescent-micrographs were quantified using AlphaDigiDoc software (Cell Biosciences, ON, Canada), ImageJ software (NIH), and MicroP software [17]. All values are expressed as the mean ± the standard error of the mean (SEM) and were analyzed using Student's *t*-test with two-tailed distribution between groups as indicated in the figures. All calculations were performed by Microsoft Excel 2010.

3. Results

3.1. MCA Promotes Mitochondrial Biogenesis in hMSCs. The overall mitochondrial dehydrogenase activity of hMSCs was measured at 24 h after MCA treatment. The mitochondrial dehydrogenase activity of the MCA-treated hMSCs was 65.6% higher than that of the nontreated control hMSCs (Figure 1(a)). Concurrently, the mitochondrial mass of the MCA-treated cells was 143.5% larger than the nontreated cells (Figure 1(b)). The total cell number of both groups at 24 h did not differ much (Figure 1(c)). We next observed the mitochondrial network using confocal microscopy: the mitochondria were vitally stained with fluorescent dye, MitoTracker Red. We found that the morphology of mitochondria were markedly altered after MCA treatment in hMSCs (Figure 1(d)). The changes of mitochondrial morphology were stratified with MicroP software [17]. The mitochondria were classified into five types according to the characteristics of their morphology: small globules, linear tubules, loops, branched tubules, and twisted tubules. The globular mitochondria decreased from 40.7% to 25.2%, while branched and tubular mitochondria increased from 22.7% and 33.8% to 31.1% and 45.1%, respectively. (Figure 1(e), upper panel). In addition, we also noted that the average length of the mitochondria in MCA-treated cells significantly outscored those without treatment (Figure 1(e), lower panel, linear: 22.0 pixels versus 13.9 pixels; branched: 25.7 pixels versus 15.5 pixels). The width of the mitochondria did not differ in both treatments.

The cellular bioenergetics was also evaluated in hMSCs after treatment with MCA for 24 h. Marked reduction of mitochondrial respiration was observed in H_2O_2-treated cells as compared to the control and MCA-treated cells (Figure 1(f)). The mitochondrial respiration efficiency of hMSCs were significantly improved after MCA treatment as compared to the control or monotreated cells (NAC or AAP alone).

3.2. MCA Enhances TNT Formation. Previous studies have shown that cellular components can be transported between two separated cells by TNTs. Cytoplasm exchange, which includes mitochondria as well, occurs when TNTs form. The mitochondria from healthy hMSCs and injured hMSCs were labeled with MitoTracker Red and MitoTracker Green, respectively. Both cells were subjected to 1 : 1 coculture. The formation of intercellular TNTs between the donor and recipient cells enabled mitochondrial exchange through the TNTs (Figure 2(a)). After 24 h coculture, most of the mitochondria were found in the recipients, that is, the H_2O_2-treated cells, and contained both MitoTrackers (Figure 2(a), yellow insets). Selected (*x*-*y*) sections, obtained from confocal microscopy, and 2.5-dimensional reconstructions (as represented in Figure 2(b)) allowed us to identify the transport of mitochondria as the two fluorochromes were from the same plane.

We next investigated whether the formation of TNTs between the donors and recipients could be enhanced by MCA treatment. Figures 3(a) and 3(b) clearly demonstrated that the numbers of TNTs increased significantly after MCA treatment, while they decreased dramatically when microtubule-disrupting agent nocodazole (50 μM) was included in the medium during the coculture period. MCA treatment also led to an increased number of long TNTs (Figures 3(c) and 3(d)). The average lengths of TNTs were 53.5 μm and 28.5 μm in coculture containing MCA-treated and control hMSCs, respectively (Figure 3(d)). Moreover, the TNTs that were more than 50 μm in length was 35.7% in the coculture containing MCA-treated hMSCs (Figure 3(e)). Interestingly, MCA also increased the numbers of TNTs that connected two or more cells when compared to the non-MCA-treated coculture (44% versus 34%, Figure 3(b)).

3.3. MCA Enhances Mitochondrial Transfer. We also observed not only that MCA increased the number and length of TNTs (Figure 3) but also that the morphology of the mitochondria was different between the MCA-treated and control cells. In Figures 4(a) and 4(b), the MitoTracker Red-labeled mitochondria from the MCA-treated hMSCs were much longer than those from the control. Interestingly, the mitochondria that resided along the TNTs were predominantly labeled with MitoTracker Red (Figure 4(b), also in Figure 2(a)). In order to make sure that the mitochondria were transferred or originated from the healthy hMSCs, we labeled the healthy hMSCs with or without MCA-treatment with MitoTracker Red (for mitochondria labeling) and CFDA (for cell labeling)

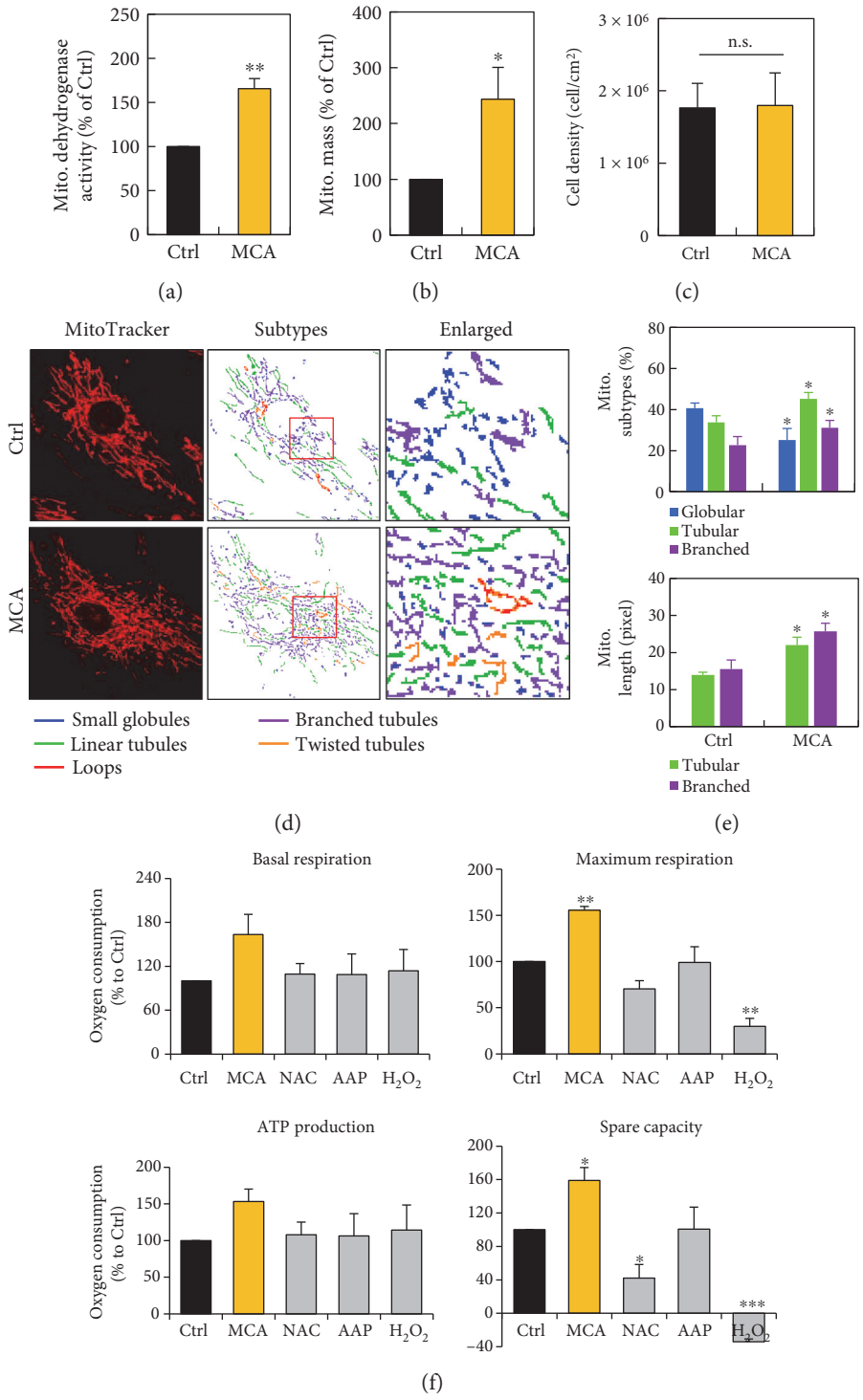

Figure 1: MCA improved mitochondrial biogenesis and bioenergetics in hMSCs. Mitochondrial dehydrogenase activity (a) and mitochondrial mass (b) of hMSCs treated with or without MCA for 24 h was assessed by CCK-8 assay and flow cytometric analysis of MitoTracker Red-labeled mitochondria, respectively. (c) The cell density of hMSCs with or without MCA treatment for 24 h was assessed by counting the harvested cells and normalized to the area of the culture flask. (d) The mitochondria of the hMSCs with or without MCA treatment were labeled with MitoTracker Red and subjected to confocal microscopy. The mitochondria were classified using MicroP software according to their morphology: small globules, linear tubules, loops, branched tubules, and twisted tubules. Three major types of mitochondria were quantified: globular, tubular, and branched ((e), upper panel), as well as their total length ((e), lower panel). (f) Mitochondrial bioenergetics of the indicated cells was determined by oxygen consumption rate (OCR) using Oroboros Oxygraph-2k analyzer. The MCA consisted of 2 mM NAC and 0.2 mM AAP. The concentrations of NAC and AAP were 2 mM and 0.2 mM, respectively, in monotreatments. OCR measured at basal respiration (upper left), maximal respiration (upper right), ATP-coupled respiration (lower left), and spare capacity (lower right) were shown. $^{*}p < 0.05$, $^{**}p < 0.01$, $^{***}p < 0.001$, as compared to the control (Ctrl); n.s., not significant.

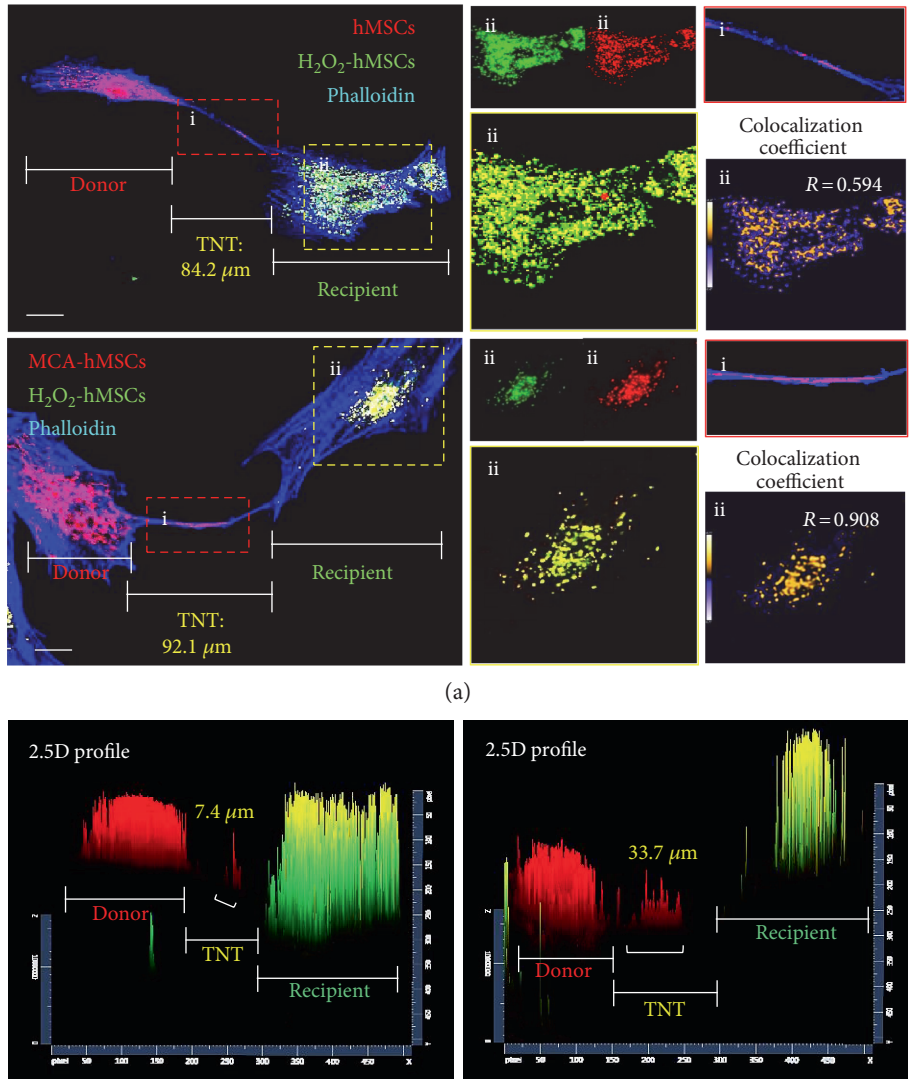

Figure 2: Mitochondria transfer was enhanced in hMSCs after MCA treatment. (a) Representative images of mitochondria transfer to H_2O_2-treated hMSCs from hMSCs with (right panel) or without (left panel) MCA treatment. The MitoTracker Red-labeled mitochondria from the healthy hMSCs were also clearly seen in TNT formed between the recipient and donor (inset i). Both MitoTracker Red- and Green-labeled mitochondria were found in the recipient cells (inset ii). The Pearson correlation coefficient are also shown to demonstrate the colocalization of the MitoTracker Red and Green labelled mitochondria after coculture [30]. The results showed that the colocalization coefficient in the (ii) of upper panel (24 h coculture of control hMSCs and H_2O_2-treated hMSCs) is 0.594, while that in the (ii) of lower panel (24 h coculture of MCA-treated hMSCs and H_2O_2-treated hMSCs) is 0.908. The colocalization coefficient can be further represented as pseudocolor changes: orange dots represent highly overlapping, while purple dots represent no overlapping. A 2.5-dimensional fluorescence reconstruction analysis of the respective images in (a) further confirmed that the red fluorescence was predominantly found in the TNT form between MCA-treated hMSCs and H_2O_2-treated hMSCs (b). Scale bar: 20 μm.

and cocultured these cells with H_2O_2-treated hMSCs. After 24 h incubation, the total cells were harvested and subjected to flow cytometric analysis. The CFDA-free cells, that is, the H_2O_2-treated hMSCs, were gated and the fluorescence of MitoTracker Red was measured. The transfer of the MitoTracker Red-mitochondria from the MCA-treated cells significantly increased when compared to the control (30.5% versus 16.3%, Figure 4(c), right panel).

3.4. MCA-hMSCs Rescue Injured Cells by Reducing Oxidative Stress. We next determined whether this mitochondrial transfer/donation was associated with reduction of oxidative stress. Oxidative stress was assessed by measuring mitochondrial ROS using MitoSOX Red (Figure 5(a)). In this experiment, the healthy cells were labeled with CFDA before coculture. After 24 h incubation, all cells were harvested, stained with MitoSOX Red, and subjected to flow cytometric analysis. Coculture with MCA-treated hMSCs markedly decreased the ROS level in the mitochondria of the recipient cells as compared to that of the control hMSCs (Figure 5(b), 32.4% versus 15.2%), whereas the ROS level in the donors' mitochondria (with or without MCA treatment) did not

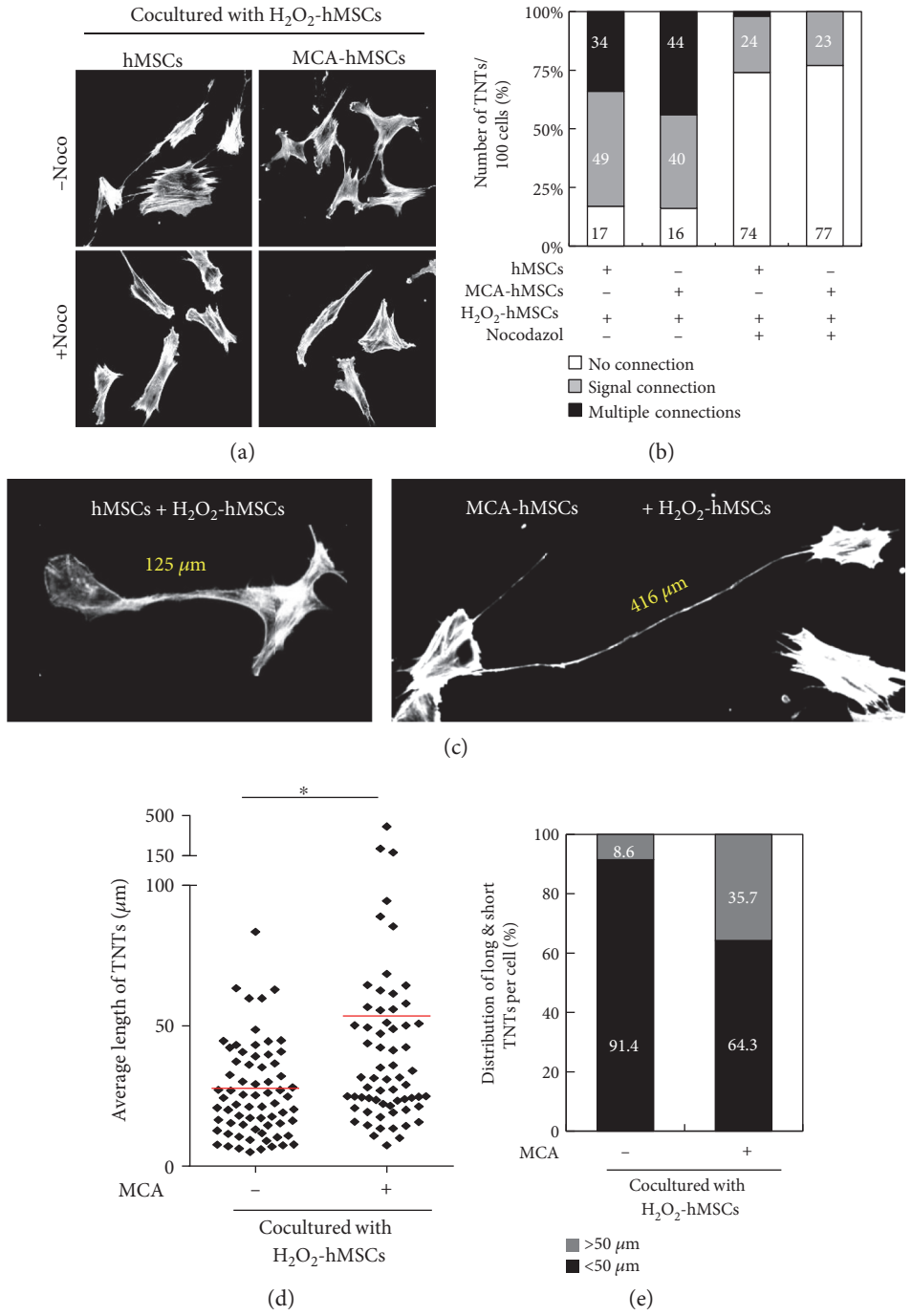

Figure 3: MCA enhanced TNT formation after coculture. TNTs decreased when microtubule-disrupting agent nocodazole (50 μM) was included in the coculture system (a). The number of TNTs were enumerated and classified per 100 cells, and the proportion of TNTs that connected multiple cells increased from 34% to 44% after MCA treatment (b). Nocodazole almost disrupted multiple connected-TNTs in the coculture system. A representative image of long TNT after MCA treatment in the coculture system is shown in (c). The average length of TNTs formed in coculture containing H_2O_2-treated hMSCs and hMSCs with or without MCA were 53.5 μm and 28.5 μm, respectively (d). TNTs that were more than 50 μm in length was 35.7% in the coculture containing MCA-treated and H_2O_2-treated hMSCs as compared to only 8.6% in the non-MCA-treated hMSCs coculture (e). $^*p < 0.05$, as compared to the non-MCA-treated hMSCs coculture. Scale bar: 20 μm.

differ much (Figure 5(c)). Most importantly, the viability of the recipients also increased significantly if they were cocultured with healthy hMSCs (Figure 5(d), 79.2% and 71.7% in MCA-treated and control hMSCs, respectively).

3.5. Maintenance of $\Delta\Psi m$ after Coculture with MCA-hMSCs. In addition to reducing mitochondrial ROS in the recipients, we further demonstrated that this mitochondria transfer/donation also contributed to the maintenance of $\Delta\Psi m$. The

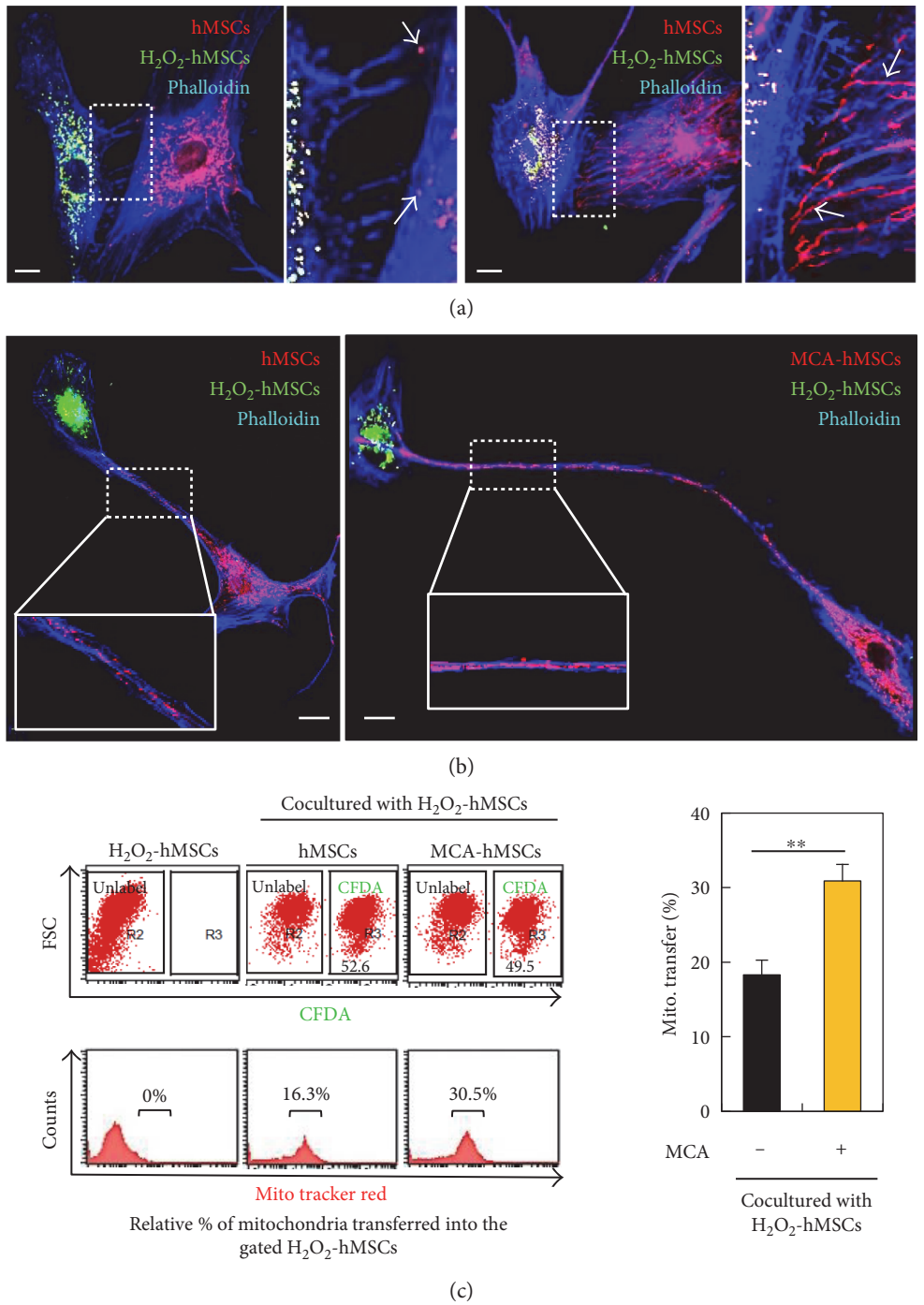

Figure 4: MCA enhanced mitochondria transfer to the injured hMSCs. (a) The MitoTracker Red-labeled mitochondria from the MCA-treated hMSCs were longer than the non-MCA-treated hMSCs in the coculture, as well as the numbers of TNTs formed (see enlarged insets). The actin was stained with phalloidin (blue fluorescence) in both coculture. (b) The MitoTracker Red-labeled mitochondria that resided along the TNTs were also longer in coculture containing MCA-treated hMSCs (right panel and inset) as compared to the one with non MCA-treated hMSCs (left panel and inset). (c) Healthy hMSCs with or without MCA treatment were labeled with CFDA and MitoTracker Red before coculture. After 24 h coculture with H_2O_2-treated hMSCs, all cells were harvested and subjected to flow cytometric analysis. The CFDA-unlabeled cells were gated and the MitoTracker Red fluorescence was quantitated. The proportion of cells containing red fluorescence was 30.5% in coculture containing MCA-treated hMSCs as compared to the 16.3% in the control hMSCs coculture. $^{**}p < 0.01$.

cocultured cells were stained with JC-1 and subjected to confocal microscopy. As shown in Figure 6(a), mitochondria with higher $\Delta\Psi$m (red fluorescent) were dominant. The red and green fluorescence were further quantitated by flow cytometry, and the results demonstrated that the mitochondria with lower $\Delta\Psi$m were significantly reduced in coculture

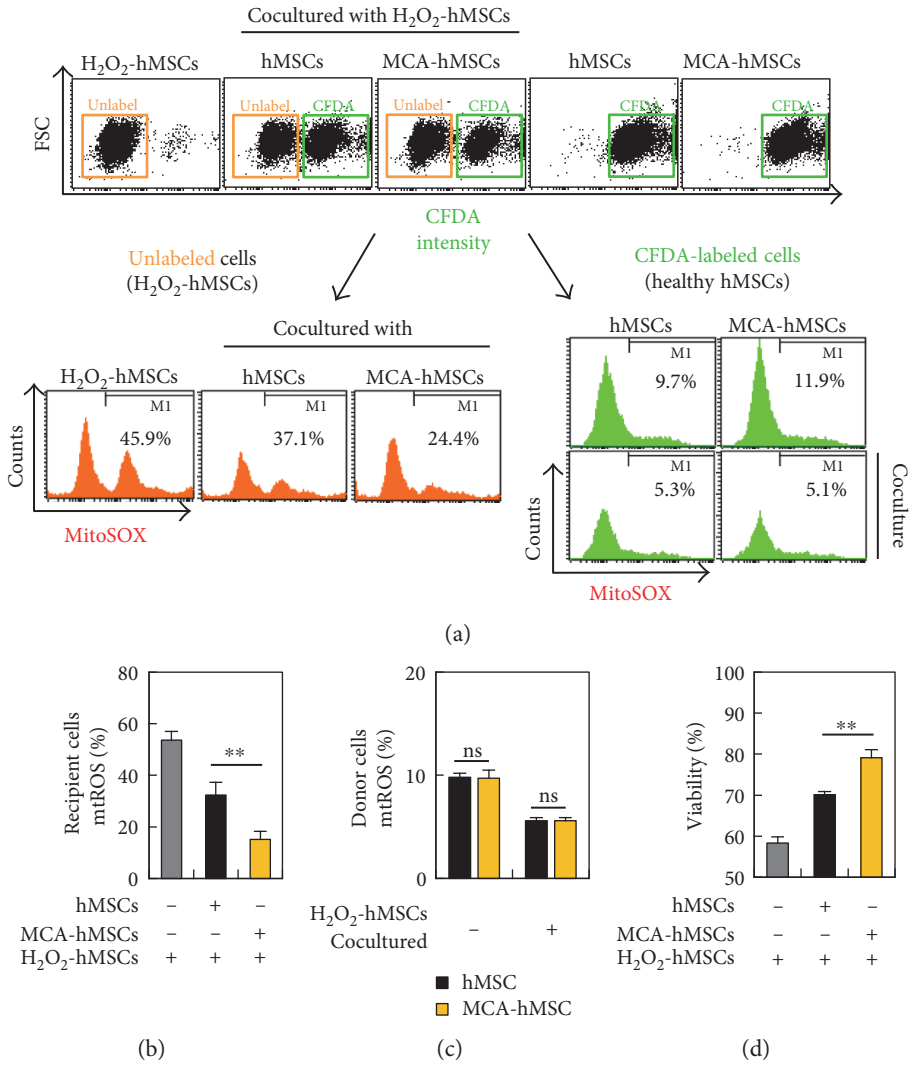

Figure 5: MCA-hMSCs rescued injured cells by reducing oxidative stress. (a) Healthy hMSCs with or without MCA treatment were labeled with CFDA before coculture. After 24 h coculture with H_2O_2-treated hMSCs, all cells were harvested, stained with and MitoSOX Red, and subjected to flow cytometric analysis. The florescence of MitoSOX Red was determined separately in the CFDA-labeled and CFDA-unlabeled cells. The proportion of injured cells (CFDA-unlabeled) with MitoSOX Red in coculture containing MCA-treated hMSCs was 24.4% as compared to the 37.1% in the control hMSCs coculture (b). However, the proportion of MitoSOX Red cells in the CFDA-labeled healthy cells did not differ much (c). The viability of injured cells increased after coculture (d). $^{**}p < 0.01$, as compared with the control.

containing healthy hMSCs (Figures 6(b) and 6(c)). The reduction was further enhanced in coculture containing MCA-treated hMSCs (Figures 6(b) and 6(c)). Addition of nocodazole significantly reduced this mitochondrial rescue effect, indicating that TNT formation was the key component in mitochondria transfer/donation (Figures 6(b) and 6(c)).

3.6. MCA Treatment Reduces Mitochondrial Fragmentation and Drp1 S616 Phosphorylation. We nest investigated whether the protection of cell against oxidative damage, reduction of mitochondrial ROS, and maintenance of $\Delta\Psi m$ were reflected in mitochondrial dynamics. By using MicroP analysis, we quantitated the mitochondrial morphological changes after coculture. H_2O_2 caused fragmentation of almost 90% of mitochondria in the hMSCs (Figures 7(a) and 7(b)). However, coculture with healthy hMSCs reduced the proportion of globular mitochondria significantly (Figure 7(b)). Among them, coculture containing MCA-treated cells further reduced mitochondrial fragmentation to 68.1% when compared to the control hMSCs (78.5%) (Figure 7(b)). Concurrently, the proportion of the relative healthier linear tubular mitochondria consisted 14.8% and 26.0% in coculture containing control and MCA-treated hMSCs, respectively. In addition, the average length of the mitochondria in coculture containing MCA-treated hMSCs also significantly outscored those without MCA treatment or H_2O_2-monotreated cells (Figure 7(c)).

Recruitment and/or retention of Drp1 in the mitochondria have been implicated in mitochondrial dynamics [18, 19]. The polymerization of Drp1 is an early and obligatory step for mitochondrial fission and fragmentation. We next tried to explore the possible mechanism of how MCA reduced mitochondrial fragmentation in hMSCs by monitoring Drp1 phosphorylation (Drp1 S616) and Mfn2 expression.

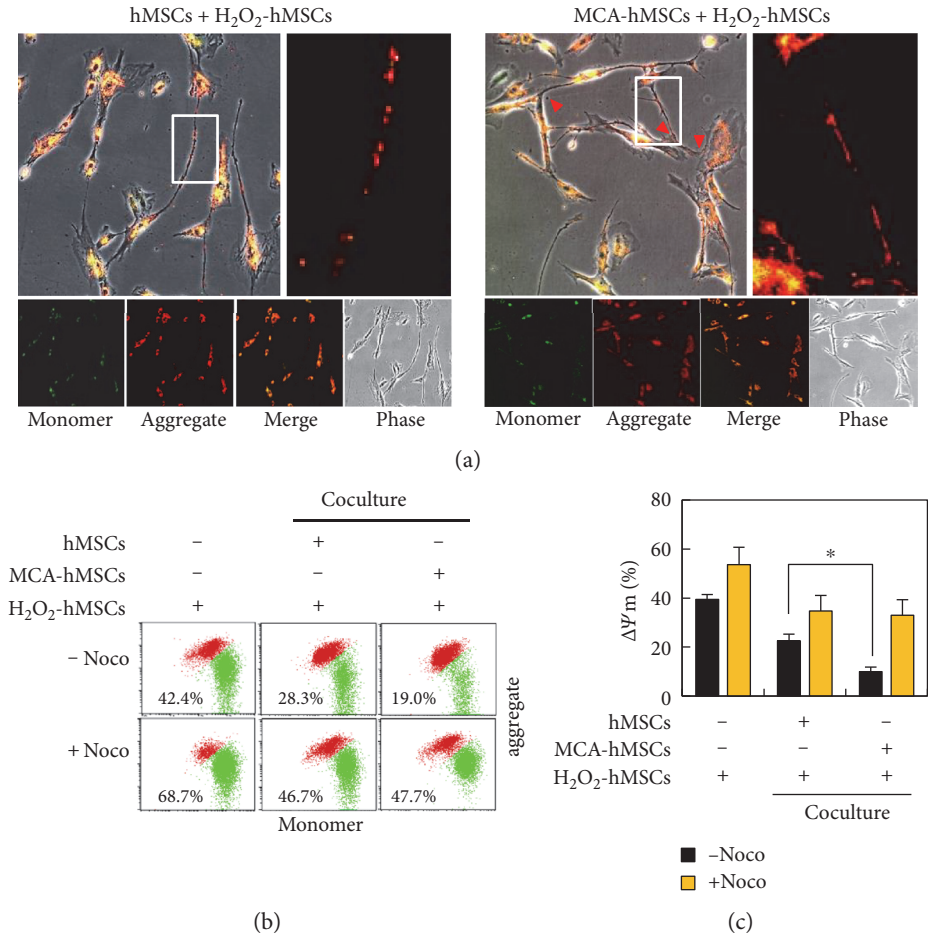

Figure 6: Maintenance of mitochondrial membrane potential (ΔΨm) after coculture with MCA-hMSCs. (a) The ΔΨm was measured using JC-1 in hMSCs coculture system. The JC-1 was mostly red (indicating higher ΔΨm) in coculture containing MCA-treated hMSCs (right panel), and the mitochondria appeared to be longer as compared to the control hMSCs coculture (comparing the enlarged insets from the right and left panels). (b) The cocultured cells were analyzed with flow cytometry. The proportion of cells with lower ΔΨm (green fluorescence) decreased in coculture containing MCA-treated hMSCs. The rescue of ΔΨm in the coculture decreased significantly in coculture medium containing nocodazole (c). $^*p < 0.05$.

As shown in Figure 7(d), Western blot analysis revealed that exposure of hMSCs to H_2O_2 induced an increase in mitochondrial Drp1 S616, while Drp1 S616 was decreased in MCA-treated hMSCs, as well as in the coculture system. Notably, although MCA treatment increased Mfn2 expression in hMSCs, it did not alter the total expression of Mfn2 after coculture.

3.7. Mitochondria Transfer/Donation Helps in Maintaining Mitochondrion Quality in the Injured hMSCs. Besides affecting mitochondrial dynamics by regulating Drp1 S616, we next investigated the fate of the damaged mitochondria in the H_2O_2-treated hMSCs after coculture with MCA-treated cells. MitoTracker Red and Green were used to label mitochondria in the healthy and H_2O_2-treated cells, respectively, before coculture. At 6 h after coculture, the total cells were subjected to fluorescent confocal microscopy. Numerous tubular intact mitochondria showed strong red fluorescence, while green fluorescence was found majorly in dots and short tubules (Figure 8(a)). Some of these dots and short tubules also harbored MitoTracker Red when the images were merged (insets in Figure 8(a)). The numbers of red fluorescent mitochondria also increased drastically in hMSCs pretreated with MCA (Figure 8(a), right panel), echoing the finding that MCA could increase mitochondrial mass in Figure 1(c).

We next investigated the fate of these dotted and short tubular mitochondria at 6 h after coculture with healthy hMSCs. The whole cells were labeled with MitoTracker Green and CytoPainter LysoRed. CytoPainter LysoRed selectively accumulates in lysosomes probably via the lysosome pH gradient and can be used to study autophagy, including mitophagy. Interestingly, some of the green fluorescent mitochondrial aggregates colocalized with LysoRed after we merged the images (Figure 8(b)). The colocalization of both cellular components was more prominently found in coculture that consisted of H_2O_2-treated and MCA-treated hMSCs (Figure 8(b), and the enlarged insets at the right panel). Fluorescence intensity analysis of the insets in Figure 8(b), especially in the two insets from MCA-hMSCs + H_2O_2-hMSCs, further confirmed that the green fluorescence was in the same plane of the red fluorescence (Figure 8(c)).

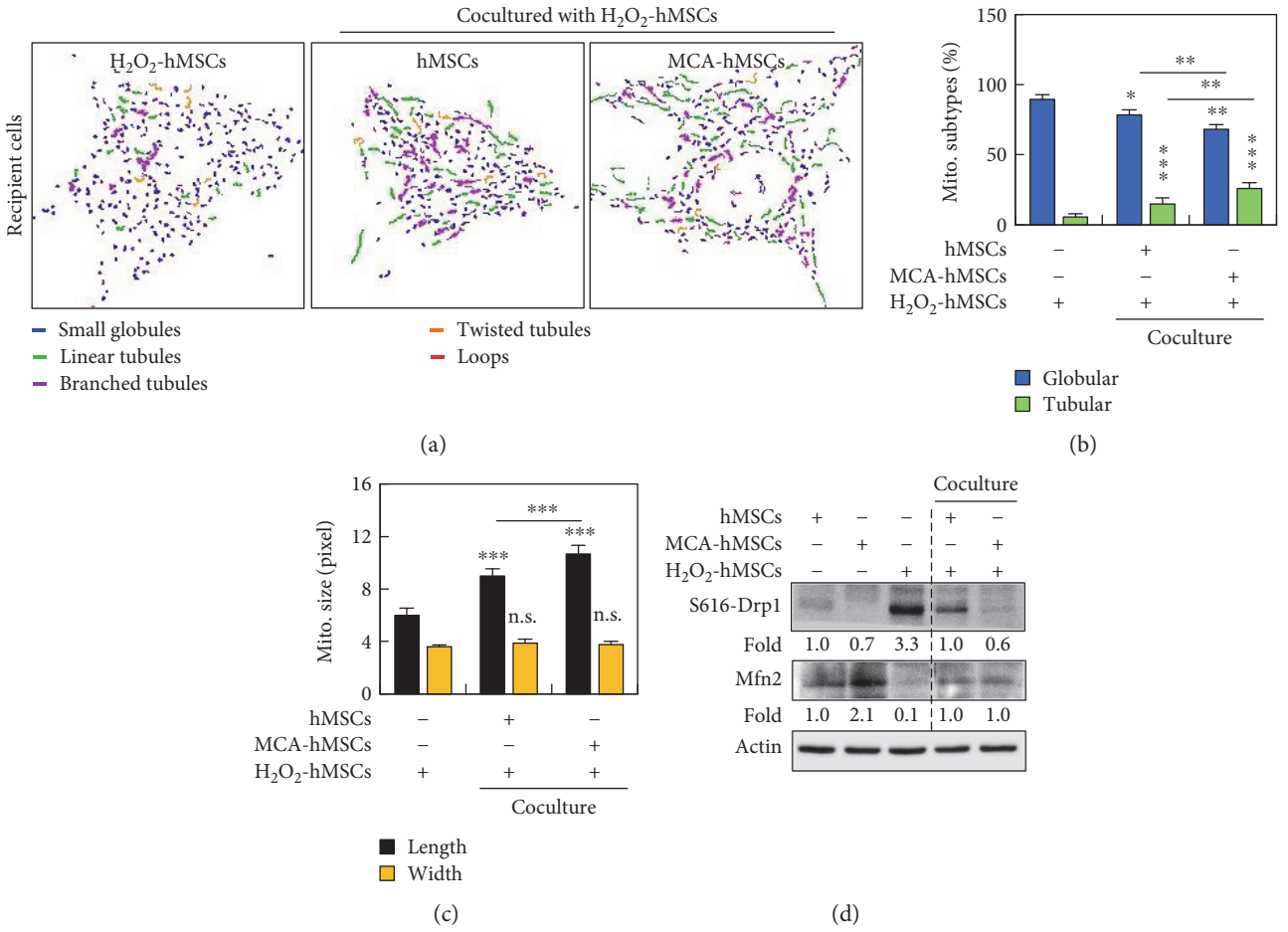

Figure 7: MCA reduced mitochondrial fragmentation. (a) Representative images of mitochondrial morphology after cocultured. The mitochondria can be classified into small globular, linear tubular, branched tubular, twisted tubular, and looped types, using MicroP software. The two major types of mitochondria, the globular and tubular, were enumerated and the results were shown in (b). In coculture containing MCA-treated hMSCs, the proportion of globular mitochondria decreased, while the proportion of the healthier tubular mitochondria increased significantly. (c) The length of the mitochondria in the coculture containing MCA-treated hMSCs was longer than that in the control hMSCs coculture. The width of the mitochondria from both coculture did not differ. (d) Western blot analysis of Drp1 S616 and Mfn2. The fold ratios of lanes 2 and 3 were obtained after comparing to lane 1, while that of lane 5 were obtained after comparing to lane 4. $^{*}p < 0.05$, $^{**}p < 0.01$, $^{***}p < 0.001$, n.s., not significant. Scale bar: 20 μm.

The colocalization of fragmented mitochondria and lysosome could be a consequence of mitophagy, a mechanism that has been implicated in mitochondrial quality maintenance [20].

4. Discussion

Stem cell therapy is an important measure to restore tissue damage due to injury and might serve as an alternative to tissue or organ transplantation [21]. Besides successful application of hematopoietic stem cell transplantation in blood disorders or cancer patients, the therapeutic application of stem cells from other sources are not fully tested in human due to lack of exact mechanisms, poor viability of transplanted cells at the site of injury, poor integration of implanted cells with the damaged tissues, and ethical consideration [22]. Stem cells of other sources include embryonic stem cells, adult stem cells, and tissue/organ-specific progenitor cells. Among them, adult stem cells, especially tissue-derived MSCs, have attracted the interest of most researchers because they can be easily obtained from the bone marrow, adipose tissue, synovium, periosteum, and placenta without much ethical consideration [23]. However, the lack of exact mechanism and problem of low viability after transplantation remained unsolved. When MSCs enter the injury site, they usually die because of the harsh microenvironment and failure to integrate/adhere to the remaining tissue. In order to overcome the abovementioned problems, especially in hMSCs-based cell therapy, many strategies have been developed [22]. Genetic modification of MSCs before transplantation is less practical due to regulatory obstacles of gene therapy. Preconditioning of MSCs with chemicals, bioactive factors, and even hypoxia culture [24–26] seems much easier to approach. Furthermore, MSCs can be transplanted in allogeneic ways as they are less immunogenic [27].

Our previous studies show that NAC and AAP (termed MCA in current study) cotreatment could promote hMSCs

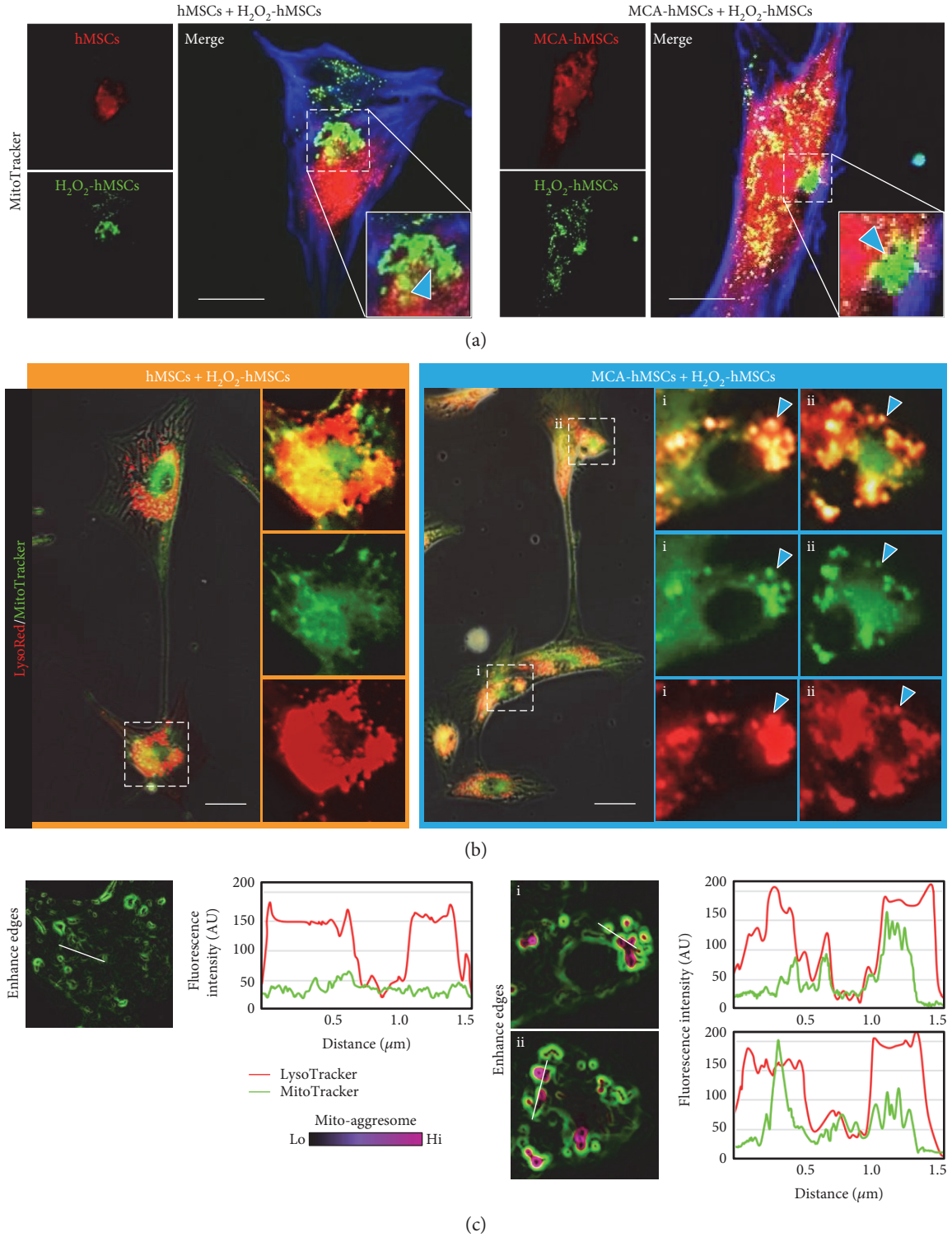

FIGURE 8: Mitochondria transfer helped regulating mitochondria quality in the injured hMSCs. (a) The mitochondria from the H_2O_2-hMSCs were labeled with MitoTracker Green, while the mitochondria from the healthy hMSCs were labeled with MitoTracker Red, respectively, before 6 h coculture. The number of MitoTracker Red-labeled mitochondria in the recipients increased in coculture containing MCA-treated hMSCs, while the MitoTracker Green-labeled mitochondria were shorter and tended to form aggregates (arrowheads in the enlarge insets). (b) Both cocultured cells were stained with MitoTracker Green and LysoRed to identify the fate of the short mitochondria. Many mitochondrial aggregates in the coculture containing MCA-treated hMSCs colocalized with LysoRed-labeled lysosomes (arrowheads in the enlarged insets of the right panel). (c) Fluorescence intensity analysis of the respective insets in (b) confirmed that the green fluorescence was in the same plane of the red fluorescence. Scale bar: 20 μm.

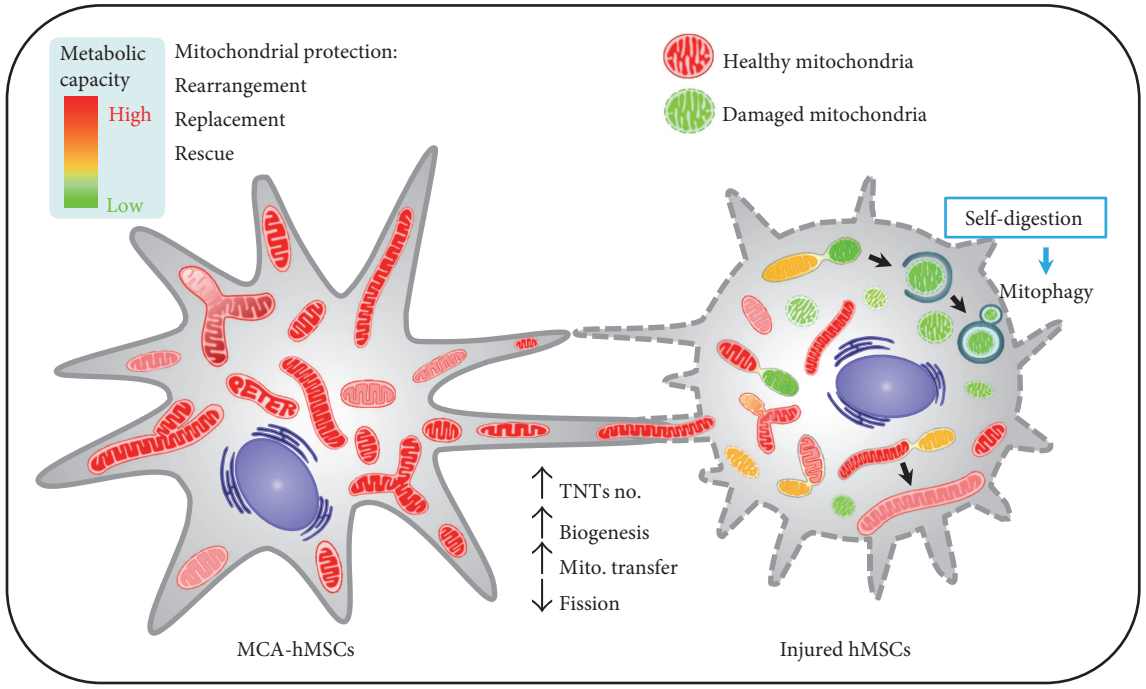

Figure 9: A schematic diagram showing TNT formation between injury and MCA-treated hMSCs. MCA can energize mitochondria and increase the number of TNTs in hMSCs. These healthy mitochondria can be transferred to the injured cells via TNTs and subsequently ameliorate oxidative stress, decrease mitochondrial damage/fragmentation/fission, and increase the turnover of damaged mitochondria by mitophagy.

entrance into S-phase by suppressing cyclin-dependent kinase inhibitors, which resulted in cell proliferation and yet retained their differentiation ability [15]. In addition, MCA also helped hMSCs to cope with H_2O_2-induced cell death by inhibiting cell death and maintaining mitochondria integrity [16].

In this study, using a coculture system that consisted of healthy and H_2O_2-trerated hMSCs, we demonstrated that MCA enhanced the protection potential of healthy hMSCs by mitochondria transfer/donation through TNTs. MCA initially promoted the increase of mitochondrial mass, respiratory capacity, and TNT formation. These "energized" mitochondria were transferred to the recipients via TNTs and decreased the oxidative stress of the H_2O_2-treated hMSCs. The $\Delta\Psi m$ of the injured cells was also stabilized after mitochondria transfer/donation. Concurrently, we also observed enhanced mitophagy in the coculture system, implicating that damaged mitochondria were being eliminated in order to maintain cell physiology (Figure 9). Although our findings indicate that functional mitochondria transfer/donation from MCA-treated hMSCs protects injured cells against H_2O_2-induced mitochondrial damage, the mechanisms of mitochondria transfer/donation remain unclear. Mechanistically, although the total Mfn2 did not increase after coculture, the decrease of Drp1 S616 was evidenced. Mfn2 and Drp1 are important regulators of mitochondrial fusion and fission, respectively.

Jiang et al. [28] demonstrated that human iPS-derived MSCs could also donate their functional mitochondria to rescue corneal epithelial cells under rotenone-induced oxidative stress via increased TNT formation between the two cell types. They further showed that the increased TNTs was associated with oxidative inflammation-activated NFκB/TNFαip2 signaling pathways that could be attenuated by NAC. Recent study has also revealed the possible mechanism of how mitochondria were transported in the TNTs: overexpression of Miro1, a mitochondrial Rho-GTPase, in mouse MSCs leads to enhanced mitochondrial transfer and rescue of epithelial injury, while knockdown of Miro1 in MSCs failed to do so [29]. Interestingly, Miro1 overexpression did not alter the anti-inflammatory factors of the MSCs, thus excluding the paracrine effects of MSCs in stem cell therapy.

5. Conclusion

This study reveals the protective effects of MCA in promoting the therapeutic potential of hMSCs by energizing mitochondria and enhancing mitochondria transfer/donation via TNTs (Figure 9). The pretreatment of hMSCs with antioxidants (MCA in current study) thus provides a novel strategy to enhance the therapeutic outcome of stem cell-based therapy in tissue injury.

Conflicts of Interest

The authors claim that there is no conflict of interest on this work.

Acknowledgments

This work was supported by Grant nos. TCRD105-01, TCRD-I101-05-02 (both granted to Cheng-Yoong Pang), and SC-5-2 (granted to Li-Yi Sun) from Hualien Buddhist Tzu Chi General Hospital and Buddhist Tzu Chi Medical Foundation, Taiwan.

References

[1] A. I. Caplan, "Mesenchymal stem cells," *Journal of Orthopaedic Research*, vol. 9, no. 5, pp. 641–650, 1991.

[2] P. A. Zuk, M. Zhu, P. Ashjian et al., "Human adipose tissue is a source of multipotent stem cells," *Molecular Biology of the Cell*, vol. 13, no. 12, pp. 4279–4295, 2002.

[3] O. K. Lee, T. K. Kuo, W. M. Chen, K. D. Lee, S. L. Hsieh, and T. H. Chen, "Isolation of multipotent mesenchymal stem cells from umbilical cord blood," *Blood*, vol. 103, no. 5, pp. 1669–1675, 2004.

[4] N. Souidi, M. Stolk, and M. Seifert, "Ischemia-reperfusion injury: beneficial effects of mesenchymal stromal cells," *Current Opinion in Organ Transplantation*, vol. 18, no. 1, pp. 34–43, 2013.

[5] H. K. Eltzschig and T. Eckle, "Ischemia and reperfusion—from mechanism to translation," *Nature Medicine*, vol. 17, no. 11, pp. 1391–1401, 2011.

[6] X. Y. Zhu, A. Lerman, and L. O. Lerman, "Concise review: mesenchymal stem cell treatment for ischemic kidney disease," *Stem Cells*, vol. 31, no. 9, pp. 1731–1736, 2013.

[7] M. Ott, M. Ott, V. Gogvadze, S. Orrenius, and B. Zhivotovsky, "Mitochondria, oxidative stress and cell death," *Apoptosis*, vol. 12, no. 5, pp. 913–922, 2007.

[8] J. Hou, Z. P. Han, Y. Y. Jing et al., "Autophagy prevents irradiation injury and maintains stemness through decreasing ROS generation in mesenchymal stem cells," *Cell Death & Disease*, vol. 4, no. article e844, 2013.

[9] A. Rustom, R. Saffrich, I. Markovic, P. Walther, and H. H. Gerdes, "Nanotubular highways for intercellular organelle transport," *Science*, vol. 303, no. 5660, pp. 1007–1010, 2004.

[10] H. H. Gerdes, A. Rustom, and X. Wang, "Tunneling nanotubes, an emerging intercellular communication route in development," *Mechanisms of Development*, vol. 130, no. 6–8, pp. 381–387, 2013.

[11] D. Torralba, F. Baixauli, and F. Sánchez-Madrid, "Mitochondria know no boundaries: mechanisms and functions of intercellular mitochondrial transfer," *Frontiers in Cell and Developmental Biology*, vol. 4, p. 107, 2016.

[12] B. L. Tang, "MIRO GTPases in mitochondrial transport. Homeostasis and pathology," *Cell*, vol. 5, no. 1, p. 1, 2015.

[13] J. Pasquier, B. S. Guerrouahen, H. Al Thawadi et al., "Preferential transfer of mitochondria from endothelial to cancer cells through tunneling nanotubes modulates chemoresistance," *Journal of Translational Medicine*, vol. 11, no. 1, p. 94, 2013.

[14] E. Y. Plotnikov, T. G. Khryapenkova, S. I. Galkina, G. T. Sukhikh, and D. B. Zorov, "Cytoplasm and organelle transfer between mesenchymal multipotent stromal cells and renal tubular cells in co-culture," *Experimental Cell Research*, vol. 316, no. 15, pp. 2447–2455, 2010.

[15] L. Y. Sun, C. Y. Pang, D. K. Li et al., "Antioxidants cause rapid expansion of human adipose-derived mesenchymal stem cells via CDK and CDK inhibitor regulation," *Journal of Biomedical Science*, vol. 20, no. 1, p. 53, 2013.

[16] C. J. Li, L. Y. Sun, and C. Y. Pang, "Synergistic protection of N-acetylcysteine and ascorbic acid 2-phosphate on human mesenchymal stem cells against mitoptosis, necroptosis and apoptosis," *Scientific Reports*, vol. 5, p. 9819, 2015.

[17] J. Y. Peng, C. C. Lin, Y. J. Chen et al., "Automatic morphological subtyping reveals new roles of caspases in mitochondrial dynamics," *PLoS Computational Biology*, vol. 7, no. 10, article e1002212, 2011.

[18] W. Bleazard, M. C. JM, E. J. King et al., "The dynamin-related GTPase Dnm1 regulates mitochondrial fission in yeast," *Nature Cell Biology*, vol. 1, no. 5, pp. 298–304, 1999.

[19] E. Smirnova, L. Griparic, D. L. Shurland, and A. M. van der Bliek, "Dynamin-related protein Drp1 is required for mitochondrial division in mammalian cells," *Molecular Biology of the Cell*, vol. 12, no. 8, pp. 2245–2256, 2001.

[20] R. J. Youle and D. P. Narendra, "Mechanisms of mitophagy," *Nature Reviews. Molecular Cell Biology*, vol. 12, no. 1, p. 9, 2011.

[21] S. J. Forbes and N. Rosenthal, "Preparing the ground for tissue regeneration: from mechanism to therapy," *Nature Medicine*, vol. 20, no. 8, pp. 857–869, 2014.

[22] S. Lee, E. Choi, M. J. Cha, and K. C. Hwang, "Cell adhesion and long-term survival of transplanted mesenchymal stem cells: a prerequisite for cell therapy," *Oxidative Medicine and Cellular Longevity*, vol. 2015, Article ID 632902, p. 9, 2015.

[23] A. M. DiMarino, A. I. Caplan, and T. L. Bonfield, "Mesenchymal stem cells in tissue repair," *Frontiers in Immunology*, vol. 4, p. 201, 2013.

[24] X. Hu, S. P. Yu, J. L. Fraser et al., "Transplantation of hypoxia-preconditioned mesenchymal stem cells improves infarcted heart function via enhanced survival of implanted cells and angiogenesis," *The Journal of Thoracic and Cardiovascular Surgery*, vol. 135, no. 4, pp. 799–808, 2008.

[25] S. M. Chacko, S. Ahmed, K. Selvendiran, M. L. Kuppusamy, M. Khan, and P. Kuppusamy, "Hypoxic preconditioning induces the expression of prosurvival and proangiogenic markers in mesenchymal stem cells," *American Journal of Physiology-Cell Physiology*, vol. 299, no. 6, pp. C1562–C1570, 2010.

[26] C. P. Chang, C. C. Chio, C. U. Cheong, C. M. Chao, B. C. Cheng, and M. T. Lin, "Hypoxic preconditioning enhances the therapeutic potential of the secretome from cultured human mesenchymal stem cells in experimental traumatic brain injury," *Clinical Science*, vol. 124, no. 3, pp. 165–176, 2013.

[27] R. P. Herrmann and M. J. Sturm, "Adult human mesenchymal stromal cells and the treatment of graft versus host disease," *Stem Cells Cloning*, vol. 7, pp. 45–52, 2014.

[28] D. Jiang, F. Gao, Y. Zhang et al., "Mitochondrial transfer of mesenchymal stem cells effectively protects corneal epithelial cells from mitochondrial damage," *Cell Death & Disease*, vol. 7, no. 11, article e2467, 2016.

[29] T. Ahmad, S. Mukherjee, B. Pattnaik et al., "Miro1 regulates intercellular mitochondrial transport & enhances mesenchymal stem cell rescue efficacy," *The EMBO Journal*, vol. 33, no. 9, pp. 994–1010, 2014.

[30] J. Adler and I. Parmryd, "Colocalization analysis in fluorescence microscopy," in *Cell Imaging Techniques: Methods and Protocols*, D. J. Taatjes and J. Roth, Eds., pp. 97–109, Humana Press, New York, 2012.